Modified gravity and alternatives to single field inflation

Mariaveronica De Angelis

Doctor of Philosophy in Mathematics
School of Mathematical and Physical Sciences
University of Sheffield

July 2025

Supervisor: Prof. Carsten van de Bruck

To my parents Eleonora and Antonio

Abstract

Motivated by the need to understand the origin of inflation and address theoretical limitations of general relativity, this thesis investigates four complementary directions beyond standard single-field inflation. Each approach is rooted in well-motivated extensions of gravity and multifield inflationary dynamics, aiming to bridge fundamental theory and cosmological observations. After introducing the theoretical foundations of modified gravity and inflation, the thesis presents original research across four main themes: multifield inflation with kinetic couplings, scale-invariant models, non-local gravity, and cyclic cosmologies.

First, multifield models with non-trivial kinetic couplings are analysed. Arising from conformal transformations in non-minimally coupled theories, these models exhibit rich dynamics including adiabatic and isocurvature perturbations. Using our sampling algorithm, the thesis explores their predictions and compares them with cosmological data.

Second, the R^2 scale-invariant inflationary model is studied, where mass scales emerge dynamically via spontaneous symmetry breaking. This model addresses the hierarchy problem and yields predictions consistent with current observations, offering an interesting alternative to Starobinsky and α-attractor scenarios.

Third, the thesis examines inflation in non-local hybrid metric-Palatini gravity, inspired by attempts to include quantum corrections through non-local operators. Reformulating the theory with auxiliary fields, we identify stable configurations and investigate how non-local terms deform the inflationary potential in observable ways.

Finally, a non-inflationary alternative is explored: the cyclic universe. A general framework is developed to study the evolution of primordial gravitational waves across cosmological cycles. The impact of initial conditions and vacuum choice is assessed, with implications for the robustness of gravitational wave predictions.

Together, these results offer novel insight into early-universe cosmology, proposing viable alternatives to standard inflation, and guiding future observational and theoretical research.

Declaration of authorship

The content of this thesis is the result of the author's original research, carried out in collaboration with the supervisor. Specifically, the material in Chapter 4 was developed solely in collaboration with the supervisor, whereas Chapter 5, Chapter 6, and Chapter 7 also include contributions from additional collaborators. These chapters are based on five papers, all of which have been published in peer-reviewed journals. The papers are the outcome of research conducted at the University of Sheffield between October 2021 and September 2025:

- M. De Angelis and C. van de Bruck, "Adiabatic and isocurvature perturbations in extended theories with kinetic couplings", *JCAP* **10** 023 (2023), arXiv: 2304.12364;
- W. Giarè, M. De Angelis, C. van de Bruck and E. Di Valentino, "Tracking the multifield dynamics with cosmological data: a Monte Carlo approach", *JCAP* **12** 014 (2023), arXiv: 2306.12414;
- M. De Angelis, A. Smith, W. Giarè and C. van de Bruck, "Gravitational waves in a cyclic Universe: resilience through cycles and vacuum state ", *JCAP* **06** 036 (2024), arXiv: 2403.00533;
- C. Cecchini, M. De Angelis, W. Giarè, M. Rinaldi and S. Vagnozzi, "Testing scale-invariant inflation against cosmological data ", *JCAP* **07** 058 (2024), arXiv: 2403.04316;
- F. Bombacigno, M. De Angelis, C. van de Bruck and W. Giarè, "Inflation in non-local hybrid metric-Palatini gravity ", *JCAP* **05** 025 (2025), arXiv: 2403.04316.

The material in Part I represents a review of the general area of research, its motivation and its recent developments. The contents of Part II constitute original research and provide a detailed exposition of the papers mentioned above, with the exception of the first section of Chapter 7 where a brief review is included. Finally, Part III contains appendices.

Contributions

The work presented in Chapter 4 is based on the papers [1] and [2]. I carried out all of the theoretical development, including the formulation of the model and the analysis by writing a general Python code, under the guidance of the supervisor. The only exception is the implementation of the MCMC code in [2], which was developed by a collaborator.

The content of Chapter 5 is based on [3]. While the model under investigation was originally formulated in the literature by some of the authors (see [4]), my contribution consisted in applying the formalism and numerical code developed in [1] and [2]. I also verified that analytical results match with numerical outcomes and theoretical predictions are in agreement with observations. The development of the numerical plots was equally shared between myself and a collaborator.

The work presented in Chapter 6 is based on [5]. I contributed in part to the formulation of the theoretical framework, and I performed the analysis of the dynamics using the code I had previously developed in [1].

The material in Chapter 7 is based on [6]. The analytical work and numerical analysis were equally shared between myself and a collaborator.

Sheffield, *July 2025*

Mariaveronica De Angelis

Contents

List of Figures

List of Tables

Introduction

Understanding the physical processes that shaped the early Universe remains one of the most pressing open questions in modern cosmology. While the standard cosmological model, built upon general relativity (GR) and the inflationary paradigm, explains a broad range of observations with remarkable accuracy [7–11], it leaves unanswered fundamental theoretical challenges. Among them are the physical origin of the inflationary potential [12], the nature and generation of mass scales, the naturalness of initial conditions [13], and the ultraviolet (UV) completion of gravity [14–16].

This thesis is motivated by the need to address these challenges through the exploration of theoretical extensions to the standard inflationary scenario. Specifically, we focus on four main directions. The first three include multifield inflation with kinetic couplings, scale-invariant models where mass scales arise dynamically, and non-local modifications of gravity inspired by attempts to improve UV behaviour. Lastly, we investigate an alternative "inflationary" scenario, a cyclic model where the universe undergoes repeated phases of contraction and expansion. This model offers a novel perspective on avoiding the inflationary phase and provides insights into the universe's evolution prior to the hot Big Bang phase. Each framework offers a distinct perspective on fundamental problems and introduces characteristic phenomenological features that can be compared to observational data.

Our approach is guided by four core questions:

1. In multifield models of inflation, the dynamics can be significantly altered by interactions between the fields. These interactions open new avenues for generating observable features beyond what is predicted by single-field models. This raises the question of whether kinetic couplings between fields during inflation could yield predictions that better align with observational data, or generate distinctive signatures such as isocurvature modes and non-Gaussianities.

2. The mass of the Higgs boson highlights the hierarchy problem, where fundamental scales differ by many orders of magnitude [17, 18]. Without a protective mechanism, quantum effects tend to drive mass parameters toward very large values,

meaning the observed small masses require extremely precise adjustments of the underlying parameters – a situation known as fine-tuning. Classical scale invariance, if broken dynamically, could provide a natural mechanism for these scales, including those driving inflation, to emerge without excessive fine-tuning. Could this framework also offer clear criteria to distinguish between different inflationary models?

3. Non-local modifications of gravity have been proposed as a way to capture quantum gravitational effects at cosmological scales [19]. Could these non-local hybrid models produce dynamically stable inflationary scenarios and provide insights into quantum gravity corrections?

4. Finally, going beyond inflationary dynamics: can cyclic cosmological scenarios reproduce key observational features, and how robust are their predictions for primordial gravitational waves, particularly regarding vacuum choice and contributions from earlier cycles?

In what follows, we briefly introduce the various frameworks used to address the above questions, outline the methods, and present the structure of the thesis, explaining the logical flow from foundational principles to detailed phenomenological analysis.

CONCEPTUAL MOTIVATIONS. The inflationary paradigm was introduced to resolve key shortcomings of the Hot Big Bang model, such as the horizon and flatness problems [7, 20], and has succeeded in predicting a nearly scale-invariant spectrum of primordial fluctuations [21, 22]. Despite its empirical success, several conceptual questions remain.

Origin of mass scales: standard inflation relies on introducing explicit mass parameters by hand. Scale-invariant models propose instead that mass scales can arise dynamically via spontaneous symmetry breaking [4, 23–25], offering an elegant resolution to the hierarchy problem.

Number of fields: High-energy completions of gravity often include multiple scalar fields [26]. Multifield inflation can naturally emerge in these settings, leading to richer dynamics and potentially observable signatures beyond single-field models [27–29].

Ultraviolet completion and non-locality: GR is non-renormalisable in the UV [15]. Modifications such as non-local operators (*e.g.* inverse d'Alembertian terms) can soften UV divergences and might capture aspects of quantum gravity corrections [19]. By investigating these directions, we aim to clarify their theoretical consistency and study whether they can produce inflationary scenarios compatible with current observations.

Alternatives to inflation: While inflation remains the dominant paradigm, it is not the only mechanism capable of explaining the observed near scale invariance and flat-

ness [30–32]. Cyclic models provide a qualitatively different framework that can predict distinct features in the primordial tensor spectrum [33–37]. By studying the cyclic scenario, we explore the robustness of its predictions, particularly the suppression of tensor modes [38], and assess the implications of different choices of vacuum state and initial conditions.

METHODOLOGY AND APPROACH. Our analysis starts from the action principle for each theoretical framework, deriving the corresponding equations of motion and identifying the dynamical degrees of freedom. For multifield models, we consider general two-field systems with non-trivial kinetic couplings arising from conformal transformations in non-minimally coupled theories. We analyse the background evolution, perturbations, and observational signatures. In scale-invariant models, we study the spontaneous breaking of classical scale invariance and its role in dynamically generating the Planck scale and inflationary scale. The resulting inflationary observables such as the spectral index, tensor-to-scalar ratio, and number of e-folds, are then compared to established models like Starobinsky inflation [39]. For non-local and hybrid gravity models, we reformulate non-local terms as local scalar-tensor theories using auxiliary fields. This allows us to study stability, ghost conditions, and the inflationary potential's deformation due to non-local operators. Finally, in studying the cyclic universe model, we start by reviewing its background dynamics and the sequence of cosmological phases characterising each cycle. Our analysis focuses on the production and evolution of primordial gravitational waves, beginning in the dark energy phase of the previous cycle. We develop a general formalism to track tensor perturbations across the phases, making no restrictive assumptions about the initial vacuum state. This approach allows us to assess the sensitivity of predictions to vacuum choice and to quantify the contribution of modes generated during earlier phases. By combining analytical estimates with numerical integration, we investigate the impact of these contributions on the observable tensor spectrum and examine the backreaction constraints required to preserve the consistency of the cyclic scenario.

STRUCTURE OF THE THESIS. The thesis is divided into two parts. Part I establishes the theoretical foundations necessary for understanding the *original* extensions developed in Part II.

Part I: Foundations

Chapter 1: "*About Gravity*" introduces the geometric description of gravity in GR, highlighting its basis in the equivalence principle and general covariance. We discuss the Einstein field equations, derived from the Einstein-Hilbert action, and explain why GR is highly successful yet theoretically incomplete for what concern cosmology. The chapter also outlines motivations for modified gravity theories, including metric and Palatini $f(R)$ models, hybrid metric-Palatini gravity, and non-local extensions.

Chapter 2: "*Structure and Dynamics of the Isotropic Universe*" applies GR to cosmology. We derive the Friedmann equations starting from the assumption of spatial homogeneity and isotropy (the cosmological principle) and introduce the standard ΛCDM model. The chapter also discusses the role of inflation in explaining the observed large-scale structure and its theoretical motivations.

Chapter 3: "*The Theory of Inflation*" focuses on the dynamics of inflation. We explain the slow-roll approximation, derive predictions for scalar and tensor perturbations, and discuss key observables. The chapter motivates why multifield dynamics and modified gravity extensions might be necessary to address fine-tuning, generate richer phenomenology, or connect inflation to fundamental theories.

Part II: Beyond Standard Inflation

Chapter 4: "*Multifield Inflation with Kinetic Couplings*" investigates two-field inflationary models where the fields are coupled through a non-trivial field-space metric. We derive background and perturbation equations, analyse adiabatic and isocurvature modes, and perform numerical analyses to explore the impact of kinetic couplings on observables.

Chapter 5: "*Scale-Invariant Inflation*" studies models where classical scale invariance is imposed at the level of the action. We explore how spontaneous symmetry breaking dynamically generates mass scales, derive inflationary dynamics, and compare predictions with observational constraints. Finally, we comment on the possibility of distinguishing the model from Starobinsky and α-attractor inflation [40]. Overall, we argue that scale-invariant inflation is in excellent health, and possesses features which make it an interesting benchmark for tests of inflation from future CMB data.

Chapter 6: "*Inflation in Non-local Hybrid Modified Gravity*" focuses on non-local extensions of hybrid metric-Palatini gravity. Using auxiliary fields, we analyse ghost conditions, derive inflationary dynamics, and examine how non-local terms lead to defor-

mation of the Starobinsky-like potential offering a new way to test the robustness of the model.

Chapter 7: "*Alternative Mechanisms to Inflation*" explores an alternative paradigm to inflation: the cyclic universe model. Motivated by the need to test the robustness of inflationary predictions and the possibility of resolving the initial singularity, we provide a detailed analysis of primordial gravitational wave production in cyclic cosmologies. In particular, we investigate how the choice of vacuum state and contributions from earlier phases, such as the dark energy epoch of the preceding cycle, affect the tensor spectrum observed today. This complementary study sheds light on the predictivity of cyclic models and their viability as alternatives to inflation.

Chapter 8: "*Conclusions*" discusses the main results and future directions.

Finally, supplementary material for Chapter 1, Chapter 4, Chapter 5 and Chapter 6 is present in the appendices in Part III.

Our goal is to contribute to the broader effort of connecting fundamental physics with cosmological observations, by examining models that remain close to data but originate from deeper theoretical motivations.

Part I | Foundations

1 About gravity

General Relativity (GR) is the theory of gravity formulated by Einstein in 1915. It is founded on two core principles: the equivalence principle, which establishes a deep connection between the effects of gravitation and acceleration, and the principle of general covariance, which states that the laws of physics should take the same form in all coordinate systems. Together, these principles lead to a radical shift in how gravitational phenomena are understood. In GR, gravity is no longer described as a force acting instantaneously at a distance, but rather as a manifestation of the curvature of spacetime, determined by the distribution of energy and matter. In this geometric picture, spacetime is modelled as a four-dimensional differentiable manifold, whose structure is encoded in the metric tensor $g_{\mu\nu}(t, \mathbf{x})$. This symmetric tensor determines distances, time intervals, and angles, and thus fully characterises the geometry of spacetime. Importantly, it does so in a way that is independent of the observer's frame of reference, reflecting the principle of general covariance. A crucial conceptual consequence of this framework is the role played by spacetime itself. Because GR is invariant under diffeomorphisms – or coordinate transformations – points on the manifold have no physical meaning on their own. Only relations between dynamical quantities are physically meaningful. In this sense, coordinates in GR are not physical quantities but arbitrary labels used to parametrise a fully covariant theory of geometry. This distinguishes GR from other theories where diffeomorphism invariance, in the form of reparametrisation invariance, can be artificially imposed and later undone; the theory of GR is inherently covariant, and there is no non-covariant formulation to return to.

In this chapter of the thesis we delve into the dynamics of spacetime as described by GR in Section 1.1, beginning with the Einstein field equations. We then move beyond GR in Section 1.2 to explore modified theories of gravity, which are motivated by both theoretical and observational challenges. Particular attention is given to extensions formulated in the metric, Palatini, hybrid metric-Palatini approaches, and non-local gravity, as well as to theories incorporating scale invariance. These generalised frameworks offer alternative descriptions of gravitational dynamics, often with additional degrees of freedom or geometric structures. They provide fertile ground for addressing open problems

in fundamental physics, such as the nature of dark energy, the origin of cosmic inflation, and the behaviour of gravity at high energies or in strong-field regimes. Here, we set the stage for a detailed exploration of theories of gravity, laying the mathematical and conceptual groundwork needed for the discussions in later chapters.

1.1 The dynamics of spacetime in General Relativity

The dynamics of spacetime is specified by its metric denoted by $g_{\mu\nu}(t, \mathbf{x})$, which connects the observer-dependent coordinates x^μ with the invariant distance between events via the line element ds^2. The invariant line element is

$$ds^2 = g_{\mu\nu}(t, \mathbf{x}) dx^\mu dx^\nu, \tag{1.1}$$

where $dx^0 = dt$ is the time coordinate and dx^i with $i = \{1, 2, 3\}$ are the spatial coordinates. We use a mostly plus convention for the metric signature and natural units in which $c = \hbar = 1$.

The concept of proper time plays a fundamental role in describing the motion of particles on curved spacetime. Proper time, denoted by $\Delta\tau$, is defined as the invariant interval measured along a timelike worldline ($ds^2 < 0$) between two events. Mathematically, if two events A and B are connected by a timelike path γ parametrised by λ such that $\lambda(0) = A$ and $\lambda(1) = B$, the proper time is given by

$$\Delta\tau = \int_\gamma \sqrt{-ds^2} = \int_0^1 d\lambda \sqrt{-g_{\mu\nu} \frac{dx^\mu}{d\lambda} \frac{dx^\nu}{d\lambda}}, \tag{1.2}$$

which directly follows from the metric's role in determining the distance between events. This definition emphasises that proper time is an intrinsic measure – independent of any coordinate system – and it serves as the "clock" along a particle's worldline. The importance of proper time becomes even more evident when we consider the motion of freely falling systems. According to the Equivalence Principle, at any spacetime point one can choose a set of coordinates $\{\xi^\mu\}$ defining a locally inertial frame (LIF) in which the metric takes the Minkowskian form at that point,

$$ds^2 = -(d\xi^0)^2 + (d\xi^1)^2 + (d\xi^2)^2 + (d\xi^3)^2 = \eta_{\mu\nu} d\xi^\mu d\xi^\nu, \tag{1.3}$$

where $\eta_{\mu\nu}$ =diag$(-1, 1, 1, 1)$. In this LIF, and only locally, the equations of motion of a

freely falling particle reduce to those of Special Relativity,

$$\frac{d^2\xi^\alpha}{d\tau^2} = 0, \tag{1.4}$$

indicating that, at a given event, the worldline is tangent to a straight line in the locally inertial coordinates. When we describe the same motion in a general coordinate system x^μ, the metric takes the general form $g_{\mu\nu}$ and the transformation from ξ^α to $x^\alpha = x^\alpha(\xi^\alpha)$ introduces additional terms. These terms are encoded in the Christoffel symbols of the Levi-Civita connection,

$$\Gamma^\alpha_{\mu\nu} = \frac{1}{2} g^{\lambda\alpha}\big(g_{\nu\lambda,\mu} + g_{\mu\lambda,\nu} - g_{\mu\nu,\lambda}\big), \tag{1.5}$$

which in general do not vanish, even in flat spacetime, since they depend on the choice of coordinates. They therefore do not represent intrinsic curvature; curvature is instead encoded in the Riemann tensor $R_{\mu\nu\sigma\rho}$ which will be introduced later in the chapter. The equation of motion in the general coordinates becomes the geodesic equation,

$$\frac{d^2x^\alpha}{d\tau^2} + \Gamma^\alpha_{\mu\nu}\frac{dx^\mu}{d\tau}\frac{dx^\nu}{d\tau} = 0. \tag{1.6}$$

Here, the term involving the Christoffel symbols represents the gravitational "force" that, in Newtonian mechanics, would be identified with the gradient of the gravitational potential (as well as the additional apparent accelerations). The metric g is identified with the gravitational potential. Thus, starting from the invariant definition of proper time we are naturally led to the concept of geodesic motion.

For massless particles, such as photons, the situation is somewhat different since proper time is identically zero. Indeed, these particles move along null geodesics $ds^2 = 0$ and the definitions given in (1.2) and (1.6) no longer apply (*i.e.* the derivation of the geodesic equation using proper time fails). Instead, one introduces an affine parameter λ that labels points along the curve and defines $k^\mu = dx^\mu/\lambda$, which plays the role of a tangent vector to the null trajectory (*i.e.* $k^\mu k_\mu = 0$). The equation of motion then takes the covariant form $k^\mu\nabla_\mu k^\nu = 0$, where ∇_μ is the covariant derivative such that $\nabla_\mu k^\nu = \partial_\mu k^\nu + \Gamma^\nu_{\mu\sigma}k^\sigma$. However, for massive particle, by defining the four-velocity of a particle as $u^\mu = dx^\mu/d\tau$ and its four-momentum $P^\mu = m\,u^\mu$ where $P^\mu = (E, \mathbf{p})$ and $E^2 = m^2 + p^2$, it is possible to rewrite (1.6) in the compact form

$$P^\mu\nabla_\mu P^\nu = 0. \tag{1.7}$$

To complete the picture, we now address how geometry itself is not fixed but dynam-

ically determined by the distribution of matter and energy. We start by considering the Einstein-Hilbert action, where R denotes the Ricci scalar, a geometrical quantity built from the metric $g_{\mu\nu}(t, \mathbf{x})$, an arbitrary scalar quantity known as cosmological constant Λ, and the action of generic matter as

$$S = \frac{M_P^2}{2} \int d^4x \sqrt{-g}\,(R - 2\Lambda) + \int d^4x \sqrt{-g}\,\mathcal{L}_M, \tag{1.8}$$

where $M_P^2 = 1/(8\pi G)$ is the reduced Planck mass, g is the determinant of the metric $g_{\mu\nu}$ and $\mathcal{L}_M$ is the matter Lagrangian density. The negative sign in the brackets of (1.8) is a convention and the factor of 2 is a choice to simplify later results. To derive the field equations, we vary the total action with respect to the metric. From the first term in (1.8) we have

$$\delta[\sqrt{-g}\,(R - 2\Lambda)] = \sqrt{-g}\left(R_{\mu\nu} - \frac{1}{2}g_{\mu\nu}R + \Lambda g_{\mu\nu}\right)\delta g^{\mu\nu} + (\text{total derivative terms}), \tag{1.9}$$

where $R_{\mu\nu} \equiv R^{\sigma}_{\mu\sigma\nu}$ is the symmetric Ricci tensor obtained by the contraction of the Riemann curvature tensor $R^{\lambda}_{\mu\sigma\nu} = \partial_\sigma\Gamma^{\lambda}_{\nu\mu} - \partial_\nu\Gamma^{\lambda}_{\sigma\mu} + \Gamma^{\lambda}_{\sigma\rho}\Gamma^{\rho}_{\nu\mu} - \Gamma^{\lambda}_{\nu\rho}\Gamma^{\rho}_{\sigma\mu}$. The total derivative terms arise from the variation of $R_{\mu\nu}$ and can be neglected under appropriate boundary conditions. This feature is specific to the Einstein–Hilbert action and explains why the metric and Palatini formulations of general relativity yield equivalent dynamics. As will be discussed later, this equivalence is generally lost in extended theories of gravity, where higher-order or non-minimal curvature terms are present. Setting the total variation $\delta S = 0$ for arbitrary $\delta g^{\mu\nu}$ and incorporating the matter variation from the second term of (1.8) giving the stress-energy tensor

$$T_{\mu\nu} \equiv \frac{-2}{\sqrt{-g}} \frac{\delta(\sqrt{-g}\,\mathcal{L}_M)}{\delta g^{\mu\nu}}, \tag{1.10}$$

via

$$\delta S_M = -\frac{1}{2} \int d^4x \sqrt{-g}\,T_{\mu\nu}\,\delta g^{\mu\nu}, \tag{1.11}$$

we obtain

$$G_{\mu\nu} = R_{\mu\nu} - \frac{1}{2}g_{\mu\nu}R = 8\pi G\,T_{\mu\nu} - \Lambda g_{\mu\nu}, \tag{1.12}$$

where $G_{\mu\nu}$ is the so-called Einstein tensor and the term $\Lambda g_{\mu\nu}$ in (1.12) acts as a uniform energy density filling space. The left-hand side of Einstein's equation (1.12), related to the spacetime geometry, is directly connected with the matter content of spacetime, in the form of matter or a cosmological constant. Originally, the cosmological constant Λ was introduced to explain a static Universe, by balancing gravity's effects, and to

keep the Universe from contracting; but it was later discarded after the discovery of the Universe's expansion by Edwin Hubble. Decades later, the concept resurfaced as a key ingredient in explaining the accelerated expansion of the Universe: observations clearly point to the presence of an "energy" in the Universe that behaves like a cosmological constant. This is why Λ is usually included in the action (1.8). Furthermore, in (1.12), the term $\Lambda g_{\mu\nu}$ is the only relevant operator at low energies (and it is clearly covariant). This is because, at low energies, the physics is dominated by operators with dimension ≤ 4 in $4D$ spacetime, as operators with higher dimensions are suppressed by powers of the cutoff scale [41]. Moreover, as the metric $g_{\mu\nu}$ is covariant and satisfies $\nabla^\mu g_{\mu\nu} = 0$, the Einstein tensor (1.12) satisfies the contracted Bianchi identities $\nabla^\mu G_{\mu\nu} = 0$. As a result, the conservation of the energy-momentum tensor

$$\nabla^\mu T_{\mu\nu} = 0, \tag{1.13}$$

is automatically ensured by the Einstein field equations and is fully compatible with the presence of a cosmological constant in (1.8). The component $\nu = 0$ corresponds to energy conservation, while the remaining spatial components express momentum conservation.

1.2 Beyond General Relativity

Modified gravity theories, often referred to as Extended Theories of Gravity (ETGs), emerge from the need to extend or modify Einstein's General Relativity to address both its theoretical and observational shortcomings [42, 43]. In the standard formulation of GR, the gravitational dynamics is governed by the Einstein-Hilbert action, which is linear in the Ricci scalar R. Although this description has been extremely powerful in modelling Solar System gravitational phenomena and in other situations where weak gravitational forces are at play [44, 45], this paradigm faces difficulty in handling extremely high-energy contexts – where quantum effects are expected to apply [19, 46–49] – and to the largest cosmological scales, where phenomena such as dark energy and dark matter dominate [50].

To overcome these limitations, modified gravity theories suggest adding to the gravitational Lagrangian extra terms, like higher-order curvature invariants (*e.g.* $f(R)$ models), non-minimal couplings with matter, and extra degrees of freedom in the form of scalar or tensor fields [43, 51, 52]. These modifications are not arbitrary; they are tightly constrained by symmetry principles inherited from the gauge-theoretical formulation of gravity. By ensuring that any added terms respect the fundamental symmetries – such as diffeomorphism invariance – these theories maintain the successful predictions of GR

in the appropriate limits while offering new mechanisms to explain cosmic acceleration without resorting to unknown forms of energy.

In the ultraviolet (UV) regime, such modifications aim to address the issues of quantising gravity by providing a renormalisable or effective framework that could capture quantum corrections. Conversely, in the infrared (IR) domain, they may offer alternative explanations for astrophysical observations – such as flat galaxy rotation curves – by effectively altering the gravitational force at large distances. For instance, the inclusion of higher-order terms in the gravitational action can lead to Yukawa-like corrections in the weak-field limit, thereby modifying Newtonian dynamics without the need for additional exotic matter components [15, 53, 54].

Overall, modified gravity theories represent a versatile framework that not only preserves the empirical successes of GR but also opens new avenues for exploring the interface between classical gravitational physics and quantum phenomena. This approach is pivotal in addressing some of the most pressing questions in contemporary cosmology and high-energy physics, ultimately seeking a more complete and unified understanding of gravity across all scales.

1.2.1 Modified gravity

As previously discussed, one of Einstein's straightforward modifications to GR was the inclusion of a cosmological constant. While conceptually appealing, this change still reveals discrepancies between theoretical predictions and observations [8, 55]. One of the simplest ways to generalise the Einstein-Hilbert action is replacing R with a more general function $f(R)$, so that the action becomes

$$S = \frac{M_P^2}{2} \int d^4x \, \sqrt{-g} \, f(R) + S_M, \tag{1.14}$$

with S_M denoting the matter action. This is sufficiently general to encapsulate some of the basic characteristics of higher-order gravity, but at the same time, these functions are simple enough to allow for straightforward analysis. Many different $f(R)$ models have been explored (see *e.g.* [51, 52, 56–59]), however, since GR has been extensively tested and confirmed on local scales, it follows that $f(R)$ reduces to R within the solar system at the present day [60].

Variation of (1.14) leads to the following fields equation for the metric, resulting in a change in the Einstein tensor

$$f'(R)R_{\mu\nu} - \frac{1}{2}f(R)g_{\mu\nu} - \nabla_\mu\nabla_\nu f'(R) + g_{\mu\nu}\Box f'(R) = \kappa T_{\mu\nu}, \tag{1.15}$$

where $\kappa \equiv M_P^{-2}$ and $f'(R) \equiv df/dR$. According to (1.15), the metric satisfies a system of fourth-order partial differential equations and the modification of the action results in an additional scalar degree of freedom, identified by $f'(R)$. In standard GR, $f'(R)$ reduces to 1 and the additional degree of freedom vanishes. By rewriting (1.15) in the form

$$R_{\mu\nu} - \frac{1}{2}g_{\mu\nu}R = \frac{\kappa}{f'(R)}T_{\mu\nu} - \frac{g_{\mu\nu}}{2f'(R)}[Rf'(R) - f(R)] + \frac{1}{f'(R)}[\nabla_\mu\nabla_\nu f'(R) - g_{\mu\nu}\Box f'(R)], \tag{1.16}$$

it becomes evident that the right-hand side acts as an effective source for the metric. Besides the matter contribution, the additional terms involving derivatives of $f'(R)$ represent the influence of a new scalar degree of freedom arising from the curvature itself. The scalar curvature satisfies a second-order differential equation,

$$3\Box f'(R) + Rf'(R) - 2f(R) = \kappa T, \tag{1.17}$$

which can be obtained by taking the trace of (1.15). By means of (1.15) and (1.17), both the metric $g_{\mu\nu}$ and the scalar curvature R are dynamical. In GR, the metric is the sole dynamical field, and the matter distribution entirely dictates its behaviour through the field equations (1.12). The scalar curvature R is also determined by the local matter content, but via the algebraic relation $R = -\kappa T$. Hence, the physical interpretation of (1.15) and (1.17) highlights the crucial role of the scalar curvature in the field equations of $f(R)$ theories. However, (1.17) indicates that the true dynamical quantity is $f'(R)$ rather than R itself, indeed, $f'(R)$ is the only term in the field equations that is explicitly influenced by differential operators. We can then define

$$\begin{aligned} \phi &\equiv f'(R), \\ V(\phi) &\equiv \phi R(\phi) - f(R(\phi)), \end{aligned} \tag{1.18}$$

where $R(\phi)$ is obtained by inverting the first relation. This inversion is only possible if $f''(R) \neq 0$, ensuring that ϕ is an independent scalar degree of freedom and that the theory differs from GR. Using these definitions, the field equations can be recast as

$$R_{\mu\nu} - \frac{1}{2}g_{\mu\nu}R = \frac{\kappa}{\phi}T_{\mu\nu} - \frac{1}{2\phi}g_{\mu\nu}V(\phi) + \frac{1}{\phi}[\nabla_\mu\nabla_\nu\phi - g_{\mu\nu}\Box\phi], \tag{1.19}$$

$$3\Box\phi + 2V(\phi) - \phi\frac{dV}{d\phi} = \kappa T. \tag{1.20}$$

This slight change of notation helps to identify (1.19) and (1.20) with the Brans-Dicke

theory with parameter $\omega = 0$ [61]. One can effectively rewrite the action as a scalar-tensor theory defining the *Jordan* frame (JF) as

$$S_J = \frac{M_P^2}{2} \int d^4x\sqrt{-g}[\phi R - V(\phi)] + S_M(g_{\mu\nu}, \psi). \tag{1.21}$$

This formulation is dynamically equivalent to the original $f(R)$ action because substituting the definition (1.18) and eliminating ϕ via its algebraic equation of motion recovers the initial $f(R)$ form. In other words, S_J simply introduces ϕ as an auxiliary field whose dynamics reproduce those encoded in $f(R)$. To remove the non-minimal coupling[1], we consider a conformal rescaling of the metric

$$\tilde{g}_{\mu\nu} = f'(R)g_{\mu\nu} \equiv \phi\, g_{\mu\nu}, \tag{1.22}$$

and the scalar field redefinition $\phi \longrightarrow \tilde{\phi}$ with

$$d\tilde{\phi} = M_P \sqrt{\frac{3}{2}} \frac{d\phi}{\phi}, \tag{1.23}$$

for which we obtain the associated action

$$\begin{aligned} S_E = \int d^4x\sqrt{-\tilde{g}}\left[\frac{M_P^2}{2}\tilde{R} - \frac{1}{2}\tilde{g}^{\mu\nu}\partial_\mu\tilde{\phi}\partial_\nu\tilde{\phi} - e^{-2\sqrt{\frac{2}{3}}\frac{\tilde{\phi}}{M_P}}V(\tilde{\phi})\right] \\ + S_M\left(e^{-\sqrt{\frac{2}{3}}\frac{\tilde{\phi}}{M_P}}\tilde{g}^{\mu\nu}, \psi\right), \end{aligned} \tag{1.24}$$

in the *Einstein* frame (EF). The action (1.24) is now written with the "new" scalar field $\tilde{\phi}$ minimally coupled to the Ricci curvature and has a canonical kinetic energy. For a more general derivation, see Appendix A.

The choice between the JF and EF in scalar-tensor theories remains a topic of debate due to their mathematical equivalence but potential physical inequivalence [62]. A conformal transformation relates the two frames, ensuring that the underlying dynamics are equivalent; however, physical inequivalence may arise once one specifies which metric – $g_{\mu\nu}$ in the JF or $\tilde{g}_{\mu\nu}$ in the EF – defines physical measurements such as lengths, times, and particle trajectories.

In the JF, the gravitational coupling is dynamically determined by the scalar field, leading to a varying effective gravitational constant. While this preserves the standard conservation of energy-momentum and ensures that massive test particles follow geodesics, it complicates analytical treatments and observational constraints. In con-

[1] By non-minimal coupling we mean a scalar degree of freedom (in this case known as ϕ) that interacts with the metric and the curvature scalar.

trast, the EF reformulates the theory to resemble GR with a fixed gravitational coupling, simplifying the equations and making it more manageable. However, this comes at the cost of introducing a non-trivial coupling between the scalar field and matter

$$\tilde{T}_{\mu\nu} = -e^{-\sqrt{\frac{2}{3}}\frac{\tilde{\phi}}{M_P}} T_{\mu\nu}, \tag{1.25}$$

which manifests as a fifth force acting on test particles, thereby violating standard geodesic motion[2]. Furthermore, while massless particles such as photons propagate identically in both frames, the motion of massive bodies differs, making the physical equivalence of the two formulations uncertain. The transformation between frames due to follows (1.22) implies that physical quantities such as masses and distances can be frame-dependent. This directly affects cosmological and astrophysical interpretations, where solar system experiments and cosmic evolution models typically favour the JF due to its closer alignment with GR predictions. While both frames offer valuable insights, the question of which is "physical" ultimately depends on the context: the JF is often preferred for direct experimental comparisons, while the EF is advantageous for theoretical and high-energy considerations.

THE PALATINI FORMALISM. In the Palatini formalism [64], instead of using the standard metric variation of the Einstein-Hilbert action, the Einstein equations are derived by independently varying the action with respect to both the metric and an independent connection. While the action remains formally unchanged, the Riemann and Ricci tensors are now constructed using this independent connection, denoted as $\Gamma^{\lambda}_{\mu\nu}$ (whereas the Levi-Civita connection are denoted by $\{^{\alpha}_{\mu\nu}\}$). Notably, the metric is not required to obtain the Ricci tensor from the Riemann tensor. To distinguish this formulation, the Ricci tensor associated with $\Gamma^{\lambda}_{\mu\nu}$ is denoted as $\mathcal{R}_{\mu\nu}$, and the corresponding Ricci scalar is given by $\mathcal{R} = g^{\mu\nu}\mathcal{R}_{\mu\nu}(\Gamma)$. The key idea behind the Palatini formalism is to treat the connection Γ, which defines the Ricci tensor, as an entity independent of the metric g on the spacetime manifold $\mathcal{M}$, typically assuming it to be torsion-free. When the action depends on functions of curvature invariants, such as $f(\mathcal{R})$, or when it is non-minimally coupled to a scalar field, the Palatini and metric variational principles lead to different field equations, resulting in distinct theories [65, 66]. However, in the standard Hilbert-Einstein theory, the Palatini formulation turns out to be equivalent to the metric approach. This equivalence arises because the field equations for the independent connection ultimately lead to the Levi-Civita connection of the metric g, thereby reducing the theory to the usual

[2] In order to screen the fifth force, the so called chameleon mechanism was introduced, see [63].

metric formulation. The action of Palatini gravity takes the form

$$S_{Pal} = \frac{M_P^2}{2} \int d^4x\sqrt{-g}\, f(\mathcal{R}) + S_M(g_{\mu\nu}, \psi). \tag{1.26}$$

The matter action S_M is assumed to depend solely on the metric and matter fields. This assumption means that the independent affine connection does not enter the matter sector, so that the variation of S_M with respect to the independent connection vanishes. For tensor fields this simply implies a minimal coupling prescription through the Levi-Civita connection of $g_{\mu\nu}$. For spinor fields, however, the situation is different: since they do not transform as tensors under spacetime diffeomorphisms, the Levi-Civita connection cannot act on them. Their coupling to gravity requires a local Lorentz frame, encoded in the tetrad e_a^μ (which maps world indices μ to flat tangent-space indices a), together with the associated spin connection ω_μ^{ab} which defines parallel transport in the local Lorentz frame. Thus the metric alone is insufficient to define a covariant derivative on spinors, making the tetrad formalism indispensable for fermionic matter. This is the standard choice in Palatini $f(R)$ theories: the independent connection becomes compatible with a conformally related metric, as we will show later. Under this assumption, variation of the action yields the field equations

$$f'(\mathcal{R})\mathcal{R}_{(\mu\nu)} - \frac{1}{2}f(\mathcal{R})g_{\mu\nu} = \kappa\, T^M_{\mu\nu}, \tag{1.27}$$

$$\bar{\nabla}_\alpha(\sqrt{-g}\, f'(\mathcal{R})g^{\mu\nu}) = 0, \tag{1.28}$$

denoting by $\mathcal{R}_{(\mu\nu)}$ the symmetrical part of $\mathcal{R}_{\mu\nu}$ and $\bar{\nabla}$ the covariant derivative built from the independent connections. (1.27) and (1.28) are obtained by varying with respect to the metric and the connection, respectively. For detailed calculations see [67, 68]. This assumption plays a crucial role in deriving Einstein's equations from the linear form of the action (1.26) and is a defining feature of the Palatini formalism. Indeed, we are implicitly assuming that parallel transport is determined by the Levi-Civita connection of the metric $\{^\alpha_{\mu\nu}\}$ introduced in (1.5), rather than the independent connection $\Gamma^\lambda_{\mu\nu}$. It is straightforward to show that the connection components

$$\Gamma^\lambda_{\mu\nu} = \{^\lambda_{\mu\nu}\} + \frac{1}{2f'}[2\delta^\lambda_{(\mu}\partial_{\nu)}f' - g_{\mu\nu}g^{\lambda\sigma}\partial_\sigma f'], \tag{1.29}$$

are the Christoffel symbols of the auxiliary metric $h_{\mu\nu}$ mentioned in what follows. In this setting, the metric g determines the causal structure of spacetime, whereas the connection Γ governs the trajectories of particles moving within it. We stress that, by means of the trace of (1.27), $\mathcal{R} = \mathcal{R}(T)$ and $f'(\mathcal{R}) = f'(T)$. More in detail, the connection Γ

is compatible with the conformal metric $h_{\mu\nu} = f'(\mathcal{R})\, g_{\mu\nu}$ in order to satisfy (1.28), so $\mathcal{R}_{\mu\nu}(\Gamma) = R_{\mu\nu}(h)$ and thus $\mathcal{R}(h) = h^{\mu\nu}\mathcal{R}_{\mu\nu}(\Gamma) = \frac{1}{f'(\mathcal{R})} g^{\mu\nu}\mathcal{R}_{\mu\nu}(\Gamma) = \frac{\mathcal{R}}{f'(\mathcal{R})}$. Hence, we can rewrite (1.27) as

$$G_{\mu\nu}(h) = \frac{\kappa}{f'(T)} T_{\mu\nu} - \Lambda(T) h_{\mu\nu}, \tag{1.30}$$

where $\Lambda(T) \equiv (\mathcal{R}\, f' - f)/(2f'^2) = (f + \kappa\, T)/(2f'^2)$ and we dropped the dependence of T in the notation. If one chooses to ignore the original physical motivations behind the construction of the theory in the JF and instead interprets the EF metric $h_{\mu\nu}$ as the physical metric defining the geodesics of free particles (thereby redefining the physical observables), then (1.30) can be viewed as describing a theory with a density-dependent effective Newton constant and a varying cosmological constant $\Lambda(T)$ [69–76].

The Palatini action (1.26) can be rewritten in the scalar-tensor representation making use of the relation

$$\mathcal{R} = R + \frac{3}{2f'^2}(\nabla_\mu f'\, \nabla^\mu f') + \frac{3}{f'}\Box f' \tag{1.31}$$

as

$$S_J = \frac{M_P^2}{2}\int d^4x\sqrt{-g}\left(\phi R + \frac{3}{2\phi}\partial_\mu\phi\partial^\mu\phi - V(\phi)\right) + S_M(g_{\mu\nu}, \psi). \tag{1.32}$$

The above is identified as the action of a Brans-Dicke theory with parameter $\omega_0 = -3/2$, in the presence of a field potential [61, 77]. Consequently, in the EF it is recast as

$$S_E = \int d^4x\sqrt{-\tilde{g}}\left(\frac{M_P^2}{2}\tilde{R} - U(\phi)\right) + S_M(\phi^{-1}\tilde{g}_{\mu\nu}, \psi), \tag{1.33}$$

where $U(\phi) = M_{\rm P}^2 V(\phi)/(2\phi)$. Note that in this setting, there is no redefinition for the scalar.

Despite offering an alternative variational principle, the Palatini formulation of $f(R)$ gravity exhibits several notable shortcomings that challenge its viability as a modified theory of gravity. One key issue is the nontrivial coupling between matter and geometry, which arises because the independent connection depends explicitly on the matter content through the trace of the energy-momentum tensor. This leads to problematic consequences, such as the breakdown of the equivalence principle. The Palatini approach also struggles to reproduce the correct Newtonian and post-Newtonian limits in the presence of non-relativistic matter, raising compatibility concerns with solar system tests. Furthermore, in this formulation there are no propagating fields (see (1.27)) as opposed to the metric formalism (see (1.17)), this does not necessarily result in a more consistent theory as the screening mechanism is not required to screen forces that are not observed (see footnote 2). The resulting field equations are nonlinear in the matter sector, leading to technical and conceptual difficulties such as curvature singularities in

compact stars [78, 79] – features that are not present in the metric formulation and are generally regarded as unphysical. Taken together, these limitations suggest that, despite its theoretical appeal, the Palatini formulation faces significant obstacles that must be addressed for it to serve as a viable framework for modified gravity.

THE HYBRID METRIC-PALATINI FORMALISM. A promising development is the hybrid metric-Palatini gravity, which combines features of both formalisms by adding a Palatini $f(R)$ term to the Einstein-Hilbert action [54, 80–84]. This theory overcomes many of the difficulties of previous models while remaining consistent with cosmological, galactic, and local gravitational tests [85–87]. Notably, in its scalar-tensor formulation, it includes a light, long-range scalar field that modifies large-scale dynamics without affecting solar system behaviour. Perturbative analyses also indicate that this model is free from instabilities [88]. An extension of this framework, known as generalised hybrid metric-Palatini gravity, was proposed in [81]. In this model, the action depends on both the metric and Palatini curvature scalars. This generalisation preserves the beneficial features of the original hybrid theory [89, 90], and further investigations have shown the existence of stable static cosmological solutions [91], compatibility with large-scale structure observations [92], and a well-posed initial value problem under general conditions [93].

The generalised hybrid metric-Palatini gravity is described by the action

$$S = \frac{M_{\rm P}^2}{2}\int d^4x\sqrt{-g}f(R,\mathcal{R}) + S_M(g_{\mu\nu},\psi). \tag{1.34}$$

Varying the action with respect to the metric and the independent connection, we obtain the field equations

$$\begin{aligned} f'(R)R_{\mu\nu} + f'(\mathcal{R})\mathcal{R}_{\mu\nu} - \frac{1}{2}g_{\mu\nu}f(R,\mathcal{R}) - (\nabla_\mu\nabla_\nu - g_{\mu\nu}\Box)f'(R) = \kappa T_{\mu\nu}, \\ \bar{\nabla}_\alpha(\sqrt{-g}\, f'(\mathcal{R})g^{\mu\nu}) = 0. \end{aligned} \tag{1.35}$$

The second equation implies, again, that $\bar{\Gamma}^\lambda_{\mu\nu}$ is the Levi-Civita connection of a conformally related metric $h_{\mu\nu} = f'(\mathcal{R})g_{\mu\nu}$.

To facilitate the analysis, we reformulate the theory in a scalar-tensor form by introducing auxiliary fields α and β, leading to the action

$$S = \frac{M_{\rm P}^2}{2}\int d^4x\sqrt{-g}[f(\alpha,\beta) + f_\alpha(R-\alpha) + f_\beta(\mathcal{R}-\beta)] + S_M(\psi,g_{\mu\nu}), \tag{1.36}$$

where $f_\alpha = \partial f/\partial\alpha$ and $f_\beta = \partial f/\partial\beta$. Defining scalar fields $\phi \equiv f_\alpha$ and $\chi \equiv f_\beta$, and

introducing the potential

$$V(\phi, \chi) = -f(\alpha, \beta) + \phi\alpha + \chi\beta, \tag{1.37}$$

we can invert the relations $\phi \equiv f_\alpha$ and $\chi \equiv f_\beta$ to express α and β in terms of ϕ and χ, provided that the Hessian of $f(\alpha, \beta)$ is non-degenerate:

$$\det \begin{pmatrix} f_{\alpha\alpha} & f_{\alpha\beta} \\ f_{\beta\alpha} & f_{\beta\beta} \end{pmatrix} \neq 0$$

This guarantees that the Legendre-type transform is well defined, and the action can be rewritten without explicit dependence on α and β as

$$S = \frac{M_P^2}{2} \int d^4x\sqrt{-g}[\phi R + \chi\mathcal{R} - V(\phi, \chi)] + S_M(\psi, g_{\mu\nu}). \tag{1.38}$$

It is important to emphasise that, in this representation, the scalar fields do not correspond to actual matter fields, but rather serve as alternative representations of the curvature terms R and $\mathcal{R}$. Furthermore, since we have chosen the signs in the definitions of the scalar fields to ensure positive kinetic energies, there is no need to be concerned about ghost instabilities. Then, by means of $h_{\mu\nu} = \chi g_{\mu\nu}$, the Palatini scalar (1.31) can be rewritten as

$$\mathcal{R} = R + \frac{3}{\chi^2}\partial^\mu\chi\partial_\mu\chi - \frac{3}{\chi}\Box\chi, \tag{1.39}$$

and the above can be replaced in the action

$$S = \frac{M_P^2}{2} \int d^4x\sqrt{-g}\left[(\phi + \chi)R - \frac{3}{2\chi}\partial^\mu\chi\partial_\mu\chi - V(\phi, \chi)\right] + S_M(\psi, g_{\mu\nu}). \tag{1.40}$$

One can define a new scalar field $\xi = \phi + \chi$ in order to simplify the analysis. Thus, (1.40) can be rearranged as

$$S = \frac{M_P^2}{2} \int d^4x\sqrt{-g}\left[\xi R - \frac{3}{2\chi}\partial^\mu\chi\partial_\mu\chi - V(\xi - \chi, \chi)\right] + S_M(\psi, g_{\mu\nu}), \tag{1.41}$$

where only the scalar field ξ is coupled to the metric Ricci scalar. By varying (1.41) with respect to the metric, we obtain

$$R_{\mu\nu} - \frac{1}{2}g_{\mu\nu}R - \frac{1}{\xi}\left(\nabla_\mu\nabla_\nu\xi - g_{\mu\nu}\Box\xi\right) + \frac{3}{2\xi\chi}\partial_\mu\chi\,\partial_\nu\chi - \frac{1}{2}g_{\mu\nu}\left(\frac{3}{2\chi}\,\partial_\rho\chi\,\partial^\rho\chi - W(\xi, \chi)\right) = \frac{\kappa}{\xi}T_{\mu\nu}, \tag{1.42}$$

where $W(\xi,\chi) = V(\xi-\chi,\chi)$, while the equations for ξ and χ are given by

$$R = \frac{\partial W(\xi,\chi)}{\partial \xi}, \tag{1.43}$$

$$\frac{3}{2\chi^2}\partial_\mu\chi\partial^\mu\chi - \frac{3\Box\chi}{\chi} - \frac{\partial W(\xi,\chi)}{\partial\chi} = 0. \tag{1.44}$$

By taking the trace of (1.42), resulting in

$$R = \frac{3\Box\phi}{\phi} - \frac{3}{2\xi\phi}\partial_\mu\xi\,\partial^\mu\xi + \frac{2W}{\phi} - \frac{\kappa T}{\phi}, \tag{1.45}$$

and plugging it into (1.43) and (1.44), we obtain a set of coupled differential equations

$$\begin{aligned} \Box\xi + \frac{1}{2\chi}\partial_\mu\chi\partial^\mu\chi + \frac{2W(\xi,\chi) - \xi W_\xi}{3} &= \frac{\kappa}{3}T, \\ \Box\chi - \frac{1}{2\chi}\partial^\mu\chi\partial_\mu\chi - \frac{\chi}{3}W_\chi &= 0, \end{aligned} \tag{1.46}$$

where $W_\xi \equiv \partial W/\partial\xi$, $W_\chi \equiv \partial W/\partial\chi$. Note that ξ is coupled to matter while χ is not[3]. This distinction has significant implications for the resulting cosmological dynamics.

NON-LOCAL GRAVITY. We now summarize the key aspects of non-local gravity theories. Unlike their local counterparts, these models incorporate non-local operators into the effective action to bridge gravity and quantum theory.

Depending on the form of the non-locality, such theories fall into two main families: *Infinite Derivative Theories of Gravity* (IDGs) and *Integral Kernel Theories of Gravity* (IKGs). IDGs employ analytic transcendental functions of the covariant d'Alembertian operator $\Box$. For example, the model of [94] resolves classical black-hole and Big Bang singularities [49]. By contrast, IKGs rely primarily on the inverse operator $\Box^{-1}$. First studied in [19], it was shown that applying $\Box^{-1}$ to the scalar curvature R naturally drives the late-time acceleration of the universe without invoking dark energy. In their quest to unify gravity with the other fundamental interactions, IDGs provide a renormalisable and unitary framework for quantum gravity [48], while IKGs address infrared quantum corrections arising from quantum field theory in curved spacetime [95]. Despite these attractive features, no existing local or non-local theory has yet succeeded in resolving all large-scale structure challenges while remaining fully compatible with current observations.

[3] In this context, although the transformation $\xi = \phi + \chi$ may appear to artificially link the variables ξ and χ, it in fact preserves the full dynamical content of the theory. This can be further confirmed by deriving the equations of motion for the original fields directly from equation (1.40), for more details see [54].

Here, we focus in IKGs as we are interested in investigating cosmology. The inverse d'Alembertian operator acts on curvature invariants [96], such as the Ricci scalar R. Among the simplest models there is

$$\mathcal{L} = \sqrt{-g}[f_1(R) + f_2(\Box^{-1}R, \Box^{-2}R, .., \Box^{-n}R)], \tag{1.47}$$

where n is a positive integer. To make these non-local models analytically tractable, the theory is treated in a local form by introducing auxiliary scalar fields – such as U_i and Lagrange multipliers λ_i – which effectively encode the action of the inverse d'Alembertian operator. This reformulation allows for the application of standard techniques in classical and quantum field theory. However, a key aspect of this theory is the identification of propagating degrees of freedom and the detection of ghost fields – degrees of freedom with negative kinetic energy – which signal a pathological instability in the theory [96]. The starting point is the non-local action (1.47). To localise it, the Lagrange multipliers λ_i and auxiliary fields U_i are introduced, which leads to

$$\begin{aligned} S = \int d^4x\sqrt{-g}\Big[& f_1(\sigma) + \frac{\partial f_1}{\partial \sigma}(R-\sigma) + f_2(U_1, ..., U_n) \\ & + \lambda_1(R - \Box U_1) + \lambda_2(U_1 - \Box U_2) + ... + \lambda_n(U_{n-1} - \Box U_n)\Big], \end{aligned} \tag{1.48}$$

where we assume $\partial^2 f_1/\partial\sigma^2 \neq 0$ in order to be on shell and $\partial f_2/\partial U_n \neq 0$. The term f_2 by itself does not introduce ghosts, provided the background theory (set by f_1) is stable

$$\frac{\partial f_1}{\partial R} > 0 \quad \rightarrow \quad \frac{\partial f_1}{\partial \sigma} > 0. \tag{1.49}$$

The action (1.48) can be rewritten in the form

$$S = \int d^4x\,\sqrt{-g}\left[\left(\lambda_1 + \frac{\partial f_2}{\partial \sigma}\right)R + f_1 + f_2 - \frac{\partial f_2}{\partial \sigma}\,\sigma - \lambda_1\Box U_1 + \sum_{i=2}^{n}\lambda_i\,(U_{i-1} - \Box U_i)\right], \tag{1.50}$$

in which $M_P^2 = 1$. Since each U_i depends on R and $R = \sigma$ on-shell, it follows that $f_2(U_1, \ldots, U_n) = f_2\big(U_1(\sigma), \ldots, U_n(\sigma)\big)$. Therefore, f_2 acquires an implicit dependence on σ through the auxiliary fields U_i. We define

$$\Phi = \lambda_1 + \frac{\partial f_2}{\partial \sigma}, \tag{1.51}$$

and we use the invertibility $\sigma = \sigma(\Phi, \lambda_1)$, to rewrite the action as

$$S = \int d^4x \sqrt{-g}\Big[\Phi R + \sum_{i=1}^{n} \nabla^\alpha \lambda_i \nabla_\alpha U_i + f_1 + f_2\big(\sigma(\Phi,\lambda_1)\big) - (\Phi - \lambda_1)\,\sigma(\Phi,\lambda_1) + \sum_{i=2}^{n} \lambda_i U_{i-1}\Big]. \tag{1.52}$$

Under a conformal transformation $g_{\mu\nu} \to \bar{g}_{\mu\nu} = \Phi\, g_{\mu\nu}$, one finds

$$S = \int d^4x \sqrt{-\bar{g}}\left[\frac{1}{2}\bar{R} - \frac{3}{4\Phi^2}\bar{g}^{\alpha\beta}\partial_\alpha\Phi\,\partial_\beta\Phi + \frac{1}{2\Phi}\sum_{i=1}^{n}\bar{g}^{\alpha\beta}\partial_\alpha\lambda_i\,\partial_\beta U_i - V(\Phi,\{\lambda_i,U_i\})\right], \tag{1.53}$$

where the potential is

$$V = \frac{1}{4\Phi^2}\Big[(\Phi - \lambda_1)\,\sigma(\Phi,\lambda_1) - f_1 - f_2 - \sum_{i=2}^{n}\lambda_i U_{i-1}\Big]. \tag{1.54}$$

Finally, we perform a field redefinitions

$$\Phi = M_{\rm P}\, q_1, \tag{1.55}$$

$$U_j = \frac{q_{j+1}}{M_{\rm P}^{2j-1}} \quad (j = 1,\dots,n), \tag{1.56}$$

$$\lambda_j = M_{\rm P}^{2j-1}\, q_{n+1+j} \quad (j = 1,\dots,n), \tag{1.57}$$

and the action takes the canonical form

$$S = \int d^4x \sqrt{-\bar{g}}\left[\frac{1}{2}\bar{R} - \frac{3}{4q_1^2}\bar{g}^{\alpha\beta}\partial_\alpha q_1\,\partial_\beta q_1 + \frac{1}{2q_1}\sum_{j=1}^{n}\bar{g}^{\alpha\beta}\partial_\alpha q_{n+1+j}\,\partial_\beta q_{j+1} - V(q_1,\dots,q_{2n+1})\right], \tag{1.58}$$

or equivalently, in the EF

$$\mathcal{S}_{EF} = \int d^4x \sqrt{-\bar{g}}\Big[\frac{1}{2}\bar{R} - \frac{1}{2}\bar{g}^{\alpha\beta}G^{kl}\,\partial_\alpha q_k\,\partial_\beta q_l - V(q)\Big], \tag{1.59}$$

with the indices $(k,l) = \{1,...,2n+1\}$. The only nonzero components of the symmetric field-space metric G^{kl} are

$$G^{11} = \frac{3}{2\,q_1^2}, \qquad G^{\,j+1,\,j+1+n} = -\frac{1}{2\,q_1}, \quad j = 1,\dots,n. \tag{1.60}$$

At this stage, we perform the final field redefinition

$$q_1 = Q_1, \quad q_{j+1} = Q_{2j} - \frac{Q_{2j+1}}{2}, \quad q_{j+1+n} = Q_{2j} + \frac{Q_{2j+1}}{2}, \quad j = 1, \dots, n. \tag{1.61}$$

In the new $\{Q\}$ basis, the kinetic matrix diagonalises with

$$\widehat{G}^{11} = \frac{3}{2\,q_1^2}, \quad \widehat{G}^{2j,2j} = -\frac{1}{q_1}, \quad \widehat{G}^{2j+1,2j+1} = \frac{1}{4\,q_1}, \quad j = 1, \dots, n. \tag{1.62}$$

Therefore, independently of the sign of q_1, the theory always contains n ghost modes. The only known exception is the particularly simple coupling model

$$\mathcal{L} = \sqrt{-g}\, R(\Box^{-1} R), \tag{1.63}$$

which can be rendered ghost-free under the condition

$$\frac{6}{q_1} f'(\Box^{-1} R) > 1, \tag{1.64}$$

where q_1 is a field-dependent quantity [96]. In Chapter 6, we will further investigate (1.47) and (1.63) within the hybrid metric-Palatini formalism, studying the implications for cosmology.

1.2.2 Scale-invariant gravity

Dilatation symmetry, often referred to as scale invariance, is the invariance of a system under rescaling of spacetime coordinates and fields such that the action remains unchanged. Under this *global* spacetime rescaling[4], spacetime coordinates transform as

$$x^\mu \longrightarrow \bar{x}^\mu = e^{-\omega}\, x^\mu, \tag{1.65}$$

where ω is a spacetime-independent parameter. In particular, the primary focus will be on scaling dimension (or weight), which is the power of the rescaling factor. Indeed, the desirable property is to have a field that transforms as

$$\bar{\phi}(\bar{x}) \equiv e^{\Delta\omega}\, \phi(x) = e^{\Delta\omega}\, \phi(e^{\omega}\bar{x}), \tag{1.66}$$

[4] The term global it is sometimes referred to as rigid and indicates that the scaling factor is a constant (as opposed to a local or position-dependent Weyl/conformal transformation where ω would be replaced by a function $\Omega(x)$).

where Δ is the scaling weight. The inverse scaling factor e^{ω} appears in the argument because we place ourselves at $\bar{x}$ and then ask what the field configuration was at the point we originated from – that is, the point obtained by applying the inverse transformation to $\bar{x}$, an *active* transformation in which the field is truly shifted. In four-dimensional spacetime, classically invariant models are formulated under such transformations providing that each term in the action has a scaling weight of four. Since $d^4x \to e^{-4\omega}d^4x$ and $\sqrt{-\bar{g}} = \sqrt{-g}$ due to $\bar{g}_{\mu\nu}(\bar{x}) = g_{\mu\nu}(e^{\omega}\bar{x})$, employing (1.66)

$$\mathcal{L}_{\text{kin}} \to \frac{e^{(2\Delta+2)\omega}}{2}\,\partial_\mu\phi\partial^\mu\phi, \tag{1.67}$$

we obtain $\Delta = 1$. Focusing on the gravitational sector, note that the Christoffel symbols and Ricci tensor transform under

$$\begin{aligned}\Gamma^{\rho}_{\mu\nu}(x) &\to e^{\omega}\,\Gamma^{\rho}_{\mu\nu}(e^{\omega}\bar{x}),\\ R_{\mu\nu}(x) &\to e^{2\omega}R_{\mu\nu}(e^{\omega}\bar{x}).\end{aligned} \tag{1.68}$$

This scaling behaviour results in an action that remains invariant [97], given by

$$S = \int d^4x\sqrt{-g}\left(\frac{\xi}{6}\,\phi^2 R + \frac{\alpha}{36}\,R^2 - \frac{1}{2}\partial_\mu\phi\partial^\mu\phi - \frac{\lambda}{4}\phi^4\right), \tag{1.69}$$

where a non-minimally coupled scalar field with quartic potential is considered to preserve the scale-invariance of the action. In this formulation, α, ξ and λ are positive, dimensionless parameters that can be constrained by comparison with data.

Another approach to discuss scaling is to keep the spacetime point fixed[5] but introduce a rescaling of the spacetime metric tensor as $\bar{g}_{\mu\nu}(x) = e^{2\beta}g_{\mu\nu}(x)$ and the field transforms as $\bar{\Phi}(x) = e^{-\beta}\,\Phi(x)$, where β is the scaling factor (different in general from ω). The invariance of the action (1.69) is still satisfied. Indeed, in a fully diffeomorphism-invariant theory, the absence of dimensionful parameters in the action implies that the theory has a global scale symmetry, then a spacetime dilatation is equivalent to an internal scaling, in the sense that they can not be physically discriminated because the two classes of transformations act indistinguishably on the space of solutions. On the other hand, in a theory that is invariant only under a restricted class of diffeomorphis, *e.g.* in Unimodular gravity [98–101], the absence of dimensional parameters will guarantee only invariance under dilatation. Clearly, performing both transformations (which we call product symmetry) with the specific choice of $e^{\omega} = e^{\beta}$, leaves again the action

[5] An *internal* transformation is a change of the fields themselves at fixed spacetime points, without modifying the coordinates.

unchanged. This two-parameter structure forms an Abelian group[6]. The theory can be seen as a special case of scalar-tensor theory in the JF.

This class of theories goes beyond mathematical elegance: scale-invariant gravity offers a compelling framework to address fundamental open questions in modern physics and cosmology. Several features make it particularly attractive:

- One of the long-standing puzzles in theoretical physics is the origin of *fundamental mass scales*, such as the Planck scale or the electroweak scale. In scale-invariant theories, all such scales are absent at the classical level and emerge dynamically, typically through spontaneous or quantum breaking of scale invariance. This provides a natural mechanism for scale generation, circumventing the need for inputting mass parameters by hand.

- The inclusion of dimensionless couplings avoids the introduction of new mass scales in the theory, which is crucial as it prevents the imposition of a "natural" cutoff, such as the Planck scale, from the very beginning. The higher-derivative terms (*e.g.* R^2) add extra terms to the equations of motion for the gravitational field. These terms modify the behaviour of gravity at very high energies and can improve the way gravity behaves in the UV limit, especially when embedded in more general frameworks like asymptotically safe gravity[7] or conformal extensions[8]. This opens pathways toward constructing a renormalisable or even UV-complete gravitational theory without requiring full string theory machinery.

- Because all couplings are dimensionless, the theory is predictive. The parameters ξ, α, λ can be directly constrained using cosmological observables.

We will delve deeper into the connection between scale-invariant gravity and cosmology in Chapter 5.

[6] An Abelian group is a mathematical structure where elements can be combined using an operation (*e.g.* addition or composition), and the result doesn't depend on the order in which they are combined.

[7] In this framework, gravity becomes well-defined (renormalisable) at very high energies. It suggests that the gravitational theory can be made finite at high energies, preventing the usual problems of infinities, by fine-tuning the couplings [102, 103].

[8] Conformal extensions refer to theories where gravity may be coupled to other fields in a way that respects conformal symmetry, allowing the theory to remain consistent and finite at high energies.

2 | Structure and dynamics of the isotropic Universe

The modern understanding of the Universe on the largest scales is built on the principles of homogeneity and isotropy, which are encapsulated in the cosmological principle. These symmetries form the foundation of the Friedmann-Lemaître-Robertson-Walker (FLRW) metric, a solution to Einstein's field equations that describes a spatially homogeneous and isotropic expanding (or contracting) universe.

This chapter introduces the mathematical and physical framework used to model the large-scale dynamics of the Universe under the assumption of isotropy and homogeneity. We begin by constructing the FLRW metric in Section 2.1 and reviewing its key geometrical features, including the classification of spatial curvature. We then go through the Einstein field equations and show how they lead to the Friedmann equations in Section 2.2, which govern the expansion rate as a function of the matter and energy content of the cosmos. In Section 2.3, we explore the behavior of different components of the ΛCDM model – such as radiation, matter, and vacuum energy – and how their relative densities evolve with cosmic expansion. Special attention is given to the roles of the Hubble parameter and the scale factor, which together characterise the Universe's expansion history.

2.1 The Robertson-Walker geometry

In this section, we explore the properties of a homogeneous and isotropic universe, whose spatial geometry is described by a maximally symmetric 3D space[1]. Our goal is to extract cosmological insights directly from the structure of the spacetime metric without relying on Einstein's field equations. In particular, we focus on characterising particle motion against an expanding background to establish its kinematic properties and to shed light on certain phenomenological aspects of the observed Universe. Specifically, we examine the motion of nearby galaxies (*i.e.* the Hubble law).

[1] Which was studied long before by Gauss, Lobachevsky, and Riemann.

In cosmology, the spacial geometry of such a universe is conventionally represented by the Robertson-Walker (RW) line element.

2.1.1 Kinematics of the isotropic Universe

Even though our observable Universe is full of highly inhomogeneous structures such as stars, galaxies and galaxy clusters, the fundamental assumption of modern cosmology is that it can be considered homogeneous and isotropic when viewed on sufficiently large scales.

It is well established that any spatially homogeneous and isotropic spacetime that evolves over time can be decomposed into space-like slices [104, 105]. Consequently, we can represent our spacetime as a manifold $\mathcal{M} = \mathbb{R} \times \Sigma$ where $\mathbb{R}$ denotes the time direction and Σ is a three-dimensional, homogeneous, and isotropic hypersurface. By choosing a foliation where the time threading is orthogonal to these slices, the metric satisfies $g_{0i} = 0$[2]. Furthermore, due to the homogeneity of spacetime, the time intervals between the slices are the same everywhere. As a result, we can choose a universal time coordinate t such that $g_{00} = -1$. These coordinates are known as *comoving coordinates*. Notice that only a comoving observer (*i.e.* one at rest in these coordinates) perceives the Universe as isotropic; any observer moving relative to these coordinates will detect anisotropies – for instance, via the Doppler effect – since a non-zero velocity introduces a preferred direction, breaking rotational symmetry.

The metric can be written as

$$ds^2 = -dt^2 + a^2(t) dl^2_{\mathrm{RW}}, \tag{2.1}$$

where the time-dependent dimensionless function $a(t)$ is called the scale factor and dl^2_{RW} denotes the spatial line element of a three-space

$$dl^2_{\mathrm{RW}} = h^{\mathrm{RW}}_{\alpha\beta} dx^\alpha dx^\beta = \frac{dR^2}{1 - KR^2} + R^2(d\theta^2 + \sin^2\theta d\phi^2), \tag{2.2}$$

with $R = a(t)r$ is the physical distance, θ and ϕ being the usual spherical coordinates, $K(t) = k/a^2(t)$ being the time-dependent curvature in terms of the scale factor and a constant k. Thus, one can rewrite [106]

$$ds^2 = -dt^2 + a^2(t)\left[\frac{dr^2}{1 - kr^2} + r^2 d\Omega^2\right], \tag{2.3}$$

[2] If non-zero, the g_{0i} component would fix a preferred direction because it transforms as a three-vector under spatial coordinate transformations.

where $d\Omega^2$ denotes the metric of the unit 2-sphere. This metric is known as the Friedmann-Lemaître-Robertson-Walker metric and shows how the RW geometry forms the spatial part of it. In (2.3), k takes one of the values $\{+1, 0, -1\}$. Depending on the sign of k, we identify three distinct possibilities. When $k > 0$, space has positive curvature, corresponding to a closed universe; if $k = 0$, the space is flat, representing a flat universe; and when $k < 0$, the space is negatively curved, describing an open universe.

In the context of the ADM formalism [107], we can also express the metric in the form

$$ds^2 = -N(t)^2 dt^2 + a^2(t)\left[\frac{dr^2}{1-kr^2} + r^2 d\Omega^2\right], \tag{2.4}$$

where $N(t)$ is the lapse function. This function controls the rate at which time flows between different spatial hypersurfaces (constant-time slices) and dictates how proper time is measured relative to the time coordinate t. Specifically, the lapse function relates the proper time $d\tau$ (1.2) and the coordinate time dt through

$$d\tau = N(t)\, dt. \tag{2.5}$$

If $N(t) = 1$, the proper time matches the coordinate time t[3]. In this gauge, time and space coordinates are treated differently since the scale factor $a(t)$ multiplies only the spatial line element. This becomes particularly important when studying the propagation of light. For this reason, it is convenient to introduce conformal time η defined by

$$d\eta \equiv \frac{dt}{a(t)}, \tag{2.6}$$

where t is the proper (or cosmic) time. When expressed in terms of conformal time, the FLRW metric takes a more symmetric form

$$ds^2 = a^2(\eta)\left[-d\eta^2 + \frac{dr^2}{1-kr^2} + r^2(d\theta^2 + \sin^2\theta d\phi^2)\right], \tag{2.7}$$

where $a(\eta)$ is the scale factor as a function of conformal time (note that this is the same as working in the *conformal* gauge with $N(t) = a(t)$). This formulation is especially useful for analysing causal structures and the behaviour of massless particles like photons.

[3]Here, coordinate time matches also cosmic time as the FLRW coordinates are chosen to follow comoving observers.

2.1.2 Particle motion

This subsection highlights an important aspect of how a particle's momentum evolves as it moves through a FLRW spacetime.

The path of a test particle in an expanding universe follows a geodesic (see (1.6)) determined by the FLRW metric (2.3). To understand the key effects, we focus on the zero component of the geodesic equation

$$\frac{du^0}{ds} + \frac{\dot{a}}{a}u^2 = 0. \tag{2.8}$$

Here, $u^2 = a^2 h^{\mathrm{RW}}_{\alpha\beta} u^\alpha u^\beta$ is the squared magnitude of the particle's spatial velocity. For a massive particle, the 4-velocity satisfies $u^\mu u_\mu = -1$. Then, by substituting it into the FLRW metric we obtain the normalisation condition $(u^0)^2 = u^2 + 1$, leading to the relation $u^0 du^0 = u du$. Hence, (2.8) simplifies to

$$\frac{du}{dt} + \frac{\dot{a}}{a}u = 0, \tag{2.9}$$

where we used $u^0 ds = dt$. This differential equation has a straightforward solution

$$u \propto \frac{1}{a}. \tag{2.10}$$

If the particle has a rest mass m_0, then its momentum is $p = m_0 u$, which also scales inversely with $a(t)$. This behaviour – commonly known as redshifting of momentum – is a direct result of the Universe's expansion. Importantly, this conclusion is independent of the specific choice of affine parameter and thus holds even for massless particles like photons. For photons, this leads to

$$E = p = \frac{2\pi}{\lambda} \propto \frac{1}{a}, \tag{2.11}$$

where E is the energy and λ is the wavelength. Consider a photon emitted at the time t_e and observed at the time t_0, the ratio of their wavelengths satisfies

$$\frac{\lambda_0}{\lambda_e} = \frac{a(t_0)}{a(t_e)} \equiv 1 + z, \tag{2.12}$$

where z denotes the redshift. Since $a(t_0) > a(t_e)$ in an expanding universe, the observed wavelength is longer than the emitted one, confirming the redshift effect. Additionally, comoving distances between observers also scale with the cosmic scale factor, just like photon wavelengths. Therefore, any physical length l_{phys} must be understood as a func-

tion of time via $l_{\text{phys}}(t) = a(t)l$. This time-dependent nature of all physical scales reflects the non-static geometry of an expanding universe.

2.1.3 The Hubble law

In this subsection, we will explain how the recession of galaxies – observed as redshifts – is not due to actual motion through space but is instead a kinematical effect of the expansion of the Universe described by the FLRW geometry.

Galaxies, modelled as free-falling, pressureless particles (*i.e.* dust), remain at fixed comoving coordinates. Their apparent motion arises because the space between them expands. This phenomenon – the Hubble flow – can be captured locally (for nearby galaxies, $z \ll 1$) by the *Hubble law*

$$v = H_0 d, \tag{2.13}$$

where v is the apparent recessional velocity, d the proper distance, and H_0 the Hubble constant. Its derivation involves expressing the scale factor near the present time t_0 as a Taylor expansion

$$a(t) \simeq a_0 + \dot{a}_{t=t_0}(t - t_0) + \dots, \tag{2.14}$$

which, when plugged into the redshift (2.12) gives

$$\frac{a}{a_0} = \frac{1}{1+z} = 1 - H_0(t_0 - t) + .., \tag{2.15}$$

in which the Hubble parameter is defined as $H(t) \equiv \dot{a}/a$, along with its present value, the Hubble constant $H_0 \equiv H(t_0)$. To obtain (2.13) we need to connect the observed redshift to the light travel time of the emitting galaxy. To relate this time interval to the distance, we consider a null geodesic (light path, see (2.3))

$$\int_t^{t_0} \frac{dt}{a(t)} = \int_0^r \frac{dr'}{\sqrt{1 - kr'^2}}, \tag{2.16}$$

that for a flat universe ($k = 0$) results in $t_0 - t = a_0 r$. This result leads to $(t_0 - t) \approx d$, where $d = a_0 r$ is the present distance to the source. We can then write

$$z = H_0 d + \dots, \tag{2.17}$$

where we used the expansion $1/(1+z) \simeq 1 - z$ for $z \ll 1$. By treating the geometric redshift of photons from a galaxy as a Doppler shift caused by a physical velocity v, we recover the familiar form of Hubble law at low redshift (2.13). It may be extended to include higher-order terms in the expansion of the scale factor. However, the extension to

higher-order terms raises subtle issues concerning the definition of distance in cosmology and its determination. Recall that the physical (or proper) distance at cosmic time t[4] between an observer at $r = 0$ and a source at comoving coordinate r is $d(t)_{\rm phys} = a(t)r$. In practice, proper distance is not directly observable. Instead, cosmological distances are typically inferred from *standard candles* – objects of known intrinsic luminosity, such as Supernovae Ia. The luminosity distance d_L relates to the proper distance via

$$d_L = d(1 + z), \tag{2.18}$$

and repeating the steps above, one can find that

$$H_0 d_L = z + \frac{1}{2}(1 + q_0)z^2 + \dots, \tag{2.19}$$

where $q_0 \equiv -\ddot{a}/(a\,H^2)$ at $t = 0$ is the deceleration parameter of the Universe.

THE HUBBLE LENGTH AND THE COSMOLOGICAL HORIZON. Here we introduce two fundamental length scales relevant to cosmology. The Hubble length, defined as

$$L_H(t) \equiv H^{-1}(t) \equiv \frac{a(t)}{\dot{a}(t)}, \tag{2.20}$$

is the characteristic length scale associated with the expansion rate, representing the typical distance over which causal processes can occur in a Hubble time[5] (*i.e.* H^{-1}(t)). The cosmological horizon – or particle horizon – defined as

$$d_H = a(t)\int_0^t \frac{dt'}{a(t')}, \tag{2.21}$$

measures the maximum physical distance that light could have travelled since the beginning of the Universe. The distinction between these two scales is crucial. Indeed, while the Hubble radius defines a sort of causal boundary for local processes, the particle horizon sets the limit on the size of the observable Universe. In particular, this implies that spatial regions which are separated by more than one cosmological horizon cannot be in thermal equilibrium. Also, since comoving distances are constant by definition (*i.e.* $dl_{\rm phys} = a(t)dl_{\rm RW}$), the ratio between the horizon and any given comoving distance decreases as we move backwards in time. In other words, objects that are in causal contact today were not necessarily in causal contact in the past. We anticipate that the horizon

[4] Cosmic time is the proper time measured by comoving observers in an FLRW universe, and it serves as the time coordinate that tracks the expansion of the universe.

[5] In our convention the Hubble time coincides with the Hubble length as $c = 1$.

paradox (explained in Section 2.3) is resolved in the inflationary scenario through an early period of de Sitter expansion, as we will discuss in Chapter 3.

2.2 The FLRW cosmology

2.2.1 Field equations for the homogeneous & isotropic Universe

The evolution of a universe described by the FLRW metric follows from Einstein's field equations. To understand how the Universe changes over time, we must define its matter content, which is represented through the energy-momentum tensor (1.10). For a universe that is homogeneous and isotropic, we will consider as a form for matter that of a *perfect fluid*. The energy-momentum tensor of such a fluid includes only time-dependent pressure P and energy density ρ, ensuring uniformity in space

$$T_{\mu\nu} = (\rho + P)u_\mu u_\nu + P g_{\mu\nu}. \tag{2.22}$$

For an observer moving with the fluid, the 4-velocity simplifies $u_\mu = (-1, 0, 0, 0)$, and the energy-momentum tensor becomes diagonal with components $T^\mu{}_\nu = (-\rho, P, P, P)$. Each fluid can be characterised by an equation of state $w \equiv P/\rho$, where typical values for ordinary matter obey the strong energy condition $w \geq -1/3$ (see [108]). The $\nu = 0$ component of the energy-momentum conservation equation (1.13) leads to the continuity equation

$$\dot{\rho} + 3H\rho(1 + w) = 0, \tag{2.23}$$

where w is the equation of state parameter. Solving this differential equation considering $w = \text{const.}$, gives the evolution of the energy density ρ in terms of the scale factor

$$\rho(t) = \rho(t_0)a(t)^{-3(1+w)}, \tag{2.24}$$

where $\rho(t_0)$ is the present day energy density, and the scale factor is normalised so that $a(t_0) = 1$. This result shows how the energy density of a given component changes as the Universe expands, with the rate of change determined by the value of w.

Let us examine four key types of perfect fluids commonly encountered in cosmology and determine how their energy densities evolve with the scale factor, using (2.24).

Pressureless matter (dust). In this case $w = 0$, meaning the pressure P is zero. The energy density then scales as $\rho_m \propto a^{-3}$, reflecting the fact that, as the Universe expands, the volume increases and matter becomes more diluted. This description applies to ordinary

baryonic matter after recombination[6] as well as to cold dark matter, which interacts primarily through gravity and only very weakly (if at all) via other forces.

Radiation. When the fluid consists of highly relativistic particles, it is characterised by $w = 1/3$. The energy density in this case scales as $\rho_r \propto a^{-4}$. The additional factor of a^{-1} compared to matter, arises from the redshifting of particle energies due to their wave-like nature as the Universe expands, since $E \propto a^{-1}$ (see (2.11)).

Cosmological constant Λ. Here $w = -1$, which violates the strong energy condition typical of ordinary matter. The energy density remains constant, $\rho_\Lambda \propto$ const, meaning that energy is effectively created as the Universe expands – a behaviour fundamentally different from that of matter or radiation.

By substituting the FLRW metric (2.3) into the Einstein field equation (1.12), we obtain

$$\begin{aligned} H^2 \equiv \left(\frac{\dot{a}}{a}\right)^2 &= \frac{\rho}{3M_{\mathrm{P}}^2} - \frac{k}{a^2} + \frac{\Lambda}{3}, \\ \frac{\ddot{a}}{a} &= -\frac{\rho\,(1+3w)}{6M_{\mathrm{P}}^2} + \frac{\Lambda}{3}, \end{aligned} \tag{2.25}$$

for the (tt)-component and (ij)-component respectively. These are referred to as the *Friedmann equations*. However, we will occasionally refer to the latter specifically as the "acceleration equation". The first equation illustrates that the Universe expansion rate is determined by the total energy density, the spatial curvature, and the cosmological constant. When both $\Lambda = 0$ and $k = 0$, the presence of matter alone is enough to drive expansion, *i.e.* $(\dot{a}/a > 0)$. Meanwhile, the second equation shows that if $\Lambda = 0$, ordinary matter that satisfies the strong energy condition leads to a decelerating expansion, meaning $\ddot{a} < 0$.

The total energy content of the Universe is made up of a mix of the different fluid components discussed above. Thus, the overall energy density and pressure can be expressed as the sum of the individual contributions

$$\rho(t) = \sum_i \rho_i(t), \qquad P(t) = \sum_i P_i(t). \tag{2.26}$$

It is useful to introduce a density parameter for each component, defined as $\Omega_i(t) \equiv \rho_i(t)/\rho_c(t)$, where $\rho_c(t) \equiv 3M_{\mathrm{P}}^2 H(t)^2$ is the critical density. These individual parameters contribute to the total density parameter $\Omega(t)$, which is related to the spatial curvature

[6] Recombination refers to the epoch when the expanding Universe cooled enough ($T \sim 3000$ K) for free photon and electrons to combine into neutral hydrogen atoms.

through the relation

$$\Omega(t) = \sum_i \Omega_i(t), \qquad \Omega(t) + \Omega_k(t) = 1, \tag{2.27}$$

where $\Omega_k(t)$ represents the curvature contribution. We define the various $\Omega_i(t)$ at the present time with the subscript 0 as $\Omega_{i,0} \equiv \rho_{i,0}/\rho_{c,0}$ where the critical density today is $\rho_{c,0} \equiv 3M_{\rm P}^2 H_0^2$. This gives us the set $\{\Omega_{r,0}, \Omega_{m,0}, \Omega_{k,0}, \Omega_{\Lambda,0}\}$ representing the present-day energy density fractions of each cosmological component (*i.e.* radiation, matter, curvature and cosmological constant). For simplicity, we will omit the subscript 0 when referring to present-day density parameters, unless it is necessary to highlight their time dependence. Hence employing (2.20) and (2.12), the Hubble rate in (2.25) takes the form

$$H^2(z) = H_0^2[\Omega_r(1+z)^4 + \Omega_m(1+z)^3 + \Omega_k(1+z)^{-2} + \Omega_\Lambda]. \tag{2.28}$$

2.2.2 Asymptotic solution towards the Big Bang

Once the relation (2.24) is specified, the Friedmann equation can be solved exactly, resulting in the power-law scale factor behaviours discussed above. In the limit $a \to 0$ – *i.e.* approaching the Big Bang – and for any fluid with $w > -1/3$, the curvature contribution becomes subdominant with respect to the energy density. Accordingly, one may write

$$H^2 \approx \frac{\rho_0}{3M_{\rm P}^2} a^{-3(1+w)}, \tag{2.29}$$

which yields

$$a(t) = \left(\frac{t}{\bar{t}}\right)^{\frac{2}{3(1+w)}}, \qquad \bar{t} \equiv \frac{2M_{\rm P}}{(1+w)\sqrt{3\rho_0}}, \tag{2.30}$$

where $\bar{t}$ is an integration constant, usually taken to be the age of the Universe to ensure the scale factor today is fixed to unity. This solution shows that for any equation-of-state parameter satisfying $w > -1$, the scale factor goes to zero as $t \to 0$, and the energy density diverges according to

$$\rho(t) = \frac{4M_{\rm P}^2}{3(1+w)^2}\, t^{-2}, \tag{2.31}$$

thereby signalling a diverging solution towards the Big Bang (in this framework, spacetime is geodesically incomplete; this means that geodesics (1.6) cannot be extended to arbitrary values of affine parameter in the past direction). Introducing the reduced Planck time $t_{\rm P} = M_{\rm P}^{-1}$ and reduced Planck density $\rho_{\rm P} \equiv t_{\rm P}^{-4} = O(10^{117}\text{GeV/cm}^3)$, one may

equivalently write

$$\rho(t) = \frac{\rho_{\rm P}}{6\pi\,(1+w)^2}\left(\frac{t_{\rm P}}{t}\right)^2. \tag{2.32}$$

This form shows that for $t \lesssim t_{\rm P}$, classical Friedmann evolution must be replaced by a quantum-gravity description or alternative mechanisms as big bounce or cyclic universe, which we will discuss in Section 3.5 and in particular in Chapter 7.

2.3 The ΛCDM model

The determination of cosmological parameters relies on a variety of assumptions, including the choice of data sets, prior distributions, and analysis techniques. In what follows, we quote present-day values for the energy density parameters of radiation, matter, spatial curvature, and the cosmological constant as obtained from fitting *Planck* temperature, polarisation, and lensing data within the six-parameter ΛCDM model [9]

$$\begin{aligned} \Omega_r &= (9.02 \pm 0.21)\times 10^{-5}, \quad \Omega_m = 0.3153 \pm 0.0073, \\ |\Omega_k| &< 5\times 10^{-3}, \quad \Omega_\Lambda = 0.6847 \pm 0.0073, \end{aligned} \tag{2.33}$$

with quoted uncertainties corresponding to the 68% confidence level (CL) and upper limits at 95%. These values indicate that approximately 70% of the Universe's energy content is in the form of dark energy – an unknown component with an equation of state parameter measured as $w = -1.03 \pm 0.03$ (68% CL) based on combined Planck, Pantheon Supernovae, and BAO data [9]. This result is consistent with dark energy behaving like a cosmological constant Λ, justifying the interchangeable use of the two terms. A large value of Ω_Λ is required to account for the observed accelerated expansion of the Universe, a phenomenon first discovered in 1998 through observations of type Ia supernovae [10, 109] and later confirmed by Cosmic Microwave Background (CMB) data from WMAP [110].

Despite its success in explaining cosmic acceleration, the introduction of Λ raises theoretical challenges. The nature of dark energy remains unknown – it could stem from physics beyond the Standard Model or modifications to general relativity, as explored in alternative gravity theories (see [52, 111] and Subsection 1.2.1). A natural candidate is vacuum energy, yet quantum field theory predicts its magnitude to be vastly larger than what is observed, leading to the so-called *cosmological constant problem* – a major open issue in contemporary physics [112].

Matter accounts for roughly 30% of the total energy density today, but only about 5% of this is ordinary, baryonic matter ($\Omega_b = 0.049$). The majority is *cold dark matter* (CDM), with $\Omega_c = 0.262$, a non-relativistic form of matter that interacts primarily

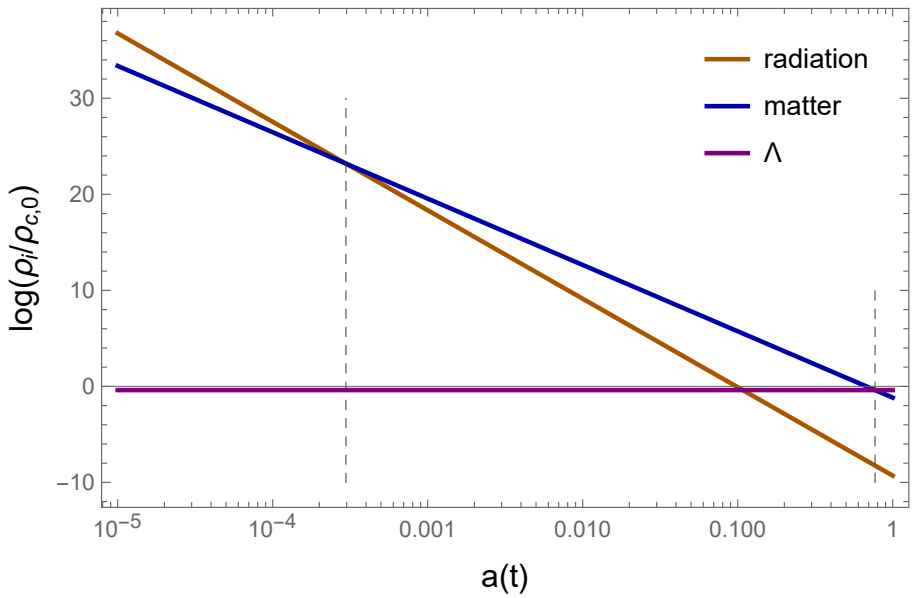

Figure 2.1: Dimensionless energy density $\rho_i(t)/\rho_{c,0}$ plotted against the scale factor (in log scale), showing the evolution of radiation, matter, and the cosmological constant in the ΛCDM model. The dashed grey lines indicate the point for which $\rho_r = \rho_m$ and the transition to the dark-energy-dominated era, respectively.

through gravity and, at most, weakly through other forces. Its presence is crucial to the formation of large-scale structures in the Universe and is supported by evidence from galaxy rotation curves, gravitational lensing, and the dynamics of galaxy clusters [113]. However, the fundamental nature of CDM particles remains elusive, and understanding their properties is a key focus in modern cosmology.

Radiation contributes only a tiny fraction of the current energy budget, primarily in the form of CMB photons. Observational constraints also suggest that the spatial curvature of the Universe is extremely small, favouring a flat geometry. The smallness of both Ω_r and Ω_k implies that Ω_Λ and Ω_m approximately add up to 1, consistent with the ΛCDM framework (2.27).

Using these measured values (2.33) and (2.24), we can determine the evolution of different eras of the Universe

$$\frac{\rho_i(t)}{\rho_{c,0}} = \Omega_i \, a(t)^{-3(1+w)}, \tag{2.34}$$

as depicted in Figure 2.1. The logarithm of the energy density parameters for radiation, matter, and dark energy is plotted as a function of the scale factor $a(t)$. Initially, radiation dominates and its energy density decreases rapidly until it becomes equal to that of matter – a time known as matter-radiation equality $a_{eq}(t)$. Thereafter, the Universe enters a matter-dominated phase, followed by a transition to the dark energy-dominated

era as the matter density drops below ρ_Λ. This sequence outlines the thermal history of the Universe and complements the earlier discussion at the beginning of Section 2.2.

As the simplest cosmological model, ΛCDM relies on just six parameters to accurately fit current observational data and has demonstrated remarkable agreement with measurements over the past two decades[7]. Despite its success, the physical origin of the cosmological constant remains unclear, and the fundamental nature of dark energy and dark matter – which together account for approximately 95% of the Universe's total energy content – continues to pose a major challenge for modern cosmology, highlighting the need for further theoretical and observational investigation.

2.3.1 Puzzles within the Big Bang cosmology

While the standard Big Bang cosmology, together with the Universe composition as prescribed by the ΛCDM model, elegantly describes a broad range of observations – from primordial nucleosynthesis to today's accelerated expansion – it nevertheless hinges on exquisitely special initial conditions. In particular, the early Universe would have had to be arranged so that causally disconnected regions share the same temperature, its spatial curvature would have been vanishingly small, and unwanted topological defects[8]would have been essentially absent.

To see how acute this fine-tuning is, we can divide it into three classic *Big Bang puzzles* and, as we will see, a mechanism that solves one of them (dubbed horizon problem, as explained below) automatically resolves the others. However, the Big Bang singularity itself is not resolved by that mechanism.

HORIZON PROBLEM. One of the major puzzles in standard Big Bang cosmology stems from the extraordinary uniformity of the cosmic microwave background (CMB). Measurements show that the CMB exhibits an almost perfect blackbody spectrum at a temperature of $T = 2.725$ K, with temperature fluctuations suppressed to a level of $\Delta T/T \sim 10^{-5}$, see Figure 2.2.

Despite this remarkable isotropy, standard radiation – or matter – dominated expansion predicts that regions separated by more than a few degrees on the sky at the time of recombination could have never been in causal contact. The observable homogeneity, therefore, cannot be the result of local causal processes within the conventional Hot[9] Big Bang framework. The issue becomes evident when considering the concept of the parti-

[7] It may now be facing its first significant test, as discrepancies in measurements – such as of the Hubble constant H_0 and weak lensing – challenge its framework (see [9, 114–130] and [131–137] respectively).

[8] Monopoles are a type of topological defect. For further details, see [138–140].

[9] The word "Hot" refers specifically to the standard cosmological model describing the Universe after it became extremely hot, dense, and began expanding from an early relativistic thermal state.

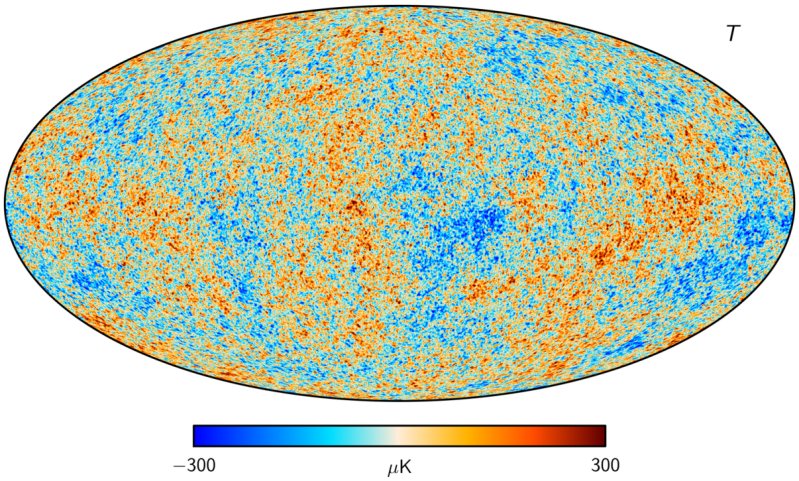

Figure 2.2: Red and blue regions indicate hotter and cooler spots, respectively, in the *Planck* 2018 map of the CMB temperature anisotropies [141].

cle horizon (2.21), which defines the maximum comoving distance that light could have travelled since the beginning of the Universe. In a spatially flat ($k = 0$) FLRW metric, the spacetime interval can be written as

$$ds^2 = a^2(\eta)(-d\eta^2 + dr^2), \tag{2.35}$$

for particles travelling in the radial direction. For a photon trajectory (*i.e.* $ds^2 = 0$), the comoving distance[10] travelled by light between two conformal times (2.6) is

$$\Delta\eta = \int_{a_i}^{a_f} \frac{d\ln a}{aH}. \tag{2.36}$$

Here, $(aH)^{-1}$ is the *comoving* Hubble radius. By using (2.24), it can be rewritten as

$$(aH)^{-1} = (H_{\rm rec} a_{\rm rec}^{\frac{3}{2}(1+w)})^{-1} a^{\frac{1}{2}(1+3w)}. \tag{2.37}$$

Inserting (2.37) into (2.36) yields

$$\Delta\eta_{rec} = \frac{2}{1+3w} \left(H_{\rm rec} a_{\rm rec}^{\frac{3}{2}(1+w)}\right)^{-1} a^{\frac{1}{2}(1+3w)} \Big|_0^{a_{\rm rec}}. \tag{2.38}$$

For any fluids satisfying $w > -1/3$, the early time contribution (*i.e.* $a = 0$) vanishes and the integral evaluates to

$$\Delta\eta_{\rm rec} = \frac{2}{1+3w} (H_{\rm rec} a_{\rm rec})^{-1}, \tag{2.39}$$

[10] The maximum distance a CMB photon could have covered stretches from the initial singularity, where $a = 0$, up to the time of recombination $a_{\rm rec}$ when the CMB was emitted.

which is manifestly finite. In other words, before recombination the particle horizon spans only a limited comoving distance. Consequently, photons emanating from widely separated points on the last-scattering surface could not have been in causal contact under standard Big Bang evolution. To quantify the largest angle on the sky over which causal contact was possible, one defines twice the comoving particle horizon at recombination (see footnote 6)

$$\theta_{\text{casual}} \equiv 2\theta_{hor} = 2\frac{\Delta\eta_{\text{rec}}}{d_A}, \tag{2.40}$$

where d_A is the comoving distance from us to the last-scattering surface. Equivalently, converting the notation to the redshift z,

$$\theta_{\text{casual}} = 2\frac{\int_{z_{\text{rec}}}^{\infty} dz/H(z)}{\int_0^{z_{\text{rec}}} dz/H(z)} \simeq 2.3\ \text{deg}, \tag{2.41}$$

obtained by considering (2.28) and (2.33) with $z_{\text{rec}} = 1080$. Thus, any two points on the CMB separated by more than ~ 2 deg could have never exchanged signals prior to recombination under the standard model, see Figure 2.3.

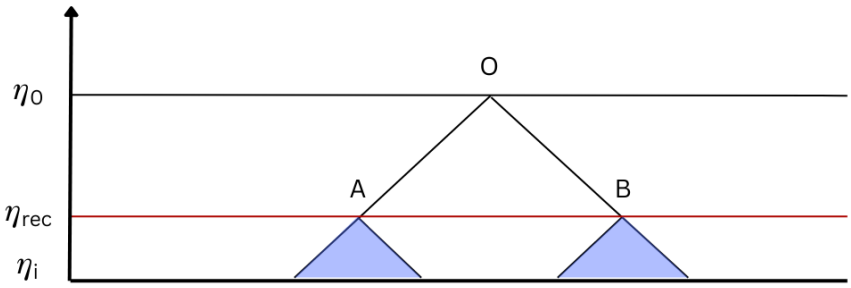

Figure 2.3: Spacetime diagram of comoving coordinate r vs conformal time η. The past light cones of two CMB photons (A and B), both observed today at O, fail to overlap if one follows the Big Bang history – underscoring the horizon problem.

FLATNESS PROBLEM. The Friedmann equation (2.25) relates the expansion rate H to the energy density ρ and the spatial curvature k. Taking into account the definition of the density parameter (2.27), we can relate

$$\Omega_k \equiv 1 - \Omega(t) = -\frac{k}{(aH)^2}. \tag{2.42}$$

Thus, the deviation from flatness grows with time because aH typically decreases in a decelerating universe. Maintaining $|\Omega_0 - 1| \leqslant 10^{-2}$ today [9] would require an extraordinarily fine-tuned initial condition. Indeed, considering that the Universe is matter-

dominated just before and around $z_{\rm eq} \sim 10^4$, we use the matter-era scaling to obtain

$$|\Omega_{\rm eq} - 1| \sim |\Omega_0 - 1|(1 + z_{\rm eq})^{-1} \leqslant 10^{-6}. \tag{2.43}$$

At early times (*e.g.* Planck time), $|\Omega - 1|$ must have been incredibly small, of order of 10^{-60}. This extremely small number reflects how precisely the initial conditions must be fine-tuned for the Universe to remain nearly flat, and highlights the need for a mechanism that dynamically enforces or preserves flatness.

MONOPOLE (RELICS) PROBLEM. Despite theoretical expectations, magnetic monopoles have never been observed [142] – an inconsistency that the standard Hot Big Bang cosmology cannot readily explain. This constitutes the so-called monopole problem. Grand Unified Theories (GUTs) [143, 144], which are extensions of the Standard Model based on larger gauge groups and expected to unify the fundamental interactions at energies above 10^{16} GeV, predict the copious production of magnetic monopoles during the spontaneous symmetry-breaking phase transitions as the Universe cools [145–147]. Without a mechanism to suppress them, the resulting monopole abundance would vastly exceed observational limits, leading to a catastrophic overclosure of the Universe. However, given our limited understanding of physical processes at extremely high energies, the monopole problem remains a subject of debate. Indeed, it is not universally accepted as a major shortcoming of the standard Hot Big Bang theory.

3 | The theory of inflation

In the early 1980s, the idea of *cosmic inflation* revolutionised our understanding of the Universe's earliest moments. Originally proposed by Alan Guth in 1981 [7], inflation describes a very brief period of extremely rapid and accelerated expansion that occurred just after the Big Bang. Driven by the potential energy of a scalar field known as the *inflaton*, this expansion stretched space by an enormous factor in a fraction of a second. The motivation for inflation arose from several fundamental puzzles left unresolved by the standard Big Bang cosmology. As mentioned in Section 2.2, there were three main issues that needed to be addressed. The horizon problem asks why distant regions of the cosmic microwave background (CMB) have almost identical temperatures despite never being in causal contact in standard cosmology. The flatness problem concerns the question of why the Universe today appears so close to spatial flatness, requiring an extraordinary fine-tuning of initial conditions. The monopole problem arises from the absence of hypothetical relics like magnetic monopoles, which are predicted by grand unified theories but have never been observed. While Guth's original *old inflation* model solved these problems conceptually, it introduced a new issue known as the "*graceful exit problem*". In this model, the Universe expands exponentially while trapped in a false vacuum (a high-energy state) which is a local but not global minimum of the potential; quantum tunnelling allows the field to overcome the energy barrier and transition to the true vacuum (a low-energy state), but this process occurs non-uniformly, forming tiny spherical "bubbles" of true vacuum that spontaneously nucleate within the surrounding false vacuum. To exit inflation, bubbles of the true vacuum must form and collide to reheat the Universe. However, if the bubble nucleation rate is too low, as required for sufficient inflation, the bubbles remain rare and widely separated due to rapid expansion. They do not merge efficiently, leading to large inhomogeneities. This makes it impossible to end inflation smoothly and uniformly across space. This led to two key developments. Andrei Linde's *new inflation* and later *chaotic inflation* models [148] introduced the idea that inflation could happen via the *slow-roll* of a scalar field down a gently sloping potential, avoiding violent bubble collisions and ensuring a long enough inflationary phase. Alexei Starobinsky independently proposed a model of inflation [39] based on modifications of

Einstein's gravity, adding an R^2 term to the gravitational action (essentially working with an $f(R) = R + R^2$ model, see (1.69)), which we will discuss in Section 3.4. This led to an exponential expansion without invoking a scalar field directly, and its predictions remain remarkably consistent with current observations. Together, these approaches established inflation as a dynamical and predictive framework. Quantum fluctuations of the inflaton field, stretched beyond the Hubble radius during inflation, become frozen and re-enter later as classical perturbations, seeding the formation of large-scale structure and imprinting the nearly scale-invariant spectrum observed in the CMB.

This chapter explores these foundational aspects of inflation in detail. We start with Section 3.1, where we explore: classical dynamics of single-field inflation, the successes of inflation in explaining the large-scale homogeneity, isotropy, and flatness of the Universe; the slow-roll approximation, a regime where the inflaton potential energy dominates over its kinetic energy, leading to quasi-exponential expansion; the crucial phase of reheating where the inflaton decays and transfers its energy into radiation and matter, smoothly connecting inflation to the standard Hot Big Bang evolution. In Section 3.2 we explore the generation of inflationary perturbations, namely how quantum fluctuations during inflation translate into temperature anisotropies in the CMB and ultimately lead to the cosmic structures we see today. In Section 3.3 we introduce *multifield models*, where more than one scalar field drive inflation, enriching the dynamics and allowing new observational signatures. We then focus on modified gravity in the inflationary context in Section 3.4, in particular on the Starobinsky model of inflation. We also discuss alternatives to inflation in Section 3.5.

3.1 Classical dynamics of single-field inflation

We begin with the action for a scalar field ϕ [7, 106, 149–155] – commonly called the inflaton – minimally coupled to gravity

$$S = \int d^4x \sqrt{-g} \left[\frac{R}{2} - \frac{1}{2} g^{\mu\nu} \partial_\mu \phi \, \partial_\nu \phi - V(\phi) \right], \tag{3.1}$$

where R is the Ricci scalar and $V(\phi)$ the inflaton potential. In this chapter we set $M_{\rm P}^2 = 1$, and assume spatial homogeneity, $\phi = \phi(t)$. The energy-momentum tensor (1.10) follows from variation with respect to $g^{\mu\nu}$,

$$T_{\mu\nu} = \partial_\mu \phi \, \partial_\nu \phi - g_{\mu\nu} \left[\tfrac{1}{2} g^{\rho\sigma} \, \partial_\rho \phi \, \partial_\sigma \phi + V(\phi) \right]. \tag{3.2}$$

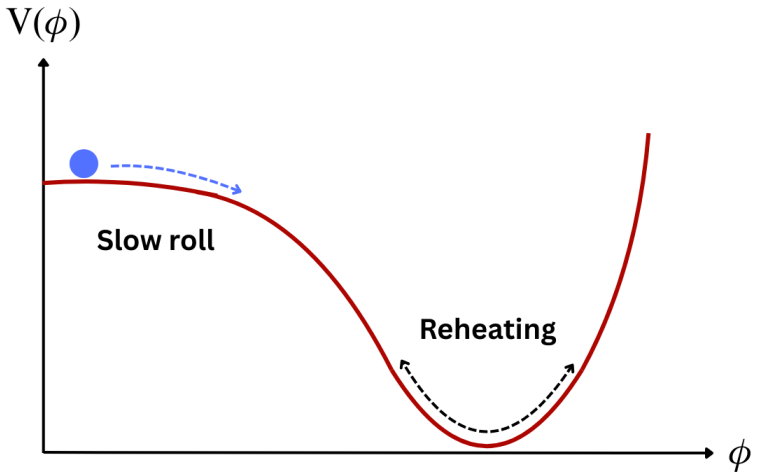

Figure 3.1: The typical shape of a good inflationary potential.

In a FLRW background, once (3.2) is contracted with the inverse of the metric $T^{\mu}_{\nu} = T_{\lambda\nu}g^{\lambda\mu}$, its (00) and (ij)-components yield

$$T^0_0 = -\rho, \qquad T^i_j = P\delta^i_j, \tag{3.3}$$

where

$$\rho = \frac{1}{2}\dot{\phi}^2 + V(\phi)\,, \tag{3.4}$$

$$P = \frac{1}{2}\dot{\phi}^2 - V(\phi)\,, \tag{3.5}$$

with dots denoting time derivative. Inflation requires potential domination

$$\frac{1}{2}\dot{\phi}^2 \ll V(\phi), \tag{3.6}$$

which implies that the inflaton field rolls slowly down its potential, see Figure 3.1. Consequently, inflation under this assumption is referred to as *slow-roll inflation*. The equation-of-state parameter is then

$$w = \frac{P}{\rho} = \frac{\frac{1}{2}\dot{\phi}^2 - V(\phi)}{\frac{1}{2}\dot{\phi}^2 + V(\phi)} \simeq -1, \tag{3.7}$$

violating the strong energy condition $w \geq -1/3$ (see [108]) and driving accelerated expansion. Indeed, by means of (2.24), an almost constant energy density, $\rho \simeq$ const, implies an almost constant Hubble rate, so that the Universe undergoes exponential ex-

pansion. The scale factor evolves as

$$a(t) \simeq a_{\rm in}\, e^{H\,(t-t_{\rm in})}, \tag{3.8}$$

describing a quasi-de Sitter spacetime, where a_{in} is the scale factor at the onset of this phase, t_{in}. In a spatially flat universe (cf (2.3) with $k = 0$), the Friedmann equations read

$$H^2 = \frac{1}{3}\left(\frac{1}{2}\,\dot{\phi}^2 + V(\phi)\right), \tag{3.9}$$

$$\dot{H} = -\frac{1}{2}\,(\rho + P) = -\frac{1}{2}\,\dot{\phi}^2\,. \tag{3.10}$$

Differentiating the first and using the second yields the inflaton equation of motion,

$$\ddot{\phi} + 3H\dot{\phi} + V'(\phi) = 0, \tag{3.11}$$

also known as the *Klein-Gordon equation*, where $V'(\phi) = dV/d\phi$. Given $V(\phi)$ and initial conditions, these determine $\phi(t)$ and $H(t)$ dynamically. Inflation ends once $\frac{1}{2}\,\dot{\phi}^2 \ll V(\phi)$ is no longer satisfied and $w > -\frac{1}{3}$.

3.1.1 Success of Inflation

In Subsection 2.3.1 we demonstrated that cosmological fluids satisfying the strong energy condition – that is, with an equation of state parameter $w > -\frac{1}{3}$ – lead to a finite comoving particle horizon. Specifically, for a constant $w > -\frac{1}{3}$, the contribution from the lower limit of integration $a = 0$ vanishes (2.38), implying that the earliest contributions to the conformal time are negligible yielding a finite comoving horizon at recombination (2.39). However, the situation changes dramatically if the Universe was instead dominated at early times by a fluid with $w < -\frac{1}{3}$. In that case, the early-time contribution to the integral diverges

$$\eta_i = \frac{2}{1+3w}\left(H_{\rm rec}a_{\rm rec}^{\frac{3}{2}(1+w)}\right)^{-1} a^{\frac{1}{2}(1+3w)}\Big|_{a\to 0} \to -\infty. \tag{3.12}$$

If this phase persists long enough, it allows previously casually disconnected regions (A and B in Figure 3.2) enough conformal time to become casully connected – thereby offering a resolution to the horizon problem. Indeed, by extending the conformal time back to $\eta_i = -\infty$, the past light-cones of two distant CMB photons (labelled as A and B in Figure 3.2) now intersect prior to the standard Big Bang evolution, within a new phase starting at $\eta_{\rm in}$ and ending at $\eta_{\rm end}$, during which the strong energy condition is violated. The key physical consequence of the strong energy condition violation is the behavior

of the Hubble radius (2.20). In this regime, the Hubble radius decreases with time

$$\frac{d}{dt}(aH)^{-1} < 0. \tag{3.13}$$

Using the definition of the Hubble parameter $H(t)$ of (2.20), the above condition implies

$$\frac{\ddot{a}}{a^2} > 0, \tag{3.14}$$

which is the signature of an *accelerated expansion*. Thus, a shrinking Hubble radius – associated with a phase where $w < -\frac{1}{3}$ – not only alters the causal structure of the Universe but also corresponds to a period of inflationary-like growth that can solve the *horizon problem*.

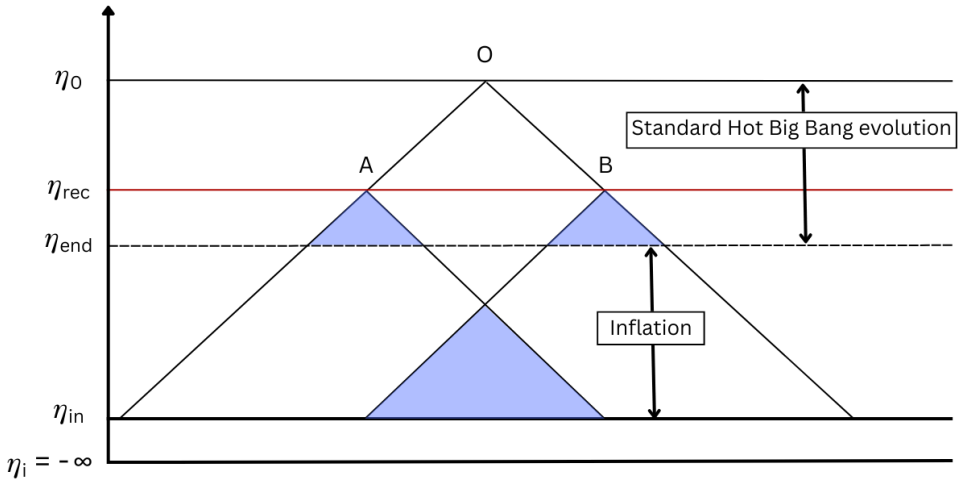

Figure 3.2: The figure shows two CMB photons, emitted (or last scattered) at points A and B and observed today at point O. The horizon problem is resolved by introducing an early phase of cosmic evolution – preceding the standard Big Bang expansion – in which the Universe is dominated by a fluid with an equation of state parameter $\omega < -1/3$. This phase, occurring between the initial singularity and the onset of standard cosmology η_{in}, allows for causal contact between regions A and B that would otherwise be casually disconnected.

The resolution of the *flatness problem* is rooted in the dynamical evolution of the density parameter Ω during this inflationary de Sitter-like expansion, as the deviation from flatness (2.42) shrinks rapidly. Specifically, the relation between its initial and final values is given by

$$|\Omega_f - 1| = |\Omega_i - 1|e^{-2N}, \tag{3.15}$$

where

$$N \equiv \log\frac{a_{end}}{a_{ini}} = \int_{N_{in}}^{N_{end}} dN = \int_{t_{in}}^{t_{end}} H(t)\,dt, \tag{3.16}$$

is the number of e-folds of inflation measuring its duration, namely the number of times the Universe expands by factor of e. Following the end of inflation, Ω_k begins to grow again, scaling as a^2 during the radiation-dominated era and as a during the matter-dominated era. Assuming the standard Friedmann evolution begins at the Planck scale, the curvature term is amplified by roughly a factor of 10^{60} between the end of inflation and today. This yields the estimate

$$|\Omega_0 - 1| \simeq 10^{60}|\Omega_i - 1|e^{-2N} \leq 10^{-2}, \tag{3.17}$$

where the inequality reflects current observational bounds on the spatial curvature. Solving this condition places a lower bound on the number of e-folds required for inflation to resolve the flatness problem: $N \simeq 65$. In other words, 65 e-folds are needed to dynamically flatten the Universe to the precision we observe today, providing a natural explanation for its near-flat geometry.

3.1.2 The slow-roll approximation

Analysing the dynamics of the inflaton field under the slow-roll condition (3.6) enables the derivation of approximate analytical solutions. The slow-roll approximation is most effectively described through a hierarchy of small parameters derived either from the inflaton potential $V(\phi)$ or from the Hubble rate $H(\phi)$ during inflation. Therefore, starting from (3.9), we have

$$3H^2 \approx V(\phi). \tag{3.18}$$

Then, we can rewrite (3.6) into the equivalent form

$$\frac{|\dot{H}|}{H^2} \ll 1. \tag{3.19}$$

Moreover, taking the derivative of (3.18), and using the above, we also obtain

$$V'(\phi) \approx -3H\dot{\phi}, \tag{3.20}$$

implying $|\ddot{\phi}| \ll 3H|\dot{\phi}|$. Thus, it is useful to introduce the following potential slow-roll parameters as

$$\epsilon_V \equiv \frac{1}{2}\left(\frac{V'}{V}\right)^2, \qquad \eta_V \equiv \frac{V''}{V}, \tag{3.21}$$

$$\xi_V^2 \equiv \frac{V'V'''}{V^2}, \qquad v_V^3 \equiv \frac{V'^2V''''}{V^3}. \tag{3.22}$$

Another useful hierarchy is defined as

$$\epsilon_0 \equiv -\frac{\dot{H}}{H^2}, \quad \epsilon_{i>0} \equiv \frac{d\log\epsilon_{i-1}}{d\log k}. \tag{3.23}$$

At leading order in the slow-roll expansion, the potential slow-roll parameters can be related to the Hubble rate hierarchy through $\epsilon_0 \simeq \epsilon_V$, $\epsilon_1 \simeq 4\epsilon_V - 2\eta_V$. Unlike the potential parameters, the $\{\epsilon_i\}$ parameters are more directly linked to the background dynamics. Throughout the slow-roll regime, all of these quantities are expected to remain small, with the limit $1 \gg |\epsilon_V| \simeq |\epsilon_0| \to 0$ signalling the onset of inflation.

The parameters ϵ_V and η_V characterise the shape of the inflaton potential and control the dynamics of inflation. Specifically, ϵ_V measures the flatness of the potential and determines the ratio between the kinetic and potential energy of the inflaton, while η_V quantifies the curvature of the potential and affects the acceleration of the field. When $\epsilon_V, |\eta_V| \ll 1$, the friction term $3H\dot{\phi}$ in (3.11) dominates the Klein-Gordon equation, leading to a quasi-exponential expansion (see (3.8)). In this regime, the slow-roll solution acts as an attractor [156], meaning that the dynamics of the inflaton rapidly converge to the slow-roll trajectory regardless of the initial conditions, ensuring a period of sustained inflation and generating a nearly scale-invariant spectrum of perturbations.

3.1.3 Reheating

When the inflationary condition (3.18) breaks down, inflation ends, and the inflaton field typically rolls into a potential well (see Figure 3.1) and starts to oscillate around its minimum, where it decays leading to particle production. This phase is known as *reheating* [157–164], and plays a crucial role in filling the Universe with particles.

During inflation, the Universe undergoes exponential expansion, smoothing out curvature and inhomogeneities. However, this process also dilutes any pre-existing matter or radiation, leaving the post-inflation Universe nearly empty and dominated by a coherently oscillating scalar field. At this stage, the Hot Big Bang conditions have not yet been realised: there are no particles or radiation, only an enormous amount of energy stored in the scalar field which solves the monopole problem (by diluting any previously produced magnetic monopoles to negligibly low densities). Because the energy density during inflation remains nearly constant, the total energy $E_i = \rho V_i$ increases exponentially with the volume of the Universe. When inflation ends and the inflaton field begins to oscillate, this energy can be efficiently converted into radiation and particles – a process that depends on the specific form of the scalar potential and how the inflaton couples to matter. Typically, reheating occurs rapidly, as we show below. During the oscillatory phase, if the potential is approximately quadratic near its minimum (*i.e.*

$V(\phi) \approx \frac{m^2}{2}\phi^2$), the inflaton behaves like a simple harmonic oscillator

$$\ddot{\phi} + m^2\phi \simeq 0. \tag{3.24}$$

Solving this equation alongside the Friedmann equation (2.25), we obtain the time-dependent solution

$$\phi(t) = \frac{\sqrt{6}}{m} H \cos(mt), \tag{3.25}$$

describing rapid oscillations of the inflaton field – as the mass becomes large – about the potential minimum with frequency set by the mass m. During this phase, the Hubble time H^{-1} is much longer than the oscillation period m^{-1}, allowing us to neglect the Hubble damping term in the equation of motion. Substituting this solution into the expression for the pressure of the inflaton field (3.5), and averaging[1] over several oscillations yields

$$\langle P \rangle = 3H^2 \langle 1 - 2\cos^2(mt) \rangle \simeq 0. \tag{3.26}$$

This shows that the inflaton, when oscillating in a quadratic potential, behaves like a pressureless, non-relativistic fluid – effectively cold matter. Hence, the equation of state during reheating is $w = 0$. The duration of reheating, measured in terms of e-folds

$$\Delta N_{\rm rh} = N_{\rm rh} - N_{\rm end}, \tag{3.27}$$

depends on both w and the energy density at the end of reheating $\rho_{\rm rh}$. It is given by

$$\Delta N_{\rm rh} \equiv \frac{1}{3(1+w)} \log\left(\frac{\rho_{\rm end}}{\rho_{\rm rh}}\right), \tag{3.28}$$

where $\rho_{\rm end}$ is the energy density at the end of inflation. In the typical case where $w = 0$, reheating mimics a matter-dominated epoch.

We can write the energy continuity equation for the inflaton, considering (3.5), as

$$\dot{\rho} + 3H\rho = -3HP = \frac{3H}{2}(m^2\phi^2 - \dot{\phi}^2). \tag{3.29}$$

It gradually loses energy and the right-hand side averages to zero over one period by means of (3.26), yielding the long-term behavior

$$\langle \dot{\rho} \rangle + 3H\langle \rho \rangle = 0. \tag{3.30}$$

It is evident that this equation describes a matter-like decay of the energy density. As

[1] We use the angular brackets to represent averages in this chapter.

the inflaton continues to oscillate near the minimum, it may decay into other particles. If this decay is slow, the energy evolution is modified as

$$\langle\dot{\rho}\rangle + (3H + \Gamma)\langle\rho\rangle = 0, \tag{3.31}$$

where Γ represents the decay rate of the inflaton and the term $-\Gamma\langle\rho\rangle$ accounts for the energy transferred to the produced particles. In some cases, especially when the inflaton decays into bosons, this process can be highly efficient and non-linear, a regime known as *preheating*[2]. Eventually, the particles interact and thermalise, restoring equilibrium at a certain temperature. This marks the transition to the standard Hot Big Bang evolution.

3.2 Inflationary perturbations

The origin of primordial perturbations lies in the quantum nature of the inflaton field during inflation. While the inflaton field ϕ evolves classically along its potential $V(\phi)$, it also experiences small quantum fluctuations around its classical trajectory. Due to the rapid expansion of the Universe during inflation, these quantum fluctuations are stretched to superhorizon scales, where $\lambda_{\rm phys} > L_H$ and they effectively become classical because they lose causal contact, undergo decoherence and freeze in amplitude [21, 165–167]. These classicalised fluctuations provide the seeds for the primordial power spectra of scalar and tensor perturbations – ultimately leading to the formation of cosmic structures [149, 151, 168, 169]. To rigorously describe these quantum fluctuations, it is necessary to account not only for perturbations in the inflaton field $\delta\phi$ but also for perturbations in the spacetime metric [106, 170–172]

$$ds^2 = -(1 + 2A)\, dt^2 + 2a(t)B_i\, dx^i dt + a^2(t)\left[(1 - 2\psi)\delta_{ij} + 2E_{ij}\right] dx^i dx^j, \tag{3.32}$$

where A is a scalar defined on spatial slices which transforms as a scalar under spatial coordinate transformations (sometimes also called 3-scalar), ψ is a 3-scalar called *spatial curvature perturbation*, $B_i = \partial_i B - S_i$ is 3-vector named *shift* and $E_{ij} = 2\partial_{ij}E + 2\partial_{(i}F_{j)} + h_{ij}$ is the 3-tensor *shear* [8]. For a full description of these quantities see [106]. Interestingly, at linear order, the combination of a fixed gauge choice and the linearised Einstein equations relates the metric and scalar field perturbations in such a way that the system reduces to a single physical degree of freedom governing the dynamics [152, 173].

[2]During preheating, the oscillating inflaton causes the effective mass of the coupled bosonic field to change periodically in time [106, 157]. This time-dependent mass acts like a driving force that can resonantly amplify specific momentum modes and certain wavelengths of the bosonic field get "pumped up" much more than others. This selective growth leads to a rapid increase in the number of particles and it is called parametric resonance [157].

A convenient approach is to work in the spatially flat gauge, where the curvature of constant-time hypersurfaces vanishes and the spatial part of the metric remains unperturbed

$$\psi = 0, \quad \text{and} \quad E_{ij} = 0, \tag{3.33}$$

therefore the spatial metric reduces to $h_{ij} = a^2(t)\delta_{ij}$. This is a gauge choice: vector and tensor perturbations are still present in general, but at linear order they decouple from the scalar sector and are neglected in the following analysis. Hence, the dynamics of scalar perturbations are captured entirely by $\delta\phi$ at linear order which allows us to treat it as the only independent physical degree of freedom. We can treat the inflaton perturbations as massless as the potential is nearly flat (3.6) so that the field mass is small compared to the Hubble scale (*i.e.* $m_\phi^2 = V''(\phi) \ll H^2(t)$). This simplifies the equations and captures the essential physics of how quantum fluctuations evolve during inflation[3]. The total field is then expressed as a sum of the background and its (generally not homogeneous) perturbations $\phi(t, \mathbf{x}) \to \phi(t) + \delta\phi(t, \mathbf{x})$. Since $\delta\phi$ is spatially inhomogeneous, its dynamics must include spatial derivatives. The exact equation of motion for the perturbations comes from expanding the full Klein-Gordon equation in an expanding spacetime, including metric perturbations,

$$\ddot{\delta\phi} + 3H\dot{\delta\phi} - a^{-2}\nabla^2\delta\phi + V''(\phi)\delta\phi + \cdots = 0,$$

where the dots represent additional terms arising from the coupling between $\delta\phi$ and metric perturbations (*e.g.* terms proportional to $\dot{\phi}\,\dot{\psi}$ or $AV'(\phi)$).

Under the slow-roll approximation and by neglecting metric perturbations to leading order, these additional terms are small compared to the dominant kinetic and gradient terms. Similarly, the inflaton mass term $V''(\phi)\,\delta\phi$ is negligible compared to $H^2\delta\phi$ due to $V''(\phi) \ll H^2(t)$. Therefore, the equation reduces at leading order to

$$\ddot{\delta\phi} + 3H\dot{\delta\phi} - a^{-2}\nabla^2\delta\phi = 0, \tag{3.34}$$

which is the massless, minimally coupled[4] Klein-Gordon equation in an expanding universe.

During inflation it is convenient to switch to conformal time (2.6), so that the scalar-field perturbation satisfies

$$\delta\phi'' + 2\frac{a'}{a}\delta\phi' - \nabla^2\delta\phi = 0, \tag{3.35}$$

[3] Later in the section we will discuss also the massive case

[4] Perturbations only feel the usual Hubble friction from the expanding metric, not additional curvature-dependent forces.

and one proceeds to quantise by promoting $\delta\phi$ to an operator and expanding in Fourier modes,

$$\delta\phi(\eta, \mathbf{x}) = \int \frac{d^3k}{(2\pi)^3}[\delta\phi_{\mathbf{k}}(\eta)\hat{b}_{\mathbf{k}}e^{i\mathbf{k}\cdot\mathbf{x}} + \delta\phi^*_{\mathbf{k}}(\eta)\hat{b}^\dagger_{\mathbf{k}}e^{-i\mathbf{k}\cdot\mathbf{x}}], \tag{3.36}$$

with creation and annihilation operators satisfying

$$[\hat{b}_{\mathbf{k}}, \hat{b}^\dagger_{\mathbf{k}'}] = \delta^3(\mathbf{k} - \mathbf{k}'), \qquad [\hat{b}^\dagger_{\mathbf{k}}, \hat{b}^\dagger_{\mathbf{k}'}] = 0. \tag{3.37}$$

Each mode $\delta\phi_{\mathbf{k}}$ then follows

$$\delta\phi''_{\mathbf{k}} + 2\frac{a'}{a}\delta\phi'_{\mathbf{k}} + k^2\delta\phi_{\mathbf{k}} = 0, \tag{3.38}$$

where $k^2 = |\mathbf{k}|^2$ is the spatial Euclidean amplitude, and defining the Mukhanov variable $u_{\mathbf{k}}(\eta) \equiv a(\eta)\delta\phi_{\mathbf{k}}(\eta)$ [21, 174], one casts the dynamics of the Fourier modes as

$$u''_{\mathbf{k}} + \left(k^2 - \frac{a''}{a}\right)u_{\mathbf{k}} = 0. \tag{3.39}$$

This equation can be considered the generalisation of the Klein-Gordon equation in an expanding universe. To define the initial vacuum state of quantum perturbations, we take the UV limit where $k^2 \gg a''/a$ (*i.e.* the Universe's expansion is low) and (3.39) reduces to

$$u''_{\mathbf{k}} + k^2 u_{\mathbf{k}} = 0, \tag{3.40}$$

with general solution

$$u_{\mathbf{k}}(\eta) = \frac{1}{\sqrt{2k}}(\alpha_k e^{-ik\eta} + \beta_k e^{ik\eta}). \tag{3.41}$$

All of the physical information about a given mode is encoded in the constants α_k and β_k, whose values are fixed by imposing boundary conditions on the perturbations in the UV regime. In fact, the canonical commutation relations for $(\hat{b}_k, \hat{b}^\dagger_k)$ translate into the requirement that the mode functions satisfy the Wronskian normalisation

$$W(u_k, u^*_k) = u_k(u^*_k)' - (u^*_k)'u_k = i, \qquad \rightarrow \qquad |\alpha_k|^2 - |\beta_k|^2 = 1, \tag{3.42}$$

exactly as in flat Minkowski space. However, this single constraint does not fully determine α_k and β_k; a second, physically motivated condition is needed to select a unique vacuum in an expanding FLRW background. We require that, in the limit $\eta \to -\infty$ (at the very beginning of inflation), modes with wavelength $\lambda \sim 1/k$ are much smaller than the Hubble radius (*i.e.* subhorizon modes). In this regime, the effects of spacetime curvature are negligible, and physics should approximate that of Minkowski space. Thus,

each mode reduces to the familiar positive-frequency Minkowski solution. This singles out $\alpha_k = 1$, $\beta_k = 0$ so that

$$u_k(\eta) \to \frac{e^{-ik\eta}}{\sqrt{2k}}. \tag{3.43}$$

The above is what defines the *Bunch-Davies vacuum* in inflationary cosmology. It is not the only discussed choice in literature (see *e.g.* [175–178] and Chapter 7), but it is of course the most reasonable choice as it does not require extra physics to generate an exited vacuum. It guarantees that at the earliest times, when all modes are deeply subhorizon, there are only the standard quantum vacuum fluctuations. In the infrared limit (or superhorizon scales $k^2 \ll a''/a$), one finds

$$u_k'' - \frac{a''}{a} u_k = 0, \tag{3.44}$$

whose solution

$$u_k(\eta) \propto a(\eta) \quad \to \quad \delta\phi_k = \text{const.}, \tag{3.45}$$

demonstrates mode freezing[5]. In a de-Sitter space, where $a(\eta) = -(H\eta)^{-1}$ and $a''/a = 2\eta^{-2}$, (3.39) becomes

$$u_k'' + \left(k^2 + \frac{2}{\eta^2}\right) u_k = 0, \tag{3.46}$$

whose general solution is

$$u_k = \frac{\alpha_k}{\sqrt{2k}} e^{-ik\eta}\left(1 - \frac{i}{k\eta}\right) + \frac{\beta_k}{\sqrt{2k}} e^{ik\eta}\left(1 + \frac{i}{k\eta}\right), \tag{3.47}$$

and with the Bunch-Davies choice simplifies to

$$u_k = \frac{e^{-ik\eta}}{\sqrt{2k}}\left(1 - \frac{i}{k\eta}\right). \tag{3.48}$$

Hence, the complete expression of the field operator $\hat{\delta\phi}$ in the de-Sitter spacetime is

$$\hat{\delta\phi}(\eta, \mathbf{x}) = \int \frac{d^3k}{(2\pi)^3} \left[\left(\frac{u_k}{a}\right) \hat{b}_{\mathbf{k}} e^{i\mathbf{k}\cdot\mathbf{x}} + \left(\frac{u_k^*}{a}\right) \hat{b}_{\mathbf{k}}^\dagger e^{-i\mathbf{k}\cdot\mathbf{x}}\right]. \tag{3.49}$$

One can now compute the two-point function around the vacuum state in the de-Sitter

[5] Note that, when the slow-roll approximation is not considered, $\delta\phi$ in the flat gauge is not conserved on super-horizon scales, while the curvature perturbation introduced later ζ is conserved outside the horizon.

limit

$$\langle 0|\hat{\delta\phi}(\eta,\mathbf{x})\hat{\delta\phi}(\eta,\mathbf{x}')|0\rangle = \int \frac{d^3k\,d^3k'}{(2\pi)^6}\left(\frac{u_k u^*_{k'}}{a^2}\right)\langle 0|\hat{b}_{\mathbf{k}}\hat{b}^\dagger_{\mathbf{k}'}|0\rangle e^{i\mathbf{k}\cdot\mathbf{x}}e^{-i\mathbf{k}'\cdot\mathbf{x}'} + \dots \tag{3.50}$$

which gives us the power spectrum of the fluctuations. Here, the only non-vanishing matrix element is indeed

$$\langle 0|\hat{b}_{\mathbf{k}}\hat{b}^\dagger_{\mathbf{k}'}|0\rangle = \langle 0|\left(\hat{b}_{\mathbf{k}}\hat{b}^\dagger_{\mathbf{k}'} - \hat{b}^\dagger_{\mathbf{k}'}\hat{b}_{\mathbf{k}}\right)|0\rangle = \langle 0|\,[\hat{b}_{\mathbf{k}},\hat{b}^\dagger_{\mathbf{k}'}]\,|0\rangle = \delta^3(\mathbf{k}-\mathbf{k}'), \tag{3.51}$$

giving

$$\langle 0|\hat{\delta\phi}(\eta,\mathbf{x})\hat{\delta\phi}(\eta,\mathbf{x}')|0\rangle = \int \frac{d^3k\,d^3k'}{(2\pi)^6}\left(\frac{u_k u^*_{k'}}{a^2}\right)e^{i\mathbf{k}\cdot\mathbf{x}}e^{-i\mathbf{k}'\cdot\mathbf{x}'}\delta^3(\mathbf{k}-\mathbf{k}') \tag{3.52}$$

$$= \int \frac{d^3k}{(2\pi)^3}\left(\frac{|u_k|^2}{a^2}\right)e^{i\mathbf{k}\cdot(\mathbf{x}-\mathbf{x}')} \tag{3.53}$$

$$\equiv \int \frac{d^3k}{(2\pi)^3}\,P_{\delta\phi}(k)\,e^{i\mathbf{k}\cdot(\mathbf{x}-\mathbf{x}')}. \tag{3.54}$$

Defining the dimensionless power spectrum

$$\mathcal{P}_{\delta\phi} \equiv \frac{k^3}{2\pi^2}P_{\delta\phi}(k) = \frac{k^3}{2\pi^2}\frac{|u_k|^2}{a^2}, \tag{3.55}$$

and since $|u_k|^2 = \frac{1}{2k}\left(1+\frac{1}{k^2\eta^2}\right)$ from (3.48), one obtains

$$\mathcal{P}_{\delta\phi}(k) = \left(\frac{H}{2\pi}\right)^2\left[1+\left(\frac{k}{aH}\right)^2\right], \tag{3.56}$$

showing that on superhorizon scales $k \ll aH$ the spectrum "freezes" to the constant amplitude

$$\mathcal{P}_{\delta\phi}(k) \approx \left(\frac{H}{2\pi}\right)^2, \tag{3.57}$$

consistent with the phenomenon of modes freezing we discussed previously (3.45).

Hence, in a conventional, non-inflationary universe dominated by matter or radiation, the comoving Hubble length (2.20) increases with time. As a result, comoving modes satisfy $k < aH$ at early times, meaning they lie outside the Hubble horizon and appear frozen. Only at late times, once inflation has ended and the horizon begins to grow again, they re-enter the horizon (*i.e.* $k > aH$), and begin to evolve dynamically, as shown in Figure 3.3. In contrast, during an inflationary phase, the comoving Hubble length decreases due to accelerated expansion. Modes that initially have small wavelengths and

behave as underdamped oscillators ($k \gg aH$) are stretched by the expansion and eventually cross outside the Hubble horizon ($k \ll aH$), while on subhorizon scales, these fluctuations originate from quantum vacuum zero-point energy, where spacetime curvature effects are negligible. Upon horizon exit, these modes become overdamped and

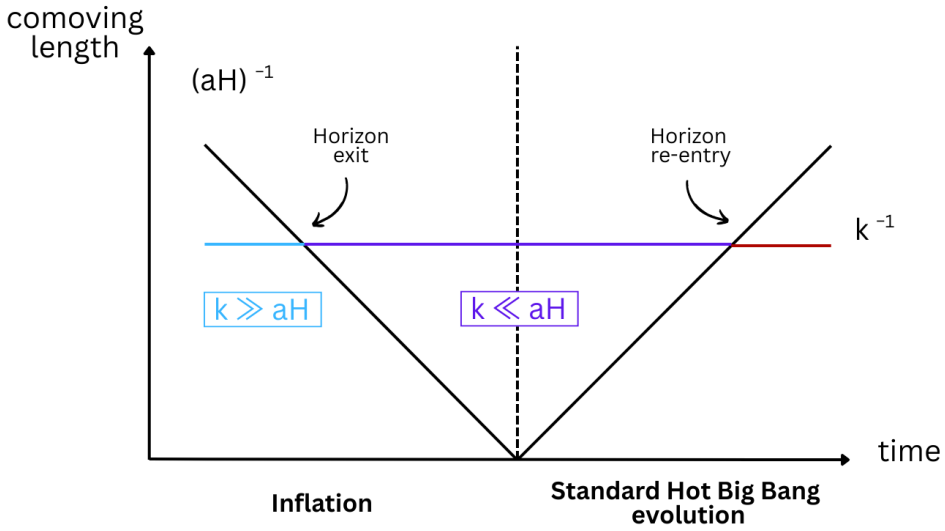

Figure 3.3: Picture of the evolution of a comoving mode with wavenumber k as it crosses the Hubble horizon during and after inflation. The sub-horizon regime ($k \gg aH$) is shaded in light blue, while the super-horizon regime ($k \ll aH$) is shaded in purple.

effectively freeze, leading to a classical spectrum of perturbations on large scales (3.57). The linear nature of their evolution ensures that these fluctuations preserve Gaussianity and remain statistically Gaussian, forming a Gaussian random field at all times. Indeed, a free (non-interacting) quantum field has a ground state that is a Gaussian wavefunctional.

Instead, for a massive or self-interacting scalar field, (3.39) modifies as

$$u_{\mathbf{k}}'' + \left(k^2 + a^2\, m^2 - \frac{a''}{a}\right) u_{\mathbf{k}} = 0. \tag{3.58}$$

In particular, we can substitute $a^2 m^2 = m^2/(H\eta)^2$ into (3.58) which gives a Bessel equation

$$u_{\mathbf{k}}'' - \left(k^2 + \frac{\nu^2 - \frac{1}{4}}{\eta^2}\right) u_{\mathbf{k}} = 0, \tag{3.59}$$

where $\nu = \sqrt{\frac{9}{4} - \frac{m^2}{H^2}}$. Massive fields with $m^2 \geq \frac{9}{4}H^2$ (with $\nu \in \mathbb{C}$) oscillate even on super-horizon scales but are underdamped as the solution scales as $u_k \propto (-\eta)^{\frac{1}{2}} \times (\text{oscillatory terms}) \sim a^{-\frac{1}{2}} \times (\text{oscillatory terms})$, suppressing the generation of perturbations. However, light fields with $m^2 < \frac{9}{4}H^2$ (with $\nu \in \mathbb{R}$) do acquire quantum fluctuations, with a nearly scale-

invariant amplitude evaluated at Hubble crossing. In particular, the inflaton field must be light during inflation, satisfying the slow-roll condition $|\eta| \ll 1$, to allow for the generation of the observed spectrum of primordial fluctuations.

However, to accurately follow the evolution of perturbations from the end of inflation into the radiation-dominated era, it is necessary to account for interactions between fields. Moreover, even in the absence of explicit interactions, gravitational backreaction must still be considered. Indeed, inflaton perturbations generate density perturbations, or more generally, perturbation in the energy-momentum tensor, which is the source for the metric. Hence, there will also be metric perturbations (3.32) which can be split into scalar and tensor parts according to their transformation properties on the spatial hypersurfaces. Vector perturbations S_i and F_i are not important as they decay with the expansion of the Universe [106].

Let us now focus on the scalar perturbation. A convenient gauge which completely fixes the coordinates is the so-called *longitudinal* or *conformal Newtonian* gauge defined by $B = E = 0$ of (3.32) which also corresponds to a basis first introduced in [179]

$$\Phi \equiv A - \frac{d}{dt}\left[a^2\left(\dot{E} - \frac{B}{a}\right)\right], \tag{3.60}$$

$$\Psi \equiv \psi + a^2 H\left(\dot{E} - \frac{B}{a}\right). \tag{3.61}$$

Hence, the perturbed scalar Einstein equations

$$\delta G^{\mu}_{\nu} = 8\pi G\, \delta T^{\mu}_{\nu}, \tag{3.62}$$

relate the scalar metric perturbations to matter perturbations via the energy and momentum constraints [8, 180]

$$3H(\dot{\Psi} + H\Phi) + \frac{k^2}{a^2}(\Psi + H(a^2\dot{E} - aB)) = \frac{1}{2}\delta T^0_0 \equiv -\frac{1}{2}\delta\rho, \tag{3.63}$$

$$\dot{\Psi} + H\Phi = -\frac{1}{2}\delta T^0_i \equiv -\frac{1}{2}\delta q. \tag{3.64}$$

If the matter content does not generate anisotropic stress at linear order in the perturbations (that is, if $\delta T^i_j = 0$ for $i \neq j$), then the two metric perturbation potentials become equal, $\Phi = \Psi$ [180]. Furthermore, we can define two commonly used gauge-invariant quantities constructed from combinations of metric and matter perturbations. The first is the curvature perturbation on uniform-density hypersurfaces, introduced in [165] as

$$-\zeta \equiv \psi + \frac{H}{\dot{\rho}}\delta\rho, \tag{3.65}$$

in the longitudinal gauge. The second is the comoving curvature perturbation [180], which measures the curvature on comoving hypersurfaces

$$\mathcal{R} \equiv \psi - \frac{H}{\rho + P}\delta q. \tag{3.66}$$

By means of (2.23), we can obtain the difference between these two curvature perturbations, which is proportional to the comoving density perturbation [179]

$$-\zeta = \mathcal{R} + \frac{H}{\dot{\rho}}\delta\rho_m, \tag{3.67}$$

where $\delta\rho_m = \delta\rho - 3H\delta q$. It is then possible to express (3.66) in the context of single-field[6] inflation by substituting (3.10) and $\delta q = -\dot{\phi}\delta\phi$, hence

$$\mathcal{R} \equiv \psi + \frac{H}{\dot{\phi}}\delta\phi. \tag{3.68}$$

It is worth noticing that during slow-roll inflation (driven by a single scalar field) $\frac{\delta\rho}{\dot{\rho}} \simeq \frac{\delta\phi}{\dot{\phi}}$ and on large scales we see that $\zeta \simeq -\mathcal{R}$ as $\delta\rho_m \simeq 0$. Alternatively, in [158] it is shown that the same definition arises by combining (3.67) with the gauge-invariant generalisation of the Poisson equation[7]

$$\frac{k^2}{a^2}\Phi = -\frac{1}{2}\delta\rho_m. \tag{3.69}$$

Thus, the power spectrum of scalar curvature perturbations is commonly given by

$$\mathcal{P}_\zeta \equiv \frac{4\pi k^3}{(2\pi)^3}|\zeta|^2. \tag{3.70}$$

This expression is derived following the same steps used for the field operator $\hat{\delta\phi}$, where one starts from the two-point correlation function in Fourier space (3.50) and defines the power spectrum as its amplitude. As we mentioned above, in a de-Sitter spacetime, the spectrum of the inflaton fluctuations is precisely scale-invariant since all modes exit the horizon with the same amplitude. Consequently, during a quasi de-Sitter phase, we expect any scale dependence to be small. This motivates parameterising the primordial scalar power spectrum using a simple power-law form

$$\mathcal{P}_s(k) = A_s\left(\frac{k}{k_*}\right)^{n_s-1}, \tag{3.71}$$

[6] In the contest of multifield inflation, explained in Section 3.3, the expression for the curvature perturbation will be different.

[7] The total matter perturbation in the longitudinal gauge is also called ϵ_m, see [181].

where $A_s = \mathcal{P}_s(k_*)$ is the amplitude evaluated at a chosen pivot scale k_*,

$$n_s - 1 \equiv \frac{d \log \mathcal{P}_s}{d \log k} \tag{3.72}$$

defines the scalar tilt and n_s is known as the spectral index.

On the other hand, tensor perturbations denoted by h_{ij} in (3.32), are defined as being both transverse $\partial^i h_{ij} = 0$ and traceless $\delta^{ij} h_{ij} = 0$. These properties ensure that tensor modes are gauge-invariant. As such, h_{ij} describes the freely propagating degrees of freedom of the gravitational field – namely, gravitational waves – which evolve independently of linear perturbations in matter. We expand any tensor perturbation h_{ij} in terms of the eigenfunctions $e_{ij}^{(P)}(\mathbf{x})$ of the spatial Laplacian, $\nabla^2 e_{ij}^{(P)} = -k^2 e_{ij}^{(P)}$, where k is the comoving wavenumber and $P = \{+, \times\}$ labels the two polarization states[8]. Factoring out the time dependence into a single amplitude $h(t)$ gives

$$h_{ij}(t, \mathbf{x}) = h(t)\, e_{ij}^{(P)}(\mathbf{x}). \tag{3.73}$$

Then, the spatial part of the Einstein equations yields a wave equation for the amplitude

$$\ddot{h} + 3H\dot{h} + \frac{k^2}{a^2} h = 0. \tag{3.74}$$

Following the steps starting from (3.36), we recover the Mukanov equation (3.39). Therefore, summing over the two polarisation states, the dimensionless tensor power spectrum is given by

$$\mathcal{P}_T = 8 \left(\frac{H}{2\pi} \right)^2 \Bigg|_{k=aH}. \tag{3.75}$$

As said before, in the quasi de-Sitter phase any scale dependence is small, so one typically adopts the power-law parametrisation

$$\mathcal{P}_T(k) = A_T \left(\frac{k}{k_*} \right)^{n_T}, \tag{3.76}$$

where $A_T = \mathcal{P}_T(k_*)$, $n_T \equiv \frac{d \ln \mathcal{P}_T}{d \ln k}$ is the tensor tilt and k_* is the chosen pivot scale. Usually, to quantify the relative strength of tensor to scalar perturbations, the ratio

$$r \equiv \frac{A_T}{A_S} \simeq 16 \epsilon_0, \tag{3.77}$$

[8] The decomposition of a perturbation field into Laplacian eigenmodes separates its spatial dependence (encoded in the known eigenfunctions $e^{i\mathbf{k}\cdot\mathbf{x}}$) from its time evolution (given by an ordinary differential equation for the amplitude of each mode).

is used, where ϵ_0 is the first Hubble slow-roll parameter (3.23).

3.3 Multifield inflation

More than four decades after Guth's seminal paper [7], inflation has proven to be remarkably successful and remains the leading paradigm for explaining the early Universe and the Hot Big Bang. Nonetheless, over the years, the simplest single-field models have revealed certain limitations and theoretical challenges. These shortcomings have motivated the scientific community to explore more general and sophisticated frameworks, notably multifield inflationary models.

3.3.1 Why multifield inflation?

A compelling motivation for multifield inflation arises from the sensitivity of inflationary dynamics to Planck-scale physics. Embedding inflation within a UV-complete framework often leads to an enriched particle spectrum, challenging the assumption that a single field governs the early Universe's dynamics. This has important implications for key observables such as the scalar spectral index n_s, the tensor-to-scalar ratio r, and primordial non-Gaussianities. Moreover, recent swampland conjectures [182] suggest that many single-field inflationary models may not be consistent with theories of quantum gravity. In particular, they constrain the scalar potential through the condition $|\nabla V| \geq c\, V/M_{\rm P}$, which disfavours the flat potentials typically used in slow-roll inflation. Multifield models, especially those involving curved (non-geodesic) trajectories in field space, have been shown to evade these constraints [183], providing a more robust theoretical foundation.

While current observations are consistent with single-field inflation, they do not exclude the presence of additional fields. Many multifield models yield observational predictions that are degenerate with the single-field case, motivating the need for next-generation experiments. Future missions such as CMB-S4 [184], LiteBIRD [185], Simons Observatory [186], and PICO [187] aim to detect B-mode polarisation in the CMB – a potential imprint of primordial gravitational waves. Large-scale structure surveys such as DESI [188], LSST [189], Euclid, and SKA [190] may also uncover signatures of primordial non-Gaussianities [191], offering further tests of multifield dynamics.

To be precise, high-energy theories that attempt to extend the Standard Model – such as string theory and supergravity – generically predict the presence of multiple scalar fields. These include compactification moduli, axions, Kaluza-Klein modes, and gauge fields [192]. This provides additional theoretical motivation for multifield inflation as a

motivated scenario.

Given these theoretical challenges and observational prospects, the study of multifield inflation has gained substantial attention in the past two decades. In the following section, we introduce the core formalism of multifield inflation, focusing on the new dynamical features that emerge from the presence of multiple interacting scalar fields. Two essential ingredients that distinguish these models from their single-field counterparts are the geometry of field space and the structure of the multifield potential, both of which can crucially affect inflationary dynamics and observables.

3.3.2 Multifield dynamics and perturbations

Extending the framework of inflation from a single field to a multifield scenario introduces two key new elements: the *field-space geometry* and the structure of the *multifield potential*. While these features enrich the inflationary dynamics and may lead to novel observational signatures, they can also introduce new issues related to fine-tuning. Analyses of this kind are usually motivated by phenomenology. The most straightforward expression for a general multifield inflationary model can be formulated as [193, 194]

$$S = \int d^4x\sqrt{-g}\left(\frac{R}{2} - \frac{1}{2}\mathcal{G}_{IJ}(\phi)\partial_\mu\phi^I\partial^\mu\phi^J - V(\phi^K)\right), \tag{3.78}$$

where the indices IJ and K stand for multiple scalar fields, $\mathcal{G}_{IJ}$ is the field-space metric that depends on the value of one scalar field, and $V(\phi^K)$ is the scalar potential. In a spatially flat FLRW Universe (2.3), the background equations of motion are given by (see, *e.g.* [194])

$$3H^2 = \frac{1}{2}\dot\sigma^2 + V, \tag{3.79}$$

$$\dot H = -\frac{1}{2}\dot\sigma^2, \tag{3.80}$$

$$D_t\dot\phi^I + 3H\dot\phi^I + \mathcal{G}^{IJ}V_J = 0, \tag{3.81}$$

where $V_J \equiv \partial V/\partial\phi^J$, and the total kinetic energy of the fields is defined with the average field

$$\dot\sigma^2 \equiv \mathcal{G}_{IJ}\dot\phi^I\dot\phi^J. \tag{3.82}$$

The covariant time derivative is defined by $D_tA^I \equiv \dot A^I + \Gamma^I_{JK}\dot\phi^J A^K$, where Γ^I_{JK} are the Christoffel symbols associated with the field-space metric. In particular, by considering a two-field model ϕ^K=$\{\phi, \chi\}$ and $\mathcal{G}_{IJ}(\phi) = \mathrm{diag}\{1, e^{2b(\phi)}\}$ with the exponential function

ensuring that the kinetic term does not change sign; (3.81) read as

$$\ddot{\phi} + 3H\dot{\phi} + V_\phi = b_\phi e^{2b}\dot{\chi}^2, \tag{3.83}$$

$$\ddot{\chi} + (3H + 2b_\phi\dot{\phi})\dot{\chi} + e^{-2b}V_\chi = 0. \tag{3.84}$$

As first introduced in [27, 193] (see also [195]), we adopt an orthonormal basis in field space to aid in interpreting the evolution and interplay of cosmological perturbations. In this basis, field-dependent quantities are decomposed into what are known as adiabatic and entropy components. An adiabatic perturbation corresponds to a shift of all fields (or all components of a fluid) in the same way so that their relative composition stays the same. An entropy perturbation changes the relative contributions of different fields. In other words, adiabatic perturbations seed curvature (metric) perturbations leading to structure formation (as we will see later) while entropy perturbations can convert into curvature perturbations in later phases. For the two-dimensional field space $\mathcal{G}_{IJ}$ defined above, the corresponding unit vectors forming this basis are

$$\mathbf{u}^I_\sigma \equiv \frac{1}{\dot{\sigma}}(\dot{\phi}, \dot{\chi}), \qquad \mathbf{u}^I_s \equiv \frac{e^{-b}}{\dot{\sigma}}(\dot{\chi}, \dot{\phi}), \tag{3.85}$$

where $\mathbf{u}^I_\sigma$ is tangent to the field trajectory in field space (defining the adiabatic component) and $\mathbf{u}^I_s$ is the orthogonal to it (defining the entropy component). By construction, they satisfy

$$\mathbf{u}^I_\sigma \mathbf{u}_{\sigma J} + \mathbf{u}^I_s \mathbf{u}_{sJ} = \delta^I_J. \tag{3.86}$$

Therefore, from (3.82) we have $\dot{\sigma}^2 \equiv \dot{\phi}^2 + e^{2b}\dot{\chi}^2$ and the adiabatic field reads as

$$d\sigma = \cos\theta\, d\phi + \sin\theta\, e^b\, d\chi, \tag{3.87}$$

in which $\cos\theta = \dot{\phi}/\dot{\sigma}$ and $\sin\theta = e^b\dot{\chi}/\dot{\sigma}$. In this notation, following [196] for convenience, the unit vectors that satisfy (3.86) are

$$\mathbf{u}^I_\sigma = (\cos\theta, e^{-b}\sin\theta), \quad \mathbf{u}^I_s = (-\sin\theta, e^{-b}\cos\theta). \tag{3.88}$$

Here, θ denotes the rotation angle relative to the tangent of the background field trajectory, see Figure 3.4. Using this formalism, we define the adiabatic and entropy perturbations, denoted by $\delta\sigma$ and δs, respectively, as

$$\delta\sigma = \mathbf{u}^I_\sigma\, \delta\phi^I, \tag{3.89}$$

$$\delta s = \mathbf{u}^I_s\, \delta\phi^I. \tag{3.90}$$

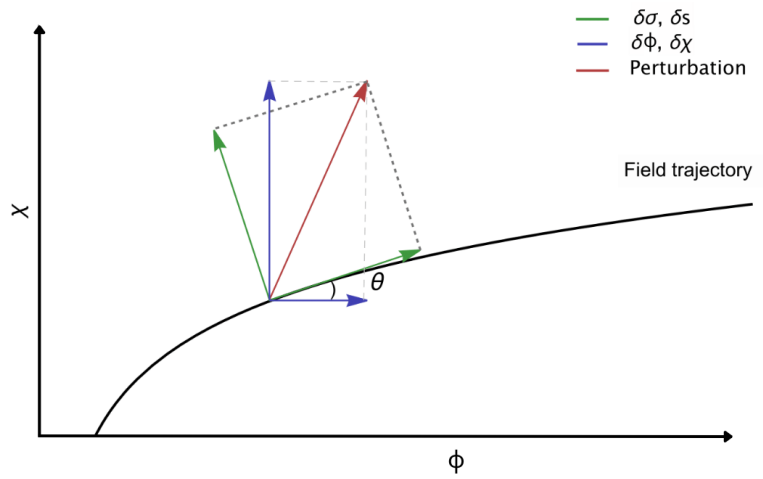

Figure 3.4: Illustration of a decomposition of a perturbation (red) into adiabatic ($\delta\sigma$) and entropy (δs) component (green) in field space. The usual perturbation components (blue) along the ϕ and χ axes are also shown.

Moreover, one can define derivatives of the potential along the adiabatic and entropy directions as follows

$$V_\sigma = \mathbf{u}_\sigma^I V_I, \qquad V_s = \mathbf{u}_s^I V_I, \tag{3.91}$$

$$V_{\sigma\sigma} = \mathbf{u}_\sigma^I \mathbf{u}_\sigma^J V_{IJ}, \qquad V_{ss} = \mathbf{u}_s^I \mathbf{u}_s^J V_{IJ}, \qquad V_{\sigma s} = \mathbf{u}_\sigma^I \mathbf{u}_s^J V_{IJ}. \tag{3.92}$$

With some manipulation, (3.81) can be recast as (see [197])

$$\ddot{\sigma} + 3H\dot{\sigma} + V_\sigma = 0. \tag{3.93}$$

In addition, the contribution of the entropy field is given by

$$\dot{\theta} = -\frac{V_s}{\dot{\sigma}} - b_\phi \dot{\sigma} \sin\theta. \tag{3.94}$$

The quantity (3.94) is commonly referred to as the turn rate of the trajectory in field space, while the corresponding dimensionless parameter characterising the deviation of the background trajectory from a field space geodesic is

$$\eta_\perp = -\frac{V_s}{H\dot{\sigma}}. \tag{3.95}$$

Making use of (3.83) and (3.84) we now write the linear perturbation equations (3.34) in the longitudinal gauge (3.61) for the fields ([193, 198–201])

$$\ddot{\delta\phi} + 3H\dot{\delta\phi} + \left(\frac{k^2}{a^2} + V_{\phi\phi} - (b_{\phi\phi} + 2b_\phi^2)\,\dot{\chi}^2\, e^{2b}\right)\delta\phi + V_{\phi\chi}\delta\chi - 2b_\phi e^{2b}\dot{\chi}\dot{\delta\chi} = 4\dot{\phi}\dot{\Phi} - 2V_\phi\Phi, \tag{3.96}$$

$$\begin{aligned}\ddot{\delta\chi} + (3H + 2b_\phi\dot{\phi})\dot{\delta\chi} + \left(\frac{k^2}{a^2} + e^{-2b}V_{\chi\chi}\right)\delta\chi + 2b_\phi\dot{\chi}\dot{\delta\phi} \\ + e^{-2b}\left(V_{\chi\phi} - 2b_\phi V_\chi + 2b_{\phi\phi}\dot{\phi}\dot{\chi}\right)\delta\phi = 4\dot{\chi}\dot{\Phi} - 2e^{-2b}V_\chi\Phi,\end{aligned} \tag{3.97}$$

Then, the energy and the momentum constraint equations (3.64) are, respectively

$$3H\left(\dot{\Phi} + H\Phi\right) + \dot{H}\Phi + \frac{k^2}{a^2}\Phi = -\frac{1}{2}\left[\dot{\phi}\,\dot{\delta\phi} + e^{2b}\dot{\chi}\,\dot{\delta\chi} + b_\phi e^{2b}\dot{\chi}^2\delta\phi + V_\phi\delta\phi + V_\chi\delta\chi\right], \tag{3.98}$$

$$\dot{\Phi} + H\Phi = \frac{1}{2}\left(\dot{\phi}\,\delta\phi + e^{2b}\dot{\chi}\,\delta\chi\right) = \frac{1}{2}\dot{\sigma}\,\delta\sigma. \tag{3.99}$$

From (3.68), the dimensionless comoving curvature[9] and isocurvature perturbations are given by

$$\zeta \equiv \frac{H}{\dot{\sigma}}\delta\sigma, \qquad \mathcal{S} \equiv \frac{H}{\dot{\sigma}}\delta s. \tag{3.100}$$

Note that perturbations that satisfy $\delta s = 0$ (*i.e.* a purely local shift along the background path) are only adiabatic and isocurvature perturbations are automatically gauge-invariant. We also point out that expressing (3.100) in a dimensionless form is needed to ensure meaningful physical interpretation and comparison with observable quantities like the CMB power spectrum.

We can also express the first of (3.100) in terms of the metric perturbation Φ [204], by rearranging (3.99) and using (3.80); this yields

$$\zeta = \Phi + \frac{H}{\dot{H}}(\dot{\Phi} + H\Phi). \tag{3.101}$$

Its evolution equation is

$$\dot{\zeta} = \frac{k^2}{a^2}\frac{H}{\dot{H}}\Phi - 2\frac{V_s}{\dot{\sigma}}\mathcal{S}, \tag{3.102}$$

and means that on super-horizon scales (*i.e.* $k/a \to 0$), the isocurvature mode is a source for the curvature perturbation. The coupling between adiabatic and isocurvature perturbations does not vanish on super-Hubble scales even when $\dot{\theta} = 0$ because of the presence of the extra term in (3.94) given by b_ϕ. This behavior differs from the case of scalar fields

[9] Note that in the literature one often finds that the symbol ζ is (mis)used to refer to the comoving curvature perturbation, particularly on super-horizon scales, due to its conservation properties – such as adiabatic modes – and widespread adoption in nonlinear and δN formalisms [202, 203].

with canonical kinetic term, as discussed in [205], where the adiabatic (curvature) and isocurvature modes decouple when $\dot{\theta} = 0$, see (3.94). To derive the equation governing the entropy perturbation δs, we differentiate (3.90) twice with respect to time and make use of (3.96) and (3.97) as well as the comoving matter perturbation (3.69) [179]. Moreover, taking into account (3.102) we finally obtain

$$\ddot{\delta s} + 3H\dot{\delta s} + \left(\frac{k^2}{a^2} + V_{ss} + 3\dot{\theta}^2 + b_\phi^2 g(t) + b_\phi f(t) - b_{\phi\phi}\dot{\sigma}^2 - 4\frac{V_s^2}{\dot{\sigma}^2}\right)\delta s = 2\frac{V_s}{H}\dot{\zeta}, \tag{3.103}$$

where the following notation is used

$$g(t) = -\dot{\sigma}^2(1 + 3\sin^2\theta) \tag{3.104a}$$

$$f(t) = V_\phi(1 + \sin^2\theta) - 4V_s\sin\theta, \tag{3.104b}$$

along with the definition of (3.92). It is evident from (3.103) that adiabatic and entropy perturbation modes interact. Indeed, (3.103) describes how the entropy mode evolves due to sourcing from the adiabatic component [193]. In other words, we can rewrite the right hand side of (3.103) using (3.95) and show that the modes are coupled in the presence of a non-zero bending of the trajectory ($\eta_\perp \neq 0$). Thus, at leading order in the slow-roll approximation, the dimensionless squared mass of the entropic mode is

$$\frac{m_s^2}{H^2} \equiv \frac{V_{;ss}}{H^2} + \epsilon_0 M_{\rm P}^2 R_{\rm fs} - \eta_\perp^2, \tag{3.105}$$

where the projection of the covariant Hessian of the potential along the entropic direction is given by $V_{;ss} = \mathbf{u}_s^I\mathbf{u}_s^J(V_{IJ} - \Gamma_{IJ}^K V_K)$ where Γ_{IJ}^K are the Christoffel symbols associated with the field-space metric. The quantity $R_{\rm fs}$ denotes the Ricci scalar of the field-space manifold. When the kinetic energy density, $\epsilon_0 H^2$, becomes sufficiently large during inflation, a negative field-space Ricci scalar $R_{\rm fs}$ can cause the effective mass of the entropy field to turn negative. This, in turn, may lead to a geometrical destabilisation [206]. In such a scenario, the entropy perturbation becomes tachyonic, destabilising the background trajectory. As a result, inflation may terminate earlier than expected, potentially altering the predicted inflationary observables [206]. Alternatively, the geometrical instability can steer the system away from its original path, redirecting it along a new, side-tracked trajectory in field space [197, 207, 208].

In Chapter 4, we will go beyond the work in the literature, allowing the kinetic coupling to depend on both fields. Our aim is to study adiabatic and isocurvature perturbations in such extended theories and test them with observations.

3.4 Modified gravity and inflation

Modified gravity theories extend or generalise GR by incorporating additional degrees of freedom or geometric structures, as discussed in Chapter 1. These modifications often arise in attempts to reconcile gravity with quantum field theory, explain the late-time cosmic acceleration without invoking dark energy, or generate inflationary dynamics from purely gravitational effects.

This part of the thesis focuses on the role of modified gravity in the context of inflation. A central example is Starobinsky inflation [209], one of the earliest and most compelling models of inflation based on a modification of the Einstein-Hilbert action. The idea is to generate inflation through a purely "quantum-gravitational" effect, by considering the case of a FLRW universe filled with massless conformally invariant quantum fields [210, 211]. Because of conformal invariance – the symmetry under local rescaling of the metric and corresponding field transformations, see footnote 4 – these massless fields do not undergo particle creation, so the stress-energy tensor is only made of terms that arise from the interaction of quantum free matter fields with a classical gravitational field. Those terms are quadratic in the space-time curvature [212, 213], and give rise to a non-vanishing expectation value for the effective stress-energy tensor, $\langle T_{\mu\nu} \rangle$ which, in the context of semi-classical gravity, sources the Einstein equations. Not only does this model arise naturally from quantum corrections to gravity, but it also provides predictions that remain in excellent agreement with current cosmological observations [9], such as the scalar spectral index n_s, and tensor-to-scalar ratio, r.

Starobinsky inflation is characterised by an $f(R)$ action of the form

$$S = \frac{M_{\rm P}^2}{2} \int d^4x \sqrt{-g} \left(R + \frac{1}{\mu^2} R^2 \right), \tag{3.106}$$

where μ is a model parameter with dimensions of mass. At low curvatures, the higher-order correction remains subdominant and thus effectively hidden. This behavior becomes clear when transitioning to the EF, where the additional scalar degree of freedom arising from the R^2 term is recast as a scalar field ϕ. Following the procedure outlined in Subsection 1.2.1, the action takes the form

$$S = \int d^4x \sqrt{-g} \left[\frac{M_{\rm P}^2}{2} R - \frac{1}{2} g^{\mu\nu} \partial_\mu \phi \, \partial_\nu \phi - \frac{M_{\rm P}^2 \mu^2}{4} \left(1 - e^{-\sqrt{\frac{2}{3}} \frac{\phi}{M_{\rm P}}} \right)^2 \right]. \tag{3.107}$$

The potential in (3.107) is flat for large values of ϕ, supporting a slow-roll inflationary phase as discussed in Subsection 3.1.2. The number of e-folds N (3.16), is calculated by

integrating the slow-roll equation

$$N \approx \int_{\phi_{\rm end}}^{\phi_i} \frac{V}{V'}\frac{d\phi}{M_{\rm P}^2} \approx \frac{3}{4} e^{\sqrt{\frac{2}{3}}\frac{\phi_i}{M_{\rm P}}}, \tag{3.108}$$

assuming $\phi_i/M_{\rm P} \gg 1$. Inverting this relation gives the field value in terms of N, allowing us to compute the slow-roll parameters (3.23) as

$$\epsilon_V \approx \frac{3}{4N^2}, \tag{3.109}$$

$$\eta_V \approx \frac{1}{N}. \tag{3.110}$$

These in turn lead to predictions for the observable inflationary parameters (3.72), (3.77) as

$$n_s \approx 1 - 6\epsilon_V + 2\eta_V \approx 1 - \frac{2}{N}, \tag{3.111}$$

$$r \approx 16\epsilon_V \approx \frac{12}{N^2}. \tag{3.112}$$

For $N \simeq 55$, these yield $n_s \approx 0.965$ and $r \approx 0.0037$ in excellent agreement with the latest Planck satellite data [9, 51]. The success of these predictions with minimal assumptions and parameters makes the Starobinsky model a benchmark in inflationary cosmology and a compelling candidate for describing the physics of the early Universe. The model presented above is also taken as a reference model for comparison with alternative scenarios. In particular, in Chapter 5 we examine a scale-invariant inflationary model and compare its predictions with those of the Starobinsky model. The aim is to test the consistency and observational viability of both models against the latest cosmological data, especially those derived from the CMB. As we will see, this comparison allows us to assess whether the scale-invariant framework offers any theoretical or observational advantages over the well-established Starobinsky paradigm.

3.5 Alternatives to inflation

While cosmic inflation has been the prevailing paradigm for explaining the early Universe's rapid expansion and the origin of large-scale structures, several alternative models have been proposed that challenge or bypass the need for an inflationary epoch. Among these, cyclic cosmologies offer compelling frameworks wherein the universe undergoes endless sequences of expansions and contractions, effectively eliminating the concept of a singular beginning. One prominent example is the ekpyrotic model, in-

troduced by Khoury, Ovrut, Steinhardt, and Turok in [34]. Rooted in string theory and higher-dimensional brane cosmology, this model posits that our observable Universe resides on a four-dimensional brane that periodically collides with a parallel brane in a higher-dimensional space. Each collision corresponds to a "Big Bang", initiating a new cycle of cosmic evolution. During the slow contraction phase preceding each bounce, the universe becomes homogeneous, isotropic, and flat, addressing the horizon and flatness problems without invoking a rapid inflationary expansion. Moreover, the ekpyrotic scenario predicts a nearly scale-invariant spectrum of cosmological perturbations, aligning with observations of the CMB.

Building upon the ekpyrotic framework, Steinhardt and Turok proposed a more comprehensive cyclic model in [35]. In this scenario, the universe undergoes an infinite sequence of cycles, each comprising a period of expansion, followed by contraction, and culminating in a bounce that initiates the next cycle. A key feature of this model is the role of dark energy, which drives the current accelerated expansion and sets the stage for the subsequent contraction phase. This cyclic approach not only addresses the initial conditions problem but also provides a mechanism for entropy dilution, ensuring that each cycle begins under similar conditions.

Another noteworthy alternative is Conformal Cyclic Cosmology (CCC), proposed by Roger Penrose [214]. In CCC, the universe is envisioned as a succession of "aeons", where the infinite future of one aeon becomes the Big Bang of the next through a conformal rescaling of spacetime. This model suggests that information could, in principle, be transmitted from one aeon to the next, potentially leaving imprints in the CMB. Penrose and Gurzadyan have claimed to identify concentric low-variance circles in the CMB data from WMAP and BOOMERANG experiments, which they interpret as evidence supporting CCC [215]. However, these claims remain controversial within the cosmological community [216].

Beyond cyclic models, other alternatives to inflation include bouncing cosmologies [32, 217, 218], where the universe undergoes a contraction phase followed by a bounce leading to expansion, and string gas cosmology [219] which attributes early-universe dynamics to thermal fluctuations in a pre-Big Bang string phase. While these models offer intriguing mechanisms for addressing the shortcomings of the standard inflationary model, they often face challenges in matching the full range of cosmological observations as precisely as inflation. Nevertheless, they continue to stimulate active research, particularly in contexts where quantum gravity, higher-dimensional theories, or scale invariance play a central role.

In Chapter 7, we continue along this path of exploring alternatives to inflation by studying the production and evolution of primordial gravitational waves in a cyclic uni-

verse, as detailed in our recent work [6]. Building on the foundations of ekpyrotic and cyclic models, we investigate whether the predictions for tensor perturbations are sensitive to the phase in which initial conditions are imposed, and how different choices of vacuum state influence the resulting spectrum. Unlike previous studies, which typically begin in the ekpyrotic phase and assume a Bunch-Davies vacuum (3.48), our analysis starts in the dark energy phase of the preceding cycle, making no prior assumptions about the vacuum. This broader approach allows us to assess the resilience of gravitational wave predictions across cycles and to derive stringent constraints on allowable deviations from the standard vacuum state. In doing so, we aim to clarify the theoretical robustness of cyclic cosmologies and contribute to the broader effort of evaluating viable alternatives to inflationary theory.

Part II | Beyond standard inflation

4 | Multifield inflation with kinetic couplings

As discussed in *Part I*, two-field models of inflation have emerged as a theoretically well-motivated extension of the single-field paradigm, offering a richer dynamics and a broader range of observational signatures [27, 220]. While the simplest models already exhibit novel features – such as the generation of isocurvature modes and trajectory-dependent perturbation evolution – they represent only a subset of the broader class of multifield theories inspired by high-energy physics. In particular, effective field theories arising from string theory, and other ultraviolet completions naturally predict non-trivial, curved field-space geometries where the field-space metric can depend on multiple fields simultaneously [150, 195, 221, 222]. Capturing the full implications of these geometries for inflationary dynamics and observables is currently an active field of research [206, 223, 224] (*e.g.* non trivial field space metric can alter the predictions for isocurvature perturbations, gravitational waves, peaks in power spectrum).

This chapter advances the discussion by presenting a generalised formalism for a two-field system in which the field-space metric is allowed to depend non-trivially on both fields. It is based on [1] and [2] and represents a substantial extension beyond previous treatments considered in *Part I*. Our formalism enables a more accurate and flexible treatment of inflationary dynamics in curved field spaces, including scenarios with strong turning trajectories and non-canonical kinetic couplings. Therefore, our goal is to exploit this formalism to derive analytical expressions for key inflationary observables. Moreover, the computational framework developed in this work evolves the full background and linear perturbation equations numerically in the slow-roll approximation, accurately tracks the coupled evolution of adiabatic and isocurvature modes on superhorizon scales, and implements the transfer matrix formalism to propagate initial conditions to late-time observables. These predictions are then interfaced with a Boltzmann integrator code, enabling a consistent comparison with cosmological data. Moreover, to compare this broad class of models with observations, we introduce a new sampling algorithm designed to efficiently explore high-dimensional parameter spaces,

accounting for the increased model complexity introduced by the general field-space dependence. Therefore, this chapter marks a key methodological development, extending the scope of multifield inflationary analyses beyond conventional assumptions and laying the groundwork for studies of more realistic inflationary scenarios motivated by fundamental theories.

The structure of the chapter is as follows. In Section 4.1 we define the theoretical framework, specifying the generalised field-space metric and associated background dynamics in Section 4.2. In Section 4.3 we outline the numerical methods used to evolve the system and compute inflationary observables; we describe the sampling strategy and its interfacing with the Boltzmann code; we apply this pipeline to a concrete example and discuss the resulting constraints.

4.1 Field equations and perturbations

The dynamics of the two-field model is governed by the action

$$S = \int d^4x\sqrt{-g}\left[\frac{R}{2} - \frac{1}{2}\mathcal{G}_{IJ}\, g^{\mu\nu}\partial_\mu\phi^I\partial_\nu\phi^J - V(\phi^I)\right], \tag{4.1}$$

with $\phi^I = \{\psi, \chi\}$ and a field-space metric $\mathcal{G}_{IJ}$ that depends on both fields. Such an action naturally arises when one begins in the JF with a nonminimal coupling $f(\psi, \chi)R$ – following the same footing of Subsection 1.2.1, in particular (1.23) – and performs a conformal transformation to the EF, yielding

$$\mathcal{G}_{IJ} = \frac{1}{2f}\delta_{IJ} + \frac{3}{2}\, h_{,I}h_{,J}, \qquad f = e^{h(\psi,\chi)}, \tag{4.2}$$

and $h(\psi, \chi)$ is any function of the fields. By an appropriate choice of field coordinates [225] this can be diagonalised to

$$\mathcal{G}_{IJ} = \begin{pmatrix} 1 & 0 \\ 0 & F(\psi, \chi) \end{pmatrix}, \tag{4.3}$$

resembling polar coordinates on the field manifold. While earlier studies have almost universally taken $F = F(\psi)$ [193, 196, 200, 225–227], our work considers the more general case $F = F(\psi, \chi)$ with dependence on both fields. This introduces an intrinsic coupling in the kinetic sector that can not be removed by simple field redefinitions, when F is taken to be a product function. This generalisation is both well-motivated by ultraviolet completions of gravity [192, 228] and crucial for capturing the full dynamics of curved field-space inflation [200, 221, 223]. To simplify the calculations and to be in line with

the literature [225], we write $F(\psi, \chi) = e^{2b(\psi,\chi)}$. In what follows, we drop the explicit ψ, χ arguments of b and the commas indicating partial derivatives, for brevity.

We begin by considering a flat FLRW Universe (2.3), and proceed by deriving the equations of motion from (4.1) for the homogeneous background

$$\ddot{\psi} + 3H\dot{\psi} + V_\psi = e^{2b} b_\psi \dot{\chi}^2, \tag{4.4}$$

$$\ddot{\chi} + (3H + 2b_\psi \dot{\psi} + b_\chi \dot{\chi})\dot{\chi} = -e^{-2b} V_\chi, \tag{4.5}$$

whereas the Friedmann equations (2.25) read

$$H^2 = \frac{1}{3}\left(\frac{1}{2}\dot{\psi}^2 + \frac{1}{2}e^{2b}\dot{\chi}^2 + V(\psi, \chi)\right), \tag{4.6}$$

$$\dot{H} = -\frac{1}{2}\left(\dot{\psi}^2 + e^{2b}\dot{\chi}^2\right). \tag{4.7}$$

To study the evolution of the field perturbations, it is convenient to move to Fourier space. The equations of motion in the Newtonian gauge are given by

$$\begin{aligned} &\ddot{\delta\psi} + 3H\dot{\delta\psi} + \left[\frac{k^2}{a^2} + V_{\psi\psi} - e^{2b}(b_{\psi\psi} + 2b_\psi^2)\dot{\chi}^2\right]\delta\psi \\ &\quad - 2b_\psi e^{2b}\dot{\chi}\dot{\delta\chi} + \left[V_{\psi\chi} - e^{2b}(b_{\psi\chi} + 2b_\psi b_\chi)\dot{\chi}^2\right]\delta\chi = 4\dot{\Phi}\dot{\psi} - 2V_\psi\Phi, \end{aligned} \tag{4.8}$$

$$\begin{aligned} &\ddot{\delta\chi} + (3H + 2b_\psi\dot{\psi} + 2b_\chi\dot{\chi})\,\dot{\delta\chi} + \left[\frac{k^2}{a^2} + e^{-2b}(V_{\chi\chi} - 2V_\chi b_\chi) + b_{\chi\chi}\dot{\chi}^2 + 2b_{\chi\psi}\dot{\psi}\dot{\chi}\right]\delta\chi \\ &\quad + 2b_\psi\dot{\chi}\dot{\delta\psi} + [2b_{\psi\psi}\dot{\psi}\dot{\chi} + e^{-2b}(V_{\chi\psi} - 2b_\psi V_\chi) + b_{\psi\chi}\dot{\chi}^2]\delta\psi = 4\dot{\Phi}\dot{\chi} - 2\Phi e^{-2b}V_\chi. \end{aligned} \tag{4.9}$$

The perturbed Einstein equations (3.62) give

$$\begin{aligned} &3H(\dot{\Phi} + H\Phi) + \dot{H}\Phi + \frac{k^2}{a^2}\Phi \\ &= -\frac{1}{2}\left[\dot{\psi}\dot{\delta\psi} + e^{2b}\dot{\chi}\dot{\delta\chi} + e^{2b}\dot{\chi}^2(b_\psi\delta\psi + b_\chi\delta\chi) + V_\chi\delta\chi + V_\psi\delta\psi\right], \end{aligned} \tag{4.10}$$

$$\dot{\Phi} + H\Phi = \frac{1}{2}\left[\dot{\psi}\delta\psi + e^{2b}\dot{\chi}\delta\chi\right]. \tag{4.11}$$

The other important quantity is the comoving curvature perturbation (3.101), which can be recast in terms of the fields

$$\zeta = \Phi + H\left(\frac{\dot{\psi}\delta\psi + e^{2b}\dot{\chi}\delta\chi}{\dot{\psi}^2 + e^{2b}\dot{\chi}^2}\right). \tag{4.12}$$

Its evolution (3.102) is given by

$$\begin{aligned}\dot{\zeta} &= \frac{k^2}{a^2}\frac{H}{\dot{H}}\Phi - 2\frac{V_s}{\dot{\sigma}}\mathcal{S} \\ &= \frac{k^2}{a^2}\frac{H}{\dot{H}}\Phi - 2H\left(\frac{V_\psi\dot{\psi}\dot{\chi}^2 e^{2b} - V_\chi\dot{\chi}\dot{\psi}^2}{(\dot{\psi}^2 + e^{2b}\dot{\chi}^2)^2}\right)\left(\frac{\delta\psi}{\dot{\psi}} - \frac{\delta\chi}{\dot{\chi}}\right) \\ &\equiv \frac{k^2}{a^2}\frac{H}{\dot{H}}\Phi - H\left[\frac{1}{2}\frac{d}{dt}\left(\frac{e^{2b}\dot{\chi}^2 - \dot{\psi}^2}{e^{2b}\dot{\chi}^2 + \dot{\psi}^2}\right) + \dot{C}\right]\left(\frac{\delta\psi}{\dot{\psi}} - \frac{\delta\chi}{\dot{\chi}}\right),\end{aligned} \tag{4.13}$$

where

$$\dot{C} = \frac{2}{\dot{\sigma}^2}\left(b_\psi\dot{\psi}\dot{\chi}^2 e^{2b}\right) = 2b_\psi\dot{\psi}\sin^2\theta. \tag{4.14}$$

Here we used (4.4), (4.5), (4.10), (4.11) and the relation

$$\frac{\delta\psi}{\dot{\psi}} - \frac{\delta\chi}{\dot{\chi}} \equiv -\frac{\dot{\sigma}e^{-b}}{\dot{\psi}\dot{\chi}}\delta s. \tag{4.15}$$

We note that the frictional damping (4.14) of the χ field by ψ is the same obtained by [193] in the case of $b = b(\psi)$.

As in Subsection 3.3.2, we now rotate our field basis from $\{\psi, \chi\}$ to the tangent and normal directions along the background trajectory, namely (3.85) which naturally separates adiabatic and isocurvature perturbations. Hence, the inflationary dynamics can be described by σ and θ, (3.93) and (3.94) respectively. It is important to note that, also here, the structure of (3.93) and (3.94) is the very same as in the case for $b = b(\psi)$ since ψ has a canonical kinetic term and χ does not (see (4.3)). However, the assumption of having $b(\phi^I)$, with $I = \{1, 2\}$, affects the feeding of the curvature perturbations indirectly, as we will show below. In this generalisation, (3.103) reads as

$$\begin{aligned}&\ddot{\delta s} + 3H\dot{\delta s} + \left(\frac{k^2}{a^2} + V_{ss} + 3\dot{\theta}^2 - \dot{\sigma}^2 b_{\psi\psi} + b_\psi^2\tilde{g}(t) + b_\psi\tilde{f}(t) + b_\chi\tilde{l}(t) - 4\frac{V_s^2}{\dot{\sigma}^2}\right)\delta s \\ &\quad = \frac{2V_s}{H}\dot{\zeta},\end{aligned} \tag{4.16}$$

where now

$$\tilde{g}(t) = -\dot{\sigma}^2(1 + 3\sin^2\theta), \tag{4.17a}$$

$$\tilde{f}(t) = V_\psi(1 + \sin^2\theta) - 4V_s\sin\theta, \tag{4.17b}$$

$$\tilde{l}(t) = -e^{-2b}\cos^2\theta V_\chi. \tag{4.17c}$$

The additional dependence of the field metric on χ enters only indirectly via the evolution of the fields. In the case of (4.16), there is an explicit dependence on b_χ, changing

the effective mass of the entropy perturbation δs.

Before applying these equations to the slow-roll regime and to specific models, it is instructive to relate our findings to other formulations in the literature. Although a comprehensive comparison lies beyond the scope of this work, one can envisage constructing a "dictionary" between our approach and the more geometric treatments, for example those described in [183, 225, 229]. As a concrete example, we compare our expression for the effective mass of the entropy perturbation with the result derived in [229] for a multifield model (3.105). In our parametrisation we find (3.95) becomes

$$\eta_\perp = \frac{\dot{\theta}}{H} + b_\psi \frac{\dot{\sigma}}{H} \sin\theta, \tag{4.18}$$

while the projection of the covariant Hessian of the potential along the entropic direction reads

$$V_{;ss} = V_{ss} + 2b_\psi e^{-b} \sin\theta\cos\theta V_\chi + b_\psi(1-\sin^2\theta)V_\psi - b_\chi e^{-2b}\cos^2\theta V_\chi, \tag{4.19}$$

and the Ricci scalar of the field space is

$$R_{\rm fs} = -2\left(b_\psi^2 + b_{\psi\psi}\right). \tag{4.20}$$

We highlight that the Ricci scalar depends only on derivatives with respect to ψ, not on the derivatives with respect to χ. Collecting terms and considering the super-horizon scales, yields

$$m^2_{s(\rm eff)} = V_{;ss} + \epsilon_0 M_{\rm P}^2 R_{\rm fs} H^2 - \eta_\perp^2 H^2 \equiv V_{ss} + 3\dot{\theta}^2 - \dot{\sigma}^2 b_{\psi\psi} + b_\psi^2 \tilde{g}(t) + b_\psi \tilde{f}(t) + b_\chi \tilde{l}(t), \tag{4.21}$$

where $\tilde{g}(t)$, $\tilde{f}(t)$, $\tilde{l}(t)$ are time-dependent functions whose explicit forms follow from (4.19). In particular, the term proportional to b_χ traces back to the non-trivial projection in (4.19), and its sign is determined by the product $b_\chi V_\chi$. As we will show below, in the slow-roll approximation this contribution can be related directly to the velocity of the χ field.

When the kinetic energy parameter $\epsilon_0 H^2 M_{\rm Pl}^2$ grows sufficiently during inflation and $R_{\rm fs} < 0$, the effective mass (4.21) can turn tachyonic, leading to geometric destabilisation, as discussed in Subsection 3.3.2. In the models studied here, however, turns in the field trajectory occur only towards the end of inflation, when entropy fluctuations have already decayed sufficiently. Having established the exact evolution equations for curvature and entropy perturbations, we now proceed to their large-wavelength limit in the slow-roll regime.

As noted in Subsection 3.1.2, we adopt the slow–roll approximation for both scalar fields, under which

$$\begin{aligned} \epsilon_0 \equiv -\frac{\dot{H}}{H^2} \ll 1 \quad &\Longrightarrow \quad \mathcal{G}_{IJ}\dot{\phi}^I\,\dot{\phi}^J \ll V(\phi^I), \\ \epsilon_1 \equiv \frac{\dot{\epsilon}_0}{H\,\epsilon_0} \ll 1 \quad &\Longrightarrow \quad 2\dot{\phi}^I D_t\dot{\phi}_I \ll H\mathcal{G}_{IJ}\,\dot{\phi}^I\,\dot{\phi}^J, \end{aligned} \tag{4.22}$$

and thus we do not consider scenarios like hyperinflation, angular inflation, or side-tracked inflation [227, 230–234]. The background equations (4.5), (4.4) and the Friedmann equation (4.6) simplify to

$$\begin{gathered} \dot{\sigma}\cos\theta = \dot{\psi} \simeq -\frac{V_\psi}{3H}, \quad \dot{\sigma}\sin\theta e^{-b} = \dot{\chi} \simeq -\frac{V_\chi}{3H}e^{-2b}, \\ H^2 \simeq \frac{V(\psi,\chi)}{3M_{\rm Pl}^2}, \end{gathered} \tag{4.23}$$

whose solutions for the turn rate and adiabatic acceleration read

$$-\frac{\dot{\theta}}{H} \simeq \eta_{\sigma s} + \frac{\dot{\sigma}}{H}b_\psi \sin\theta\cos^2\theta + \frac{\dot{\sigma}}{H}b_\chi e^{-b}\sin^2\theta\cos\theta, \tag{4.24}$$

$$\frac{\ddot{\sigma}}{H\dot{\sigma}} \simeq \epsilon_0 - \eta_{\sigma\sigma} - \frac{\dot{\sigma}}{H}b_\psi \sin^2\theta\cos\theta - \frac{\dot{\sigma}}{H}b_\chi e^{-b}\sin^3\theta, \tag{4.25}$$

in which

$$\eta_{IJ} \equiv \frac{V_{IJ}}{3H^2}. \tag{4.26}$$

It is then clear that the kinetic coupling contributes already at horizon crossing through the slow-roll parameters. At horizon crossing ($k_* = aH$), the curvature-perturbation power spectrum (3.71) is

$$\mathcal{P}_\zeta^* \simeq \frac{H^2}{8\pi^2\epsilon_0}, \tag{4.27}$$

and the spectral index (3.72) can be recast in terms of the slow-roll parameters

$$n_* = \left.\frac{\mathrm{d}\ln\mathcal{P}_\zeta}{H\mathrm{d}t}\right|_* = \frac{1}{H}\left[\frac{\epsilon_0}{H^2}\left(\frac{2H\dot{H}\epsilon_0 - \dot{\epsilon}_0 H^2}{\epsilon_0^2}\right)\right]\Bigg|_* = -2\epsilon_{0*} - \epsilon_{1*}. \tag{4.28}$$

Now, substituting (4.22) into the above and making use of

$$\dot{\epsilon}_0 = 2H\epsilon_0(2\epsilon_0 - \eta_{\sigma\sigma} - \sqrt{2\epsilon_0}b_\psi\sin^2\theta\cos\theta - e^{-b}\sqrt{2\epsilon_0}b_\chi\sin^3\theta), \tag{4.29}$$

we arrive at

$$n_* = -6\epsilon_0 + 2\eta_{\sigma\sigma} + 2\sqrt{2\epsilon_0}b_\psi\sin^2\theta\cos\theta + 2e^{-b}\sqrt{2\epsilon_0}b_\chi\sin^3\theta. \tag{4.30}$$

Note that in the limit of a flat field metric, (4.30) is equal to the expression presented in [235]. We also relate the higher-order running that describes the successive scale dependence of the primordial power spectrum beyond the leading-order tilt, as

$$\begin{aligned}\alpha_* \equiv & \left.\frac{\mathrm{d}n}{H\mathrm{d}t}\right|_* = -2\left.\frac{\dot{\epsilon}_0}{H} - \frac{\dot{\epsilon}_1}{H}\right|_* \\ = & -24\epsilon_0^2 - 4\eta_{\sigma s}^2 + 16\epsilon_0\eta_{\sigma\sigma} - 2\bar{\xi}_1^2\sin^4\theta e^{-2b} - 2\bar{\xi}_1\xi_1\sin^3\theta\cos\theta e^{-b} - 2\bar{\xi}_1\xi_1\sin^3\theta\cos^3\theta e^{-b} \\ & - 4\bar{\xi}_1\xi_1\sin^5\theta\cos\theta e^{-b} - 6\bar{\xi}_1\eta_{\sigma\sigma}\sin^3\theta e^{-b} - 14\bar{\xi}_1\eta_{\sigma s}\sin^2\theta\cos\theta e^{-b} - 2\bar{\xi}_1^2\sin^6\theta e^{-2b} \\ & + 6\bar{\xi}_1^2\sin^4\theta\cos^2\theta e^{-2b} + 16\bar{\xi}_1\epsilon_0\sin^3\theta e^{-b} + 2\bar{\xi}_{12}\sin^3\theta\cos\theta e^{-b} + 2\bar{\xi}_2\sin^4\theta e^{-2b} \\ & + 2\xi_2\sin^2\theta\cos^2\theta + 2\xi_1\eta_{\sigma s}\sin^3\theta - 12\xi_1\eta_{\sigma s}\sin\theta\cos^2\theta - 6\xi_1\eta_{\sigma\sigma}\sin^2\theta\cos\theta \\ & \left. - 4\xi_1^2\sin^2\theta\cos^4\theta + 16\xi_1\epsilon_0\sin^2\theta\cos\theta - 2\alpha_{\sigma\sigma\sigma}\right|_*,\end{aligned} \tag{4.31}$$

where, following [196], we have introduced new higher-order slow-roll parameters

$$\begin{aligned}\xi_1 &= \sqrt{2\epsilon_0}b_\psi, \quad \xi_2 = 2\epsilon_0 b_{\psi\psi}, \\ \bar{\xi}_1 &= \sqrt{2\epsilon_0}b_\chi, \quad \bar{\xi}_2 = 2\epsilon_0 b_{\chi\chi}, \quad \bar{\xi}_{12} = 2\epsilon_0 b_{\chi\psi},\end{aligned} \tag{4.32}$$

and $\alpha_{IJK} \equiv V_\sigma V_{IJK}/V^2$. One can similarly derive a formula for the running of the running,

$$\beta_* \equiv \left.\frac{\mathrm{d}\alpha}{H\mathrm{d}t}\right|_*, \tag{4.33}$$

but given its complexity we omit its explicit expression here.

4.1.1 Super-horizon scales

Building on Subsection 3.3.2, where we showed that on super-Hubble scales the curvature perturbation is driven solely by the entropy mode (see (3.102)), we can express the evolution of curvature and isocurvature perturbations entirely in terms of slow-roll parameters

$$\begin{aligned}\dot{\zeta} &\simeq -2\frac{V_s}{\dot{\sigma}}\mathcal{S} = AH\mathcal{S}, \\ \dot{\mathcal{S}} &\simeq \frac{H}{\dot{\sigma}}\dot{\delta s} + \left(\frac{\dot{H}}{H^2} - \frac{\ddot{\sigma}}{H\dot{\sigma}}\right)\frac{H^2}{\dot{\sigma}}\delta s = BH\mathcal{S}.\end{aligned} \tag{4.34}$$

In the above, A and B are time-dependent dimensionless functions

$$\begin{aligned}A &= -2\eta_{\sigma s} + 2\xi_1\sin^3\theta - 2\bar{\xi}_1 e^{-b}\sin^2\theta\cos\theta = 2\frac{\dot{\theta}}{H} + 2\xi_1\sin\theta, \\ B &= -\eta_{ss} + \eta_{\sigma\sigma} - 2\epsilon + \xi_1\cos\theta(1+2\sin^2\theta) + \bar{\xi}_1 e^{-b}\sin\theta(2\sin^2\theta - 1) + \frac{\xi_1^2}{3} + \frac{\xi_2}{3}.\end{aligned} \tag{4.35}$$

This result follows from substituting (4.16), (4.24), and (4.25), and imposing that on super-horizon scales $|\ddot{\delta s}| \ll 3H|\dot{\delta s}|$, $|\ddot{\delta\sigma}| \ll 3H|\dot{\delta\sigma}|$. To obtain the curvature-perturbation spectrum at the end of inflation, it is then essential to relate the curvature and entropy perturbations at the horizon crossing with the ones at the end of inflation, most conveniently expressed in the transfer-matrix formalism [236]

$$\begin{pmatrix} \zeta \\ \mathcal{S} \end{pmatrix} = \begin{pmatrix} 1 & \mathcal{T}_{\zeta\mathcal{S}} \\ 0 & \mathcal{T}_{\mathcal{S}\mathcal{S}} \end{pmatrix} \begin{pmatrix} \zeta \\ \mathcal{S} \end{pmatrix}_*, \tag{4.36}$$

where

$$\begin{aligned} \mathcal{T}_{\zeta\mathcal{S}}(t_*, t) &= \int_{t_*}^{t} A(t')H(t')\mathcal{T}_{\mathcal{S}\mathcal{S}}(t_*, t')dt', \\ \mathcal{T}_{\mathcal{S}\mathcal{S}}(t_*, t') &= \exp\left(\int_{t_*}^{t'} B(t'')H(t'')dt''\right). \end{aligned} \tag{4.37}$$

Although the functions introduced in equation (4.35) remain effectively constant throughout most of the slow-roll phase, they can change appreciably towards the end of inflation. For this reason, when evaluating the time integrals in equation (4.37), we retain the full time dependence of A and B rather than treating them as fixed parameters. Thus, we express the curvature power spectrum at the end of inflation in terms of its value at Hubble exit by introducing the transfer angle Θ, according to

$$\mathcal{P}_\zeta = (1 + \mathcal{T}^2_{\zeta\mathcal{S}})\mathcal{P}^*_\zeta \equiv \frac{\mathcal{P}^*_\zeta}{\cos^2\Theta}. \tag{4.38}$$

Here, the modification is due to the transfer function $\mathcal{T}_{\zeta\mathcal{S}}$ from entropy to curvature perturbations, and the transfer angle Θ is defined by

$$\cos^2\Theta = (1 + \mathcal{T}^2_{\zeta\mathcal{S}})^{-1}. \tag{4.39}$$

Because $\mathcal{T}_{\zeta\mathcal{S}}$ is constructed from the coefficients A and B in (4.35), the transfer angle Θ encodes direct information about the underlying field-space geometry. Even if adiabatic and isocurvature modes are initially uncorrelated, any bending of the background trajectory in field space during inflation produces a non-zero $\mathcal{T}_{\zeta\mathcal{S}}$ and thus induces a correlation between ζ and δs. This offers an alternative perspective on the discussed result (3.103) and then generalised in our work, (4.16). Moreover, we can also obtain explicit

formulas for the spectral index and its runnings evaluated at the end of inflation

$$\begin{aligned} n_s &\simeq n_* - 2\sin\Theta(A_*\cos\Theta + B_*\sin\Theta), \\ \alpha_s &\simeq \alpha_* + 2\cos\Theta(A_*\cos\Theta + B_*\sin\Theta)\times(A_*\cos 2\Theta + B_*\sin 2\Theta), \\ \beta_s &\simeq \beta_* - 2\cos\Theta(A_*\cos\Theta + B_*\sin\Theta)\times(B_*\cos 2\Theta - A_*\sin 2\Theta) \\ &\quad\times(A_* + 2A_*\cos 2\Theta + B_*\sin 2\Theta). \end{aligned} \tag{4.40}$$

4.2 Investigation of some kinetic couplings

In this section, we briefly apply the general formalism of Section 4.1 to three case studies of two-field inflationary models. They all share the potential

$$V = \frac{1}{2}m_\psi^2\psi^2 + \frac{1}{2}m_\chi^2\chi^2 + g^2\psi^2\chi^2, \tag{4.41}$$

in which m_I ($I = \{\psi, \chi\}$) denotes the masses of the fields and g a coupling constant, but differ in their field-space metric.

Bilinear coupling model. In the bilinear coupling model, we set $b(\psi,\chi) = -c\frac{\psi\chi}{M_P^2}$ (with c a constant). We find numerically that the background trajectory stays almost solely along the ψ-direction until ψ reaches its minimum at zero – so the entropic direction is almost exactly aligned with the χ-axis, see Figure 4.1. Since the χ-field does not evolve significantly, its effective mass squared $m_s^2 \simeq V_{;ss} \approx m_\chi^2$, remains large compared to H^2, *i.e.*

$$\eta_{ss} \equiv \frac{V_{;ss}}{3H^2} \gg 1. \tag{4.42}$$

A large η_{ss} means that the isocurvature perturbations in χ are heavy and decay exponentially. In particular, the first of (4.34) in terms of e-fold can be recast as

$$\frac{d\mathcal{S}}{dN} = B\mathcal{S}, \tag{4.43}$$

where B is as in (4.35) and whose solution is

$$\mathcal{S}(N) \propto e^{\int^N B(\tilde{N})d\tilde{N}}. \tag{4.44}$$

This means that, $B > 0$ gives exponential growth of the entropy mode, while $B < 0$ (as in the heavy-mass limit) gives exponential decay. This can be better understood with

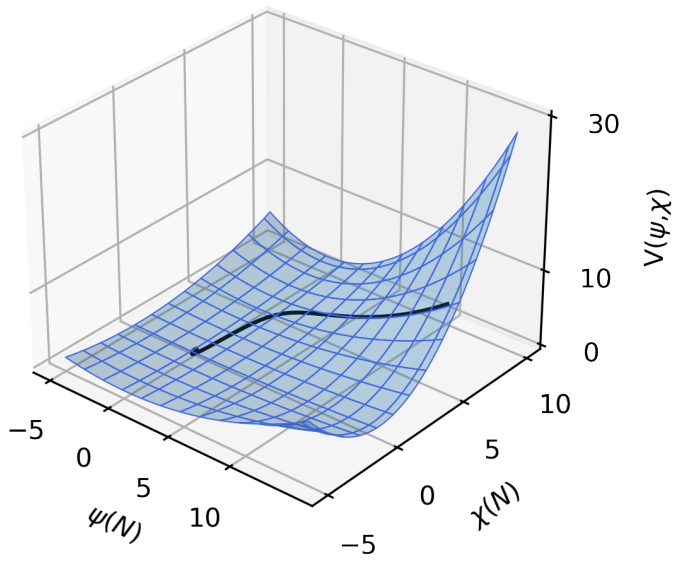

Figure 4.1: Field trajectory on the potential $V(\psi, \chi)$ for $c = -0.05$ (the values for ψ and χ are in Planck units). The values used here are those commonly found in the literature: $m_\psi = 3 \cdot 10^{-6}$ $M_{\rm P}$, $m_\chi = 6 \cdot 10^{-6}$ $M_{\rm P}$, $g = 10^{-6}$, $N = 55$ e–folds.

the second transfer function (4.37)

$$\mathcal{T}_{\mathcal{SS}} = \frac{\mathcal{S}(N)}{\mathcal{S}(N_*)} = e^{\int_{N_*}^{N} B(\tilde{N}) d\tilde{N}}, \tag{4.45}$$

that encapsulates the net growth or decay of isocurvature fluctuations over inflation. If $|\mathcal{T}_{\mathcal{SS}}| < 1$, isocurvature modes have decayed by the end of inflation, if $|\mathcal{T}_{\mathcal{SS}}| > 1$ they have been amplified. In this scenario, ψ remains near its minimum ($\psi = 0$) until very late, leaving χ effectively frozen, resulting in $|\mathcal{T}_{\mathcal{SS}}| = 0.29 < 1$. Once ψ reaches its minimum and χ becomes dynamical, the bending of the trajectory can in principle mediate a transfer of isocurvature fluctuations into the curvature perturbation. However, since δs was already suppressed by the earlier large-mass phase, there is no sufficient residual isocurvature power available for conversion, and consequently the resulting enhancement of $\mathcal{P}_\zeta$, see (4.38), remains small. Indeed, we find $|\mathcal{T}_{\zeta\mathcal{S}}| = 0.04 \ll 1$.

LOGARITHMIC COUPLING MODEL. In the logarithmic coupling scenario, we define $2b(\psi, \chi) = \ln\left[(a\psi + b\chi)^2 / M_{\rm Pl}^2\right]$. We find numerically that the background trajectory undergoes a pronounced turn shortly before the end of inflation, when the linear com-

bination $(a\psi + b\chi)$ passes through zero. Indeed, as $(a\psi + b\chi) \to 0$, the kinetic term for χ disappears, so variations in χ no longer contribute meaningfully to the dynamics. The entropic direction becomes effectively massless. So entropy perturbations stop decaying and momentarily "freeze", allowing them to be efficiently transferred into the curvature perturbation via the sharp turn (3.95). Hence, the net result is that a substantial fraction of the surviving entropy power is converted into curvature modes, yielding an order-unity amplification given by

$$\frac{\mathcal{P}_\zeta}{\mathcal{P}^*_\zeta} = \frac{2.01 \times 10^{-9}}{3.14 \times 10^{-10}} \approx 6, \tag{4.46}$$

by the end of inflation. An amplification of the primordial power spectrum between horizon exit and the end of inflation can significantly increase the abundance of primordial black holes (PBHs). In particular, if the curvature perturbation grows on super-horizon scales, the enhanced modes will lead to larger density contrasts upon re-entry, increasing the probability of PBH formation.

4.3 Tracking the multifield dynamics with cosmological data

Adiabatic and isocurvature modes can persist beyond the end of inflation and influence how perturbations evolve during the radiation-dominated era. This has important implications for cosmology, as these modes can leave measurable imprints on the early Universe that we can test using astrophysical and cosmological observations. For that reason, it is essential to use current data to uncover clues about inflation and gain insight into some properties of the fields that drove it [237–253]. In particular, recent high-precision measurements of the CMB – including its temperature fluctuations and polarization – have given us the ability to tightly constrain both adiabatic and isocurvature contributions [241, 254]. This opens a valuable window into testing multifield inflation models. However, making accurate predictions from general multifield theories remains difficult, because observable quantities are sensitive to many factors. For example, different initial conditions for the fields can lead to different trajectories in field space, which in turn can shift predictions for observables like the scalar amplitude, spectral index, and tensor modes. This makes comparing multifield models with observations more complicated than in the simpler single-field case. Moreover, many standard tools used in cosmological data analysis – like Boltzmann solvers and sampling algorithms

– are either not aware of the physics of inflation or assume single-field potential[1]. To address this challenge, this section introduces a new numerical framework that can accurately compute predictions for general multifield inflation models, including those with non-trivial field-space geometries. Our method has three main components. First, we solve the full background equations numerically across the entire inflationary period. Once a slow-roll regime is confirmed, we apply a first-order slow-roll approximation to compute key observables, such as the scalar power spectrum (4.27), tensor-to-scalar ratio (3.77), and isocurvature modes. We also track how adiabatic and isocurvature perturbations evolve on super-horizon scales and how entropy modes convert into curvature modes after horizon crossing, using the transfer matrix formalism (4.37). Second, we link our predictions to the well-established Boltzmann code to compute the complete cosmological evolution and produce CMB observables. Finally, we constrain the model's parameter space using a novel sampling algorithm that efficiently explores the large number of possibilities and isolates the regions that match observations.

4.3.1 Integration scheme and sampling method

After specifying the field-space metric $\mathcal{G}_{IJ}$ and the initial field values ϕ^K with their velocities, we integrate the full equations of motion (4.4), (4.5) for up to $N_{\max} = 10^4$ e-folds. Throughout this integration we compute the slow-roll parameter ϵ_0 from (3.23) and identify the first occurrence of $\epsilon_0 = 1$ as a candidate end of inflation. Should this condition not be reached within $N_{\max}$ e-folds, the model is discarded. On the other hand, if the condition $\epsilon_0 = 1$ is satisfied, we verify that none of the fields, when normalised to their initial values, exceed a prescribed threshold[2]; if they do, we continue integrating until this criterion is met, simultaneously confirming that ϵ_0 does not subsequently fall below unity. If we get back to $\epsilon_0 < 1$, the corresponding point at which $\epsilon_0 = 1$ coincides again with all fields below the threshold is then adopted as the true end of inflation. Next, we measure the total number of e-folds ΔN elapsed between the initial condition and the established end of inflation, imposing the requirement $\Delta N \geqslant 100$ to ensure sufficient expansion for the observed large-scale homogeneity and isotropy. In cases where $\Delta N < 100$, we perform a backward integration from the original initial conditions to determine whether the deficit arises from an unfortunate choice of starting

[1] A few numerical tools for multifield inflation have been developed as well. See, *e.g.* [255].

[2] For the bilinear coupling model analysed in what follows, we set $\psi/\psi_{\text{ini}} \leqslant 10^{-3}$, $\chi/\chi_{\text{ini}} \leqslant 10^{-2}$. We emphasise that this diagnostic is included specifically to identify and exclude models exhibiting a double-inflation phase, see *e.g.* [256–259]. Although in the case study model of this section a secondary phase of inflation is exceedingly unlikely – since the end of the fields' motion generally marks a permanent end to inflation – our algorithm is fully equipped to detect and accommodate such behavior, as demonstrated in Appendix B.

point or from an intrinsic inability of the model to sustain slow-roll; models exhibiting pathological behavior under this test are rejected. Having secured a valid inflationary trajectory of adequate duration, we reconstruct the evolution of the fields and slow-roll parameters over the full interval. We then select $N_* = 55$ e-folds before the end of inflation as the horizon-crossing epoch, record all relevant slow-roll parameters at that instant, and integrate the super-horizon dynamics of both adiabatic and isocurvature perturbations. Finally, employing the transfer-matrix formalism described in Subsection 4.1.1, we compute the primordial scalar power spectrum and associated observables at the end of inflation.

Upon successful termination of the integration, we extract all primary inflationary observables – namely, the scalar amplitude A_s, the scalar spectral index n_s, its running α_s, the running of the running β_s, and the tensor-to-scalar ratio r. These quantities serve as initial conditions for the Boltzmann solver "Code for Anisotropies in the Microwave Background"`CAMB`[3] [261, 262], together with the ΛCDM parameters $\Omega_b h^2$, $\Omega_c h^2$, $\theta_{\rm MC}$ and τ. In this way, we translate the multifield inflationary predictions into the standard cosmological observables – CMB temperature and polarisation power spectra and the matter power spectrum – under both canonical and extended background models. To compare theory with data, we then perform a Monte Carlo exploration of the multifield parameter space (of order 10^6 samples). At each step, we draw the fields' initial conditions and model parameters from prescribed priors, integrate the background and perturbations (applying the end-of-inflation and minimum-ΔN consistency checks described above), and compute the resulting A_s, n_s, α_s, β_s, and r. We retain only models that simultaneously satisfy the following conditions:

- $A_s \in [1.5\,,\ 2.5] \times 10^{-9}$
- $n_s \in [0.94\,,\ 0.99]$
- $\alpha_s \in [-0.2\,,\ 0.2]$
- $\beta_s \in [-0.2\,,\ 0.2]$
- $r < 0.1$

where the ranges chosen reflect the bounds of the values measured by the most recent CMB experiments [263, 264]. This step is not strictly necessary, as one could – in principle – include all models in the analysis and assign them a likelihood, even if their predictions lie outside the target observational ranges. In such cases, the models would

[3] Note that the same procedure can be applied to interface our algorithm with the "Cosmic Linear Anisotropy Solving System", (`CLASS`) code [260].

receive a log-likelihood of negative infinity and contribute nothing to the final parameter constraints, leading to identical overall results. However, due to the broad prior volume[4] often explored in multifield scenarios, the space of possible outcomes can be highly unpredictable, resulting in a large number of models that fall well outside observationally viable regions. To avoid the unnecessary computational cost of evaluating likelihoods for models that are already strongly disfavored by data – and which would not influence the posterior – we apply this filtering step as a practical efficiency measure. Therefore, accepted models are then passed to `CAMB`, and we record the full set of cosmological outputs alongside their input parameters. In this way, we generate a chain of models that are equivalent to those produced by typical Markov Chains Monte Carlo (MCMC) technique, assigning to each retained model a likelihood constructed as a multivariate Gaussian,

$$\mathcal{L}_{\rm ike} \propto \exp\left(-\frac{1}{2}\left(\mathrm{x}-\mu\right)^{\mathrm{T}}\Sigma^{-1}\left(\mathrm{x}-\mu\right)\right), \tag{4.47}$$

where x are the predicted observables, and μ and Σ are the mean and covariance derived from the Planck 2018 TT, TE, EE, low-ℓ and lensing data [9, 265–267], together with the BICEP/Keck Array X B-mode likelihood [264]. We refer to Appendix B for further details. The resulting posterior distributions then yield robust constraints on the multifield inflationary parameters.

4.3.2 Predictions

Concretely, we demonstrate and validate every aspect of our methodology using the bilinear coupling model introduced in Section 4.2. Once the field-space metric and the self-interaction potential are specified, the formalism developed in the previous section can be directly applied, and the multifield dynamics can be numerically solved using the integration scheme outlined in Subsection 4.3.1. In particular, the evolution of the fields – and thus their trajectory in field space – depends on the model's free parameters (namely m_ψ, m_χ, g and c) as well as on the initial conditions ($\psi_{\rm ini}$, $\dot{\psi}_{\rm ini}$, $\chi_{\rm ini}$, $\dot{\chi}_{\rm ini}$). In this subsection, we examine the role of each of these parameters separately, focusing on their impact on both the inflationary dynamics and the resulting cosmological observables. This step provides a clearer understanding of the model's behavior and helps interpret the outcomes of the full Monte Carlo exploration presented in the next subsection. We begin by assessing the stability of the model's predictions under variations in the initial field values. In particular, we investigate how the trajectories in field

[4] In Bayesian inference or parameter estimation, the prior represents our initial assumptions about the values parameters can take, before considering data. The prior volume refers to the size or range of the parameter space over which these priors are defined.

space respond to random changes in the initial positions $\psi_{\rm ini}$ and $\chi_{\rm ini}$, while keeping the model parameters fixed and setting the initial velocities $\dot{\psi}_{\rm ini} = \dot{\chi}_{\rm ini} \approx 0$. The resulting trajectories are shown in Figure 4.2. Although different initial field values can lead to

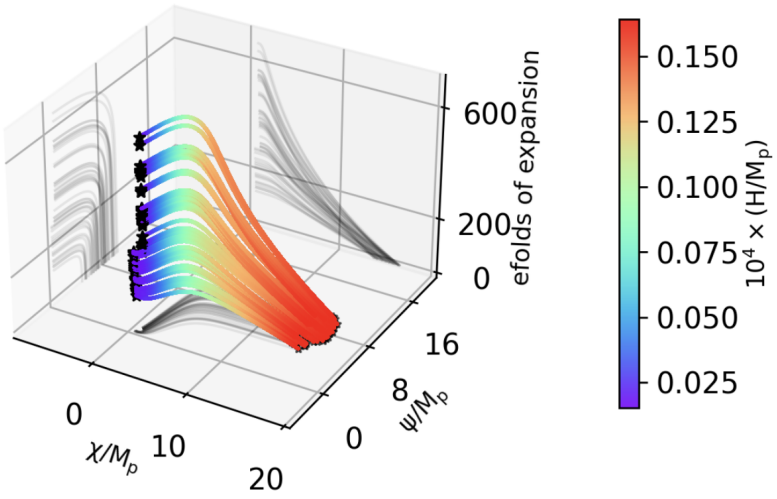

Figure 4.2: Field trajectories and their projections in different 2D-planes in grey as functions of the e-folds of expansions between the beginning of the integration and the end of inflation. The integration process begins at $N = 0$ with randomly selected initial conditions, represented by a black star-like dot in the figure. The end of inflation marked by another black star-like dot is determined using the method explained in Subsection 4.3.1. The color-bar shows the value of the Hubble parameter along the field trajectories. For all trajectories, the model's free parameters are in Planck unit and fixed to: $m_\psi = 1.58 \times 10^{-6}$, $m_\chi = 3.86 \times 10^{-6}$, $c = -0.06$, and $g = 2 \times 10^{-8}$.

inflationary phases of different duration, they generally leave the predicted cosmological observables unaffected. This suggests that the physical predictions of the model are largely insensitive to the choice of initial conditions.

In contrast, variations in the model's free parameters – particularly the parameter c, which governs the curvature of the field-space manifold – have a more pronounced impact on the dynamics. The value of c significantly influences the interaction between curvature and isocurvature modes during the super-horizon evolution, from horizon exit to the end of inflation. Specifically, as c is gradually decreased (*i.e.* made more negative), the velocity of the χ field remains nearly constant, and it becomes effectively frozen for an extended period. It only reenters the dynamics once the ψ field approaches the minimum of the potential, see Figure 4.3. This behavior directly affects the degree to which isocurvature modes can source the curvature perturbation. Indeed, as discussed in Section 4.2, the more rapid the turn the faster isocurvature modes decay and the less they are able to source the curvature modes. Conversely, increasing c leads to the rapid suppression of χ, effectively reducing the system to a single-field regime. In this limit, curvature and isocurvature modes become almost uncorrelated. However, if the trajectory in field space exhibits curvature from horizon crossing through to the end of infla-

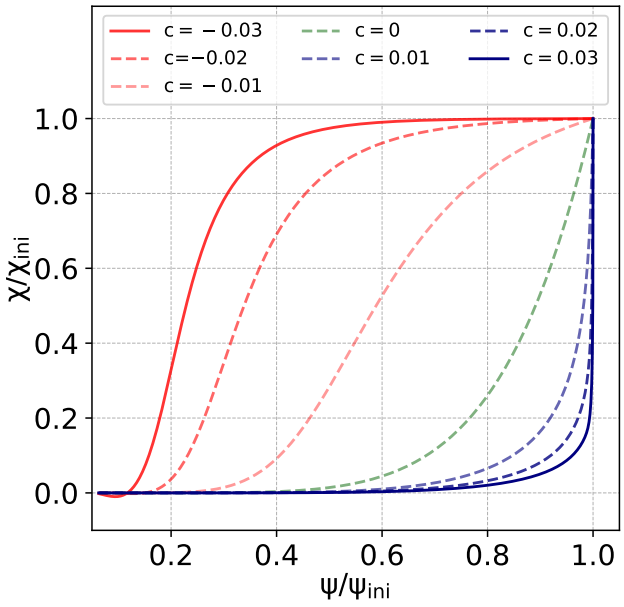

Figure 4.3: Effects of the field-space curvature parameter c on the evolution of the fields in the $\psi - \chi$ plane. Field values are normalised to their respective initial conditions, so all trajectories begin at the point $(1, 1)$, while the origin $(0, 0)$ represents the idealised end of inflation. Red and blue trajectories correspond to negative and positive values of c, respectively, as indicated in the legend. The green curve denotes the case of a flat field-space metric, $\mathcal{G}_{IJ} = \text{diag}\{1, 1\}$, (*i.e.* $c = 0$). All other model parameters are fixed to $m_\psi = 1.58 \times 10^{-6}$, $m_\chi = 3.86 \times 10^{-6}$, and $g = 2 \times 10^{-8}$.

tion, an important coupling between the two sectors emerges – potentially introducing significant correlation that can amplify or suppress the final curvature power spectrum, as illustrated in Figure 4.4.

Turning to the influence of the field masses, Figure 4.4 demonstrates that increasing or decreasing m_χ and m_ϕ respectively raises or lowers the power in the temperature-anisotropy spectrum. To see why, recall from (4.23) that on the slow-roll trajectory

$$V_\psi \simeq -3\dot{\psi}H, \qquad V_\chi \simeq -3\dot{\chi}e^{2b(\psi,\chi)}H. \tag{4.48}$$

For our quartic interaction potential (4.41), one computes

$$V_{\chi\chi} = 2b_\chi V_\chi - 3e^{2b(\psi,\chi)}\dot{H}, \tag{4.49}$$

using $\frac{dH}{d\chi} = \frac{\dot{H}}{\dot{\chi}}$. It follows that the effective mass of the χ field can be written as

$$m_\chi^2 = 2b_\chi V_\chi + \frac{3}{2}\dot{\sigma}^2 e^{2b(\psi,\chi)} - 2g^2\psi^2, \tag{4.50}$$

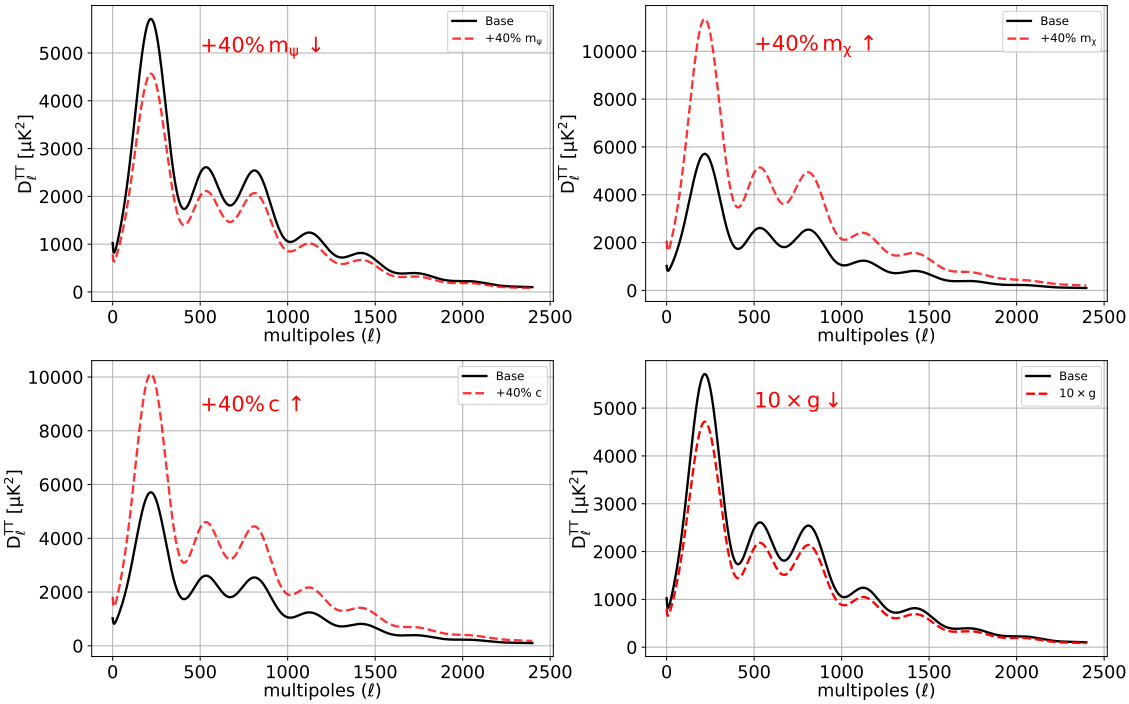

Figure 4.4: Impact of varying model parameters on the CMB angular power spectrum, as shown across the different panels/legends of the figure. The black curve represents the baseline model, defined by the following set of parameter values: $m_\psi = 1.58 \times 10^{-6}$, $m_\chi = 3.86 \times 10^{-6}$, $c = -0.06$, and $g = 2 \times 10^{-8}$.

so that on the slow-roll trajectory defined by (4.49) there is a correlation between the mass m_χ and the coupling b_χ. By contrast, one finds for the ψ mass

$$m_\psi^2 = \frac{3}{2}\dot{\sigma}^2 - 2g^2\chi^2, \tag{4.51}$$

which implies that a larger m_ψ drives a faster change in the Hubble parameter (since $\dot{\sigma} \simeq -\dot{H}$). This shortens the duration of inflation and thereby reduces the overall amplitude of the scalar power spectrum, as seen in Figure 4.4. Moreover, the same figure confirms that raising either c or m_χ boosts the initial power-spectrum amplitude, in accordance with (4.50).

4.3.3 Monte Carlo analysis and parameter constraints

We are now ready to employ the sampling procedure described in Subsection 4.3.1 to map out the parameter space of our multifield model. Our exploration spans the four free parameters (m_ψ, m_χ, c, and g) together with the fields initial values ($\psi_{\rm ini}$, $\chi_{\rm ini}$) which, as shown in Subsection 4.3.2, determine the inflationary trajectory. To cover a broad region of model space, we draw each parameter and initial condition from wide, uniform priors

(see Table 4.1), generating as many distinct combinations as there are Monte Carlo steps. At each step, we integrate the background and perturbation equations, compute the full field evolution, and extract all primordial observables – including A_s, n_s, α_s, β_s and r. We then evaluate each sample against CMB data by means of our Gaussian likelihood (4.47). Using this framework, we perform a comprehensive Monte Carlo analysis of over

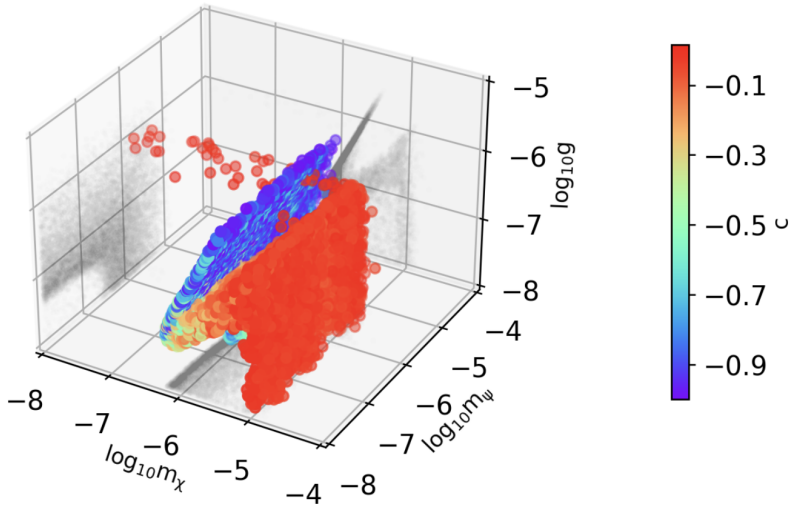

Figure 4.5: Distribution of the models in the 4D parameter space. The box has the size of the prior volume.

5×10^6 iterations, ultimately retaining roughly 2×10^4 viable models – each associated with its own likelihood. From this ensemble, we extract posterior distributions for every sampled parameter and for derived quantities such as the super-horizon entropy transfer. Table 4.1 summarises our numerical findings, while Figure 4.5 illustrates the spread of accepted models within the four-dimensional prior volume. Figure 4.6 then presents the 68% and 95% confidence-level contours for all key parameters and observables. Our first check concerns the primordial inflationary observables. For the amplitude of scalar spectrum, we find $A_s = (2.109 \pm 0.033) \times 10^{-9}$ at 68% CL, in perfect agreement with the model-independent analysis performed with the full Planck and BK18 likelihoods. Similarly, for the spectral index we get $n_s = 0.9621^{+0.0053}_{-0.0047}$ at 68% CL, while for the amplitude of primordial gravitational waves we obtain an upped bound $r < 0.04$ at 95% CL. Finally, the higher-order runnings are constrained to $\alpha_s = \left(-0.74^{+0.37}_{-0.32}\right) \times 10^{-3}$ and $\beta_s = \left(-0.103^{+0.088}_{-0.004}\right) \times 10^{-3}$ at 68% CL, favoring slightly negative values but remaining consistent with zero at the 95% level. One significant aspect of our method is yielding direct observational bounds on each model parameter. At the 95% confidence level, we find the following upper limits (in Planck units): $m_\psi < 2.30 \times 10^{-6}$ and $m_\chi < 1.01 \times 10^{-5}$. Each of these values lies well within the limits, confirming that our results are driven by the data rather than prior choices (meaning that we adopted uninformative ranges,

Initial Conditions	**Constraints**	**Unifrom Prior Ranges**
$\psi_{\rm ini}/M_p$	–	$\psi_{\rm ini}/M_p \in [14\,,\,17]$
$\chi_{\rm ini}/M_p$	–	$\chi_{\rm ini}/M_p \in [10\,,\,4]$
Model's Parameters	**Constraints**	**Unifrom Prior Ranges**
m_ψ	$< 2.30 \cdot 10^{-6}$	$\log_{10}(m_\psi) \in [-8\,,\,-4]$
m_χ	$< 1.01 \cdot 10^{-5}$	$\log_{10}(m_\chi) \in [-8\,,\,-4]$
c	< -0.0211	$c \in [-1\,,\,1]$
g	$< 9.72 \cdot 10^{-7}$	$\log_{10}(g) \in [-8\,,\,-5]$
Primordial spectra	**Constraints**	
A_s	$(\,2.109 \pm 0.033\,) \cdot 10^{-9}$	
n_s	$0.9621^{+0.0053}_{-0.0047}$	
α_s	$\left(-0.74^{+0.37}_{-0.32}\right) \times 10^{-3}$	
β_s	$\left(-0.103^{+0.088}_{-0.0040}\right) \times 10^{-3}$	
r	< 0.04	
Entropy Transfer	**Constraints**	
Θ	< -0.686	
$A_\star$	> -1.71	
$B_\star$	> -0.341	

Table 4.1: External priors and observational constraints at 1σ (68% CL) or upper bounds at 2σ (95% CL) on parameters.

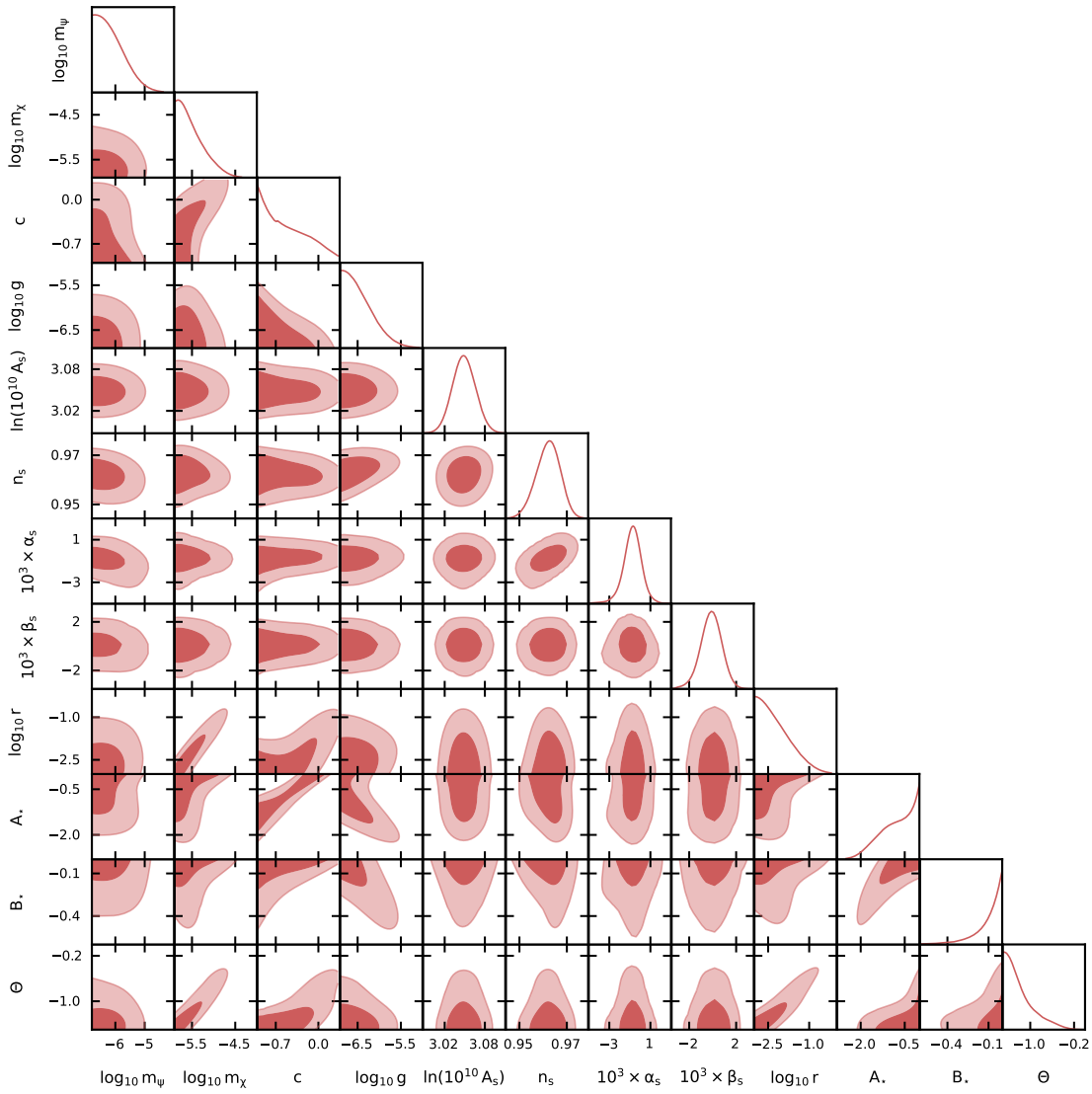

Figure 4.6: Contour plots at 1σ (68% CL) and upper bounds at 2σ (95% CL) on parameters.

without introducing any unwanted bias in the parameter space). To understand how these parameters interplay, recall from Figure 4.4 that making c more negative amplifies CMB temperature anisotropies, whereas increasing g suppresses it. Consequently, more negative c values are only allowed alongside larger g, a trend clearly visible in the 4D scatter of Figure 4.5 and in the 68%/95% contours of Figure 4.6. The strong preference for $c < 0$ originates in the geometry of field space: positive c exponentially flattens $\mathcal{G}_{IJ}(\phi^K)$, effectively freezing one field and reducing the model to a single quadratic inflaton. Such single-field quadratic models predict a tensor-to-scalar ratio that is already excluded by the latest B-mode limits from BK18 and the Planck temperature and polarisation data, thereby ruling out $c > 0$. Finally, our algorithm allows us to derive constraints on any relevant physical quantities in the model, including parameters and functions that govern the transfer of entropy between adiabatic and isocurvature perturbations. For instance, we obtain a 95% CL upper limit on the transfer angle parameter of (4.39), $\Theta < -0.686$, quantifying the correction to inflationary observables between horizon exit and the end of inflation. Likewise, we constrain the transfer-matrix functions $A(t)$ and $B(t)$ that encode the time-dependent coupling between curvature and entropy perturbations. Evaluated at horizon crossing, these are $A_* > -1.71$ and $B_* > -0.341$ at 95% CL. These results underscore how, in multifield scenarios with a curved field-space metric, the dynamics of isocurvature modes and their transfer into the curvature sector decisively shape the final observable predictions, as emphasised in [1].

The work presented in this chapter on multifield inflation with kinetic couplings lays the foundation for future studies exploring more generalised theories of gravity. Indeed, in Chapter 5, we will apply the numerical method developed here to study and analyse a scale-invariant quadratic inflationary model, and we will also compare its predictions with those of competing models such as Starobinsky inflation. Furthermore, in Chapter 6 we will investigate hybrid metric-Palatini gravity models that incorporate non-local geometric operators in the gravitational action[5], such as terms of the form $f(\ldots, \Box^{-1}R, \ldots)$. These non-local modifications can induce deformations of well-known inflationary potentials – such as the Starobinsky potential in (3.107) – offering a novel framework to test the stability and predictive power of the model.

[5]Hybrid and non-local gravity models are introduced in Subsection 1.2.1.

5 | Scale-invariant inflation

Inflationary cosmology, first proposed to address the horizon and flatness problems as discussed in *Part I* (see Subsection 3.1.1), has become a cornerstone of the modern cosmological paradigm. Observations of the CMB have revealed a nearly scale-invariant spectrum of primordial density fluctuations ($n_s \simeq 0.96$) [263] alongside stringent upper limits on primordial tensor modes, firmly ruling out simple monomial potentials and favoring models with an extended plateau [209, 263]. Yet, maintaining such a plateau across super-Planckian field ranges presents a persistent theoretical challenge: quantum loop corrections generically induce lower-dimensional operators – such as mass terms and vacuum-energy contributions – that tend to steepen the potential [12, 150, 268]. These "dangerous" terms must either be forbidden by symmetries, which provide a natural protection, or else be suppressed through finely tuned cancellations, which raise concerns about naturalness. A powerful resolution lies in invoking scale-invariance, the requirement that no explicit mass or length scale appears in the fundamental action, as shown in Subsection 1.2.2. At the classical level, this symmetry constrains all operators in four dimensions to mass dimension four with dimensionless couplings, automatically forbidding super-renormalisable terms such as $m^2\phi^2$ or vacuum energy terms Λ^4. Quantum mechanically, an exact (or softly broken) scale symmetry ensures that loop corrections can only renormalise existing operators, producing at most logarithmic running rather than dangerous power-law divergences [269–273]. In this way, scale-invariance acts as a "gatekeeper", protecting the flat directions of the potential and avoiding large hierarchical tunings.

The Starobinsky model mentioned in *Part I* (see Section 3.4) elegantly realises these principles within the gravitational sector. By considering in the EH action operators of exactly dimension four with a dimensionless coefficient, the theory enjoys scale symmetry at high curvature. A conformal transformation to the EF reveals a single scalaron field with a potential [209]

$$V(\chi) = \frac{M_{\rm Pl}^4}{4\alpha}\left(1 - e^{-\sqrt{2/3}\,\chi/M_{\rm Pl}}\right)^2, \tag{5.1}$$

already introduced in (3.107), so that at large values of the field the potential becomes almost perfectly flat and it is not spoiled by the usual quantum corrections that would otherwise create unwanted mass or vacuum-energy terms.

Building on this success, one can incorporate a scalar sector while preserving scale symmetry. Introducing a real scalar field ϕ with a non-minimal coupling and a quartic self-interaction $\lambda\phi^4$ leads to the purely scale-invariant action of (1.69) which, on a homogeneous FLRW background, admits two de Sitter regimes – an initial saddle and a late-time attractor – between which the scalar field dynamically acquires a vacuum expectation value, spontaneously breaking scale symmetry and generating the Planck mass. Analytical investigations [4, 274–276] have shown that this scale-invariant inflationary scenario yields spectral indices well within the bounds set by current observations, even after including one-loop quantum corrections [275]. Moreover, studies of the two-field formulation in the EF demonstrate that scale symmetry effectively reduces the dynamics to a single degree of freedom, thereby eliminating isocurvature modes [23, 277]. Nonetheless, several key issues remain open. First, it is crucial to confirm the analytic results by numerically solving the full field equations throughout the entire inflationary epoch – a non trivial task given the inherent two-field nature of the model in the EF. Second, quantitative fits to the latest CMB data are needed to place precise bounds on the parameters α, ξ, λ. Third, one should assess the robustness of inflationary trajectories against changes in initial conditions, and consider priors directly on the fundamental couplings rather than on the derived observables n_s and r. Beyond these, further work is required to verify the predicted suppression of isocurvature perturbations, to compute the level of primordial non-Gaussianity, and to pinpoint observational imprints that could distinguish scale-invariant inflation from competing models such as Starobinsky's.

The present study based on [3] is dedicated to tackling these challenges, thereby strengthening the case for scale-invariant inflation as a phenomenologically viable model of the early universe. The main objectives of this chapter are the following. We outline the methodology used and demonstrate that entropy perturbations vanish as a consequence of scale symmetry in Section 5.1. We introduce a field redefinition that facilitates the analysis with our code, allowing us to derive all quantities needed for the numerical implementation. We evaluate the level of local non-Gaussianity predicted in the squeezed limit. Finally, in Section 5.2 we make comparison with competitive models of inflation such as the Starobinsky model.

5.1 Theoretical aspects

The JF action (1.69), that we report here for convenience

$$S_J = \int d^4x\sqrt{-g}\left(\frac{\xi}{6}\,\phi^2 R + \frac{\alpha}{36}\,R^2 - \frac{1}{2}\partial_\mu\phi\partial^\mu\phi - \frac{\lambda}{4}\phi^4\right), \tag{5.2}$$

(where α not to be confused with the running of the spectral index α_s) is dynamically equivalent to the following formulation involving an auxiliary scalar field

$$S_J = \int d^4x\sqrt{-g}\left[\left(\frac{\alpha\psi^2}{18} + \frac{\xi\phi^2}{6}\right)R - \frac{\alpha\psi^4}{36} - \frac{1}{2}\partial_\mu\phi\partial^\mu\phi - \frac{\lambda}{4}\phi^4\right], \tag{5.3}$$

as the equation of motion for the field implies $\psi^2 = R$. Note this is not the most general action quadratic in curvature invariants [278, 279] – as it lacks a term quadratic in the Weyl tensor. However, our aim is to study cosmology and on a flat FLRW background, which is conformally flat, the Weyl tensor vanishes identically. Therefore, including a $C^2_{\mu\nu\rho\sigma}$ term does not affect the classical dynamics (this statement may not hold at the perturbative level, see [280], however such effects lie beyond the scope of our study). Since the auxiliary field satisfies the constraint $\psi^2 = R$ on shell, the action (5.3) matches the class of two-scalar scale-invariant models analysed in [23] (and earlier in the context of Higgs-dilaton models in [277]). To transition to the EF, we perform the Weyl rescaling

$$\tilde{g}_{\mu\nu} = e^{2\omega(x)}g_{\mu\nu}\,, \tag{5.4}$$

with the conformal factor defined by

$$\omega \equiv \frac{1}{2}\ln\frac{2}{M^2}\left(\frac{\alpha\psi^2}{18} + \frac{\xi\phi^2}{6}\right), \tag{5.5}$$

where here M is an arbitrary parameter with mass dimension 1. Introducing the field $\mathfrak{f} = Me^{-\omega}$ the action takes the compact EF (4.1) form

$$S_E = \int d^4x\sqrt{-g}\left[\frac{M^2}{2}R - \frac{1}{2}\mathcal{G}_{IJ}g^{\mu\nu}\partial_\mu\phi^I\partial_\nu\phi^J - V(\phi^I)\right], \tag{5.6}$$

where the scalar field multiplet and field-space metric are given by

$$\phi^I \equiv \begin{pmatrix}\phi\\ \mathfrak{f}\end{pmatrix}, \qquad \mathcal{G}_{IJ} \equiv \begin{pmatrix}e^{2b(\mathfrak{f})} & 0\\ 0 & 6e^{-2b(\mathfrak{f})}\end{pmatrix}, \tag{5.7}$$

with $b(\mathfrak{f}) \equiv \ln(\mathfrak{f}/M)$.

The corresponding EF potential becomes

$$V(\phi^I) = V(\phi, \mathfrak{f}) = -\frac{3\xi\phi^2\mathfrak{f}^2}{2\alpha} + \frac{\Omega\phi^4\mathfrak{f}^4}{4\alpha M^4} + \frac{9M^4}{4\alpha}, \tag{5.8}$$

where we have defined

$$\Omega \equiv \alpha\lambda + \xi^2 . \tag{5.9}$$

Scale symmetry implies the existence of a conserved Noether current, which can be computed under an infinitesimal Weyl transformation,

$$\begin{aligned} g_{\mu\nu} &\longrightarrow e^{-2\epsilon(x)} g_{\mu\nu} \simeq (1 - 2\epsilon(x)) g_{\mu\nu}, \\ \phi &\longrightarrow e^{-\epsilon(x)} \phi \simeq (1 - \epsilon(x))\phi, \\ \psi &\longrightarrow e^{-\epsilon(x)} \psi \simeq (1 - \epsilon(x))\psi. \end{aligned} \tag{5.10}$$

The Noether current is defined as

$$K_\mu = \frac{\delta \mathcal{L}}{\delta \partial_\mu \epsilon(x)}. \tag{5.11}$$

In our case, to calculate it, we can split the Lagrangian of (5.3) into the parts that will contribute to the current when varied

$$\begin{aligned} \mathcal{L}_\phi &= -\frac{1}{2}(\partial\phi)^2, \\ \mathcal{L}_1 &= \frac{\alpha}{18}\sqrt{-g}\,\psi^2 R, \\ \mathcal{L}_2 &= \frac{\xi}{6}\sqrt{-g}\,\phi^2 R. \end{aligned} \tag{5.12}$$

Starting with $\mathcal{L}_\phi$ we find that

$$\frac{\delta \mathcal{L}_\phi}{\delta(\partial_\mu \epsilon(x))} = \phi \partial_\mu \phi, \tag{5.13}$$

by means of $\delta(\partial\phi)^2 = 2\partial^\mu\phi\delta(\partial_\mu\phi)$ and $\delta(\partial_\mu\phi) = -(\partial_\mu\epsilon)\phi - \epsilon\partial_\mu\phi$ in which we neglected the second term as it does not contribute to K_μ. Variation of $\mathcal{L}_1$ gives

$$\begin{aligned} \delta\mathcal{L}_1 &= \frac{\alpha}{18}\Big((-4\epsilon\sqrt{-g})\psi^2 R + \sqrt{-g}(-2\epsilon\psi^2)R + \sqrt{-g}\psi^2(2\epsilon R + 6\Box\epsilon)\Big) \\ &= \frac{\alpha}{18}\Big(-4\psi^2 R + 6\psi^2\partial^\mu\partial_\mu\epsilon\Big), \end{aligned} \tag{5.14}$$

in which we substitute $\delta(\sqrt{-g}) = -4\epsilon\sqrt{-g}$ and $\delta R = 2\epsilon R + 6\Box\epsilon$, and the covariant

derivatives reduce to partial derivatives. Moreover, we can rewrite

$$\psi^2 \partial^\mu \partial_\mu \epsilon = \partial_\mu (\psi^2 \partial^\mu \epsilon) - (\partial_\mu \psi^2) \partial^\mu \epsilon, \tag{5.15}$$

and ignoring the first term on the right hand side because it is a boundary term. Hence,

$$\frac{\delta \mathcal{L}_1}{\delta(\partial_\mu \epsilon(x))} = -\frac{2\alpha}{3} \psi \partial_\mu \psi. \tag{5.16}$$

The very same procedure applies for $\mathcal{L}_2$; one obtains

$$\frac{\delta \mathcal{L}_1}{\delta(\partial_\mu \epsilon(x))} = -2\xi \phi \partial_\mu \phi. \tag{5.17}$$

By substituting all the results into (5.11), the Noether current takes the form

$$K_\mu = (2\xi + 1)\, \phi \partial_\mu \phi + \frac{2}{3} \alpha\, \psi \partial_\mu \psi. \tag{5.18}$$

One can introduce the scalar function

$$K = \frac{1}{2} \left[(2\xi + 1)\phi^2 + \frac{2\alpha}{3} \psi^2 \right], \tag{5.19}$$

so that $K_\mu = \partial_\mu K$. Strictly speaking, K is not conserved in the sense of a constant of motion; rather, it satisfies the massless free field equation

$$\Box K = 0. \tag{5.20}$$

In a spatially flat FLRW universe, this reads

$$\ddot{K} + 3H\dot{K} = 0, \tag{5.21}$$

whose general solution is

$$K = c_1 + c_2 \int \frac{dt}{a^3(t)}, \tag{5.22}$$

where $a(t)$ is the scale factor. The second term decays rapidly due to the expansion of the universe, so K dynamically approaches a constant. This reflects a *dynamical freezing* rather than exact conservation, and it constrains the field motion in the $(\phi, \mathfrak{f}^{-1})$ plane to an elliptical trajectory. Expressing K in terms of $\mathfrak{f} = Me^{-\omega}$ with ω as in (5.5), we have

$$K \equiv \frac{M_{\rm P}^2}{2} \left(\frac{\phi^2}{M_{\rm P}^2} + \frac{6M_{\rm P}^2}{\mathfrak{f}^2} \right), \tag{5.23}$$

as also derived in [277], and setting $c_1 = M_{\rm P}^2$ without loss of generality gives the ellipse

$$\frac{\phi^2}{M_{\rm P}^2} + \frac{6M_{\rm P}^2}{\mathfrak{f}^2} = 2 \quad \rightarrow \quad \mathfrak{f} = \frac{\sqrt{6}M_{\rm P}^2}{\sqrt{2M_{\rm P}^2 - \phi^2}}\,. \tag{5.24}$$

This trajectory is illustrated in Figure 5.1 and aligns with numerical solutions of the background equations of motion. The approach of K to a constant is thus a dynamical consequence of the expansion for a free massless field, rather than a strict statement of conservation, illustrating how symmetries can effectively constrain multifield dynamics.

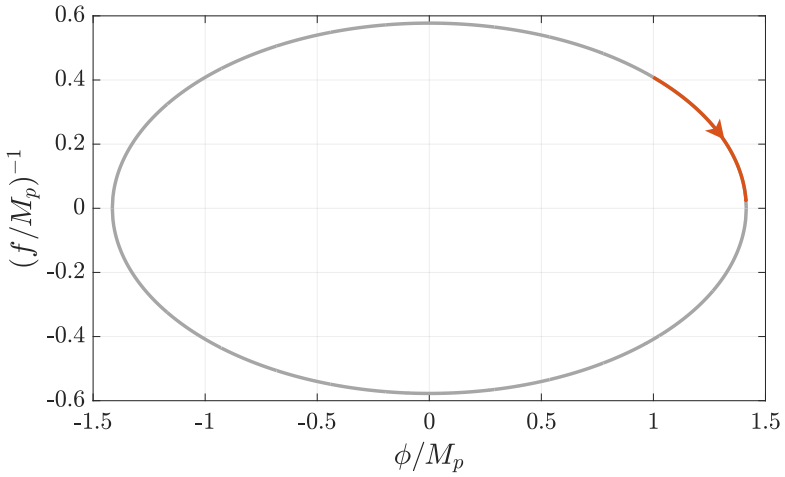

Figure 5.1: The grey curve shows the analytical expression of the ellipse from (5.24) with $c_1 = M_{\rm P}^2$, while the red curve represents the field trajectory obtained by numerically solving the background equations. The arrow indicates the direction of evolution, and the numerical integration is performed up to the end of inflation.

Examples include Higgs inflation, where $SU(2)$ symmetry appears as an $SO(4)$ symmetry in field space [281], the Higgs-dilaton model of inflation [282, 283] and the scale-invariant generalisation of [284].

Given that, we proceed with presenting the key analytical results that underpin the theoretical framework of the model, serving as a foundation for the numerical analysis to follow.

5.1.1 Vanishing of entropy perturbation

In this subsection we outline the methodology used and demonstrate that entropy perturbations vanish as a consequence of scale symmetry.

To facilitate the interpretation of the evolution of cosmological perturbations and their interrelation, we introduce an orthonormal basis in field space, as discussed in Subsection 3.3.2. This allows us to decompose field-dependent quantities into adiabatic

and entropy components. For the two-dimensional field space defined in (5.7), the unit vectors forming the orthogonal basis (3.86) are given by

$$\mathbf{u}_\sigma^I \equiv \frac{1}{\sqrt{e^{2b}\dot{\phi}^2 + 6e^{-2b}\dot{\mathfrak{f}}^2}}\left(\dot{\phi}, \dot{\mathfrak{f}}\right), \quad \mathbf{u}_s^I \equiv \frac{1}{\sqrt{e^{2b}\dot{\phi}^2 + 6e^{-2b}\dot{\mathfrak{f}}^2}}\left(-\sqrt{6}e^{-2b}\dot{\mathfrak{f}}, \frac{e^{2b}}{\sqrt{6}}\dot{\phi}\right). \tag{5.25}$$

By means of (3.82), we can write

$$\dot{\sigma}^2 \equiv e^{2b}\dot{\phi}^2 + 6e^{-2b}\dot{\mathfrak{f}}^2, \tag{5.26}$$

where the adiabatic field σ is defined via:

$$d\sigma = e^b \cos\theta d\phi + \sqrt{6}e^{-b}\sin\theta d\mathfrak{f}, \tag{5.27}$$

in which $\cos\theta = e^b\dot{\phi}/\dot{\sigma}$ and $\sin\theta = \sqrt{6}e^{-b}\dot{\mathfrak{f}}/\dot{\sigma}$. In this notation, the unit vectors that satisfy (3.86) are

$$\mathbf{u}_\sigma^I = \left(e^{-b}\cos\theta, \frac{e^b}{\sqrt{6}}\sin\theta\right), \qquad \mathbf{u}_s^I = \left(-e^{-b}\sin\theta, \frac{e^b}{\sqrt{6}}\cos\theta\right), \tag{5.28}$$

to be in line with [196], as discussed in Subsection 3.3.2. Within this formalism, adiabatic and entropy perturbations, which we denote by $\delta\sigma$ and δs, are defined by (3.90). In particular, we can evaluate the entropy perturbations by imposing the constraint given in (5.24)

$$\delta s = \sqrt{6}e^{-b}\cos\theta\delta\mathfrak{f} - e^b\sin\theta\delta\phi = \left[\frac{12e^{-b}M_{\rm P}^2\phi}{(2M_{\rm P}^2 - \phi^2)^{3/2}}\cos\theta - e^b\sin\theta\right]\delta\phi = 0\,, \tag{5.29}$$

following directly by substituting the explicit forms of $\sin\theta$ and $\cos\theta$, and using $\dot{\mathfrak{f}} = (\partial\mathfrak{f}/\partial\phi)\dot{\phi}$. This demonstrates that entropy perturbations vanish in our model as a direct consequence of the constraint in (5.24), which itself originates from the conservation of the Noether current associated with scale symmetry. Hence, in the two field model, the absence of entropy perturbations is ultimately a manifestation of scale invariance[1]. An important implication of this result is that it eliminates concerns about a tachyonic mass for entropy perturbations – a known issue in many multifield inflationary models with hyperbolic field space geometry, where it can prematurely end inflation [206]. In contrast, scale invariance in our setup offers protection against such geometric instabilities. Furthermore, the formalism adopted here is not affected by the apparent destabilisation

[1] This is not true in the three field framework [285].

effects explored in [286], where the need for a careful definition of the entropy variable when assessing the presence of growing isocurvature modes is emphasised. Given our result in (5.29), the decomposition of perturbations into components tangent and normal to the inflationary trajectory is well-defined and free from such ambiguities.

5.1.2 Field redefinition and observable predictions

In the following analysis, we demonstrate that the dynamical content of the model can be effectively shifted onto a single field, allowing for a single-field description of inflation. The remaining field behaves as a spectator throughout the inflationary evolution. Starting from (5.23), we define new fields

$$\rho = \sqrt{6} M_{\rm P} \, \text{arcsinh}\left(\frac{\phi \mathfrak{f}}{\sqrt{6} M_{\rm P}^2}\right), \tag{5.30}$$

$$\chi = \frac{M_{\rm P}}{2} \ln\left(\frac{\phi^2}{2M_{\rm P}^2} + \frac{3M_{\rm P}^2}{\mathfrak{f}^2}\right). \tag{5.31}$$

Hence, the Lagrangian density in the EF (4.1) becomes

$$\frac{\mathcal{L}_E}{\sqrt{-g}} = \frac{M^2}{2} R - \frac{1}{2}\partial_\mu \rho \partial^\mu \rho - 3\cosh^2\left(\frac{\rho}{\sqrt{6}M}\right) \partial_\mu \chi \partial^\mu \chi - V(\phi^I), \tag{5.32}$$

in which

$$\phi^I \equiv \begin{pmatrix} \rho \\ \chi \end{pmatrix}, \qquad \mathcal{G}_{IJ} \equiv \begin{pmatrix} 1 & 0 \\ 0 & e^{2b(\rho)} \end{pmatrix}, \tag{5.33}$$

and the coupling is now defined as

$$b(\rho) = \frac{1}{2} \ln\left[6\cosh^2\left(\frac{\rho}{\sqrt{6}M_{\rm P}}\right)\right]. \tag{5.34}$$

The scalar potential in the $\{\rho, \chi\}$ basis depends only on ρ and can be written as

$$V(\phi^I) = V(\rho) = \frac{9M_{\rm P}^4}{4\alpha}\left[1 - 4\xi \sinh^2\left(\frac{\rho}{\sqrt{6}M_{\rm P}}\right) + 4\Omega \sinh^4\left(\frac{\rho}{\sqrt{6}M_{\rm P}}\right)\right]. \tag{5.35}$$

The shape of (5.35) is that of a "Mexican hat" potential with a nonzero minimum. The vacuum expectation value of the field leads to a residual vacuum energy, which effectively acts as a cosmological constant. As shown in [97], one can tune the couplings so that the R^2 and ϕ^4 contributions cancel this constant exactly, though not in agreement with observational spectral indices. For phenomenologically viable parameters, the left-over vacuum energy is large and requires an additional cancellation mechanism – *e.g.*

via a third, scale-symmetric field that participates in inflation rather than remaining a spectator, as explored in [285]. Extending our analysis to include such a field is an interesting avenue for future work. At the background level, the homogeneous KG equations are

$$\ddot{\rho} + 3H\dot{\rho} + V_\rho = b_\rho\, e^{2b(\rho)}\dot{\chi}^2, \tag{5.36}$$

$$\ddot{\chi} + 3H\dot{\chi} + 2b_\rho\,\dot{\chi}\dot{\rho} = 0. \tag{5.37}$$

The Einstein equations determining the evolution of the scale factor are

$$H^2 = \frac{1}{3}\left(\frac{\dot{\rho}^2}{2} + e^{2b(\rho)}\frac{\dot{\chi}^2}{2} + V(\rho)\right), \tag{5.38}$$

$$\dot{H} = -\frac{1}{2}\left(\dot{\rho}^2 + e^{2b(\rho)}\dot{\chi}^2\right), \tag{5.39}$$

in which we set $M_{\rm P}^2 = 1$. From the above, χ clearly behaves as the Goldstone mode: it settles to a constant value. Consequently, the only active degree of freedom driving inflation is ρ, in agreement with the fact that $V(\phi^I) = V(\rho)$. Indeed, In the slow-roll regime, (5.37) reduces to the single-field inflationary equation for ρ. Equivalently, in the rotated field basis (3.88), one finds $\theta \approx 0$. The evolution on the entropy direction (3.94) vanishes identically, so the background trajectory remains straight and flat. There is no potential coupling between adiabatic and entropy perturbations (since $V_s = 0$) either. Therefore, all dynamics reduces to the tangent field σ, which in slow roll (4.25) reduces to

$$\frac{\ddot{\sigma}}{H\dot{\sigma}} \simeq \epsilon_0 - \eta_{\rho\rho}. \tag{5.40}$$

In this regime, equations (4.27) and (4.28) hold. Inserting the two Friedmann equations (5.38) and (5.39) in the definition of ϵ_0 given in (3.23), and further employing (5.40) we get

$$\dot{\epsilon_0} \simeq 2\epsilon_0 H(2\epsilon_0 - \eta_{\rho\rho}), \tag{5.41}$$

which, inserted in (4.28), gives

$$n_* \simeq -6\epsilon_0 + \eta_{\rho\rho}. \tag{5.42}$$

On the other hand, its running (4.31) takes the form

$$\alpha_* \simeq -24\epsilon_0^2 + 16\epsilon_0\eta_{\rho\rho} + 2\sqrt{2\epsilon_0}\cos\theta\frac{V_{\rho\rho\rho}}{3H^2}, \tag{5.43}$$

and the running of the running (4.33) is

$$\beta_* \simeq -192\epsilon_0^3 + 64\epsilon_0^2\eta_{\rho\rho} - 32\epsilon_0\eta_{\rho\rho}^2 + \frac{8\sqrt{2}\epsilon_0^{3/2}\cos\theta V_{\rho\rho\rho}}{H^2} - \frac{2\sqrt{2\epsilon_0}\cos\theta\eta_{\rho\rho}V_{\rho\rho\rho}}{3H^2} + \\ + \frac{4\epsilon_0\cos^2\theta V_{\rho\rho\rho\rho}}{3H^2}. \tag{5.44}$$

To generate the predictions, we need the derivatives of the potential (5.35) up to fourth order, and those of the function (5.34) up to second order. We derive these expressions explicitly in Appendix C; these will be useful later for numerical implementation.

In the same vein as in the previous section, moving on super-horizon scales, we can also evaluate – in the slow-roll regime – the dimensionless function A (4.35) which reduces to

$$A = 2\xi_1 \sin\theta \simeq 0\,, \tag{5.45}$$

with $\xi_1 \equiv \sqrt{2\epsilon_0}b_\rho$ which demonstrates that isocurvature modes do not influence the adiabatic spectrum. Indeed, since $\theta \approx 0$ and hence $A \approx 0$, the cross-transfer $\mathcal{T}_{\zeta\mathcal{S}}$ vanishes (see (4.37)) and the final spectrum remains identical to its value at horizon crossing (*i.e.* it is simply multiplied by 1).

5.1.3 Non-gaussianity

Starting from the fact that the inflationary dynamics is effectively governed by the field ρ, as demonstrated in the previous section, we expect observables such as non-Gaussianities to reflect the behavior of a single-field inflation model with canonical kinetic terms. Primordial cosmological perturbations are usually expressed in terms of the curvature perturbations on uniform energy density hypersurfaces (3.101) and (4.12). Moreover, when evaluated on a final uniform-density slice at time t_c, ζ can be written as the spatial variation in the number of e-folds between an initial flat slice at t_* and the comoving slice at t_c,

$$\zeta(t_c, \mathbf{x}) \simeq \delta N(t_c, t_*, \mathbf{x}). \tag{5.46}$$

This "δN relation"[202, 203] allows us to track the full nonlinear evolution of super-horizon perturbations without solving the complete set of perturbed field equations. The spatial variation can be expanded as

$$\delta N(t_c, t_*, \mathbf{x}) = N_I(N, \phi_*^J)\delta\phi_*^I(\mathbf{x}) + \frac{1}{2}N_{IJ}(\phi_*^K)\delta\phi_*^I(\mathbf{x})\delta\phi_*^J(\mathbf{x}) + \dots \tag{5.47}$$

up to second order in the field fluctuations $\delta\phi_*^I(\mathbf{x}) \equiv \phi_*^I(\mathbf{x}) - \phi_*^I$. For small $\delta\phi_*^I(\mathbf{x})$, the two points $\phi_*^I(\mathbf{x})$ and the background value ϕ_*^I lie on a unique geodesic in field space,

which we parametrise by λ. Introducing the tangent-space vector $Q^I = d\phi^I/d\lambda|_{\lambda=0}$, which transforms covariantly under field-space coordinate transformations [287, 288] we can express $\delta\phi^I$ in terms of Q^I as

$$\delta\phi^I = Q^I - \frac{1}{2!}\Gamma^I_{JK}Q^JQ^K + \dots , \tag{5.48}$$

and hence recast (5.47) in a manifestly covariant form as

$$\zeta(N,\mathbf{x}) = N_I(N,\phi^J_*)Q^I_*(\mathbf{x}) + \frac{1}{2}\mathcal{D}_I\mathcal{D}_JN(N,\phi^K_*)Q^I_*(\mathbf{x})Q^J_*(\mathbf{x}) + \dots , \tag{5.49}$$

again truncating at second order. We now consider the correlation functions of the curvature perturbation in Fourier space. The two-point function is parametrised as

$$\langle\zeta(\mathbf{k}_1)\zeta(\mathbf{k}_2)\rangle = (2\pi)^3\delta^3(\mathbf{k}_1+\mathbf{k}_2)P_\zeta(k_1) = (2\pi)^3\delta(\mathbf{k}_1+\mathbf{k}_2)\frac{2\pi^2}{k_1^3}\mathcal{P}_\zeta(k_1)\,, \tag{5.50}$$

where $P_\zeta(k)$ and $\mathcal{P}_\zeta(k)$ are respectively the power spectrum and reduced power spectrum, and the three-point correlation function defines the bispectrum:

$$\langle\zeta(\mathbf{k}_1)\zeta(\mathbf{k}_3)\zeta(\mathbf{k}_3)\rangle = (2\pi)^3\delta^3(\mathbf{k}_1+\mathbf{k}_2+\mathbf{k}_3)B_\zeta(k_1,k_2,k_3)\,. \tag{5.51}$$

By definition, a purely Gaussian field has vanishing connected higher-point functions beyond the two-point function; thus any nonzero bispectrum signals primordial non-Gaussianity. Improved upper limits on the amount of non-Gaussianity critically test inflationary dynamics: minimal single-field slow-roll predicts negligible signals, while measurable non-Gaussianities points to additional fields, non-trivial kinetic structure, or non-standard vacua. Observationally, non-Gaussianities leave imprints in the CMB bispectrum and on large-scale structures. Even small levels affect the abundance and clustering of rare objects, impacting the thermal and ionisation history. Therefore, studying primordial non-Gaussianities provides a unique and powerful probe of the physics of the very early universe and guides model-building in inflationary cosmology. A common phenomenological parameterisation of "local" or "squeezed"[2] non-Gaussianities is given by their magnitude with the parameter $f_{\rm NL}$

$$f_{\rm NL} = \frac{5}{6}\frac{B_\zeta(k_1,k_2,k_3)}{P_\zeta(k_1)P_\zeta(k_2) + \text{c.p.}}\,, \tag{5.52}$$

[2]Different inflationary (or alternative) mechanisms yield bispectra peaking on characteristic triangular configurations in momentum space. The squeezed triangle arises in models where curvature perturbations are generated or modulated by a second light field outside the horizon [289–291].

where c.p. denotes cyclic permutations of k_1,k_2 and k_3. We stress that the δN formalism is only valid in the squeezed limit of the three-point correlation function ($k_3 \ll k_1 \simeq k_2$). Following [287] and using (5.49), we find the power spectrum

$$\mathcal{P}_\zeta = \left(\frac{H_*}{2\pi}\right)^2 \mathcal{G}_*^{IJ} N_I N_J = \left(\frac{H_*}{2\pi}\right)^2 N_\rho^2 , \tag{5.53}$$

where $N \simeq \int d\rho/(M_p\sqrt{2\epsilon_0(\rho)})$. Hence, in the slow-roll regime, the non-Gaussianity parameter becomes (for detailed derivation see Appendix C)

$$f_{\rm NL} = \frac{5}{6}\frac{\mathcal{G}_*^{IK} N_K \mathcal{G}_*^{JL} N_L \mathcal{D}_I N_J}{(\mathcal{G}_*^{KH} N_H N_K)^2} = \frac{5}{6}\frac{N_\rho^2 (N_{\rho\rho} - \Gamma^\rho_{\rho\rho} N_\rho)}{N_\rho^4} = \frac{5}{6}\frac{N_{\rho\rho}}{N_\rho^2} \simeq \frac{5}{3} M \epsilon_0(\rho) \frac{\partial}{\partial\rho}\frac{1}{\sqrt{2\epsilon_0(\rho)}} . \tag{5.54}$$

This expression coincides exactly with the result found in single-field inflation with a canonical kinetic term [292]. This agreement reflects the fact that, as noted above, our model's inflationary evolution is effectively governed by the field ρ with a canonical kinetic structure. Since slow-roll dynamics suppress $f_{\rm NL}$, the predicted non-Gaussianity remains well below current observational bounds. Nevertheless, one should also include the comparably small contribution arising at horizon crossing. Employing the Maldacena consistency relation – naturally incorporated in the δN framework [293] – one obtains

$$f_{\rm NL} = \frac{5}{12}(1 - n_s). \tag{5.55}$$

We have explicitly checked that, over the region of parameter space constrained by the numerical analysis presented in the following section, $f_{\rm NL}$ remains well below the current upper bounds on non-Gaussianity from the Planck temperature and polarisation bispectra. In particular, Planck constrains the local amplitude to $f_{\rm NL}^{\rm local} = -0.9 \pm 5.1$ [294]. For instance, at our benchmark point $\xi = 0.00039, \alpha = 1.87 \times 10^{10}, \Omega = 1.64 \times 10^{-7}, \rho_* = 5.15\, M_{\rm P}$, we obtain $f_{\rm NL}^{\rm local} = -0.015$, well within current observational bounds. Note that large-scale structure constraints on $f_{\rm NL}^{\rm local}$ are at least an order of magnitude weaker [248, 283, 295–297]. We focus on the local amplitude for three reasons: first, it peaks in the squeezed limit – where one of the three momenta is much smaller than the others – which is precisely where the δN formalism applies. Second, the local shape provides a clean diagnostic to discriminate between single-field and multifield inflation: single-field models predict an unobservably small local non-Gaussianity [298, 299], while multi-field models can generate a sizable signal [290, 300]. Third, the local amplitude is the most tightly constrained among the standard bispectrum shapes considered in cosmological data analyses. These shapes are: the local shape which peaks in the squeezed configuration and is associated with superhorizon evolution or modulation by light fields; the

equilateral shape, which peaks when all three momenta are of similar magnitude, typically arising in models with non-canonical kinetic terms or higher-derivative interactions [301, 302]; and the orthogonal shape, which has a more complex structure and was designed to be orthogonal to the local and equilateral templates, capturing certain higher-derivative models [303]. They serve as benchmarks in CMB analyses, notably those by the Planck collaboration [294], which place the tightest current bounds on primordial non-Gaussianities.

5.2 Cosmological constraints

The theoretical parametrisation described in Subsection 5.1.2 leaves three free parameters – ξ, Ω, α. We perform a Monte Carlo analysis with the aim of exploring the 3D parameter space, comparing the model's predictions against observational data. In doing so, we follow exactly the sampling strategy discussed in Section 4.3 employing an algorithm designed to cover a large parameter volume and pinpoint the subregion where theory and observations are in best agreement. The procedure of our sampling algorithm is as follows.

1. **Parameters and initial conditions Sampling**: at each Monte Carlo iteration, we draw the three model parameters (ξ, Ω, α) and the fields' initial values from uniform priors (see rightmost column of Table 5.1). This simultaneously explores both parameter space and sensitivity to initial conditions.

2. **Fields evolution and inflation-end test**: for each chosen parameter set and initial field values from step 1, we numerically solve the fields' equations of motion and track their evolution over the inflationary potential, allowing up to $N_{\max} = 10^7$ e-folds to accommodate the possibility of an extended slow-roll phase that could lead to eternal inflation. During integration, we monitor the slow-roll parameter ϵ_0 and declare the trajectory eternally inflating – and thus discard it – if ϵ_0 never reaches unity before $N_{\max}$. If ϵ_0 occurs at some $N < N_{\max}$, we mark that point as the end of inflation, then apply the checks from Subsection 4.3.1. Furthermore, we check: no re-entry into a slow-roll regime, $\epsilon_0 \neq 0$ throughout the evolution, and a total of $\Delta N > 70$ e-folds to ensure the observed universe's homogeneity and isotropy. Only trajectories passing all these tests advance to step 3; otherwise, we return to step 1 to sample anew.

3. **Observable reconstruction**: once the trajectory passes all the end-of-inflation

checks, we reconstruct the full evolution of the fields and slow-roll parameters as a function of N. In particular, at $N_* = 55$[3] e-folds before the end, we extract all relevant observables: the scalar power-spectrum amplitude A_s, its spectral index n_s, the running α_s, and the tensor-to-scalar ratio $r = A_T/A_s$. Our numerical code also implements the transfer-matrix formalism (4.37) [236] to capture any super-horizon exchange between isocurvature and curvature modes. However, as shown analytically in Subsection 5.1.2, scale invariance enforces $\mathcal{T}_{\zeta\mathcal{S}} = 0$ and we confirm numerically that entropy transfer vanishes. Consequently, the inflationary observables are fixed at horizon crossing – just as in single-field models – and remain unchanged through to the end of inflation, since $1 + \mathcal{T}_{\zeta\mathcal{S}} = 1$ (4.38).

4. **Likelihood evaluation and chain construction**: we save the model's predicted observables as a sequence of points, analogous to an MCMC chain, as we discussed in Subsection 4.3.1. Each point's likelihood is evaluated using a multi-dimensional normal distribution,

$$\mathcal{L} \propto \exp\left(-\frac{1}{2}\,(\boldsymbol{x}-\boldsymbol{\mu})^T\,\Sigma^{-1}\,(\boldsymbol{x}-\boldsymbol{\mu})\right), \tag{5.56}$$

where the parameter vector $\boldsymbol{x} = (A_s,\, n_s,\, \alpha_s,\, r)$, and $\boldsymbol{\mu}$ and Σ are the mean vector and covariance matrix derived from the joint Planck 2018 (TT, TE, EE + lensing) analysis [265, 267] combined with the 2018 BICEP/Keck foreground-cleaned B-mode likelihood [264]. For details see Appendix B.

5. **Iteration**: The algorithm then returns to step 1 and repeats, gradually building up the posterior distribution over $\{\xi,\, \Omega,\, \alpha\}$.

Using this procedure, we accumulate 7×10^4 sample points – each assigned its computed likelihood – allowing us to place bounds on the model's free parameters and to investigate correlations both among those parameters and among derived observables (*e.g.* n_s, A_s, r, etc.). Although the output resembles an MCMC chain, our algorithm is purely random, as discussed in Appendix B. The algorithm does not require a proposal distribution or acceptance criterion (such as Metropolis-Hastings [305]), and every sample carries equal weight by construction. Consequently, there is no formal convergence metric (*e.g.*

[3] Estimating the exact value of N_* would necessitate a detailed treatment of reheating, which lies outside the scope of this work. However, fixing it to 55 in the Einstein frame is well justified: as we demonstrate below in (5.62), the same n_s - r relation familiar from Starobinsky inflation (see (3.111) and (3.112)) applies here. Therefore, even with reheating taken into account, the departure from the standard Starobinsky value $N_* = 55$ remains below one e-fold [304].

Initial conditions	**Constraints**	**Uniform prior ranges**
$\rho_{\rm ini}/M_{\rm P}$	(*unconstrained*)	$\rho_{\rm ini}/M_{\rm P} \in [0.1, 2]$
$\chi_{\rm ini}/M_{\rm P}$	(*unconstrained*)	$\chi_{\rm ini}/M_{\rm P} \in [0.1, 10]$
Model parameters	**Constraints**	**Uniform prior ranges**
ξ	< 0.00142	$\log_{10}(\xi) \in [-5, -1]$
α	$1.951^{+0.076}_{-0.11} \times 10^{10}$	$10^{-10} \times \alpha \in [1, 3]$
Ω	$0.93^{+0.72}_{-2.8} \times 10^{-5}$	$\Omega \in [\xi^2, 2\xi^2]$
Primordial spectra parameters	**Constraints**	
A_s	$(2.112 \pm 0.033) \cdot 10^{-9}$	(*derived*)
n_s	$0.9638^{+0.0015}_{-0.0010}$	(*derived*)
α_s	$< 1.2 \times 10^{-4}$	(*derived*)
r	> 0.00332	(*derived*)

Table 5.1: External priors and observational constraints are listed for the initial conditions of the fields ρ and χ (first two rows), the model parameters ξ (specifically $\log_{10}\xi$), α, and Ω (next three rows), and the (derived) inflationary observables that characterize the primordial scalar and tensor power spectra: A_s, n_s, α_s, and r (bottom four rows). Regarding observational constraints, we report 1σ (68% CL) intervals for two-sided bounds, and 2σ (95% CL) upper or lower limits for all other cases.

Gelman-Rubin [306]), and convergence is instead assessed empirically by verifying that parameter constraints remain stable as additional samples are added. As an additional empirical check of convergence, we verified that increasing the number of points in the chains and computing the one-dimensional marginalised posterior distributions led to consistent statistical behavior in the tails. In particular, the regions corresponding to the 5% CL were found to contain approximately 5% of the total number of models. This is precisely the expected outcome when marginalising over the parameter space and provides strong evidence that the tails of the posterior distributions were properly sampled and sufficiently populated.

Constraints on the model parameters – including the initial conditions for the fields ρ and χ – as well as on the inflationary observables associated with the primordial scalar and tensor power spectra (treated as derived parameters), are summarised in Table 5.1. For parameters consistent with two-tailed bounds, we report 68% CL intervals, while for those lacking such evidence, we quote 95% CL upper or lower bounds. Figure 5.2 displays two-dimensional joint and one-dimensional marginalised posterior probability

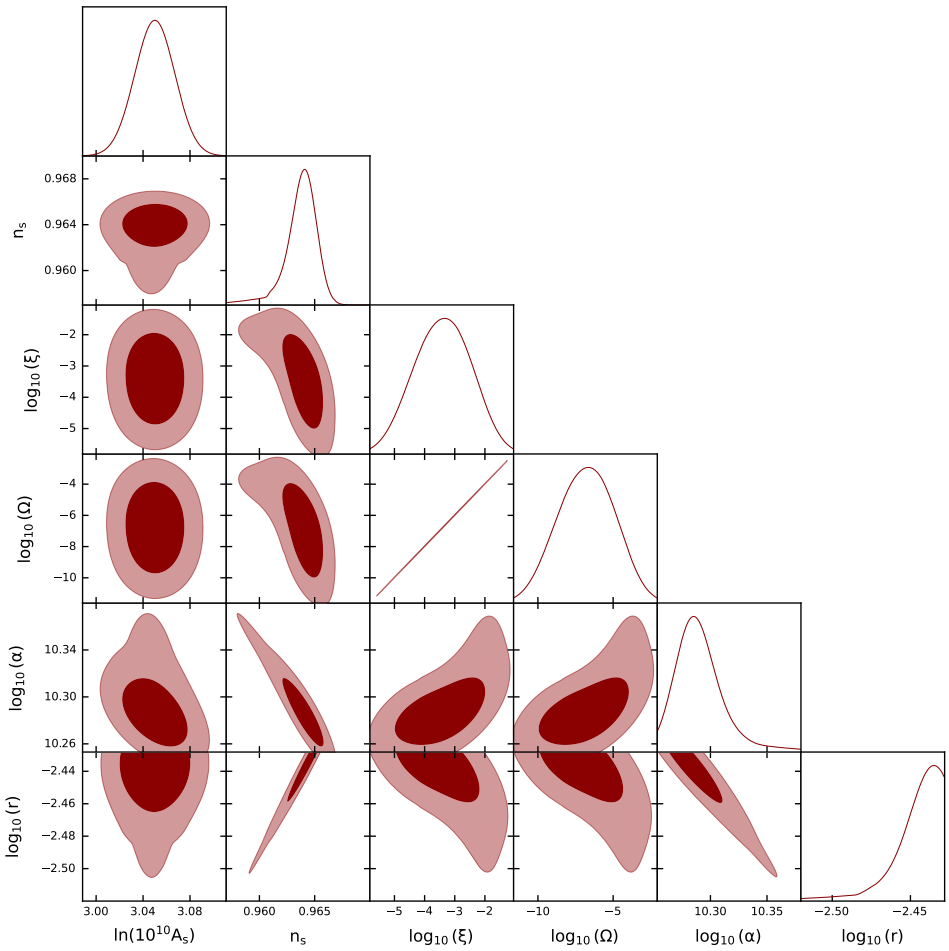

Figure 5.2: Triangular plot illustrating the two-dimensional joint and one-dimensional marginalised posterior probability distributions for a subset of parameters: the (natural logarithm of the) amplitude of primordial scalar perturbations A_s, the scalar spectral index n_s, and the (logarithms of the) coupling parameters ξ, Ω, and α. The parameters ξ and α govern the strengths of the $\phi^2 R$ and R^2 terms, respectively, in the JF action (see (1.69)), while the ratio Ω/α controls the $\sinh^4(\rho)$ term in the potential expressed in the (ρ, χ) field basis (5.35). The plot also includes the (logarithm of the) tensor-to-scalar ratio r.

distributions for a selection of parameters (excluding the distributions for the initial field values). A key result of our analysis is that, despite allowing $\rho_{\rm ini}$ and $\chi_{\rm ini}$ to vary over broad flat priors, these initial conditions remain entirely unconstrained. This outcome highlights the insensitivity of our model to the initial field values – an encouraging feature. By contrast, the three free model parameters – α, ξ, and Ω (with a flat prior imposed on $\log_{10}\xi$) – are well constrained within their prior ranges. The resulting 68% CL intervals and 95% CL limits remain away from the boundaries of the prior domains, suggesting that our constraints are driven by the underlying physics of the model rather than prior choices. To briefly recap the physical meaning of these parameters: ξ and α control the strength of the $\phi^2 R$ and R^2 terms, respectively, in the JF action (see (1.69)),

while Ω/α determines the strength of the $\sinh^4(\rho)$ term in the potential expressed in terms of the fields (ρ, χ) (see (5.35)). Given fixed values of α and ξ, the parameter Ω also determines λ, which sets the strength of the quartic interaction in the original JF action (1.69).

In more detail, the parameter α, which determines the strength of the R^2 term, is directly tied to the overall amplitude of the inflationary potential via (5.35). As a result, it significantly influences the amplitudes of both the primordial scalar and tensor power spectra. This connection is particularly clear in the correlations between α, A_s, and r, as shown in Figure 5.2. Since the amplitude of scalar perturbations A_s has been tightly constrained by Planck observations – primarily through its impact on the heights of the acoustic peaks in the CMB temperature and polarisation spectra – such measurements impose strong requirements on the amplitude of the inflationary potential. Consequently, A_s serves as a calibrator for inflationary models. This remains true in our scale-invariant framework which, reproducing the observed value $A_s = (2.112 \pm 0.033) \times 10^{-9}$,in excellent agreement with existing literature, results in the constraint $\alpha = 1.951^{+0.076}_{-0.11} \times 10^{10}$.

On the other hand, the parameter ξ, which controls the strength of the non-minimal coupling $\phi^2 R$, has a significant impact on both the scalar spectral index n_s and the amplitude of primordial tensor fluctuations via the tensor-to-scalar ratio r. As shown in the left panel of Figure 5.3, values of $\xi \sim 10^{-2}$ tend to shift n_s towards smaller values, around $n_s \sim 0.95$, whereas for $\xi \lesssim 10^{-3}$, the predictions flatten out to a plateau near $n_s \sim 0.965$, in good agreement with the Planck results. There are, however, two important caveats to this statement. First, CMB data from the Atacama Cosmology Telescope (ACT) are, in principle, compatible with $n_s = 1$, albeit with some degree of tension with Planck data [307–311]. Second, the quoted value of n_s is derived assuming the ΛCDM framework. Models involving new early-time physics – often proposed as possible resolutions of the Hubble tension [121–123, 125, 129] – typically predict higher values of n_s, in some cases approaching $n_s \approx 1$ (see, *e.g.* [312–321] for explicit examples). This trend arises because a larger scalar tilt can help compensate for shifts in the CMB spectrum induced by an enhanced early integrated Sachs-Wolfe effect, as well as modifications in the damping tail [115, 312, 319, 322, 323]. In view of these caveats, we caution against drawing too strong conclusions from the value of n_s inferred by Planck under the assumption of ΛCDM [324, 325]. Therefore, in order to maintain consistency with the observed value of n_s, excessively large values of ξ are not viable, as they would push the model into a region of parameter space where n_s becomes too small to remain in agreement with Planck data. This requirement leads to the 95% confidence level upper bound $\xi < 0.00142$. It is worth highlighting that this constraint excludes $\xi = 1$ with

very high statistical significance. In our parametrisation of the non-minimal coupling term $\phi^2 R$, the coupling appears as $\xi/6$, meaning that $\xi = 1$ corresponds to the conformal coupling. Consequently, our results rule out conformal invariance within the context of this model. This outcome is not unexpected, as conformal invariance imposes stronger symmetry constraints than scale invariance alone. It is worth noting that the low-n_s tail of the distribution is more extended than its high-n_s counterpart. This asymmetry gives rise to the somewhat non-Gaussian shapes observed in the contours of Figure 5.2. As evident from the same figure, smaller values of n_s are correlated with larger values of ξ, and vice versa. Consequently, the sharper high-n_s tail is a reflection of the lower bound imposed on the $\log_{10}\xi$ prior, which we set to $\log_{10}\xi > -5$. Naturally, the choice of this lower prior edge is somewhat arbitrary, as sampling in $\log_{10}\xi$ space prevents us from exploring arbitrarily small values of ξ (*i.e.* we cannot probe the exact $\xi \to 0$ limit). Nonetheless, our results remain robust and well-converged, even though convergence is not achieved in the strict MCMC sense. Moreover, we note that the allowed values of ξ in our analysis are significantly smaller than those typically required for the non-minimal coupling in Higgs inflation models [326–328]. As a result, our model does not suffer from the potential issues related to unitarity violation that have been raised in the context of Higgs inflation [327, 329–332]. We emphasise, however, that a direct comparison between the two scenarios is not entirely appropriate, since the scalar field driving inflation in our case is not the Higgs boson.

Regarding the parameter Ω – which, as previously discussed, controls the strength of the $\sinh^4(\rho)$ term in the potential within the (ρ, χ) field-space representation, or equivalently (once α and ξ are fixed) the strength of the quartic term in the JF action – it is important to clarify the prior range adopted in our analysis: $\Omega \in [\xi^2, 2\xi^2]$. This choice is motivated by semi-analytical considerations which indicate that, for a given value of ξ, avoiding eternal inflation requires Ω to lie within a relatively narrow range, specifically $\Omega \in [\xi^2, 1.15\,\xi^2]$ [274]. Our numerical results confirm this semi-analytical expectation. In particular, we observe that deviations from this interval tend to lead to scenarios where the numerical evolution enters a regime of eternal inflation. Consequently, we adopt the prior reported in Table 5.1, which is slightly more conservative than the analytical bound, allowing for a broader exploration of the parameter space. As with α and ξ, the parameter Ω also influences the shape of the inflationary potential and, therefore, impacts the resulting cosmological observables. This sensitivity leads to non-trivial correlations between Ω and both the model parameters and the inflationary predictions, as illustrated in Figure 5.2. In our analysis, we set a two-tailed constraint on Ω, $\Omega = 0.93^{+0.72}_{-2.8} \times 10^{-5}$.

We conclude this section with a few final remarks concerning both the predictive

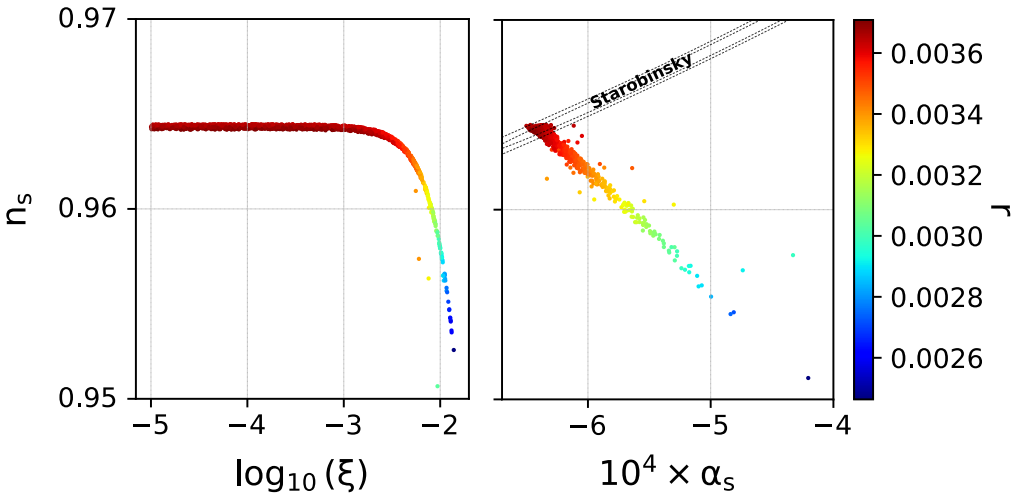

Figure 5.3: ***Left panel:*** 2D scatter plot in the $\log_{10}\xi$–n_s plane, where ξ parametrises the strength of the non-minimal coupling $\phi^2 R$ in the JF action. Points are color-coded according to the value of the tensor-to-scalar ratio r.
Right panel: 2D scatter plot in the $10^4\alpha_s$–n_s plane, where α_s denotes the running of the scalar spectral index. Points correspond to predictions from the scale-invariant model studied in this work and are color-coded by the value of the tensor-to-scalar ratio r. For comparison, predictions from Starobinsky inflation are also shown (dotted contours), though these are not color-coded by r.

power of our scale-invariant model and the distinctive features of the methodology adopted in this work. Our approach differs substantially from the standard procedures commonly found in the literature. Typically, predictions from inflationary models are compared to observational data by overlaying theoretical curves – computed at fixed benchmark values for the model parameters – onto pre-computed 2D marginalised probability contours in the n_s–r plane.[4] A representative example of this standard methodology is illustrated in Figure 8 of the Planck 2018 inflation paper [263]. In contrast, a key advantage of our method (see also [333, 334]) is that it allows us to compute fully model-dependent predictions for inflationary observables such as the tensor-to-scalar ratio r and the running of the spectral index α_s. Hence, assuming a specific model reduces the freedom to tune parameters independently, because the observables are interconnected by consistency conditions. These considerations are clearly reflected in the correlations observed within the 3D parameter space spanned by n_s, r, and α_s, as shown in the right panel of Figure 5.3. In particular, we find that more negative values of α_s are only realised when $n_s \sim 0.965$ and $r \sim 0.0036$. This region corresponds to the regime in which the effects of the non-minimal coupling $\phi^2 R$, controlled by ξ, are negligible – effectively reducing the dynamics to those of Starobinsky inflation, where the R^2 term

[4] This approach does not fully explore the parameter space of the model – it just checks how a few specific examples compare to the data.

dominates. On the other hand, lower values of $n_s \lesssim 0.96$ are associated with smaller values of r and less negative (*i.e.* smaller in absolute value) values of α_s, indicating a significant deviation from the predictions of Starobinsky-like models. It is important to note that these correlations emerge after marginalising over all free parameters of the model – namely ξ, α, and Ω – as well as over the initial conditions for the fields. Consequently, this approach provides a more comprehensive view of the correlations among inflationary observables within our specific scenario, thereby highlighting the predictive power of scale-invariant inflation. For example, we obtain the model-dependent predictions $r > 0.00332$ and $\alpha_s < 1.2 \times 10^{-4}$ (both at 95% CL), indicating a non-zero amplitude of primordial gravitational waves and a small running of the scalar spectral index. These are not generic features, but rather robust predictions that follow directly from the structure of the model. As such, they can be tested in the near future with forthcoming CMB experiments [184, 186, 335–337], providing an opportunity to either support or falsify the scenario. On the other hand, one may naturally ask whether these predictions are sufficient to distinguish this model from other competing frameworks. The next subsection is devoted to addressing both of these aspects in detail.

5.2.1 Comparison with Starobinsky inflation

As this approach differs fundamentally from the more conventional method of simply overlaying theoretical curves on pre-computed 2D marginalised n_s–r contours, our analysis should be interpreted as a model-specific prediction, as explained in the previous section. A natural question that arises is whether – and to what extent – these predictions can be distinguished from those of other well-known inflationary scenarios, such as Starobinsky inflation [39] or its α-attractor extensions [40, 338–341] (see also [342–351] for related developments). In this context, we note that Starobinsky inflation itself may be viewed as a scale-invariant model in the regime where the R^2 term dominates the dynamics – an assumption that typically holds in its standard realisation. One should therefore expect some degree of overlap in the predictions of the two frameworks, at least for specific ranges of model parameters.

We choose to compare our results against Starobinsky and α-attractor inflation not only due to their quasi-scale-invariant nature, but also because they are in excellent agreement with current observational data and are often used as benchmarks in forecasting the sensitivity of future CMB experiments.

To address these questions, in Figure 5.4 we present a comparison of the marginalised contours in the n_s–r plane for our scale-invariant inflationary model (shown in red) with those obtained for Starobinsky inflation (green) and α-attractor inflation (light blue). For the latter two models, the predictions are derived following the methodology outlined

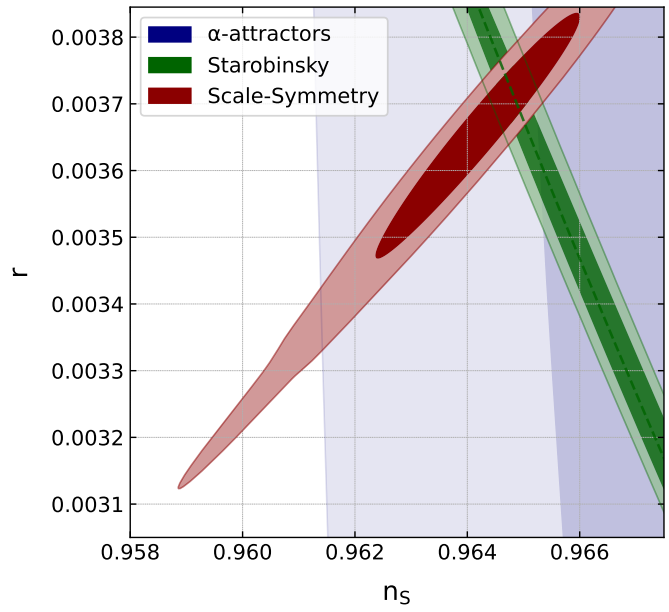

Figure 5.4: 2D contours in the n_s–r plane for the scale-invariant inflationary model studied in this work (red contours), shown in comparison with those of Starobinsky inflation (green contours) and α-attractors (light blue contours). The contours are derived using observational data from the *Planck* 2018 legacy release, combined with BICEP/Keck measurements (including BICEP2, Keck Array, and BICEP3 data up to 2018).

in [333]. This approach incorporates the relation between inflationary observables,

$$n_s \simeq 1 - \sqrt{\frac{r}{3\alpha}}, \tag{5.57}$$

with $\alpha = 1$ corresponding to the Starobinsky limit. This consistency relation is assumed within the cosmological model, and constraints are then obtained using the same dataset employed in our analysis of the scale-invariant inflationary model, to ensure a fair and meaningful comparison. Although the predictions of the three models overlap across a substantial region of parameter space, several notable differences can be identified. Most prominently, the red contours – corresponding to our scale-invariant inflationary model – exhibit a positive correlation between the amplitude of tensor modes and the scalar spectral index. That is, higher values of r are associated with higher values of n_s. This behavior stands in sharp contrast to that of Starobinsky inflation, where the two observables are related by (5.57) with $\alpha = 1$. This relation enforces a negative correlation: as r increases, n_s decreases. As a result the marginalised contours of the two models appear rotated with respect to each other in the n_s–r plane. Consequently, a significant portion of the parameter space that lies within the 68% CL region for the scale-invariant model falls outside the 95% confidence level region of Starobinsky inflation – and vice versa. In the case of the more general α-attractor scenario – where (5.57) is applied with α treated

as a free parameter – the correlation between n_s and r is effectively washed out due to marginalisation over α. When n_s is fixed, α primarily affects the tensor amplitude, effectively moving predictions vertically in the n_s–r plane between the Starobinsky limit ($\alpha = 1$) and the predictions of chaotic inflation with a quadratic potential ($V \propto \phi^2$). This flexibility allows for a wide range of r values to be accommodated by varying α, resulting in significantly broader posterior contours once α is marginalised over. Hence, the differences between scale-invariant inflation and Starobinsky inflation appear sufficiently significant to prompt further discussion regarding: their physical origin, and the implications that can be drawn in light of future, more precise CMB measurements from upcoming satellite and ground-based experiments. Our main observations are as follows:

1. With regard to the first point, we argued in the previous subsection that the parameter ξ exerts the strongest influence on the constraints in the n_s–r plane. Re-examining the left panel of Figure 5.3, we see that the predictions of Starobinsky inflation are fully recovered in the limit $\xi \to 0$, where the R^2 term dominates the dynamics. In this negligible-ξ regime we approach the familiar plateau at $n_s \simeq 0.965, r \simeq 0.0036$, precisely the region where the red (scale-invariant) and green (Starobinsky) contours overlap in Figure 5.4. Conversely, increasing ξ shifts the model toward smaller values of both n_s and r, driving it into a portion of the n_s–r plane that Starobinsky inflation cannot reach. The same trend is evident in the right panel of Figure 5.3: as long as ξ remains negligible (leftmost portion of the plot), the scale-invariant predictions (colored points) lie on top of the Starobinsky contours (dashed); once ξ becomes appreciable, the points migrate away, manifesting the distinct behaviour of the scale-invariant scenario in the full three-dimensional space spanned by n_s, r, and α_s. The fact that the predictions of scale-invariant inflation reduce to those of Starobinsky inflation in the limit $\xi \to 0$ can also be demonstrated semi-analytically, providing additional support for the robustness of our numerical results. To illustrate this, let us consider the potential slow-roll parameters (3.21), which depend only on the field ρ

$$\epsilon_V(\rho) = \frac{M_{\rm P}^2}{2}\left(\frac{V_\rho}{V}\right)^2, \qquad \eta_V(\rho) = M_{\rm P}^2\frac{V_{\rho\rho}}{V}, \tag{5.58}$$

from which the inflationary observables can be expressed as

$$n_s(\rho) \simeq 1 - 6\epsilon_V(\rho) + 2\eta_V(\rho), \qquad r(\rho) \simeq 16\epsilon_V(\rho). \tag{5.59}$$

These expressions can be computed analytically and simplify considerably in the

limit $\Omega \to \xi^2$, as discussed earlier. By additionally taking the limit $\xi \to 0$, we find

$$n_s \simeq 1 - \frac{8}{3}\xi \cosh\left(\frac{2}{3}\frac{\rho}{M_P}\right), \tag{5.60}$$

$$r \simeq \frac{64}{3}\xi^2 \sinh^2\left(\frac{2}{3}\frac{\rho}{M_P}\right). \tag{5.61}$$

Combining (5.60) and (5.61) allows us to eliminate the field dependence and obtain the following relation between the observables

$$n_s \simeq 1 - \frac{1}{3}\sqrt{3r + 64\xi^2} \simeq 1 - \sqrt{\frac{r}{3}}, \tag{5.62}$$

which is exactly the consistency relation found in Starobinsky inflation (5.57) with $\alpha = 1$. However, as soon as $\xi \neq 0$ – and thus the non-minimal coupling $\phi^2 R$ is present – the predictions of scale-invariant inflation begin to deviate from those of Starobinsky inflation. This departure is clearly visible in Figure 5.4.

2. Concerning future observations, we expect that the next generation of CMB experiments will significantly enhance our ability to constrain the amplitude of primordial tensor modes, potentially leading to their first detection. In some cases, these experiments are also projected to reduce the uncertainties on the scalar spectral index n_s. To quote a few representative forecasts (assuming a standard power-law form for the primordial spectra), the SO collaboration [186] anticipates a sensitivity of $\sigma(r) \sim 0.003$ on the tensor-to-scalar ratio, along with an expected improvement in the measurement of the scalar spectral index to $\sigma(n_s) \sim 0.003$. CMB-S4 [336] is projected to achieve even higher sensitivity, with $\sigma(r) \sim 0.001$–0.007 depending on foreground assumptions [336], and $\sigma(n_s) \sim 0.002$. Similarly, LiteBIRD [337] is expected to reach $\sigma(r) \lesssim 0.001$, although its impact on constraining n_s will be more limited – unsurprisingly, as LiteBIRD is primarily designed to probe large angular scale polarisation. These improvements in sensitivity could be decisive for testing the predictions of scale-invariant inflation. Assuming that our model provides a faithful description of the early Universe, our results based on current data predict a primordial tensor amplitude of at least $r \gtrsim 0.003$. This value lies well within the detection capabilities of all aforementioned experiments. For example, CMB-S4 is expected to detect a signal with $r > 0.003$ at up to 5σ significance [336]. Conversely, if no detection is made, CMB-S4 is forecast to place an upper bound of $r < 0.001$ at 95% CL. This implies that a null detection at that sensitivity would strongly disfavor, if not outright rule out, the scale-invariant inflationary scenario. Similar arguments apply to SO and LiteBIRD. That said, in

the optimistic case where r is detected, a key question remains: will a combined measurement of n_s and r be sufficient to distinguish between different models, such as scale-invariant and Starobinsky inflation? On one hand, the forthcoming experiments are expected to significantly tighten the allowed region in the n_s–r plane compared to current constraints from *Planck* and BICEP/Keck. Given the model-dependent differences visible in Figure 5.4, this may suggest that future observations could help discriminate between the two frameworks. Nonetheless, it is important to stress that predictions in the n_s–r plane depend sensitively on the value of ξ. Assuming that ξ takes relatively large values in nature, differences between the models can reach up to $\Delta n_s \sim 0.006$ when $r \sim 0.032$. In light of these considerations, it seems unlikely that upcoming CMB data alone will allow for a decisive distinction between scale-invariant and Starobinsky inflation at high statistical significance. This situation could change, however, if a widely accepted resolution to the Hubble tension were to shift the preferred value of n_s away from that predicted by ΛCDM. Such a shift could force us to reconsider the viability of various inflationary models altogether.

6 | Inflation in non-local hybrid modified gravity

Building on the discussion in *Part I* (Section 1.2), where we introduced the metric and Palatini formulations of gravity as distinct approaches, as well as the hybrid formalism that blends their features and the framework of non-local gravitational theories, we are now ready to present a model that unifies all these elements: *non-local hybrid metric-Palatini gravity*.

This work is based on [5] and it represents a pioneering step in the exploration of non-local modifications within the hybrid metric-Palatini framework, providing a rigorous analysis of the stability conditions of these combined theories and evaluating their viability, particularly in the context of early universe cosmology. Within the framework of hybrid gravity, we investigate non-localities introduced as powers of the inverse d'Alembert operator, assumed to act on both types of curvature scalars: the metric Ricci scalar R and the Palatini Ricci scalar $\mathcal{R}$. By doing so, we extend the analysis from the purely metric case studied in [96], incorporating Palatini contributions through the hybrid formalism developed for $f(R,\mathcal{R})$ theories in [54, 81, 352]. Following the approach of [96], we treat the non-local theory as dynamically equivalent to a local scalar-tensor model, where non-localities are localised via a suitable procedure involving auxiliary fields. We show in Section 6.1 that a naive extension of the analysis in [96] to the hybrid metric-Palatini case fails to eliminate ghost instabilities. Ghost instabilities refer to degrees of freedom with negative kinetic energy, which result in unphysical behavior such as vacuum decay and loss of unitarity in quantum theory [353–355]. Specifically, the number of ghost modes depends on the sum of the highest powers of the $\Box^{-k}$ operators acting on both metric and Palatini curvature terms. We argue that this is an inherent feature of any non-degenerate[1] non-local $F(R,\mathcal{R},\ldots,\Box^{-m}R,\ldots,\Box^{-n}\mathcal{R})$ action, even when restricting to a purely Palatini approach, in contrast with standard $f(R)$ gravity which introduces no additional degrees of freedom (for more details, see Appendix D). Building

[1] Non-degenerate action means that the kinetic matrix is invertible ensuring that the scalar field representation is meaningful and the dynamics is well-defined.

on this observation, in Section 6.2 we examine special configurations where degeneracy is explicitly broken; namely, metric $f(R)$ (or Palatini $f(\mathcal{R})$) models supplemented by Palatini (or metric) non-local terms. In these cases, the non-localities appear linearly in curvature terms, leading to deformations of the Starobinsky-like potential and offering a new way to test the robustness of the model. We show how this hybridisation can restore dynamical stability, and we derive a set of algebraic conditions that ensure the absence of ghost modes within the resulting three-dimensional scalar field space. In Section 6.3 we then explore the possibility of realising inflation in this framework. As a first step, we verify the well-posedness of the first-order slow-roll parameter, which imposes additional constraints on the derivatives of the potential and the scalar fields. We then carry out a numerical analysis of the inflationary dynamics at the background level, studying how the scalar fields trajectories over the potential and the number of e-folds depend on different choices of initial non-local terms. We focus in particular on quadratic metric $f(R)$ models with Palatini non-localities, which turn out to be the only viable setup for a finite slow-roll phase; the quadratic Palatini $f(\mathcal{R})$ models with metric non-localities instead lead to an infinite slow-roll phase along one scalar field direction. Finally, for each viable scenario that achieves the correct number of e-folds, we numerically confirm that the no-ghost condition holds throughout the scalar field evolution.

6.1 Non-localities for hybrid metric-Palatini gravity

The starting point of our analysis is the non-local gravity model introduced in Subsection 1.2.1, which we extend here by incorporating the hybrid metric-Palatini framework as developed in Subsection 1.2.1 [54, 81]. In this context, we consider the action

$$S = \int d^4x\sqrt{-g}\, F\left(R, \mathcal{R}, \Box^{-1}R, \ldots, \Box^{-m}R, \Box^{-1}\mathcal{R}, \ldots, \Box^{-n}\mathcal{R}\right), \tag{6.1}$$

where F is a function of both the Ricci scalar R, constructed from the Levi-Civita connection of the metric $g_{\mu\nu}$, and the Palatini Ricci scalar $\mathcal{R}$, which depends on an independent connection $\Gamma^{\rho}_{\mu\nu}$, namely

$$R = g^{\mu\nu}R_{\mu\nu}(g), \tag{6.2}$$

$$\mathcal{R} = g^{\mu\nu}\mathcal{R}_{\mu\nu}(\Gamma). \tag{6.3}$$

To recast the original action into a scalar-tensor representation (see Subsection 1.2.1), we introduce auxiliary scalar fields and rewrite (6.1) as

$$S = \int d^4x\sqrt{-g}\Big[F\left(R,\mathcal{R},\vec{\alpha},\vec{\beta}\right) - \lambda_1(\Box\alpha_1 - R) - \rho_1(\Box\beta_1 - \mathcal{R}) \\ - \sum_{i=2}^{m}\lambda_i(\Box\alpha_i - \alpha_{i-1}) - \sum_{j=2}^{n}\rho_j(\Box\beta_j - \beta_{j-1})\Big], \tag{6.4}$$

where $\vec{\alpha} = (\alpha_1,\ldots,\alpha_m)$ and $\vec{\beta} = (\beta_1,\ldots,\beta_n)$ are tuples of real scalar fields, and λ_i, ρ_j are the corresponding Lagrange multipliers. Varying the action with respect to the Lagrange multipliers enforces the non-local structure of the original formulation, as shown by the relations

$$\begin{aligned}
&\delta_{\lambda_1}S = 0 \Rightarrow \alpha_1 = \Box^{-1}R,\\
&\delta_{\lambda_2}S = 0 \Rightarrow \alpha_2 = \Box^{-1}\alpha_1 = \Box^{-2}R,\\
&\quad\vdots\\
&\delta_{\lambda_i}S = 0 \Rightarrow \alpha_i = \Box^{-1}\alpha_{i-1} = \Box^{-i}R,
\end{aligned}$$

and similarly for β_j and the Palatini scalar $\mathcal{R}$. This procedure ensures that the scalar-tensor representation remains dynamically equivalent to the original non-local formulation. The term $F(R,\mathcal{R},\vec{\alpha},\vec{\beta})$ can be further reformulated by introducing two auxiliary fields χ and η, yielding

$$F(R,\mathcal{R},\vec{\alpha},\vec{\beta}) = \phi(R-\chi) + \xi(\mathcal{R}-\eta) + F(\chi,\eta,\vec{\alpha},\vec{\beta}), \tag{6.5}$$

where we defined the derivatives

$$\phi \equiv \frac{\partial F}{\partial\chi}, \qquad \xi \equiv \frac{\partial F}{\partial\eta}. \tag{6.6}$$

By plugging (6.5) into the action (6.4) we achieve

$$S = \int d^4x\sqrt{-g}\Big[(\phi+\lambda_1)R + (\xi+\rho_1)\mathcal{R} - W(\phi,\xi,\vec{\alpha},\vec{\beta},\vec{\lambda},\vec{\rho}) \\ + \sum_{j=1}^{m}\nabla_\mu\alpha_j\nabla^\mu\lambda_j + \sum_{j=1}^{n}\nabla_\mu\beta_j\nabla^\mu\rho_j\Big], \tag{6.7}$$

provided the Hessian condition $F_{\chi\chi}F_{\eta\eta} - (F_{\chi\eta})^2 \neq 0$, also known as non-degenerate condition which ensures a well-defined inversion of variables:

$$\begin{cases} \chi = f(\phi, \xi, \vec{\alpha}, \vec{\beta}), \\ \eta = g(\phi, \xi, \vec{\alpha}, \vec{\beta}). \end{cases} \tag{6.8}$$

In (6.7) we also have defined the effective potential

$$W = \phi f(\phi, \xi, \vec{\alpha}, \vec{\beta}) + \xi g(\phi, \xi, \vec{\alpha}, \vec{\beta}) - F(\phi, \xi, \vec{\alpha}, \vec{\beta}) - \sum_{j=1}^{m} \alpha_{j-1}\lambda_j - \sum_{j=1}^{n} \beta_{j-1}\rho_j, \tag{6.9}$$

with the identification $\alpha_0 = \beta_0 = 0$. Next, by varying (6.7) with respect to the independent connection $\Gamma^{\rho}_{\mu\nu}$, under the assumptions of vanishing torsion $\Gamma^{\rho}_{\mu\nu} = \Gamma^{\rho}_{\nu\mu}$ and metric compatibility $\nabla_\rho g_{\mu\nu} = 0$, one obtains the connection equation (1.28)

$$\nabla_\rho \left(\sqrt{-g}\,\Xi\, g^{\mu\nu}\right) = 0, \tag{6.10}$$

where $\Xi \equiv \xi + \rho_1$. This equation admits as a solution the Levi-Civita connection associated with the conformally related metric

$$h_{\mu\nu} = \Xi g_{\mu\nu}, \tag{6.11}$$

which implies

$$\Gamma^{\rho}_{\mu\nu} = \frac{1}{2} h^{\rho\sigma}\left(\partial_\mu h_{\nu\sigma} + \partial_\nu h_{\mu\sigma} - \partial_\sigma h_{\mu\nu}\right). \tag{6.12}$$

Rewriting this expression in terms of the original metric $g_{\mu\nu}$ and the scalar field Ξ, we obtain (1.29)

$$\Gamma^{\rho}_{\mu\nu} = \{^{\rho}_{\mu\nu}\} + \frac{1}{2\Xi}\left(\delta^{\rho}_{\nu}\partial_\mu\Xi + \delta^{\rho}_{\mu}\partial_\nu\Xi - g_{\mu\nu}\partial^\rho\Xi\right), \tag{6.13}$$

where $\{^{\rho}_{\mu\nu}\}$ is (1.5). This allows us to express the Palatini Ricci scalar as (1.31)

$$\mathcal{R} = R + \frac{3}{2\Xi^2}\nabla_\mu\Xi\nabla^\mu\Xi - \frac{1}{\Xi}\Box\Xi. \tag{6.14}$$

where R is the Ricci scalar built from the Levi-Civita connection of the metric $g_{\mu\nu}$, the additional terms arise due to the independent variation of the affine connection in the Palatini formalism. Importantly, in Palatini gravity one does not need to assume from the start that the connection is torsionless and metric-compatible. A fully dynamical treatment, in which the torsion and non-metricity tensors are initially allowed, leads to the same result once the connection equations are solved. This is because such non-Riemannian components do not introduce physical propagating degrees of freedom. In-

stead, they are algebraically determined by the derivatives of the scalar field Ξ, and can be interpreted as spurious degrees of freedom – extra components of the connection that are not dynamical and can be eliminated without affecting the physics. This elimination is possible thanks to the projective symmetry of the Palatini action: under a transformation of the form $\Gamma^{\rho}_{\mu\nu} \to \Gamma^{\rho}_{\mu\nu} + \delta^{\rho}_{\mu}\xi_{\nu}$ for an arbitrary covector field ξ_{ν} the Ricci scalar R remains invariant up to a total derivative. As a result, the connection possesses redundant components that can be gauged away. After accounting for this symmetry, the remaining connection degrees of freedom can be fully expressed in terms of the metric and the scalar field, leading again to the curvature expression (6.14). Therefore, even when torsion and non-metricity are initially included, they do not yield new physics in this context and ultimately reduce to known metric-dependent terms (for all the details see, *e.g.* [356–359]).

Substituting (6.14) into the action (6.7), we finally obtain

$$S = \int d^4x\sqrt{-g}\Bigg[(\phi + \lambda_1 + \Xi)R + \frac{3}{2\Xi}\nabla_\mu\Xi\nabla^\mu\Xi - W(\phi, \xi, \vec{\alpha}, \vec{\beta}, \vec{\lambda}, \vec{\rho}) + \sum_{j=1}^{m}\nabla_\mu\alpha_j\nabla^\mu\lambda_j + \sum_{j=1}^{n}\nabla_\mu\beta_j\nabla^\mu\rho_j\Bigg]. \tag{6.15}$$

At this stage, we note that it is always possible to perform a linear field redefinition of the form

$$\begin{cases} \phi + \lambda_1 + \Xi = \Phi, \\ \lambda_i = a^{(i)}_{11}\psi^{(i)}_1 + a^{(i)}_{12}\psi^{(i)}_2, \\ \alpha_i = a^{(i)}_{21}\psi^{(i)}_1 + a^{(i)}_{22}\psi^{(i)}_2, \\ \rho_j = b^{(j)}_{11}\omega^{(j)}_1 + b^{(j)}_{12}\omega^{(j)}_2, \\ \beta_j = b^{(j)}_{21}\omega^{(j)}_1 + b^{(j)}_{22}\omega^{(j)}_2, \end{cases} \tag{6.16}$$

which is well-defined provided the Jacobian of the transformation is non-degenerate. This requirement translates into the condition

$$|J| = \prod_{i=1}^{m}\det A^{(i)}\prod_{j=1}^{n}\det B^{(j)} \neq 0, \tag{6.17}$$

where we defined the matrices

$$A^{(i)} = \begin{pmatrix} a^{(i)}_{11} & a^{(i)}_{12} \\ a^{(i)}_{21} & a^{(i)}_{22} \end{pmatrix}, \qquad B^{(j)} = \begin{pmatrix} b^{(j)}_{11} & b^{(j)}_{12} \\ b^{(j)}_{21} & b^{(j)}_{22} \end{pmatrix}, \tag{6.18}$$

and it is easy to verify that the non-degeneracy condition is simply

$$\det A^{(i)} \neq 0, \quad \det B^{(j)} \neq 0 \quad \forall\, i, j. \tag{6.19}$$

Under these conditions, the action can be rewritten as

$$\begin{aligned} S_J = \frac{1}{2\kappa^2}\int d^4x\sqrt{-g}\Bigg(\Phi R + \frac{3(\nabla\Xi)^2}{2\Xi} - W(\Phi,\Xi,\vec{\psi}_1,\vec{\psi}_2,\vec{\omega}_1,\vec{\omega}_2) + \\ + \sum_{i=1}^{m} K^{kl}_{(i)}\nabla_\mu\psi^{(i)}_k\nabla^\mu\psi^{(i)}_l + \sum_{j=1}^{n} H^{kl}_{(j)}\nabla_\mu\omega^{(j)}_k\nabla^\mu\omega^{(j)}_l\Bigg), \end{aligned} \tag{6.20}$$

with $(k,l) = 1,2$, and where the kinetic matrices $K_{(i)}$ and $H_{(j)}$ are given by

$$K_{(i)} = \begin{pmatrix} a^{(i)}_{11}a^{(i)}_{21} & \frac{1}{2}(a^{(i)}_{11}a^{(i)}_{22} + a^{(i)}_{12}a^{(i)}_{21}) \\ \frac{1}{2}(a^{(i)}_{11}a^{(i)}_{22} + a^{(i)}_{12}a^{(i)}_{21}) & a^{(i)}_{12}a^{(i)}_{22} \end{pmatrix}, \tag{6.21}$$

$$H_{(j)} = \begin{pmatrix} b^{(j)}_{11}b^{(j)}_{21} & \frac{1}{2}(b^{(j)}_{11}b^{(j)}_{22} + b^{(j)}_{12}b^{(j)}_{21}) \\ \frac{1}{2}(b^{(j)}_{11}b^{(j)}_{22} + b^{(j)}_{12}b^{(j)}_{21}) & b^{(j)}_{12}b^{(j)}_{22} \end{pmatrix}. \tag{6.22}$$

A simple choice for the matrices $A^{(i)}$ and $B^{(j)}$ is

$$A^{(i)} = B^{(j)} = \begin{pmatrix} 1 & 1 \\ 1 & -1 \end{pmatrix}, \tag{6.23}$$

which diagonalises the kinetic matrices as

$$K_{(i)} = H_{(j)} = \begin{pmatrix} 1 & 0 \\ 0 & -1 \end{pmatrix}, \qquad \forall\, i, j. \tag{6.24}$$

With this choice, the action simplifies to

$$S_J = \frac{1}{2\kappa^2}\left(\Phi R + \frac{3(\nabla\Xi)^2}{2\Xi} + (\boldsymbol{\Psi} + \boldsymbol{\Omega}) - W(\Phi,\Xi,\vec{\psi}_1,\vec{\psi}_2,\vec{\omega}_1,\vec{\omega}_2)\right), \tag{6.25}$$

where we have defined the shorthand

$$\boldsymbol{\Psi} \equiv \sum_{i=1}^{m}\left[(\nabla\psi^{(i)}_1)^2 - (\nabla\psi^{(i)}_2)^2\right], \tag{6.26}$$

$$\boldsymbol{\Omega} \equiv \sum_{j=1}^{n}\left[(\nabla\omega^{(j)}_1)^2 - (\nabla\omega^{(j)}_2)^2\right]. \tag{6.27}$$

Finally, performing a conformal transformation to the EF via $q_{\mu\nu} = \Phi g_{\mu\nu}$, the action

becomes

$$S_E = \frac{1}{2\kappa^2}\int d^4x\sqrt{-q}\left(R(q) - \frac{3(\nabla\Phi)^2}{2\Phi^2} + \frac{3(\nabla\Xi)^2}{2\Phi\Xi} + \frac{\Psi+\Omega}{\Phi} - \frac{W(\Phi,\Xi,\vec{\psi}_1,\vec{\psi}_2,\vec{\omega}_1,\vec{\omega}_2)}{\Phi^2}\right). \tag{6.28}$$

It follows that, upon fixing the total order of non-localities to be $N = n + m$, where n and m are the exponents that appear in (6.1), the theory generically contains at least N ghost-like degrees of freedom regardless of the sign of the field Φ or the specific form of the function F. Furthermore, if we impose $\Phi > 0$ to ensure the conformal transformation is well-defined, an additional ghost arises whenever $\Xi > 0$. This result is consistent with the findings of [54].

In particular, focusing on the $\Phi > 0$ branch, we can redefine the scalar fields as

$$\Phi = e^{\sqrt{\frac{2}{3}}\Phi_C}, \qquad \Xi = \sigma_\Xi \frac{\Xi_C^2}{6}, \tag{6.29}$$

where $\sigma_\Xi = \pm 1$ denotes the sign of the field Ξ. With these redefinitions, the action takes the form

$$S_E = \frac{1}{2\kappa^2}\int d^4x\sqrt{-q}\left(R(q) - (\nabla\Phi_C)^2 + \frac{\sigma_\Xi(\nabla\Xi_C)^2 + \Psi + \Omega}{e^{\sqrt{2/3}\Phi_C}} - \frac{W(\Phi,\Xi,\vec{\psi}_1,\vec{\psi}_2,\vec{\omega}_1,\vec{\omega}_2)}{e^{2\sqrt{2/3}\Phi_C}}\right), \tag{6.30}$$

where all kinetic terms are canonically normalised, up to an overall coupling to the scalar field Φ_C. A detailed discussion of the special case in which only one curvature invariant appears in the original action is presented in Appendix D, where we show that this does not affect the general conclusion regarding the structure and number of ghost fields.

6.2 Ghost free configurations

Ghost instabilities can be avoided by considering a linear coupling between the metric Ricci scalar and the non-local sector of the action, as it is shown in [96], see also Subsection 1.2.1. Here, we generalise the result I just mentioned by introducing two specific models where the dynamics is stabilised through the inclusion of non-local terms that retain the same type of coupling as in [96], but are constructed on top of standard $f(R)$-like theories.

To achieve this, we adopt the approach of [352], introducing *hybridisation* additively: we supplement the $f(R)$ sector with non-local contributions built from the type of curvature not originally present in the argument of the f function. This leads to two viable

configurations, described by the following Lagrangians:

$$\mathcal{L}_1 = f(\mathcal{R}) + R\,G(\Box^{-1}R) - V(\Box^{-1}R), \qquad \mathcal{L}_2 = f(R) + \mathcal{R}\,G(\Box^{-1}\mathcal{R}) - V(\Box^{-1}\mathcal{R}), \quad (6.31)$$

where G is a non-local operator. For completeness, we have included the function V, which does not affect the stability of the scalar degrees of freedom (as will be discussed below), but instead plays the role of a potential in the scalar-tensor representation of the theory. We also note that the configurations in (6.31) fall outside the general class discussed in Section 6.1, since the condition $F_{RR}F_{\mathcal{R}\mathcal{R}} - F_{R\mathcal{R}}^2 \neq 0$ is no longer satisfied in this case.

We begin by analysing the first case, namely a Palatini $f(\mathcal{R})$ theory supplemented with metric nonlocalities, as given by $\mathcal{L}_1$ in (6.31). Following the procedure outlined previously, the corresponding action can be recast in the scalar-tensor form

$$\begin{aligned} S_1 &= \frac{1}{2\kappa^2}\int d^4x\sqrt{-g}\Big[f(\mathcal{R}) + R\,G(\Box^{-1}R) - V(\Box^{-1}R)\Big] \\ &= \frac{1}{2\kappa^2}\int d^4x\sqrt{-g}\Big[\xi\mathcal{R} - U(\xi) + (\lambda + G(\alpha))R + \nabla^\mu\alpha\,\nabla_\mu\lambda - V(\alpha)\Big] \\ &= \frac{1}{2\kappa^2}\int d^4x\sqrt{-g}\Big[(\xi + \lambda + G(\alpha))R + \frac{3}{2\xi}(\nabla\xi)^2 + \nabla^\mu\alpha\,\nabla_\mu\lambda - (V(\alpha) + U(\xi))\Big] \\ &= \frac{1}{2\kappa^2}\int d^4x\sqrt{-g}\Big[\varphi R + \frac{3}{2\xi}(\nabla\xi)^2 + \nabla^\mu\alpha\,\nabla_\mu(\varphi - \xi - G(\alpha)) - W(\alpha,\xi)\Big], \end{aligned} \quad (6.32)$$

where, in the final line, we introduced the redefinition $\varphi \equiv \xi + \lambda + G(\alpha)$ and defined the effective potential $W(\alpha,\xi) \equiv V(\alpha) + U(\xi)$. Going to the EF via the conformal rescaling $q_{\mu\nu} = \varphi\, g_{\mu\nu}$, the action becomes

$$S_1 = \frac{1}{2\kappa^2}\int d^4x\sqrt{-q}\left[\tilde{R} - \frac{3}{2\varphi^2}(\nabla\varphi)^2 + \frac{3}{2\varphi\xi}(\nabla\xi)^2 + \frac{\nabla^\mu\alpha\,\nabla_\mu(\varphi - \xi - G(\alpha))}{\varphi} - \frac{W(\alpha,\xi)}{\varphi^2}\right], \quad (6.33)$$

where $\tilde{R}$ is the Ricci scalar associated with the EF metric $q_{\mu\nu}$. The kinetic sector of the theory is encoded in the matrix

$$K_1 = \frac{1}{\varphi}\begin{pmatrix} \frac{3}{2\varphi} & 0 & -\frac{1}{2} \\ 0 & -\frac{3}{2\xi} & \frac{1}{2} \\ -\frac{1}{2} & \frac{1}{2} & G'(\alpha) \end{pmatrix}, \quad (6.34)$$

written in the basis $(\varphi,\ \xi,\ \alpha)$. To ensure the absence of ghost instabilities, it is necessary that the kinetic matrix K_1 is positive definite. For symmetric matrices, this requirement

is equivalent to demanding that all eigenvalues are positive. Although, in principle, the eigenvalues of the kinetic matrix can be obtained by diagonalising it, the unspecified functional dependence of G on the scalar field α generally prevents an explicit derivation of the transformation between the original field basis and the diagonal one. As a consequence, the action cannot be straightforwardly expressed in a diagonal form. To overcome this limitation and facilitate the analysis of the positivity of the kinetic sector, we make use of *Sylvester's criterion*. This criterion states that a symmetric real matrix is positive definite if and only if all the leading principal minors – *i.e.* the determinants of the upper-left $k \times k$ submatrices M_k with $1 \leq k \leq n$ (where n is the matrix dimension) – are strictly positive. Applying Sylvester's criterion to the kinetic matrix K_1 given in (6.34), we obtain the following conditions:

$$\begin{aligned} \|M_1\| &= \frac{3}{2\varphi^2} > 0, \\ \|M_2\| &= -\frac{9}{4\varphi^3\xi} > 0, \\ \|M_3\| &= \frac{3(\varphi-\xi) - 18G'(\alpha)}{8\varphi^4\xi} > 0. \end{aligned} \tag{6.35}$$

Solving this system of inequalities, we find the allowed region to be

$$\varphi > 0, \qquad \xi < 0, \qquad G'(\alpha) > \frac{\varphi-\xi}{6}. \tag{6.36}$$

We discard the alternative solution corresponding to $\varphi < 0$, $\xi > 0$, and $G'(\alpha) < (\varphi-\xi)/6$, since in that case the conformal transformation used to define the EF becomes ill-defined. Finally, we observe that some of the kinetic terms in the matrix K_1 can be brought to canonical form by performing suitable field redefinitions, as outlined in Section 6.1. Specifically, we introduce the following transformations (6.29)

$$\varphi = e^{\sqrt{\frac{2}{3}}\Phi_c}, \qquad \xi = -\frac{\Xi_c^2}{6}, \qquad \Psi_c = \int \sqrt{G'(\alpha)}\, d\alpha, \tag{6.37}$$

where the definition of Ψ_c depends on the explicit form of the function $G(\alpha)$. Under these redefinitions, the action in (6.33) can be recast as

$$\begin{aligned} S_1 = \frac{1}{2\kappa^2}\int d^4x\sqrt{-q}\Bigg[\tilde{R} - (\nabla\Phi_c)^2 - (\nabla\Xi_c)^2 + \frac{(\nabla\Psi_c)^2}{e^{\sqrt{\frac{2}{3}}\Phi_c}} \\ + \frac{1}{e^{\sqrt{\frac{2}{3}}\Phi_c}}\left(\frac{d\alpha}{d\Psi_c}\nabla_\mu\Psi_c\sqrt{\frac{2}{3}}\nabla^\mu\Phi_c + \frac{\Xi_c}{3}\nabla_\mu\Xi_c\nabla^\mu\Phi_c\right) - \frac{W_1(\Psi_c,\Xi_c)}{e^{2\sqrt{\frac{2}{3}}\Phi_c}}\Bigg], \end{aligned} \tag{6.38}$$

where we emphasise that the potential term becomes separable in the fields Ψ_c and Ξ_c,

up to a global factor depending solely on Φ_c, namely

$$W_1(\Psi_c, \Xi_c) = V(\alpha(\Psi_c)) + U\left(-\frac{\Xi_c^2}{6}\right). \tag{6.39}$$

We anticipate that this peculiar structure hinders the implementation of a viable inflationary scenario. In particular, the separability of the potential fails to generate a mechanism capable of naturally slowing down the evolution of the field Φ_c, which may roll indefinitely.

As for the model $\mathcal{L}_2$, it retains the same formal structure as $\mathcal{L}_1$, with the two curvature scalars interchanged. That is, we now consider a metric $f(R)$ theory supplemented by Palatini non-localities. Applying the localisation procedure, the action becomes

$$\begin{aligned}
S_2 &= \frac{1}{2\kappa^2}\int d^4x\sqrt{-g}\left[f(R) + \mathcal{R}\,G(\Box^{-1}\mathcal{R}) - V(\Box^{-1}\mathcal{R})\right] \\
&= \frac{1}{2\kappa^2}\int d^4x\sqrt{-g}\left[\xi R - U(\xi) + (\rho + G(\beta))\mathcal{R} + \nabla_\mu\beta\nabla^\mu\rho - V(\beta)\right] \\
&= \frac{1}{2\kappa^2}\int d^4x\sqrt{-g}\left[(\xi + \rho + G(\beta))R + \frac{3\left(\nabla(\rho + G(\beta))\right)^2}{2(\rho + G(\beta))} + \nabla_\mu\beta\nabla^\mu\rho - (V(\beta) + U(\xi))\right] \\
&= \frac{1}{2\kappa^2}\int d^4x\sqrt{-g}\left[\phi R + \frac{3(\nabla\psi)^2}{2\psi} + \nabla_\mu\beta\nabla^\mu(\psi - G(\beta)) - W_2(\beta, \phi - \psi)\right],
\end{aligned}$$

where we introduced the new field definitions $\phi \equiv \xi + \rho + G(\beta)$ and $\psi \equiv \rho + G(\beta)$, keeping β unchanged. Going to the EF, the action becomes

$$S_2 = \frac{1}{2\kappa^2}\int d^4x\sqrt{-q}\left[\tilde{R} - \frac{3(\nabla\phi)^2}{2\phi^2} + \frac{3(\nabla\psi)^2}{2\phi\psi} + \frac{\nabla_\mu\beta\nabla^\mu(\psi - G(\beta))}{\phi} - \frac{W_2(\beta, \phi - \psi)}{\phi^2}\right]. \tag{6.40}$$

The corresponding kinetic matrix takes the form

$$K_2 = \frac{1}{\phi}\begin{pmatrix} \frac{3}{2\phi} & 0 & 0 \\ 0 & -\frac{3}{2\psi} & -\frac{1}{2} \\ 0 & -\frac{1}{2} & G'(\beta) \end{pmatrix}. \tag{6.41}$$

Following the analysis applied to K_1, we again employ Sylvester's criterion to determine the conditions for positive definiteness of K_2, which yield:

$$\begin{aligned}
\|M_1\| &= \frac{3}{2\phi^2} > 0, \\
\|M_2\| &= -\frac{9}{4\phi^3\psi} > 0,
\end{aligned} \tag{6.42}$$

$$\|M_3\| = -\frac{3(\psi + 6G'(\beta))}{8\phi^4\psi} > 0$$

These inequalities are simultaneously satisfied for the configuration:

$$\phi > 0, \qquad \psi < 0, \qquad G'(\beta) > -\frac{\psi}{6}.$$

We now perform the same field redefinitions as in the case of S_1, simply exchanging the roles of ξ and α with those of ψ and β, respectively

$$\phi = e^{\sqrt{\frac{2}{3}}\Phi_c}, \qquad \psi = -\frac{\Xi_c^2}{6}, \qquad \Psi_c = \int \sqrt{G'(\beta)}\, d\beta. \tag{6.43}$$

With these, the action S_2 takes the final form

$$S_2 = \frac{1}{2\kappa^2}\int d^4x\sqrt{-q}\left[\tilde{R} - (\nabla\Phi_c)^2 - \frac{(\nabla\Xi_c)^2 + (\nabla\Psi_c)^2}{e^{\sqrt{\frac{2}{3}}\Phi_c}} + \frac{1}{3}\frac{d\beta}{d\Psi_c}\frac{\Xi_c}{e^{\sqrt{\frac{2}{3}}\Phi_c}}\nabla^\mu\Psi_c\nabla_\mu\Xi_c - \frac{W_2(\Phi_c,\Psi_c,\Xi_c)}{e^{2\sqrt{\frac{2}{3}}\Phi_c}}\right]. \tag{6.44}$$

In this case, the potential exhibits the appealing feature that the U component depends simultaneously on both the Ξ_c and Φ_c fields

$$W_2(\Phi_c,\Psi_c,\Xi_c) = V(\beta(\Psi_c)) + U\left(e^{\sqrt{\frac{2}{3}}\Phi_c} + \frac{\Xi_c^2}{6}\right), \tag{6.45}$$

which can, in principle, provide a mechanism to prevent the field Φ_c from undergoing an unbounded slow-roll phase. The dependence on Ψ_c remains separable and, as discussed in Section 6.1, can generally be neglected when focusing on inflationary dynamics. We conclude this section by noting that (6.44) can be further brought into a diagonal form. However, since this transformation does not lead to significant improvements in the numerical analysis, we relegate the corresponding expression to Appendix D. In what follows, we turn our attention to an application of this framework to early-universe inflationary cosmology.

6.3 Hybrid non-local cosmology

In this section, we apply what described above to the case of a homogeneous and isotropic cosmological background given by the flat FLRW metric (2.3). To express the

equations of motion in a more compact form, we rewrite (6.38) and (6.44)

$$S_i = \int d^4x\sqrt{-q}\left[\tilde{R} - (\nabla\Phi)^2 - \frac{(\nabla\Xi)^2 + (\nabla\Psi)^2}{e^{\sqrt{\frac{2}{3}}\Phi}} + \frac{d\chi_i}{d\Psi}\nabla^\mu\Psi\left(\sigma_i\sqrt{\frac{2}{3}}\nabla_\mu\Phi + \frac{\Xi}{3e^{\sqrt{\frac{2}{3}}\Phi}}\nabla_\mu\Xi\right) - Y_i\right], \tag{6.46}$$

where $\chi_i = \{\alpha, \beta\}$ and $\sigma_i = \{1, 0\}$ for $i = \{1, 2\}$ respectively, and the generalised potential is defined as $Y_i = \frac{W_i}{e^{2\sqrt{\frac{2}{3}}\Phi}}$. To lighten the notation, we omit the subscript c. Varying the action (6.46) with respect to the scalar fields Φ, Ξ, and Ψ leads to the equations of motion

$$\Box\Phi + \frac{e^{-\sqrt{\frac{2}{3}}\Phi}}{\sqrt{6}}\left((\nabla\Xi)^2 + (\nabla\Psi)^2\right) - \frac{1}{2}\frac{\partial Y_i}{\partial\Phi} - \frac{\sigma_i}{\sqrt{6}}\nabla_\mu\left(\frac{d\chi_i}{d\Psi}\nabla^\mu\Psi\right) - \frac{\Xi}{3\sqrt{6}}e^{-\sqrt{\frac{2}{3}}\Phi}\frac{d\chi_i}{d\Psi}\nabla_\mu\Psi\nabla^\mu\Xi = 0, \tag{6.47}$$

$$\Box\Xi - \sqrt{\frac{2}{3}}\nabla_\mu\Xi\nabla^\mu\Phi - \frac{e^{\sqrt{\frac{2}{3}}\Phi}}{2}\frac{\partial Y_i}{\partial\Xi} - \frac{\Xi}{6}\left[\frac{d^2\chi_i}{d\Psi^2}(\nabla\Psi)^2 - \sqrt{\frac{2}{3}}\frac{d\chi_i}{d\Psi}\nabla_\mu\Phi\nabla^\mu\Psi + \frac{d\chi_i}{d\Psi}\Box\Psi\right] = 0, \tag{6.48}$$

$$\Box\Psi - \sqrt{\frac{2}{3}}\nabla_\mu\Psi\nabla^\mu\Phi - \frac{e^{\sqrt{\frac{2}{3}}\Phi}}{2}\frac{\partial Y_i}{\partial\Psi} - \frac{d\chi_i}{d\Psi}\left[\frac{\sigma_i}{\sqrt{6}}e^{\sqrt{\frac{2}{3}}\Phi}\Box\Phi + \frac{\Xi}{6}\Box\Xi + \frac{(\nabla\Xi)^2}{6} - \frac{\Xi}{3\sqrt{6}}\nabla_\mu\Phi\nabla^\mu\Xi\right] = 0. \tag{6.49}$$

Turning to the gravitational sector, variation with respect to the metric yields the Einstein equations (1.12). The (tt)-component gives the Friedmann equation (2.25)

$$H^2 = \frac{1}{6}\left(\dot{\Phi}^2 + e^{-\sqrt{\frac{2}{3}}\Phi}(\dot{\Xi}^2 + \dot{\Psi}^2) - \frac{d\chi_i}{d\Psi}\dot{\Psi}\left(\sigma_i\sqrt{\frac{2}{3}}\dot{\Phi} + e^{-\sqrt{\frac{2}{3}}\Phi}\frac{\Xi}{3}\dot{\Xi}\right) + Y_i\right), \tag{6.50}$$

while the (ij)-component leads to

$$\dot{H} = -\frac{1}{2}\left(\dot{\Phi}^2 + e^{-\sqrt{\frac{2}{3}}\Phi}(\dot{\Xi}^2 + \dot{\Psi}^2) - \frac{d\chi_i}{d\Psi}\dot{\Psi}\left(\sigma_i\sqrt{\frac{2}{3}}\dot{\Phi} + e^{-\sqrt{\frac{2}{3}}\Phi}\frac{\Xi}{3}\dot{\Xi}\right)\right), \tag{6.51}$$

To ensure physical viability, we impose that the leading-order slow-roll parameter (3.23) remains positive, $\epsilon_0 > 0$, thereby excluding phantom-like behavior ($w < -1$) in the single-field limit. Finally, we can recast the no-ghost condition for the kinetic matrix in

terms of the fields Φ, Ξ, and Ψ as

$$\frac{1}{6}\left(\frac{d\chi_i}{d\Psi}\right)^2\left(\sigma_i e^{\sqrt{\frac{2}{3}}\Phi}+\frac{\Xi^2}{6}\right)<1. \tag{6.52}$$

In the following, we present and analyse the numerical results obtained by integrating the equations of motion derived in this section, considering different case studies. Specifically, we distinguish between two scenarios: $V(\Box^{-1}\mathcal{R})=0$ and $V(\Box^{-1}\mathcal{R})\neq 0$. For each case, we investigate the effects of adopting different functional forms for the kinetic coupling. The numerical integration of the equations of motion is performed using the algorithm adapted from the previous chapters, suitably modified to address the features of these models.

6.3.1 The case $V(\Box^{-1}\mathcal{R})=0$

As discussed in Section 6.2, imposing this condition does not compromise the dynamical stability of the theory; it simply removes the dependence of the global potential on the field Ψ (cf (6.45)). Furthermore, for the local $f(R)$ (or $f(\mathcal{R})$ sector, we consider a minimal quadratic extension of the standard Einstein-Hilbert term, while the hybrid non-local modifications are encoded in the function G, as introduced in (6.31). This leads to study actions of the form

$$\mathcal{L}_1=a_1\mathcal{R}+b_1\mathcal{R}^2+R\,G(\Box^{-1}R),\qquad \mathcal{L}_2=a_2R+b_2R^2+\mathcal{R}\,G(\Box^{-1}\mathcal{R}), \tag{6.53}$$

which, following the procedure outlined in Section 6.2, yield the EF potential

$$Y_i(\Phi,\Xi,\Psi)=\frac{\left[(1-\sigma_i)e^{\sqrt{\frac{2}{3}}\Phi}+(-1)^{\sigma_i}\frac{\Xi^2}{6}-a_i\right]^2}{4b_ie^{2\sqrt{\frac{2}{3}}\Phi}}. \tag{6.54}$$

A necessary feature we require of the potential is the existence of a global minimum, so that the slow-roll phase can eventually end and the reheating stage can take place. In (6.54), we notice that for $\sigma_1=1$ the potential Y_1 becomes independent of the field Φ. Even if the system settles into a minimum in the (Ψ,Ξ) subspace, the evolution along the Φ-direction remains slow-rolling, and inflation does not naturally end. Since our main interest lies in standard slow-roll realisations of inflationary scenarios, we postpone to future work the analysis of alternative multifield mechanisms such as ultra-slow-roll, hybrid inflation, or rapid-turn inflation. Here, our primary aim is to demonstrate that a hybrid non-local extension of standard $f(R)$ gravity can consistently support infla-

tionary dynamics at least at the background level, without addressing the perturbative sector at this stage. Therefore, we restrict our attention to the case $\sigma_2 = 0$, in which the potential simplifies to

$$Y_2(\Phi, \Xi) = \frac{\left[e^{\sqrt{\frac{2}{3}}\Phi} + \frac{\Xi^2}{6} - a_2\right]^2}{4b_2 e^{2\sqrt{\frac{2}{3}}\Phi}}. \tag{6.55}$$

We aim to construct a plateau-like potential (by choosing the parameters a_2 and b_2) endowed with a global minimum, which enables inflation to take place. Nevertheless, the detailed shape of the potential is not strictly fixed by these values. In particular, requiring the potential to remain positive imposes the constraints $a_2 > 0$ and $b_2 > 0$, where a_2 sets the position of the minimum and $1/b_2$ determines the overall height of the potential. For this setup, the no-ghost condition can be expressed as

$$0 < \left(\frac{d\chi_2}{d\Psi}\frac{\Xi}{6}\right)^2 < 1, \tag{6.56}$$

which, depending on the choice of the function $\chi_2(\Psi)$, identifies the subregion of the $\{\Xi, \Psi\}$-plane where the scalar fields' motion must remain confined. We note that when $\sigma_2 = 0$, the field Φ does not appear in this inequality, and thus its evolution is not constrained a priori in the Φ-direction.

The explicit form of $\chi_2(\Psi)$ depends on the initial choice of the non-local coupling function G. However, since the factor $d\chi_2/d\Psi$ also enters the equations of motion (6.47) and (6.49), it is computationally convenient to specify directly different functional choices for

$$K(\Psi) \equiv \frac{d\chi_2}{d\Psi}.$$

In particular, we consider the following two cases

$$K(\Psi) = k\Psi^{1+n}, \qquad K(\Psi) = ke^{n\Psi}, \tag{6.57}$$

which we refer to as the *power-law* and *exponential* kinetic coupling scenarios, respectively. These choices determine the form of the non-diagonal kinetic terms in (6.46). The original coupling function G can be reconstructed by inverting the definition of Ψ. First, we have

$$\chi_2 - \chi_{2,0} = \int K(\Psi)\, d\Psi, \tag{6.58}$$

and then

$$G - G_0 = \int \left(\frac{d\Psi}{d\chi_2}\right)^2 d\chi_2, \tag{6.59}$$

where $\Psi = \Psi(\chi_2)$ is obtained by inverting (6.58).

Special care must be taken regarding the integration constants G_0, $\chi_{2,0}$, and Ψ_0 (the last of which may arise on the right-hand side of (6.58)). These constants can introduce unwanted contributions into the original action (6.31) and potentially spoil the dynamical consistency of the model. For instance, a nonzero G_0 generates a linear term in the scalar curvature not present in the original $f(R)$ Lagrangian, thus violating the assumptions made in Section 6.2. Moreover, specific nontrivial combinations of $\chi_{2,0}$ and Ψ_0 may have analogous effects. Hence, the constants $\{G_0, \chi_{2,0}, \Psi_0\}$ must satisfy certain mutual conditions to preserve the ghost-free nature of the theory.

As an illustrative example, consider the simplest case $K = k$. Then,

$$G(\chi_2) = G_0 + \frac{1}{k^2}(\chi_2 - \chi_{2,0}), \tag{6.60}$$

and consistency requires $G_0 = \chi_{2,0}/k^2$. By working directly with the function $K(\Psi)$, we avoid these subtleties and can search for dynamically consistent configurations more transparently within the scalar-tensor reformulation.

POWER-LAW KINETIC COUPLING. The first scenario we examine is the power-law kinetic coupling

$$K(\Psi) = k\Psi^{1+n}, \tag{6.61}$$

whose associated function $G(\chi_2)$ is derived explicitly in Appendix D. We start by focusing on the case $n = -1$, which corresponds to a constant non-local coupling term. This choice significantly simplifies the equations of motion, yielding field trajectories that mainly depend on the initial conditions. In the EF, the kinetic terms introduce non-diagonal components, which in turn affect the background evolution. From this point onward, we consider non-local contributions with $k \ll 1$ so that these terms effectively act as perturbative corrections. In Figure 6.1, we numerically integrate the complete system of equations (6.47), (6.48), and (6.49) up to the end of inflation, defined by the condition $\epsilon_0 = 1$. The numerical results indicate that inflationary solutions do exist: the scalar fields slowly roll down the potential, as illustrated in the bottom-right plot of Figure 6.1. However, careful tuning of parameters is required to simultaneously avoid ghost instabilities and achieve a sufficient number of e-folds.

In this context, the no-ghost condition (6.56) becomes

$$\left|k\,\Xi\,\Psi^{1+n}\right| < 6. \tag{6.62}$$

This inequality constrains the allowed evolution of the fields, especially in the $\{\Xi, \Psi\}$ plane.

The evolution highlights the leading role of the inflaton, identified here with the field Φ. In contrast, the Ξ field quickly decays towards zero. Given that the potential $Y_2(\Phi, \Xi)$ in (6.55) is independent of Ψ, the coupling between Ξ and Ψ originates only from the non-local term. This coupling induces an initial displacement (or "kick") in the Ψ field, after which its motion is slowed down by the expansion of the universe. It is also noteworthy that turning on the dependence of Ψ in (6.61) makes the non-local coupling dynamically relevant. Indeed, for higher values of n, the Ψ field tends to stabilise at larger values, becoming effectively frozen (see Figure 6.1). In such cases, the model effectively behaves like single-field inflation supplemented by a spectator field, as the inflationary dynamics is mainly controlled by the evolution of Φ. In the next section, we will compare these results to the case $n = 0$ when a non-vanishing potential $V \neq 0$ is included.

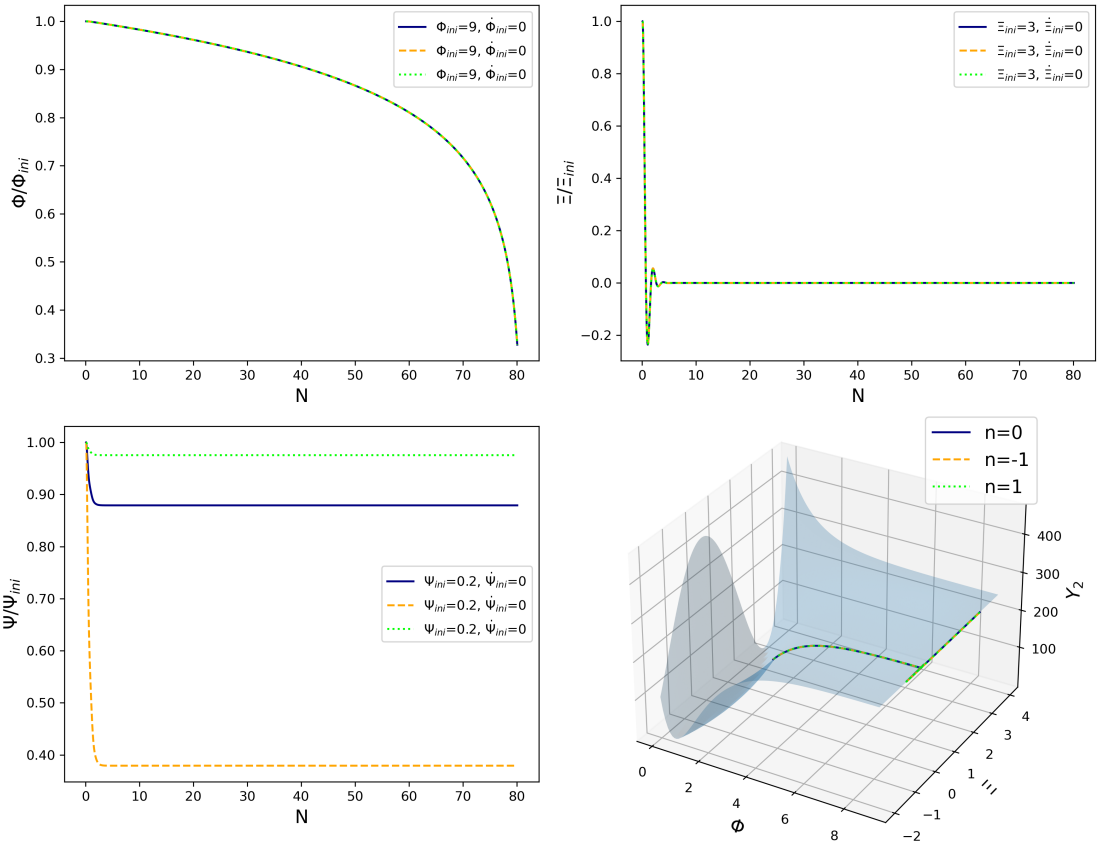

Figure 6.1: Power-law kinetic coupling case with $V = 0$: normalised field trajectories over the shaded potential $Y_2(\Phi, \Xi)$ for parameters $a_2 = 2.3$, $b_2 = 0.001$, $k = 0.1$ and different choices of n: $n = 0$ (blue), $n = -1$ (orange), and $n = 1$ (green).

EXPONENTIAL KINETIC COUPLING. We set the exponential kinetic coupling to

$$K(\Psi) = ke^{n\Psi}, \tag{6.63}$$

with the corresponding $G(\chi_2)$ function derived in Appendix D. The condition ensuring

dynamical stability takes the form

$$|k\,\Xi\,e^{n\Psi}| < 6. \tag{6.64}$$

The exponential coupling significantly influences the dynamics. As the parameter n increases toward positive values, the coupling between the fields Ξ and Ψ becomes stronger, causing the Ψ field to stabilise at lower values after an initial decline, as shown in Figure 6.2. In this regime, the Ψ field effectively becomes almost frozen, reducing the system to a single-field dynamics with a spectator field.

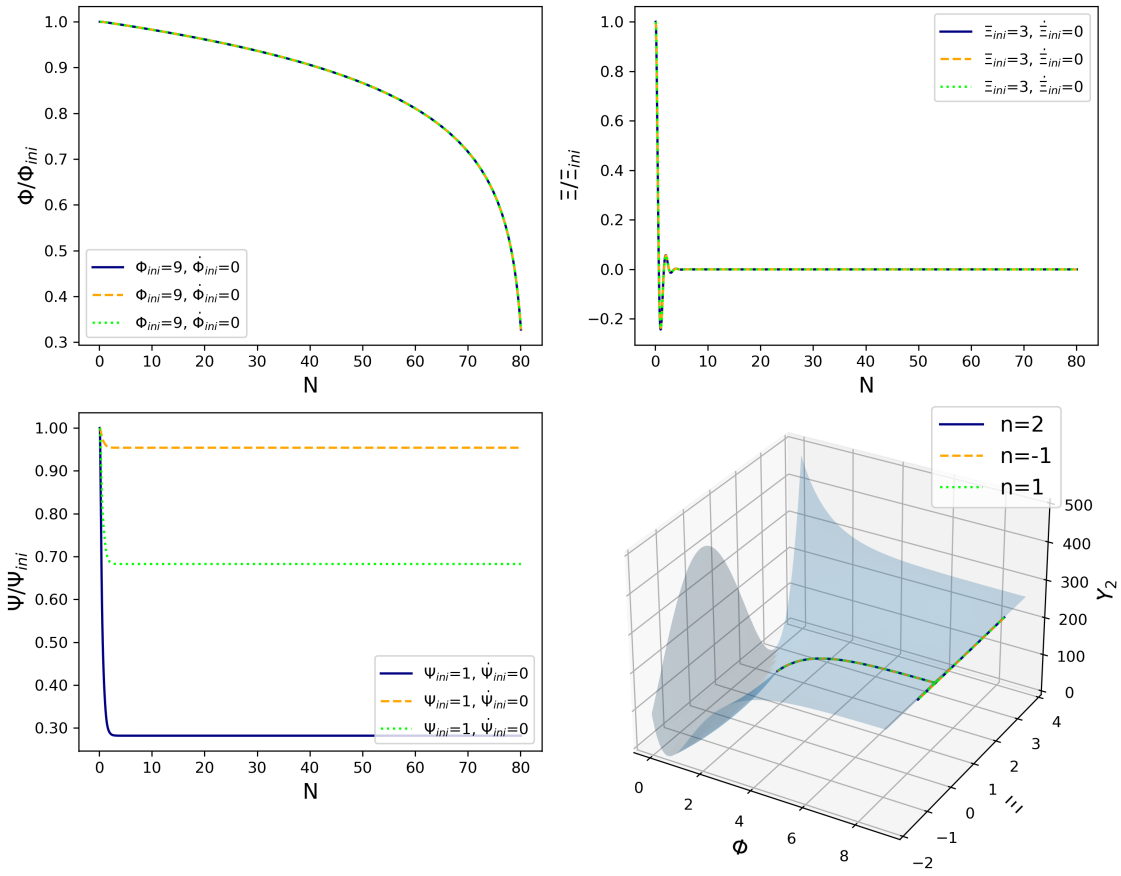

Figure 6.2: Exponential coupling case with $V = 0$: normalised field trajectories over the shaded potential profile $Y_2(\Phi, \Xi)$ for $a_2 = 2.3$, $b_2 = 0.001$, $k = 0.1$ with $n = 2$ (blue), $n = -1$ (orange), and $n = 1$ (green).

6.3.2 The case $V(\Box^{-1}\mathcal{R}) \neq 0$

IN this subsection we extend our analysis to include the case where the initial action features a non-vanishing potential term $V(\Box^{-1}\mathcal{R})$. This introduces an additional dependence on the field Ψ into the global potential Y_2, as determined by the relation (6.58).

Specifically, following the discussion at the start of Section 6.3, we choose for V a simple quadratic form, namely $V(\chi_2) = V_0\chi_2^2$, where V_0 is a constant parameter. As a result, the global potential in the EF becomes

$$Y_2(\Phi, \Xi, \Psi) = \frac{V_0\chi_2^2(\Psi) + \left(e^{\sqrt{\frac{2}{3}}\Phi} + \frac{\Xi^2}{6} - a_2\right)^2}{4b_2 e^{2\sqrt{\frac{2}{3}}\Phi}}, \tag{6.65}$$

in which non-localities introduce deformations to the Starobinsky-like potential, providing a novel pathway to test the robustness of the model. This requires the study of perturbations, which is beyond the scope of this work.

POWER-LAW KINETIC COUPLING. For the choice $K(\Psi)$ given by (6.61), we obtain

$$\chi_2 = \frac{k}{n+2}\Psi^{n+2}, \tag{6.66}$$

where, for simplicity, we set the integration constant to $\chi_{2,0} = \frac{k\Psi_0^{n+2}}{n+2}$. With this parametrisation, the potential term V takes the form

$$V(\Psi) = \frac{k^2V_0}{(n+2)^2}\Psi^{2(n+2)}. \tag{6.67}$$

Focusing on the case $n = 0$, for which $K(\Psi) \approx \Psi$, the behaviour closely resembles that discussed in Subsection 6.3.1. Furthermore, the condition $H^2/Y_{\Psi\Psi} \gg 1$ implies that the field Ψ remains light during inflation. Consequently, it becomes "Hubble-damped" and is not driven to zero by the potential; instead, its kinetic energy diminishes over time, effectively freezing the field. The variation in the coupling strength modifies the overall amplitude of the potential (see Figure 6.3), which would in turn affect the scalar spectral amplitude A_s of primordial perturbations by either enhancing or suppressing it.

EXPONENTIAL KINETIC COUPLING. For the choice $K(\Psi)$ given by (6.63), the function χ_2 becomes

$$\chi_2 = \frac{k}{n}e^{n\Psi}, \tag{6.68}$$

where we have set the integration constant to $\chi_{2,0} = \frac{k}{n}e^{n\Psi_0}$. In this setup, the potential term V is given by

$$V(\Psi) = \frac{k^2V_0}{n^2}e^{2n\Psi}. \tag{6.69}$$

The modification of the Starobinsky-like potential (6.65) by the additional $V(\Psi)$ term for $\Phi \to 0$ creates conditions suitable for inflation, depending on the specific shape of

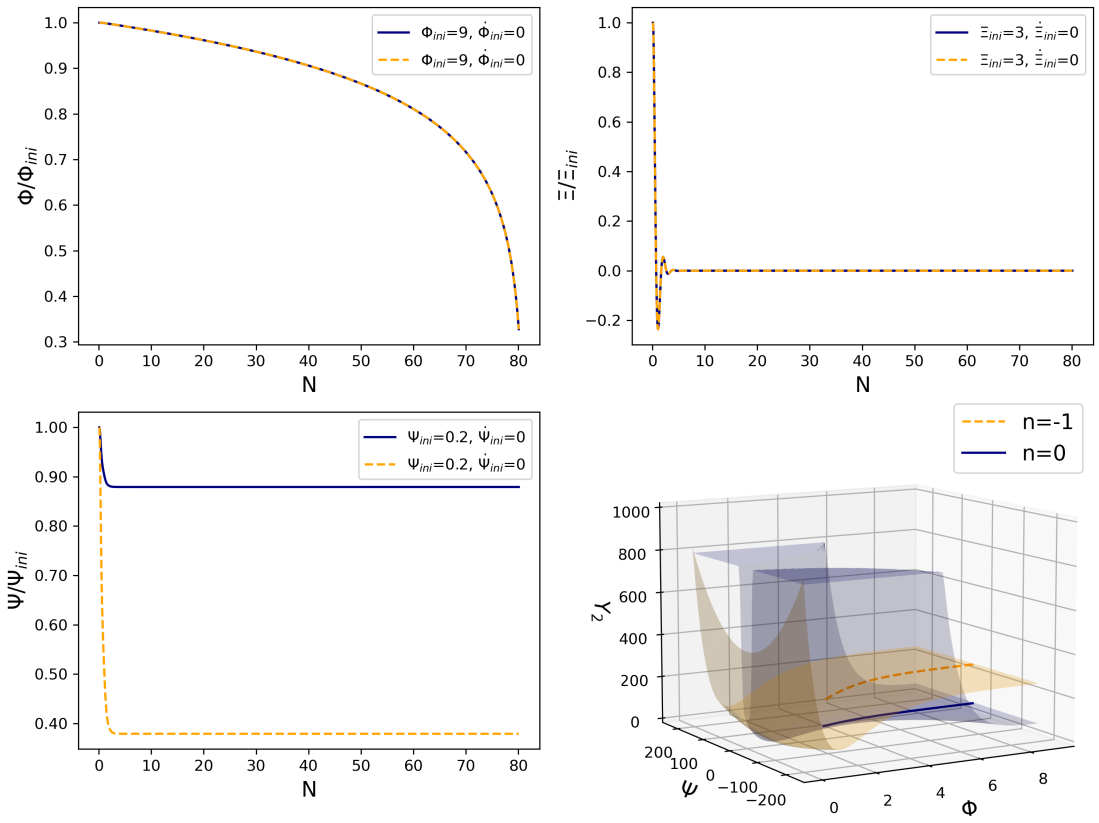

Figure 6.3: Power-law coupling with $V \neq 0$: normalised field trajectories over the shaded potential profiles $Y_2(\Phi, 0, \Psi)$ with $a_2 = 2.3$, $b_2 = 0.001$, $k = 0.1$ for $n = 0$ (blue) and $n = -1$ (orange).

$V(\Psi)$; see Figure 6.4. Also in this case, the condition $H^2/Y_{\Psi\Psi} \gg 1$ holds, ensuring that Ψ remains light during inflation. Overall, the resulting field dynamics closely resembles those of the power-law kinetic coupling scenario.

6.4 Conclusion

The main findings of our analysis are as follows. We have shown that non-degenerate hybrid metric-Palatini models, when extended with non-local terms involving inverse d'Alembertian operators, are generally affected by ghost instabilities. By reformulating the theory in a scalar-tensor representation, we make the interaction between local and non-local contributions transparent. Our analysis reveals that the number of ghost instabilities is determined by the sum of the highest powers of the $\Box^{-k}$ operators acting on the metric and Palatini curvature terms. We argue that this is an inherent feature of any non-degenerate non-local action of the form $F(R, \mathcal{R}, ..., \Box^{-m}R, ..., \Box^{-n}\mathcal{R})$, even under a purely Palatini formulation. This contrasts with standard $f(R)$ gravity, where no extra degrees of freedom arise. Our findings generalise the results of [96] obtained for

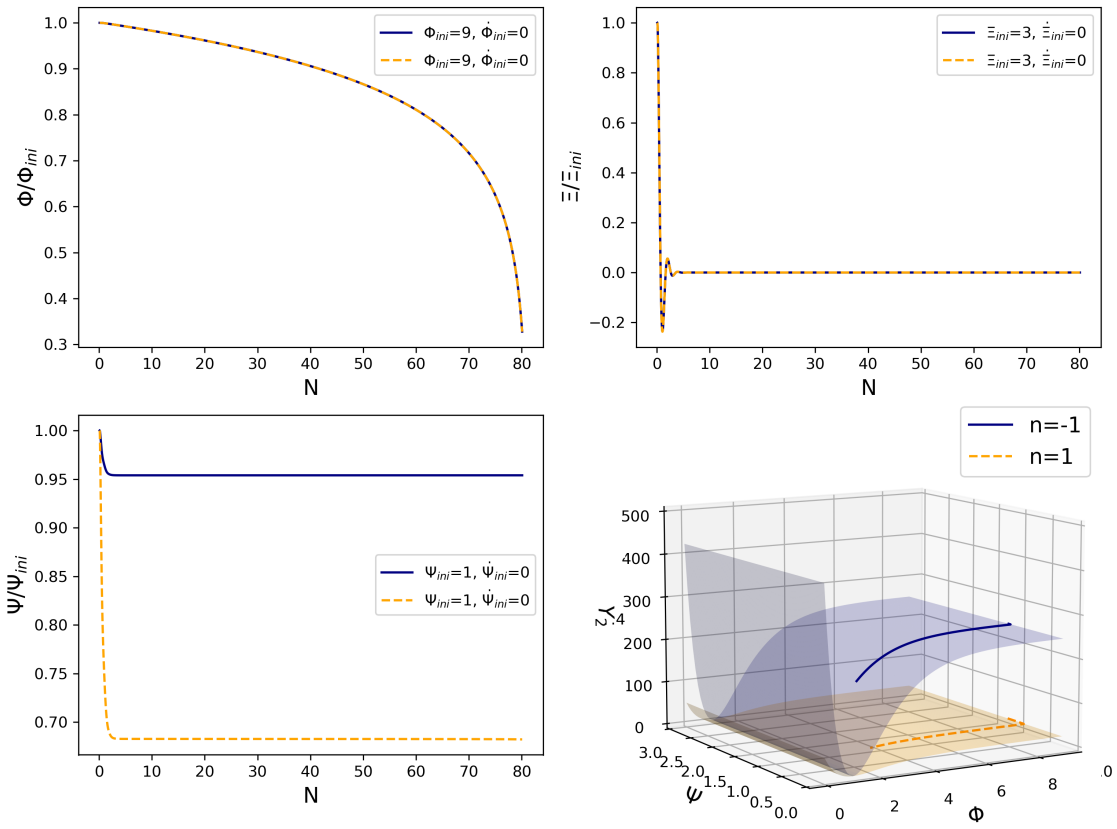

Figure 6.4: Exponential coupling with $V \neq 0$: normalised field trajectories over shaded potential profiles $Y_2(\Phi, 0, \Psi)$ with $a_2 = 2.3$, $b_2 = 0.001$, $k = 0.1$ for $n = 1$ (orange) and $n = -1$ (blue).

the purely metric case and are consistent with the known doubling of degrees of freedom in generalised hybrid metric-Palatini gravity [54, 81] compared to models involving only a single curvature scalar. Furthermore, We demonstrate that Lagrangian densities satisfying the condition $f_{RR} f_{\mathcal{R}\mathcal{R}} - f_{R\mathcal{R}}^2 \neq 0$ are sufficient to eliminate ghost instabilities, provided that the local and non-local terms are associated with different types of curvature. Specifically, we show that straightforward extensions of standard $f(R)$ theories that introduce non-local Palatini (or metric) terms – where the curvature scalars couple linearly to functions of the $\Box^{-1}$ operator – achieve this goal. These models can consistently accommodate up to three scalar degrees of freedom, whereas, by comparison, generalised hybrid models typically exhibit only two.

Building on these considerations, the second part of our work focused on a specific class of well-defined hybrid actions in which local and non-local contributions are associated with different types of curvature. We studied configurations where metric $f(R)$ (or Palatini $f(\mathcal{R})$) models are supplemented by Palatini (or metric) non-local terms, explicitly breaking degeneracy by coupling non-localities linearly to the curvature. We then explored the viability of these models in early universe cosmology, examining whether

inflation can emerge within the resulting EF multifield scenario. Our analysis investigated how non-local terms and non-minimal kinetic couplings between fields – reflecting the non-local structure of the original frame – affect the background evolution, the total number of e-folds, and the scalar field trajectories. As a preparatory step, we verified the well-posedness of the first-order slow-roll parameter, which imposed further constraints among the potential derivatives and the fields. We found that non-localities deform the Starobinsky-like potential, offering a new perspective on testing the model's robustness. Quantitatively, we examined two representative configurations based on whether the potential term $V(\Box^{-1}\mathcal{R})$ vanishes or not. In the case it does not vanish, the dynamics is dominated by the coupling between the non-local terms and the scalar fields. We showed that the qualitative behavior of the fields is largely insensitive to the specific form of the kinetic coupling $K(\Psi)$: whether K is power-law or exponential, the Ξ field quickly settles to the minimum of the potential, Ψ becomes frozen due to Hubble damping, and Φ drives inflation – effectively reducing the dynamics to a single-field scenario with a spectator field. Stability of these trajectories requires satisfying the no-ghost condition. Instead, including a quadratic potential term $V(\Box^{-1}\mathcal{R})$ enriches the inflationary dynamics by introducing additional interactions among the fields, resulting in extra constraints that naturally help end inflation. We also noted that the effective mass of the Ψ field remains light, meaning that for general initial conditions it does not evolve to zero during inflation.

Overall, our study demonstrates that non-local effects not only deform the Starobinsky-like potential, but also directly impact the background dynamics during slow-roll inflation. These effects imprint characteristic signatures, suggesting a promising new direction to test the resilience of the Starobinsky model and to probe potential non-localities in gravitational interactions at high energy scales, relevant for the inflationary Universe. Although our analysis was limited to background-level effects, it establishes a robust foundation for future studies of inflationary perturbations and their observational consequences within non-local hybrid metric-Palatini gravity.

7 Alternative mechanism to inflation

At the end of *Part I*, we provided an overview of alternative scenarios to cosmological inflation, highlighting theoretical frameworks capable of reproducing key observational features of our Universe. Among these, the cyclic universe model emerges as a particularly intriguing alternative, as mentioned at the end of Section 3.5. In this chapter, we focus on a detailed investigation of this model: we lay the groundwork by discussing its observational motivations and by setting up the formalism necessary to study its predictions for primordial gravitational waves.

As we already discussed, the most compelling observational evidence supporting cosmological inflation [7, 20, 360, 361] as the leading paradigm for the early Universe is currently provided by the Planck satellite measurement of the spectral index of scalar perturbations, $n_s = 0.9649 \pm 0.0042$ [263]. In the simplest single-field slow-roll inflationary models, the spectrum of scalar modes is expected to be nearly, though not exactly, scale-invariant [21, 166, 167, 362]. Deviations from scale-invariance is quantified by the extent to which n_s differs from unity [12, 106, 173]. Consequently, the Planck data appear in excellent agreement with the theoretical expectations of inflationary models [9, 263], excluding a Harrison-Zel'dovich scale-invariant spectrum [363–365] ($n_s = 1$) at more than 8.5σ significance and thereby lending considerable support to the inflationary framework.

That said, it is important to stress that this agreement, by itself, does not constitute definitive proof of cosmological inflation. Even adopting a flexible perspective and setting aside both the uncertainties associated with n_s constraints from CMB experiments other than Planck[1] and the potential implications of recent cosmological tensions [119–121, 125], alternative theoretical mechanisms have been proposed that also predict an almost scale-invariant spectrum of primordial density perturbations without invoking

[1] Constraints on n_s have also been obtained by WMAP [366, 367], ACT [307, 308], and the South Pole Telescope (SPT) [368, 369]. Planck remains the only experiment to exclude $n_s = 1$ at significantly more than 3σ. In contrast, ACT even shows a mild preference for $n_s = 1$ [310], as also mentioned in the previous chapters.

inflation.

A notable example is the cyclic universe scenario [30, 33, 35–37, 370, 371], which replaces the traditional Big Bang origin with a periodic cosmic history. This model has been widely discussed in contexts ranging from quantum gravity and modified gravity to gravitational waves and dark energy (see, *e.g.* [38, 372–402] or the reviews [31, 32]). Broadly speaking, each cycle includes a standard hot Big Bang phase where large-scale structure forms, followed by a slow accelerated expansion mirroring the present dark energy-dominated epoch. This late-time acceleration serves to smooth inhomogeneities and flatten spatial curvature. Subsequently, a contracting (ekpyrotic) phase generates nearly scale-invariant density perturbations, which culminates in a Big-crunch/Big-Bang transition that produces new matter and radiation, initiating the next cycle.

Both inflation and the cyclic scenario provide physical mechanisms able of generating an almost scale-invariant spectrum of scalar perturbations [403–405], and both explain the observed large-scale homogeneity of the CMB [406] and the near-flatness of spatial geometry [407–427]. At first glance, distinguishing between them is challenging when considering only scalar modes [428, 429]. However, the predictions for primordial tensor modes differ: inflation generally predicts a nearly scale-invariant (red-tilted) tensor spectrum [12, 106, 430], whereas the cyclic universe typically leads to a blue-tilted tensor spectrum with an amplitude orders of magnitude below the sensitivity of foreseeable experiments [38]. As a result, a detection of primordial gravitational waves, for example via large-scale B-mode polarisation in the CMB, would strongly favour inflation and disprove the cyclic scenario. Although this is often seen as a predictive strength of inflation, it is essential to recognise important caveats. First, primordial tensor modes have not yet been detected [264], so observationally the cyclic scenario remains viable. Second, the inflationary prediction for the tensor amplitude and tilt depends strongly on the specific model. Even within single-field slow-roll inflation, consistency relations among inflationary parameters [12, 106] can be broken by various physical effects: modified gravity [431–434], multifield dynamics [1, 2, 195, 225, 435], axion couplings [436–439], couplings to axion-gauge or spin-2 fields [440, 441], breaking of diffeomorphism invariance [442–445], higher-curvature terms [168], higher-order operators [446, 447], violations of the null energy condition [448, 449], alternative vacuum choices [176, 450, 451], sound speed resonances [452], elastic media [453], or quantum gravity-inspired effects [454–456]. Some of these mechanisms lead to blue-tilted spectra or suppress tensor amplitudes to undetectable levels [457–465], and models can even be constructed to yield arbitrarily small tensor signals [466]. This makes it difficult to falsify inflation solely by the absence of detected primordial gravitational waves, a limitation often cited in critiques of inflation's predictive power.

Turning back to the cyclic scenario, a natural question is whether similar limitations apply. In particular, it is crucial to investigate the robustness of its prediction of a suppressed tensor amplitude. To that end, we review the production of primordial gravitational waves in the cyclic Universe, clarifying several conceptual issues relevant to its predictivity. Existing literature typically calculates the tensor spectrum by imposing Bunch–Davies initial conditions in the ekpyrotic contracting phase [38]. While for scalar modes the impact of choosing initial conditions in different phases has been analysed [467], tensor modes have always been evolved starting in the ekpyrotic phase, neglecting possible contributions from tensor modes generated during the preceding dark energy phase. This motivates us to study whether these earlier contributions affect the tensor spectrum observed today, and more generally, to assess how sensitive predictions are to the choice of vacuum state. Specifically, we construct a general framework to follow the evolution of tensor modes across cycles, making no assumptions about the initial vacuum and starting the calculation from the dark energy phase of the previous cycle. Our results show that modes produced during the dark energy phase make negligible contributions on observable scales, except for corrections on the largest scales comparable to the current Hubble radius. More importantly, we find that significant excitations away from the Bunch-Davies vacuum in the dark energy phase can easily lead to backreaction problems, overwhelming the energy density of the modulus field and thereby spoiling the model's consistency. Avoiding such backreaction imposes strong constraints, effectively limiting the freedom to choose alternative vacua.

This chapter is based on [6], and with the exception of Section 7.1 where we review the cyclic model and its background dynamics, it constitutes original research. In Section 7.2 we examine the evolution of primordial gravitational waves starting from the dark energy phase of the previous cycle. In Section 7.3 we discuss the implications for predictivity, the role of vacuum choice, and the contribution of modes from earlier cycles.

7.1 Cyclic model and background dynamics

We consider a simple scalar field setup in the EF (3.1) where ϕ is a modulus field responsible for the dark energy-dominated phase, as well as the following *ekpyrotic* and *contracting kinetic* phases, discussed in more detail below. A modulus field typically refers to a scalar field that describes the size or shape of extra dimensions in theories with extra dimensions, like string theory or braneworld models. Here, it parametrises the inter-brane distance or equivalently the size of the fifth dimension [36]. In general, moduli fields are dynamical, meaning they can evolve over time and can influence the

expansion or contraction of the Universe. Assuming a spatially flat FLRW background (2.3), the scalar field ϕ obeys the standard Klein-Gordon equation (3.11). Furthermore, neglecting any coupling between the scalar field and Standard Model species, and disregarding additional contributions from these species to the total energy density, the evolution of the scale factor is determined by the Friedmann equation (3.9). In what follows, to effectively capture the dynamics of the cyclic Universe, we consider a phenomenological potential of the form

$$V(\phi) = V_0 \left(1 - e^{-c\phi/M_{\rm P}}\right) Y(\phi), \tag{7.1}$$

where V_0 is of the same order of magnitude as the vacuum energy observed in the present-day Universe, c is a positive constant, and $Y(\phi)$ is a step function that modulates the potential. The assumption of this specific potential is motivated in part by its analytical simplicity and in part by its widespread use in the literature [36, 371, 468], which facilitates a direct comparison with previous results. It is important to stress, however, that cyclic models can emerge from a wide variety of scalar field potentials, which are ultimately expected to originate from an underlying higher-dimensional theory. In single-field ekpyrotic models, however, the scalar perturbation spectrum is highly blue-tilted and far from scale-invariant [404, 469]. Therefore, reproducing the observed nearly scale-invariant scalar spectrum typically requires a two-field setup where isocurvature perturbations are converted into curvature perturbations [404] or to generalise the string-inspired potential $V(\phi) = -V_0 e^{-c\phi/M_{\rm P}}$ in [469] by adding a constant to it. This point is relevant when comparing tensor and scalar modes of the same wavelength. Without loss of generality, the essential requirement is that the potential leads to a viable spectrum of scalar perturbations. This typically needs the presence of a steep and strongly negatively curved region over field ranges relevant to observations. A potential of the form (7.1) serves multiple purposes, including modelling the dark energy responsible for the present-day accelerated expansion of the Universe. More crucially, it facilitates the transition from expansion to contraction by allowing the scalar field to roll from positive to negative values of the potential. This process keeps going until the moment when $H^2 = 0$, thereby initiating a contracting phase characterised by an equation of state $\omega \gg 1$. For instance, solving (3.9) for the scale factor shows that when the dynamics are dominated by the negative part of the potential, $V \simeq -V_0 e^{-c\phi}$ (corresponding to the *ekpyrotic* phase), the scale factor evolves as [467]

$$a(t) \sim (-t)^{\tilde{\alpha}}, \tag{7.2}$$

where t is negative and $\tilde{\alpha} = 2/c^2$. It is also convenient to introduce the conformal time (2.6), which will be frequently used in subsequent analysis. In terms of conformal time, the scale factor during the *ekpyrotic* phase evolves as

$$a(\tau) \sim \left[(-1)^{\tilde{\alpha}}(\tau - \tilde{\alpha}\tau)^{\tilde{\alpha}/(1-\tilde{\alpha})}\right]_{\tau_i}^{\tau_f}, \tag{7.3}$$

highlighting that the Universe undergoes a slow contraction while the scalar field rolls down its steep, negative potential, producing an acceptable spectrum of cosmological scalar perturbations.

In the literature, the *ekpyrotic* phase is typically taken as the starting point of the cycle, where the initial conditions for primordial perturbations are set[34, 37, 429]. Here, however, we aim to extend the standard approach by including the contribution of tensor perturbations generated during the dark energy phase of the previous cycle. The goal is to investigate whether these additional perturbations can leave any imprint on the tensor spectrum observed in the current cycle and, if not, to clarify the underlying reasons. To this end, our strategy is to begin the analysis in the dark energy phase of the previous cycle (without imposing any assumption on the vacuum state) and then evolve the system through four distinct phases: dark energy, ekpyrotic, contracting kinetic, expanding kinetic – as we explain below. Consequently, before proceeding to the explicit calculation of the tensor spectrum, it is useful to devote the next two subsections to reviewing the background dynamics of the model. We will then trace the evolution starting from the dark energy phase of the previous cycle, ensuring the continuity of the scale factor across the transitions between phases. Furthermore, we derive constraints on the model parameters by imposing minimal theoretical requirements, such as the continuity of the Hubble parameter $H(t)$ and the overall consistency of the cyclic scenario across successive cycles.

7.1.1 Evolution and continuity across stages

DARK ENERGY PHASE. We begin by considering the dark energy phase, during which the expansion rate H remains approximately constant and the scale factor $a(t)$ evolves as

$$a(t) = a(t_{\rm tr})e^{H(t-t_{\rm tr})} \quad t < t_{\rm tr}, \tag{7.4}$$

where $t_{\rm tr}$ denotes the transition time between the dark energy and the *ekpyrotic* phase. Expressing the scale factor in terms of the conformal time τ, we find

$$a(\tau) = \frac{1}{H(B-\tau)}, \tag{7.5}$$

where the constant B is determined by ensuring continuity of the scale factor at $\tau = \tau_{\rm tr}$, leading to[2]

$$B = \frac{1}{a(\tau_{\rm tr})H} + \tau_{\rm tr}. \tag{7.6}$$

Moreover, by using (7.3), the ratio of the scale factor at the transition time $\tau_{\rm tr}$ and at the end of the *ekpyrotic* phase $\tau_{\rm end}$ can be written as

$$\frac{a(\tau_{\rm tr})}{a(\tau_{\rm end})} = \left(\frac{\tau_{\rm tr} - \tau_{\rm ek}}{\tau_{\rm end} - \tau_{\rm ek}}\right)^{\alpha}, \tag{7.7}$$

where $\alpha \equiv \tilde{\alpha}/(1-\tilde{\alpha})$, and $\tau_{\rm ek} \equiv (1-2\alpha)\,\tau_{\rm end}$ corresponds to the conformal time at which the potential diverges to minus infinity.

EKPYROTIC PHASE. Next, we move to the *ekpyrotic* phase. During this stage, the potential becomes negative, and in the EF, this leads the scale factor to enter a phase of slow contraction

$$\frac{a(\tau)}{a(\tau_{\rm end})} = \left(\frac{\tau - \tau_{\rm ek}}{\tau_{\rm end} - \tau_{\rm ek}}\right)^{\alpha}, \quad \tau_{\rm tr} < \tau < \tau_{\rm end}. \tag{7.8}$$

It is worth emphasising that, since $\alpha \ll 1$, this contraction proceeds very gradually.

CONTRACTING KINETIC PHASE. Once $\tau > \tau_{\rm end}$, we enter a regime where the potential becomes negligible, that is, $\phi < \phi_{\rm end}$. During this period – known as the contracting kinetic phase – the scale factor evolves as

$$\frac{a(\tau)}{a(\tau_{\rm r})} = \left(\frac{-\tau}{(1+\chi)\,\tau_{\rm r}}\right)^{\frac{1}{2}}, \quad \tau_{\rm end} < \tau < 0, \tag{7.9}$$

where χ is a small positive parameter that quantifies the amount of radiation produced at $\tau = 0$.

EXPANDING KINETIC PHASE. In the final stage of the cycle, known as the expanding kinetic phase, the scale factor takes the form

$$a(\tau) = \left(\frac{\tau}{\tau_{\rm r}}\right)^{\frac{1}{2}}, \quad 0 < \tau < \tau_{\rm r}. \tag{7.10}$$

For convenience, we choose coordinates so that $a(\tau_{\rm r}) = 1$ at time $t_{\rm r}$, corresponding to the onset of the radiation-dominated era. The conformal time $\tau_{\rm r} = (2H_{\rm r})^{-1}$ is determined

[2]The explicit value of B is obtained by considering H_0, $a(\tau_{\rm tr})$, and $\tau_{\rm tr}$, which are specified in the following sections.

by the radiation temperature T_r, with $H_r \propto T_r^2/M_P$. Following [33], we adopt a conservative value $T_r \sim 10^7$ GeV, similar to the temperature expected at the end of reheating in standard inflationary scenario, ensuring that the model remains compatible with the successful predictions of primordial Big Bang Nucleosynthesis.

7.1.2 Parameter constraints

To ensure that the Hubble parameter returns to its initial value each cycle, we follow [467] and impose

$$\frac{H_{end}}{H_0} \approx \sqrt{\frac{-V_{end}}{V_0}}, \tag{7.11}$$

where V_{end} is the depth of the potential minimum and V_0 the height of its plateau. Since the comoving wavenumbers generated when ϕ rolls from $V \approx 0$ to $V \approx -V_{end}$ span

$$\frac{k_{max}}{k_{min}} \approx \sqrt{\frac{-V_{end}}{V_0}}, \tag{7.12}$$

we require at least $N = 60$ e-folds in the ekpyrotic phase to cover the observable range of scales [9, 263]. This in turn constrains the transition time between dark energy and ekpyrosis

$$\frac{H_{tr}}{H_{end}} = 2\,\alpha\,\tau_{end}\,\frac{a_{end}\,a_{tr}}{\tau_{tr}-\tau_{ek}} < e^{-60}. \tag{7.13}$$

Because $a(\tau) \approx$ const during the ekpyrotic contracting phase [467], (7.13) implies

$$\left|\tau_{tr}-\tau_{ek}\right| > 2\,\alpha\,\tau_{end}\,a_{end}^2\,e^{60}. \tag{7.14}$$

Next, we demand that the kinetic phases last long enough for ϕ to roll from the potential minimum ($\phi = \phi_{end}$) through the bounce ($\phi \to -\infty$) and back up past ϕ_{end} onto the plateau, initiating radiation domination. By neglecting a brief $w \gg 1$ interval, integration of the Klein-Gordon equation (3.11) under kinetic domination gives

$$\phi - \phi_{end} = c_1 \ln(t/t_{end}), \quad c_1^2 = \frac{2}{3}, \tag{7.15}$$

where t_{end} is the time to reach ϕ_{end} from the bounce. During the high–w portion, $V \approx V_0(1-e^{-c\phi})$ and one finds

$$\frac{t_r}{t_{end}} > \left(\frac{V_{end}}{V_0}\right)^{\sqrt{\frac{3}{2c^2}}}. \tag{7.16}$$

Since $t_{\rm r}/t_{\rm end} \approx \sqrt{V_{\rm end}}/H_{\rm r}$, (7.16) yields

$$H_{\rm r} \lesssim \frac{\sqrt{V_{\rm end}}}{M_{\rm P}} \left(\frac{V_0}{V_{\rm end}}\right)^{\frac{3}{2c^2}}, \tag{7.17}$$

which restricts the conformal-time ratio

$$\Gamma \equiv \left|\tau_{\rm r}/\tau_{\rm end}\right| \gtrsim \left(\frac{V_{\rm end}}{V_0}\right)^{\sqrt{\frac{2}{3c^2}}} \sim 10^8, \tag{7.18}$$

using $V_0 \sim 10^{-120} M_{\rm P}^4$ and $V_{\rm end} \sim 10^{-20} M_{\rm P}^4$ [38]. In summary, the key background constraints for our cyclic model are

$$\left|\tau_{\rm r}/\tau_{\rm end}\right| \gtrsim 10^8, \qquad (\tau_{\rm tr} - \tau_{\rm ek}) \gtrsim 10^9, \qquad \tau_{\rm r} = \frac{1}{2H_{\rm r}}. \tag{7.19}$$

7.2 General primordial tensor spectrum

In a spatially flat FLRW background (2.3) and working in synchronous gauge[3], the line element with only tensor (transverse $\partial^i h_{ij} = 0$ and traceless $\delta^{ij} h_{ij} = 0$) perturbations reads

$$ds^2 = a^2(\tau)\left[d\tau^2 - \left(\delta_{ij} + h_{ij}\right) dx^i\, dx^j\right]. \tag{7.20}$$

We work in Fourier space to highlight the contribution of each wavenumber k to $h_{ij}(t, \mathbf{x})$. Focusing on a single polarisation (3.73) and assuming statistical isotropy, one finds that each mode $h_k(\tau)$ obeys (3.74) in conformal time

$$h_k'' + 2\frac{a'}{a} h_k' + k^2 h_k = 0, \tag{7.21}$$

Introducing the rescaled variable $f_k(\tau) \equiv a(\tau)\, h_k(\tau)$, (7.21) becomes

$$f_k'' + \left(k^2 + \frac{a''}{a}\right) f_k = 0. \tag{7.22}$$

Further redefining $f_k = i\sqrt{\tau}\, u_k$ casts (7.22) into the standard form of a Bessel equation. In each phase of the cyclic model, the general solution is a linear combination of Hankel functions $H_\nu^{(1)}$ and $H_\nu^{(2)}$.

[3] In synchronous gauge comoving observers follow geodesics. Here, one demands that there be no perturbation in the (tt) and (ti)-components of the metric, *i.e.* $g_{0,\mu} = 0$ with $\mu = \{0, 1, 2, 3\}$.

7.2.1 General solutions in the different phases

For $\tau < \tau_{\rm tr}$, during which $a(\tau) = \frac{1}{H(B-\tau)}$, the general solution of (7.22) can be written in terms of Hankel functions as

$$f_k(\tau) = \sqrt{-k\eta}\left[D_1(k)\, H^{(1)}_{\frac{3}{2}}(-k\eta) + D_2(k)\, H^{(2)}_{\frac{3}{2}}(-k\eta)\right], \quad \eta \equiv \tau - B, \tag{7.23}$$

where B is given by (7.6), and $D_{1,2}(k)$ are integration constants for each mode k.

In the interval $\tau_{\rm tr} < \tau < \tau_{\rm end}$, when $a(\tau) \propto \left(\tau - \tau_{\rm ek}\right)^{\alpha}$, the solution takes the form

$$f_k(\tau) = \sqrt{y}\left[A_1(k)\, H^{(1)}_n(y) + A_2(k)\, H^{(2)}_n(y)\right], \quad y \equiv -k\left(\tau - \tau_{\rm ek}\right), \tag{7.24}$$

with $A_{1,2}(k)$ as the corresponding constants.

For the contracting kinetic phase, $\tau_{\rm end} < \tau < 0$, where $a(\tau) \propto (-\tau)^{1/2}$, one obtains

$$f_k(\tau) = \sqrt{-k\tau}\left[B_1(k)\, H^{(1)}_0(-k\tau) + B_2(k)\, H^{(2)}_0(-k\tau)\right]. \tag{7.25}$$

Finally, in the expanding kinetic phase $0 < \tau < \tau_{\rm r}$, where $a(\tau) \propto \tau^{1/2}$, the general solution is

$$f_k(\tau) = \sqrt{k\tau}\left[C_1(k)\, H^{(1)}_0(k\tau) + C_2(k)\, H^{(2)}_0(k\tau)\right]. \tag{7.26}$$

The matching is not performed at $\tau = 0$, where the metric would be singular and perturbation theory breaks down, but rather at a finite conformal time close to the transition between the two phases, where both the background and perturbations remain well defined.

In what follows, we determine the integration constants $D_{1,2}(k)$, $A_{1,2}(k)$, $B_{1,2}(k)$ and $C_{1,2}(k)$ by enforcing continuity of $f_k(\tau)$ and $f_k'(\tau)$ at each transition of phase. At $\tau = \tau_{\rm tr}$ – the boundary between dark energy and ekpyrotic stage – continuity of f_k yields

$$\sqrt{x_{\rm tr}}\left[D_1 H^{(1)}_{3/2}(x_{\rm tr}) + D_2 H^{(2)}_{3/2}(x_{\rm tr})\right] = \sqrt{y_{\rm tr}}\left[A_1 H^{(1)}_n(y_{\rm tr}) + A_2 H^{(2)}_n(y_{\rm tr})\right], \tag{7.27}$$

and continuity of f_k' yields in matrix form

$$\underline{\underline{Y}}_1\, \mathbf{A} \;=\; \underline{\underline{X}}_1\, \mathbf{D},$$

with

$$\underline{\underline{Y}}_1 = \begin{pmatrix} \sqrt{y_{\rm tr}}\, H^{(1)}_n(y_{\rm tr}) & \sqrt{y_{\rm tr}}\, H^{(2)}_n(y_{\rm tr}) \\ \sqrt{y_{\rm tr}}\, H^{(1)}_{n-1}(y_{\rm tr}) - \frac{n-\frac{1}{2}}{\sqrt{y_{\rm tr}}} H^{(1)}_n(y_{\rm tr}) & \sqrt{y_{\rm tr}}\, H^{(2)}_{n-1}(y_{\rm tr}) - \frac{n-\frac{1}{2}}{\sqrt{y_{\rm tr}}} H^{(2)}_n(y_{\rm tr}) \end{pmatrix},$$

$$\underline{\underline{X}}_1 = \begin{pmatrix} \sqrt{x_{\rm tr}}\, H^{(1)}_{3/2}(x_{\rm tr}) & \sqrt{x_{\rm tr}}\, H^{(2)}_{3/2}(x_{\rm tr}) \\ \sqrt{x_{\rm tr}}\, H^{(1)}_{1/2}(x_{\rm tr}) - \frac{1}{\sqrt{x_{\rm tr}}} H^{(1)}_{3/2}(x_{\rm tr}) & \sqrt{x_{\rm tr}}\, H^{(2)}_{1/2}(x_{\rm tr}) - \frac{1}{\sqrt{x_{\rm tr}}} H^{(2)}_{3/2}(x_{\rm tr}) \end{pmatrix},$$

$$\mathbf{A} = \begin{pmatrix} A_1 \\ A_2 \end{pmatrix}, \quad \mathbf{D} = \begin{pmatrix} D_1 \\ D_2 \end{pmatrix}, \quad x_{\rm tr} \equiv -k\,\eta(\tau_{\rm tr}), \;\; y_{\rm tr} \equiv -k(\tau_{\rm tr} - \tau_{\rm ek}).$$

At $\tau = \tau_{\rm end}$, namely the end of the ekpyrotic phase, matching gives

$$\underline{\underline{Y}}_2\, \mathbf{B} = \underline{\underline{X}}_2\, \mathbf{A},$$

with

$$\underline{\underline{Y}}_2 = \begin{pmatrix} H^{(1)}_0(x_{\rm e}) & H^{(2)}_0(x_{\rm e}) \\ \sqrt{x_{\rm e}}\, H^{(1)}_{-1}(x_{\rm e}) + \frac{1}{2\sqrt{x_{\rm e}}} H^{(1)}_0(x_{\rm e}) & \sqrt{x_{\rm e}}\, H^{(2)}_{-1}(x_{\rm e}) + \frac{1}{2\sqrt{x_{\rm e}}} H^{(2)}_0(x_{\rm e}) \end{pmatrix},$$

$$\underline{\underline{X}}_2 = \begin{pmatrix} \sqrt{2\alpha}\, H^{(1)}_n(2\alpha x_{\rm e}) & \sqrt{2\alpha}\, H^{(2)}_n(2\alpha x_{\rm e}) \\ \sqrt{2\alpha x_{\rm e}}\, H^{(1)}_{n-1}(2\alpha x_{\rm e}) - \frac{n-\frac{1}{2}}{\sqrt{2\alpha x_{\rm e}}} H^{(1)}_n(2\alpha x_{\rm e}) & \sqrt{2\alpha x_{\rm e}}\, H^{(2)}_{n-1}(2\alpha x_{\rm e}) - \frac{n-\frac{1}{2}}{\sqrt{2\alpha x_{\rm e}}} H^{(2)}_n(2\alpha x_{\rm e}) \end{pmatrix},$$

$$\mathbf{B} = \begin{pmatrix} B_1 \\ B_2 \end{pmatrix}, \quad x_{\rm e} \equiv -k\,\tau_{\rm end}.$$

At the bounce $\tau = 0$, kinetic contraction-kinetic expansion, one finds the simple relation

$$C_1 = -\sqrt{1+\chi}\, B_2, \qquad C_2 = -\sqrt{1+\chi}\, B_1.$$

7.2.2 Present day strain spectrum

We quantify the primordial gravitational-wave background via the dimensionless strain spectrum [38, 106]

$$\Delta h(k,\tau) = \frac{k^{3/2}}{\pi} \left| h_k(\tau) \right|. \tag{7.28}$$

Evaluating this during radiation domination ($\tau = \tau_{\rm r}$) using the matched solutions gives

$$\Delta h(k,\tau_{\rm r}) = \frac{k^2 \sqrt{2\,\tau_{\rm r}}}{\pi\, a(\tau_{\rm r})\, M_{\rm Pl}} \left| C_1(k)\, H^{(1)}_0(k\tau_{\rm r}) + C_2(k)\, H^{(2)}_0(k\tau_{\rm r}) \right|, \tag{7.29}$$

where we define $x_{\rm r} = k\tau_{\rm r}$. The present-day spectrum $\Delta h(k,\tau_0)$ is obtained by applying a transfer function $\mathcal{T}(k)$

$$\Delta h(k,\tau_0) = \mathcal{T}(k)\, \Delta h(k,\tau_{\rm r}), \tag{7.30}$$

with the fitting form [38]

$$\mathcal{T}(k) \approx \left(\tfrac{k_0}{k}\right)^2 \left(1 + \frac{k}{k_{\rm eq}} + \frac{k^2}{k_{\rm eq}\, k_{\rm r}}\right), \tag{7.31}$$

where

$$k_{\rm r} = a_{\rm r}\, H_{\rm r} \approx \frac{T_{\rm r}^2}{M_{\rm P}}$$

is the comoving horizon scale at radiation-domination.

Although we have set $a(\tau_{\rm r}) = 1$ internally, comparison with observations requires normalising $a(\tau_0) = 1$. Since $a \propto 1/T$, one finds

$$\frac{a(\tau_0)}{a(\tau_{\rm r})} \simeq \frac{T_{\rm r}}{T_0} \sim 10^{20},$$

so that the rescaled comoving frequency becomes $\hat{k}_{\rm r} = k_{\rm r}/a(\tau_0) \sim 10^{-1}\,\text{Hz}$. Hereafter we denote $\hat{k}_{\rm r}$ simply as $k_{\rm r}$. Using $T_0/T_{\rm r} \sim 6.6 \times 10^{-20}$, the ratio of the present horizon to the radiation-era horizon is

$$\frac{k_0}{k_{\rm r}} \sim \frac{T_0}{T_{\rm r}} \sim 6.6 \times 10^{-20}, \tag{7.32}$$

and during matter domination $H \propto a^{-3/2}$ implies

$$\frac{k_{\rm eq}}{k_0} \approx \sqrt{1 + z_{\rm eq}} \sim 10^2, \tag{7.33}$$

with $z_{\rm eq}$ the redshift of matter-radiation equality. We can also place a bound on $k_{\rm tr}$, modes on the horizon at the previous dark energy phase, which will be useful later. The comoving wavelengths of these modes are determined by the duration of the ekpyrotic phase, which we require to last at least ~ 60 e-folds in order to homogenise and flatten the universe for the next cycle. A yet more stringent bound follows from (7.11), since

$$N \simeq \ln\left(H_{\rm end}/H_0\right) \approx \ln \sqrt{\frac{-V_{\rm end}}{V_0}}. \tag{7.34}$$

Substituting V_0 at today's dark-energy density and $V_{\rm end}$ at the GUT scale yields $N \approx 115$, and implies the comoving horizon shrinks by $\sim 10^{50}$, yielding

$$\frac{k_{\rm end}}{k_{\rm tr}} \approx 10^{50}. \tag{7.35}$$

7.3 Vacuum choice and backreaction constraints

The derivation of the tensor spectrum in the previous section is completely general with respect to the choice of vacuum state and includes contributions from modes generated in the dark energy phase of the prior cycle. This framework allows us to probe two key questions: how sensitive the spectrum is to non-Bunch-Davies (non-BD) initial conditions, and whether modes from the previous cycle's dark energy era leave an observable imprint today.

In quantum field theory the vacuum state is the lowest-energy field configuration, but in an effective description (such as our cyclic model) integrating out high-energy degrees of freedom can provide the choice of vacuum to be nontrivial. Inflationary studies have shown that exotic vacua – parameterised by nonzero Bogoliubov coefficient β_k – can violate standard consistency relations and yield blue-tilted tensor spectra (*e.g.* [176, 450, 451]). In cyclic cosmology, previous works have always assumed the BD vacuum during the ekpyrotic phase [38], but if new physics at a scale M modifies the initial state in the dark energy phase, one must ensure that excited quanta do not backreact catastrophically on the modulus field. Following [450, 470, 471], we allow the Bogoliubov coefficient $\beta_k = 2\,D_2(k)\,\sqrt{\frac{k}{\pi}}$ to be nonzero, and impose a UV cutoff by requiring $\beta_k \to 0$ for modes with $k > M\,a(\tau_c)$. Following [471], we model

$$\beta_k = \beta_0 \exp\!\left[-k^2/\left(M\,a(\tau_c)\right)^2\right], \tag{7.36}$$

where $M \sim 10^{-4} M_{\rm P}$ is the effective cutoff and β_0 its amplitude. The energy density of non-BD quanta (particles associated with the non-BD vacuum due to $\beta_k \neq 0$), at time τ is

$$\rho_{\text{non-BD}} \;\sim\; \frac{1}{a(\tau)^4}\int \frac{d^3k}{(2\pi)^3}\,\left|\beta_k\right|^2 k \;\sim\; \left(\frac{a(\tau_c)}{a(\tau)}\right)^4 \beta_0^2\,M^4. \tag{7.37}$$

Requiring $\rho_{\text{non-BD}} \ll M_{\rm P}^2 H^2$ during the dark energy phase (where $H \approx H_0$) yields

$$\beta_0 \lesssim \frac{H\,M_{\rm P}}{M^2} \sim 10^{-53}, \tag{7.38}$$

an extraordinarily tight bound, independent of the precise choice of the cutoff time τ_c, because total expansion from one cycle to the next ensures $(a(\tau_c)/a(\tau_i))^4 \ll 1$. Hence, avoiding any backreaction during the dark energy phase imposes an extraordinarily tight upper bound on deviations from the Bunch-Davies vacuum. For context, the analogous constraint in inflationary cosmology is $\beta_0 < 10^{-6}$ [471], which is weaker than our result. This discrepancy arises because, although inflation and dark energy share similar background dynamics, their characteristic energy densities differ by more than 10^{100}. The

vastly higher energy scale of inflation makes it far harder for perturbations to backreact, and thus permits much larger departures from the BD vacuum. One might instead choose to fix the vacuum during the ekpyrotic phase, where H grows rapidly while a remains almost constant (7.12). In that case, one finds

$$\beta_0 < 10^{45} \quad (M \sim 10^{-4} M_{\rm P}), \tag{7.39}$$

allowing much freedom in vacuum choice for that phase. Nevertheless, one must still verify that any large deviation from the BD vacuum during ekpyrosis does not introduce pathologies in later phases. Given that the dark-energy epoch occurs at the lowest energy scale and that the cyclic model shows remarkable insensitivity to initial conditions from one cycle to the next (as we confirm in the following), we state that fixing the vacuum in the dark-energy phase is both the most restrictive and the most conservative assumption. From a model-building perspective, this makes the BD initial state the safest choice.

7.3.1 Gravitational waves produced from different phases

Our general computation of the strain spectrum of gravitational waves allows us to explore how the predicted spectrum is modified when including contributions from tensor modes produced during the dark energy phase of the preceding cycle. This, in turn, enables us to assess the robustness of these predictions by directly comparing them to those found in previous works, which typically begin in the *ekpyrotic* contracting phase. Here, we compare the strain spectrum predictions obtained in the following two scenarios:

1. Using our general calculation, starting in the dark energy phase of the previous cycle. In this case, we impose BD vacuum conditions on the coefficients D_1 and D_2 during the dark energy stage, given by

$$D_1 = \frac{1}{2}\sqrt{\frac{\pi}{k}}, \qquad D_2 = 0. \tag{7.40}$$

2. Starting the calculation in the *ekpyrotic* phase (omitting the matching at $\tau = \tau_{tr}$) and imposing BD initial conditions as adopted in [38]

$$A_1 = \frac{1}{2}\sqrt{\frac{\pi}{k}}, \qquad A_2 = 0. \tag{7.41}$$

It is important to stress that, although our calculation remains entirely general with

respect to the choice of vacuum state, significant deviations from the BD vacuum in the dark energy phase are strongly constrained, as demonstrated in the previous discussion. This provides a compelling physical motivation for imposing the BD vacuum in the dark energy phase in scenario *1*. Conversely, for scenario *2*, we adopt BD initial conditions in the *ekpyrotic* phase to remain consistent with the framework of [38], thereby facilitating a direct comparison.

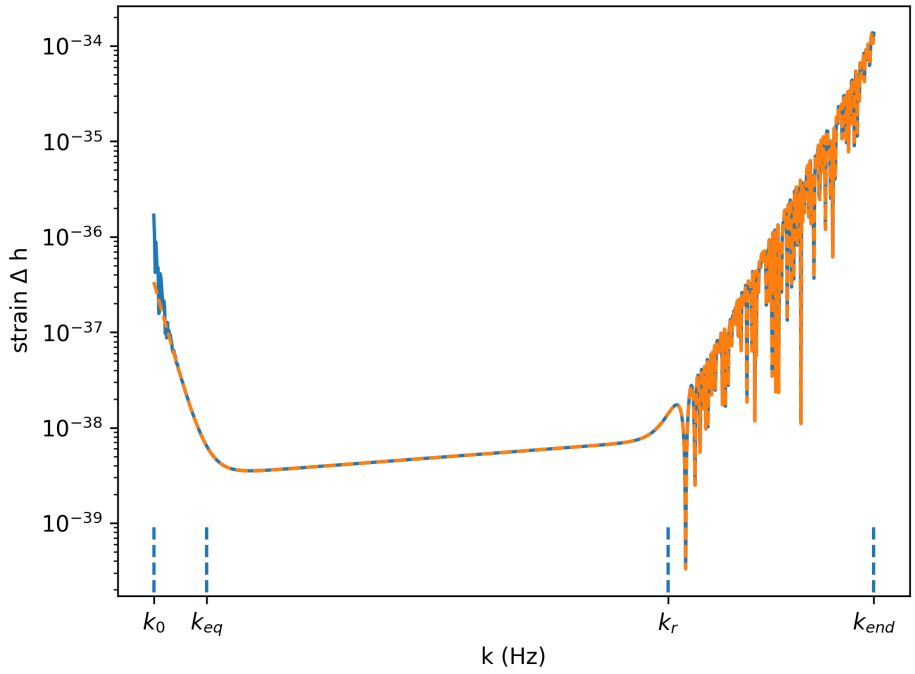

Figure 7.1: Strain spectrum as a function of comoving frequency k for gravitational waves generated when the cycle begins in the dark energy phase (blue) and in the *ekpyrotic* phase (orange). BD initial conditions are assumed in both cases. The points k_0, k_{eq}, k_r, and k_{end} denote the comoving frequencies corresponding to the present-day horizon, matter-radiation equality, the onset of radiation domination, and the *ekpyrotic*-kinetic transition, respectively.

After performing the matching across the relevant cosmological phases, the strain spectra of tensor modes for the two cases can be computed using (7.29) and (7.31). The resulting spectra are displayed in Figure 7.1, where case *1* is shown in blue and case *2* in orange. There is a difference of up to an order of magnitude in the strain amplitude Δh for modes corresponding to k_0, which is the comoving wavenumber at the horizon today. This difference can be attributed to the evolution of modes generated during the dark energy phase of the previous cycle, corresponding to case *1*. To clarify this point, we refer to Figure 7.2, which illustrates the evolution of the comoving Hubble horizon across the different phases of the model. We note that the horizon size at the end of the dark energy phase (*i.e.* $k_{\rm tr}^{-1}$) is several orders of magnitude larger than the

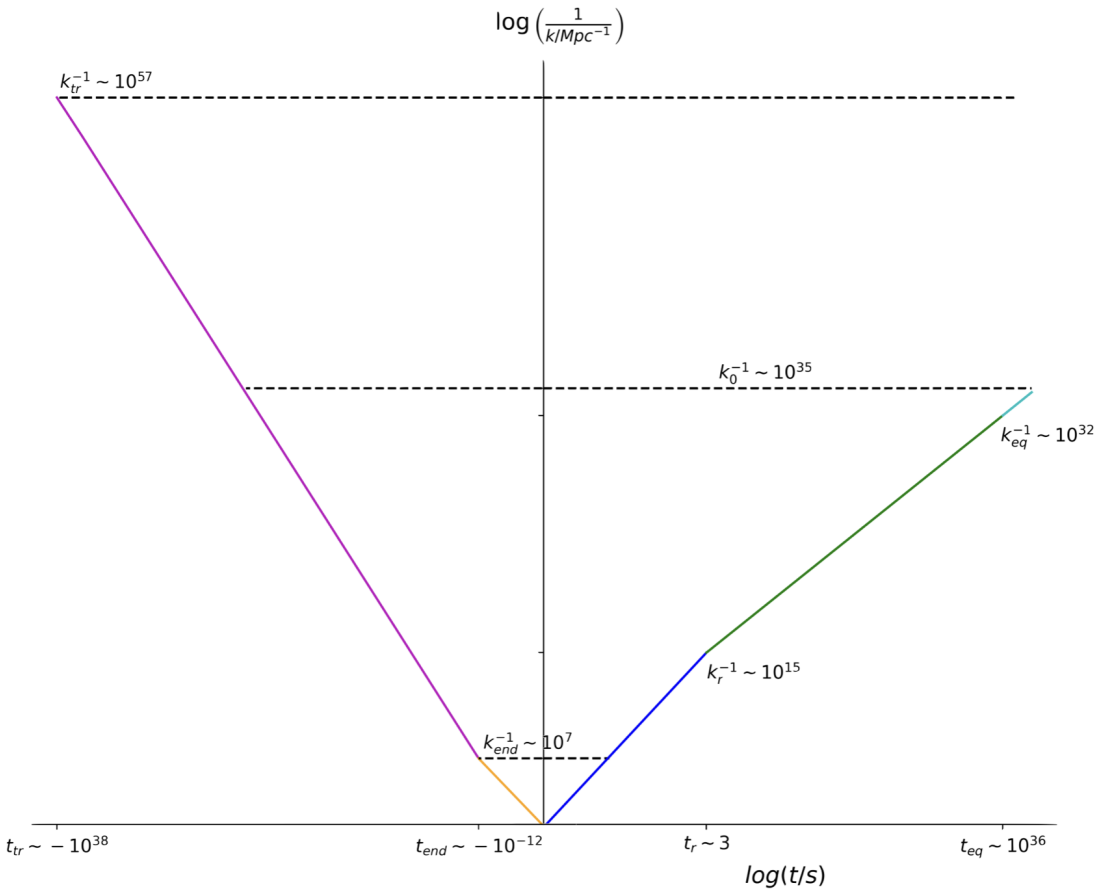

Figure 7.2: Illustrative plot showing the evolution of the comoving Hubble horizon, $(aH)^{-1}$, across the ekpyrotic, kinetic contracting, kinetic expanding, radiation-dominated, and matter-dominated phases, depicted in magenta, orange, dark blue, green, and cyan, respectively. Key horizon-crossing modes are indicated by horizontal dashed lines labeled with their corresponding comoving wavenumbers; less significant modes are also labeled.

present-day horizon (*i.e.* k_0^{-1}). This guarantees that none of these super-horizon modes could have re-entered by today. As a result, modes produced during the dark energy phase that exit the horizon become effectively frozen and experience further stretching throughout this epoch. On the other hand, sub-horizon modes generated during the same phase undergo oscillations with a decaying amplitude, following $h \propto a^{-1}$. This behaviour can be explicitly shown by solving (7.22) under the dark energy background evolution given by (7.4). As a consequence, we expect sub-horizon modes produced deep within the dark energy phase (as well as during earlier phases of the previous cycle) to decay to negligible amplitudes when compared to modes produced near the end of the same phase or during the subsequent *ekpyrotic* phase. In contrast, sub-horizon modes generated *close* to the end of the dark energy phase can persist into the *ekpyrotic* phase of the next cycle, effectively acting as additional quanta in the vacuum initial conditions

of the following *ekpyrotic* phase. This contribution is captured by the coefficient A_2 in (7.24) and may produce observable signatures on scales corresponding to the long-wavelength part of the strain spectrum. Referring again to Figure 7.1, we observe that the differences induced by these amplitude oscillations – expected from the under-damped solution of a simple harmonic oscillator – are confined to the frequency range between k_0 and $k_{\rm eq}$, before modes become frozen during the *ekpyrotic* phase. As discussed in [467], the following phases induce a red tilt on the initially scale-invariant spectrum generated during the dark energy phase. It is important to note that for an *ekpyrotic* phase lasting approximately $N \sim 115$ e-folds, the magnitude of the coefficient A_2 can reach $\mathcal{O}(10^{10})$[4] for modes between k_0 and $k_{\rm eq}$, before dropping sharply to around $\mathcal{O}(10^{-15})$ for modes near $k_{\rm r}$. This behaviour accounts for the observed discrepancy between imposing BD initial conditions in the dark energy phase, as specified in (7.40), and imposing them in the *ekpyrotic* phase, as specified in (7.41).

We conclude with an important final observation: preserving the correct background evolution of the modulus field requires the vacuum state during the dark energy phase to be BD-like. This condition implies that perturbations present in the current cycle must decay to amplitudes negligible compared to the energy density associated with the BD vacuum, preventing them from acting as additional quanta above the vacuum state. We emphasise that this requirement is naturally fulfilled by the evolution of tensor perturbations after the bounce, particularly during the subsequent radiation and matter-dominated eras. In particular, the transfer function given in (7.31) ensures that the amplitudes of short-wavelength modes – those that re-enter the horizon first and could potentially cause the most significant backreaction – are suppressed by a factor of $(k_0/k)^2$. Consequently, the amplitude of the shortest wavelength modes in the observable spectrum ($k \sim k_{\rm end}$) is reduced by more than 20 orders of magnitude during the radiation and matter eras.

As a result, the evolution through these phases ensures that the amplitude of all modes decays across every cycle before each dark energy phase, effectively restoring the vacuum to a BD state each time. This mechanism protects the dark energy phase from potential backreaction effects, underlining the robustness of the model and demonstrating that, from a theoretical perspective, imposing initial conditions in the dark energy phase remains the most conservative and reliable choice for consistent model building.

[4] A_1 remains of order unity because it matches directly to the scale-invariant amplitude inherited from the BD vacuum.

8 Conclusions

The objective of this thesis is to elucidate the phenomenology and viability of alternative and generalised models of the early Universe, providing insights into multifield inflationary dynamics, the behavior of gravitational waves and scale-invariant symmetry in cosmology. Motivated by current observational tensions and theoretical challenges in standard inflationary cosmology, these works explore a range of models that incorporate novel mechanisms, field interactions, non-local terms, and symmetry principles to understand the origin and evolution of primordial perturbations.

Chapter 4 analyses multifield inflationary models featuring non-trivial kinetic couplings, focusing on both analytical and numerical aspects. We start by deriving analytically the background field equations and linear perturbation equations for two scalar fields with a curved field-space metric, highlighting the explicit dependence on the kinetic coupling parameter. We study the decomposition of perturbations into adiabatic and isocurvature modes and analyse their evolution on super-horizon scales, providing conditions under which isocurvature modes can convert into curvature perturbations. We also analytically discuss how field-space curvature modifies the effective entropic mass and affects stability. Regarding the numerics, we implement a Monte Carlo Markov Chain (MCMC) approach to explore the parameter space, using a dedicated integration scheme for solving the background dynamics from initial random field values to the end of inflation (typically at $N \approx 55$ e-folds). We systematically sample over parameters such as the mass of the fields and both the potential and kinetic couplings, and compute inflationary observables including the scalar spectral index n_s, tensor-to-scalar ratio r, and the running parameters α_s and β_s. The numerical results show how variations in the kinetic coupling parameter impact the shape of field trajectories, the evolution of the Hubble parameter, and the predicted CMB angular power spectra. Additionally, we present posterior distributions and contour plots illustrating constraints on the model parameters at 68% and 95% confidence levels, derived by comparing theoretical predictions with observational data. The combination of analytical insight and numerical constraints confirms that kinetic couplings can significantly alter multifield dynamics, potentially leading to distinct observational imprints that can be tested with current and

future CMB data. The general formalism and the novel sample code of this work can be used to test the robustness of inflationary models.

Chapter 5 focuses on scale-invariant inflationary models, combining analytical and numerical studies to assess their viability and predictions. The chapter begins by considering a scale-invariant action involving a non-minimally coupled scalar field ψ, a quadratic curvature term R^2, and a quartic self-interaction, all preserving classical scale symmetry. A key result is the spontaneous breaking of scale symmetry via dynamical field evolution, leading to a conserved Noether charge and a characteristic elliptical field-space trajectory. The analysis demonstrates that entropy (isocurvature) perturbations vanish due to scale invariance, simplifying the dynamics effectively to a single-field system and avoiding typical multifield instabilities. Analytical expressions for slow-roll parameters, spectral index n_s, tensor-to-scalar ratio r, and their runnings are derived explicitly, revealing that in the limit of vanishing non-minimal coupling ξ, predictions coincide with Starobinsky inflation. A dedicated algorithm numerically samples the parameter space (the parameter α which determines the strength of R^2 term, the parameter ξ controlling the strength of the coupling $\phi^2 R$, Ω related to the strength of the quartic term in the JF) and solves the full background equations and perturbations. Constraints are placed using likelihoods built from Planck 2018 and BICEP/Keck data, generating posterior distributions for observables such as the spectral index n_s, the tensor to scalar ratio r, and the running parameters such as α_s. Results show that the model predicts a non-zero lower bound on $r \gtrsim 0.00332$ and small running $\alpha_s < 1.2\times10^{-4}$ (both at 95% CL), making these predictions testable with future CMB observations. Additionally, a detailed comparison with Starobinsky and α-attractor models in the $n_s - r$ plane demonstrates that, despite overlapping regions, scale-invariant inflation occupies distinct parameter space, particularly when ξ is non-negligible. Finally, the analysis robustly rules out large ξ values, excluding conformal coupling ($\xi = 1$) at high significance, and confirms that initial conditions do not strongly affect inflationary predictions. Overall, Chapter 5 validates scale-invariant inflation as a theoretically motivated and observationally viable scenario, highlighting its unique phenomenological features and potential discriminating power in future cosmological surveys.

A promising future direction is to pioneer the study of primordial black hole (PBH) formation within the framework of scale-invariant quadratic gravity. PBHs are hypothesised to form from the collapse of overdense regions in the early Universe and are of particular interest due to their potential to account for a significant fraction of dark matter. Their purely gravitational interactions make them natural dark matter candidates, and their formation history may also influence small-scale structure through inherited clustering properties. Beyond their intrinsic interest, PBHs offer a powerful probe for

testing early-Universe models. While many cosmological scenarios yield similar predictions – such as gravitational wave signatures – the study of PBHs provides an independent avenue for constraining and discriminating between theoretical frameworks.

Chapter 6 investigates inflation in the context of non-local hybrid metric-Palatini gravity, analytically and numerically exploring the effects of non-local operators on early Universe dynamics. We start by formulating the action with non-local terms expressed through inverse d'Alembertian operators acting on both metric and Palatini curvature scalars. The theory is recast into an equivalent scalar-tensor representation using auxiliary fields, allowing explicit identification of ghost conditions. A rigorous analysis demonstrates that generic non-degenerate non-local hybrid models suffer from ghost instabilities unless local and non-local terms are assigned to different curvatures. Algebraic no-ghost conditions are derived, constraining the parameter space and the functional form of the non-local couplings. We then tackle the inflationary background dynamics numerically considering the FLRW metric. Two main scenarios are considered: with vanishing and nonvanishing non-local potential ($V(\Box^{-1}\mathcal{R}) = 0$ and $V(\Box^{-1}\mathcal{R}) \neq 0$). Field equations for the scalar fields Φ, Ξ and Ψ are integrated, and we investigate how different non-local coupling choices (power-law or exponential) affect scalar field trajectories, the number of e-folds, and deformation of the potential. The results show that for metric $f(R)$ models with coupling Palatini non-localities, a finite slow-roll phase is possible with successful exit from inflation. On the other hand, considering Platini $f(R)$ models with coupling metric non-localities leads to an infinite slow-roll phase and no natural end to inflation. This scenario happens as the shape of the potential coming from the $f(R)$ does not provide the model with a global minimum. For each viable setup, the no-ghost condition is numerically verified throughout the evolution. The analysis further reveals that non-local terms deform the effective Starobinsky-like potential, offering distinctive features that could be probed observationally. Overall, Chapter 6 demonstrates that carefully constructed non-local hybrid gravity models can consistently support inflation at the background level, while also providing a framework to explore new phenomenological imprints in the early Universe.

A promising future direction is to test the robustness of the model by extending the analysis beyond the background level and investigate the evolution of cosmological perturbations. Studying both scalar and tensor perturbations in this non-local hybrid framework is essential for assessing the model's viability against observational constraints, particularly from the CMB anisotropies and large-scale structure data. This includes analysing the power spectra, spectral indices, tensor-to-scalar ratio, and potential non-Gaussian signatures. In models where non-localities deform the effective inflationary potential, perturbations can carry distinct imprints that may serve as observational dis-

criminants. Moreover, evaluating the stability of perturbations is crucial for confirming the absence of additional ghost or gradient instabilities at the linear level. Such an analysis could also clarify whether the successful exit from inflation seen in some scenarios agree with observations. Overall, the perturbative study would significantly advance the understanding of non-local hybrid gravity models and help determine their predictive power in the context of early-universe cosmology.

Chapter 7 explores an alternative to the standard inflationary paradigm by analysing cyclic cosmologies, with a particular focus on the ekpyrotic scenario. The chapter starts by reviewing a cyclic model with a phenomenological scalar potential designed to induce successive phases of expansion and contraction. The evolution of the scale factor across different cosmological epochs (ekpyrotic, kinetic contracting, bounce, and kinetic expanding phases) is derived explicitly, using both cosmic and conformal time parametrisations. Constraints on the model parameters are analytically obtained to ensure a sufficient number of e-folds ($N \sim 115$) in the ekpyrotic phase, necessary to homogenise and flatten the Universe. Moreover, model parameters such as potential depth and transition times are constrained to satisfy continuity and stability requirements. We then study the evolution of primordial tensor perturbations across cycles numerically, starting from the dark energy phase of the previous cycle, and considering different vacuum choices. Two scenarios are explored: one with Bunch-Davies (BD) vacuum imposed during the dark energy phase, and one (compared to the one already studied in literature) with BD vacuum imposed in the ekpyrotic phase. The strain spectra of gravitational waves are computed for both cases, revealing differences up to an order of magnitude in the present-day strain amplitude for the longest modes. The analysis further demonstrates that deviations from the BD vacuum can introduce backreaction problems, potentially spoiling the cyclic evolution unless strong constraints on the excited modes are imposed. It is shown that the cyclic model predictions for tensor modes remain robust under conservative vacuum choices, with contributions from previous dark energy phases decaying sufficiently before the start of the new cycle. Overall, Chapter 7 establishes that cyclic scenarios can reproduce a nearly scale-invariant scalar spectrum while predicting a suppressed tensor spectrum by validating the choice of the vacuum state.

Unlike other parts of this thesis, the analysis presented in this chapter is self-contained and does not directly point toward immediate extensions. The study provides a complete exploration of tensor perturbations within the chosen cyclic framework, offering a standalone contribution to the ongoing investigation of alternatives to inflation.

Taken together, these chapters illustrate how diverse theoretical extensions – from multifield kinetic couplings to scale-invariant models, non-local hybrid gravity, and

cyclic cosmologies – provide a rich landscape of early-universe scenarios, each offering distinctive predictions and observational signatures that help deepen our understanding of cosmic origins and guide future experimental tests.

Part III | Appendices

A | Conformal transformation between JF and EF

We start from the JF action for an $f(R)$ theory with an additional scalar field χ:

$$S_{\rm J} = \int d^4x\,\sqrt{-\tilde{g}}\left[f(\tilde{R}) - \frac{1}{2}\,\tilde{g}^{\mu\nu}\partial_\mu\chi\,\partial_\nu\chi - U(\chi)\right]. \tag{A1}$$

We introduce an auxiliary field α for which we can rewrite (A1) as

$$S = \int d^4x\,\sqrt{-\tilde{g}}\left[f(\alpha) + f'(\alpha)\,(\tilde{R}-\alpha) - \frac{1}{2}\,\tilde{g}^{\mu\nu}\partial_\mu\chi\,\partial_\nu\chi - U(\chi)\right]. \tag{A2}$$

Variation of the action with respect to α leads to $f''(\alpha)\,(\tilde{R}-\alpha) = 0$ onshell, so for $f''(\alpha)\neq 0$ we recover $\alpha = \tilde{R}$. We then define the scalaron field $\varphi \equiv f'(\alpha)$, and we define the two-field potential

$$V(\varphi,\chi) = \alpha\,\varphi - f(\alpha) + U(\chi), \tag{A3}$$

where the first two terms come from the f-gravity sector (expressed in terms of α and its "momentum" φ), and $U(\chi)$ is the potential that the original matter field carries. Once the $f(\tilde{R})$ has been chosen, we can invert the relation to express α in terms of φ and then rewrite $V(\varphi,\chi)$ purely in terms of $\{\varphi,\chi\}$. The action becomes

$$S = \int d^4x\,\sqrt{-\tilde{g}}\left[\varphi\,\tilde{R} - \frac{1}{2}\tilde{g}^{\mu\nu}\partial_\mu\chi\,\partial_\nu\chi - V(\varphi,\chi)\right]. \tag{A4}$$

Next, we perform a conformal transformation

$$\sqrt{-\tilde{g}} = \Omega^4\sqrt{-g} \qquad \tilde{g}_{\mu\nu} = \Omega^2\,g_{\mu\nu}, \qquad \tilde{R} = \Omega^{-2}\,R - 6\,\Omega^{-3}\,\Box\Omega. \tag{A5}$$

We substitute (A5) into (A4) yielding

$$S = \int d^4x\,\sqrt{-g}\left[\varphi\left(\Omega^2 R - 6\,\Omega\,\Box\Omega\right) - \frac{1}{2}\Omega^2 g^{\mu\nu}\partial_\mu\chi\,\partial_\nu\chi - \Omega^4 V(\varphi,\chi)\right]. \tag{A6}$$

We choose $\varphi\Omega^2 = 1/2\kappa$ (with $\kappa = 8\pi G$) which brings the Ricci term into canonical Einstein form. The mixed term $\varphi\,\Omega\,\Box\Omega$ can be expanded as

$$in(\text{A6}) \int d^4x\,\sqrt{-g}\,\varphi\,\Omega\,\Box\Omega = \frac{1}{2\kappa}\int d^4x\sqrt{-g}\,\frac{1}{\Omega}\,\frac{\partial_\mu(\sqrt{-g}g^{\mu\nu}\partial_\nu\Omega)}{\sqrt{-g}}, \tag{A7}$$

and then integrated by parts

$$\int d^4x\,\sqrt{-g}\,\varphi\,\Omega\,\Box\Omega = -\frac{1}{2\kappa}\int d^4x\sqrt{-g}\partial_\mu\left(\frac{1}{\Omega}\right)g^{\mu\nu}\partial_\nu\Omega = \frac{1}{2\kappa}\int d^4x\,\sqrt{-g}\,\frac{1}{\Omega^2}\,g^{\mu\nu}\partial_\mu\Omega\,\partial_\nu\Omega, \tag{A8}$$

leading to a kinetic term for φ once substituted back into (A6). The boundary term in (A8) is neglected under the assumption of a flat FLRW universe with no physical boundary. By collecting terms the action can be written as

$$S = \int d^4x\,\sqrt{-g}\left[\frac{R}{2\kappa} - \frac{3}{4\kappa\varphi^2}\,g^{\mu\nu}\partial_\mu\varphi\,\partial_\nu\varphi - \frac{1}{4\kappa\varphi}\,g^{\mu\nu}\partial_\mu\chi\,\partial_\nu\chi - \frac{V(\varphi,\chi)}{4\kappa\varphi^2}\right]. \tag{A9}$$

Finally, via a field ψ redefinition

$$\varphi = \frac{1}{2\kappa}\,e^{\beta\psi},$$

we bring (A9) to the familiar two-field EF form

$$S_{\rm E} = \int d^4x\,\sqrt{-g}\left[\frac{R}{2\kappa} - \frac{3}{4\kappa}\beta^2\,g^{\mu\nu}\partial_\mu\psi\,\partial_\nu\psi - \frac{1}{2}\,e^{-\beta\psi}\,g^{\mu\nu}\partial_\mu\chi\,\partial_\nu\chi - e^{-2\beta\psi}\,V(\psi,\chi)\right], \tag{A10}$$

with $\beta = \sqrt{2\kappa/3}$ to ensure a canonical kinetic term for ψ.

B | Double inflation and likelihood validation

B.1 Double quadratic potential and double inflation

In this appendix, we apply our numerical framework introduced in Chapter 4 to a simple two-field example – a canonical double-quadratic potential

$$V = \frac{1}{2}m_\psi^2\psi^2 + \frac{1}{2}m_\chi^2\chi^2, \tag{B1}$$

which corresponds to setting $c = 0$ and $g = 0$ in the more general parametrisation of Section 4.2. Although this model has been studied extensively in the literature, our goals here are twofold: first, to verify that our code reproduces well-known results; and second, to showcase its ability to detect and track "double inflation"scenarios, in which two distinct fields drive successive phases of accelerated expansion.[1] Figure B1 shows the tensor-to-scalar ratio r as a function of the mass ratio $\log_{10}(m_\chi/m_\psi)$ for roughly 10^4 realisations in which the scalar amplitude A_s and spectral index n_s lie within observationally allowed ranges. As noted in [224] (and confirmed here), this model generically predicts $r \gtrsim 0.13$ independently of the fields' initial conditions or mass ratio – values that exceed the current upper limits from the CMB B-mode polarization released by the Keck Array collaboration. Hence, although we do not perform a full data likelihood analysis (the model is already ruled out by its high tensor amplitude), we use our sampler to cross-validate this prediction. Indeed, even across many orders of magnitude in m_χ/m_ψ and with randomly chosen initial conditions, r remains above the 95% CL bound from the joint Planck+BK18 analysis, in excellent agreement with Figure 8 of [224]. A closer analysis of the figure reveals the presence of minor dispersion of patterns that deviate

[1] Such double-inflation behaviours arise more naturally in purely quadratic, canonical models than in the bilinear coupling case of Section 4.2.

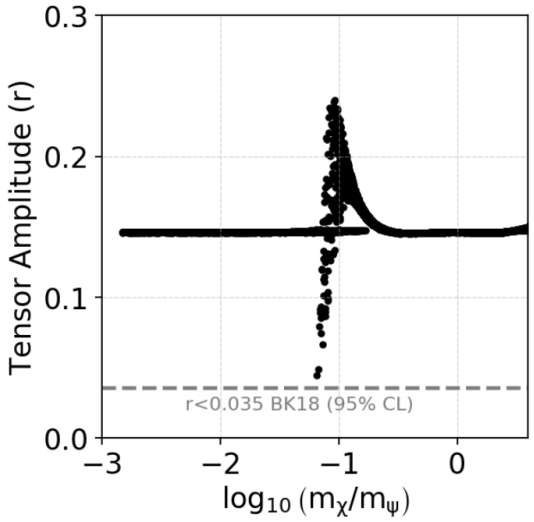

Figure B1: Predictions for the tensor-to-scalar ratio r as a function of the mass ratio $\log_{10}(m_\chi/m_\psi)$ for $\sim 10^4$ models in which the scalar amplitude A_s and spectral index n_s lie within ranges consistent with our observational constraints.

from the degeneration line between the mass ratio and the value of r. These points correspond to genuine double-inflation trajectories, where the first phase is driven by ψ and the second by χ. Reference [224] mentions these trajectories but treats them as if they were a single inflationary epoch. By contrast, our code automatically identifies each distinct inflationary stage and reconstructs its dynamics separately, producing accurate predictions for models with multiple acceleration epochs. To illustrate this feature, we select one of the lowest r ($r \sim 0.05$; still above observational bounds) and plot its detailed evolution in Figure B2. In the top panel, $\epsilon_0(N)$ first reaches unity after about 55 e-folds (grey dashed line), marking the end of the ψ-driven phase. The second and third panels show that ψ has essentially settled by this time, while χ remains dynamically active. Rather than stopping, our integrator continues and finds a second period of inflation as χ rolls. The bottom panel tracks the Hubble rate $H(N)$, throughout both stages. At each phase transition, our algorithm re-evaluates all observables – including r – thereby providing a fully consistent treatment of complicated, multi-stage inflationary dynamics.

B.2 Sampling and likelihood validation

In this appendix, we present a step-by-step description of the procedure used to construct and validate our analytical likelihood described in Section 4.3, which is based on a joint analysis of the B-mode polarization data from BK18 and the Planck 2018 measurements of temperature and polarisation anisotropies. Most importantly, we demon-

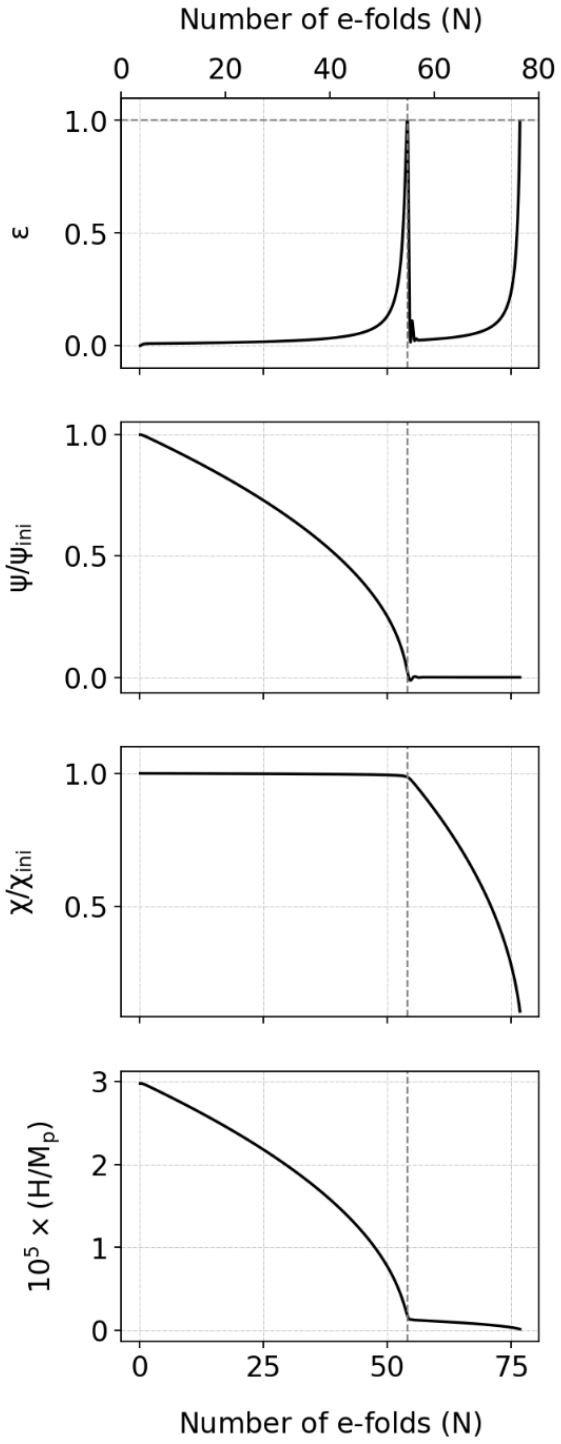

Figure B2: Evolution of the slow-roll parameter ϵ (top panel), the scalar fields ψ and χ (middle panels), and the Hubble rate H (bottom panel) in a double-inflation model featuring two successive stages of accelerated expansion.

strate that our likelihood reproduces results consistent with those obtained from standard MCMC analyses widely used in the literature. Throughout this validation, we do

Parameter	**Real likelihoods**	**This work**
$\log(10^{10}A_S)$	3.049 ± 0.016	3.051 ± 0.015
n_s	0.9624 ± 0.0044	0.9621 ± 0.0046
α_s	0.002 ± 0.010	0.002 ± 0.010
β_s	0.012 ± 0.012	0.013 ± 0.013
r	< 0.0354	< 0.0357

Table B1: Results for the ΛCDM+α_s+β_s+r model obtained using the publicly available sampler Cobaya [472], in combination with the full Planck 2018 likelihoods [9, 265, 266] and the BK18 B-mode polarization data [264] (labeled as *Real likelihoods*), are compared with the results obtained for the same model using our sampling algorithm together with the analytical likelihood defined in (4.47) (labeled as *This work*).

not assume any specific inflationary model and remain agnostic about the underlying inflationary dynamics, in keeping with the standard approach adopted in cosmological data analyses.

1. **Extended cosmological model and MCMC analysis:** As a first step, we consider an extension of the standard ΛCDM model that includes three additional parameters: the tensor-to-scalar ratio r, the running of the spectral index α_s, and the running of the running β_s. We refer to this extended model as ΛCDM+$\alpha_s + \beta_s + r$. We then perform a full MCMC analysis using the `Cobaya` sampler [472] in combination with the `CAMB` Boltzmann integrator [261, 262]. `Cobaya` incorporates the efficient "fast dragging"procedure developed in [473]. For our baseline dataset, we include:

   - Planck 2018 TT, TE, EE likelihoods, including low multipole data ($\ell < 30$) [9, 265, 266];
   - Planck 2018 lensing likelihood, based on the reconstructed lensing potential [267];
   - Bicep/Keck Array X (BK18) likelihood for CMB B-mode polarization, cleaned of foreground contamination [264].

   The resulting constraints on the extended parameter set are summarised in Table B1, and serve as updated bounds on this cosmological extension based on the

latest data.

2. **Construction of likelihood:** In the second step, we use the results of the MCMC analysis to construct our analytical Gaussian likelihood, defined in (4.47). Specifically, we adopt the mean vector μ and covariance matrix Σ derived from the posterior distribution of the ΛCDM+α_s + β_s + r model.

3. **Validation via sampling of inflationary observables:** Finally, we validate the analytical likelihood by showing that it yields equivalent constraints to those obtained using the full experimental likelihoods. To this end, we perform an independent sampling of the inflationary observables $\{A_s, n_s, \alpha_s, \beta_s\}$ using our custom sampling algorithm, and apply the analytical likelihood defined by (4.47). This approach directly samples from the observable parameter space, using the same priors as in the MCMC analysis. As this method avoids the complexity of solving inflationary dynamics for each sample – and the potential numerical issues that may arise – it is computationally efficient and allows us to evaluate approximately 10^5 models. Figure B3 shows a direct comparison between the results obtained with our analytical likelihood (labeled *This work*) and those from the full MCMC analysis using real experimental likelihoods (labeled *Real likelihoods*). One can see that both approaches yield consistent constraints for all inflationary parameters. Numerical comparisons are provided in Table B1, further confirming the validity of our method.

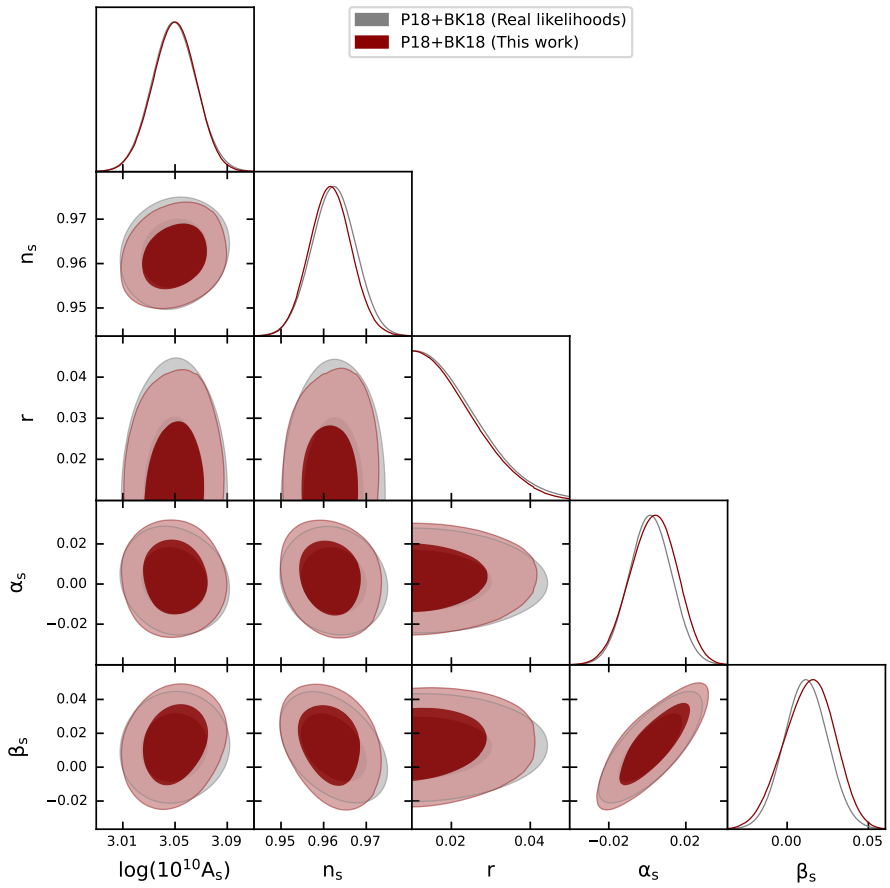

Figure B3: Comparison between the marginalised 1D and 2D posterior distributions obtained using our analytical likelihood (red curves, labeled *This work*) and those obtained from real experimental likelihoods via Cobaya (grey curves, labeled *Real likelihoods*) for the inflationary parameters $\{A_s, n_s, \alpha_s, \beta_s, r\}$. The agreement validates our approach.

C | Technical derivations for the scale-invariant model

C.1 Derivatives of $V(\rho)$ and $b(\rho)$

The derivatives of the potential $V(\rho)$ (5.35) read:

$$\begin{aligned}
V_\rho &= -\frac{9}{\sqrt{6}}\frac{\xi M^3}{\alpha}\sinh\left(\frac{2\rho}{\sqrt{6}M}\right) + 3\sqrt{6}\frac{\Omega M^3}{\alpha}\sinh\left(\frac{2\rho}{\sqrt{6}M}\right)\sinh^2\left(\frac{\rho}{\sqrt{6}M}\right),\\
V_{\rho\rho} &= -\frac{3(\xi+\Omega)M^2}{\alpha}\cosh\left(\frac{2\rho}{\sqrt{6}M}\right) + \frac{3\Omega M^2}{\alpha}\cosh\left(\frac{4\rho}{\sqrt{6}M}\right),\\
V_{\rho\rho\rho} &= -\frac{\sqrt{6}M}{\alpha}\sinh\left(\frac{2\rho}{\sqrt{6}M}\right)\left[\xi+\Omega-4\Omega\cosh\left(\frac{2\rho}{\sqrt{6}M}\right)\right],\\
V_{\rho\rho\rho\rho} &= -\frac{2(\xi+\Omega)}{\alpha}\cosh\left(\frac{2\rho}{\sqrt{6}M}\right) + \frac{8\Omega}{\alpha}\cosh\left(\frac{4\rho}{\sqrt{6}M}\right).
\end{aligned} \tag{C1}$$

The derivatives of the coupling $b(\rho)$ (5.34) are:

$$b_\rho = \frac{1}{\sqrt{6}M}\tanh\left(\frac{\rho}{\sqrt{6}M}\right), \quad b_{\rho\rho} = \frac{1}{6M^2}\frac{1}{\cosh^2\left(\frac{\rho}{\sqrt{6}M}\right)}. \tag{C2}$$

These formulas are used in the numerical implementation of (5.42), (5.43) and (5.44).

C.2 Derivation of the numerator in the $f_{\rm NL}$ expression

By definition (cf (5.52) and/or (5.54)), in terms of the bispectrum B_ζ and the power spectrum P_ζ, one has

$$f_{\rm NL} = \frac{5}{6}\frac{B_\zeta(k_1,k_2,k_3)}{P_\zeta(k_1)\,P_\zeta(k_2) + \text{c.p.}}. \tag{C3}$$

Let us calculate $B_\zeta(k_1, k_2, k_3)$. We start by considering $\zeta \simeq N_I\, Q^I + \frac{1}{2}\, \mathcal{D}_I \mathcal{D}_J N\, Q^I Q^J$ from (5.49). Hence, by inserting ζ into the three-point function (5.51), we get

$$\left\langle \left(N_I Q^I\right) \left(N_J Q^J\right) \left(\tfrac{1}{2} \mathcal{D}_K \mathcal{D}_L N\, Q^K Q^L\right) \right\rangle \sim N_I\, N_J\, \mathcal{D}_K \mathcal{D}_L N \left\langle Q^I Q^K \right\rangle \left\langle Q^J Q^L \right\rangle + \text{p.c.}\,, \tag{C4}$$

to leading order. Each contraction obeys $\langle Q^I Q^K \rangle \propto \mathcal{G}_*^{IK}\, P_Q(k)$, where $P_Q(k) = (H_*/2\pi)^2$ – by considering (5.50) and (5.53). Including the combinatorial factor (from the three ways to choose which pair arises from the quadratic piece), the bispectrum in momentum space is

$$B_\zeta(k_1, k_2, k_3) \propto N_I\, N_J\, \mathcal{D}_K \mathcal{D}_L N \left[\mathcal{G}_*^{IK}\, \mathcal{G}_*^{JL}\, P(k_1)\, P(k_2) + 2 \text{ perms.}\right]. \tag{C5}$$

In the squeezed limit $k_3 \ll k_1 \simeq k_2$, the dominant contribution becomes

$$B_\zeta(k_1, k_2, k_3) \propto N_I\, N_J\, \mathcal{D}_K \mathcal{D}_L N\, \mathcal{G}_*^{IK} \mathcal{G}_*^{JL}\, P(k_1)\, P(k_3). \tag{C6}$$

Noting that $\mathcal{D}_K \mathcal{D}_L N = \mathcal{D}_K \left(N_{,L}\right) = \mathcal{D}_K \left(\partial_L N\right)$, and relabeling dummy indices, the combination $N_I\, N_J \mathcal{D}_K \mathcal{D}_L N \mathcal{G}_*^{IK}\, \mathcal{G}_*^{JL}$ can be rewritten as $\mathcal{G}_*^{IK} N_K \mathcal{G}_*^{JL} N_L \mathcal{D}_I N_J$. Hence the full numerator takes the form $\frac{5}{6} \mathcal{G}_*^{IK} N_K \mathcal{G}_*^{JL} N_L \mathcal{D}_I N_J$ which is in agreement with (5.54).

D Analytical aspects of the EF representation

D.1 Ghosts for the purely metric and Palatini case

Following the procedure outlined in Section 6.1, it is straightforward to verify that when the original function F of (6.1) depends solely on a single curvature scalar, the resulting action in the EF takes the form

$$S_E = \frac{1}{2\kappa^2}\int d^4x\sqrt{-q}\left(R(q) - \delta_i\,(\nabla\Theta)^2 + \frac{\mathbf{\Pi}}{e^{\sqrt{\frac{2}{3}}\Theta}} - \frac{W(\Theta,\vec{\pi}_1,\vec{\pi}_2)}{e^{2\sqrt{\frac{2}{3}}\Theta}}\right), \tag{D1}$$

where $\delta_i = 0$ or $\delta_i = 1$ corresponds to the Palatini and metric configurations, respectively. Here, Θ and $\mathbf{\Pi}$ denote the scalar field and the sum of kinetic terms associated with the specific representation of the model under consideration. In the case $\delta_i = 1$, the results of [96] are recovered, *i.e.* the theory propagates N ghost-like degrees of freedom. On the other hand, choosing $\delta_i = 0$ implies that Θ lacks independent dynamics and can be entirely expressed in terms of the other scalar fields, as is typically the case in Palatini $f(\mathcal{R})$ theories. Indeed, varying (D1) with respect to Θ yields

$$2W - \frac{\partial W}{\partial\Theta} = e^{\sqrt{\frac{2}{3}}\Theta}\mathbf{\Pi}, \tag{D2}$$

which, once the potential W is specified, can in principle be solved for $\Theta = \Theta(\vec{\pi}_1,\vec{\pi}_2)$. It is important to emphasise that, even in this case, the kinetic sector $\mathbf{\Pi}$ still includes N ghost-like fields, indicating that the theory remains dynamically unstable.

D.2 Diagonalisation for $\sigma_2 = 0$

In this section, we present the diagonalised form of the action given in (6.44), obtained through the field redefinition $\Psi = \eta + \omega$, $\Xi = \eta - \omega$. This transformation leads to

the following expression

$$S_2 = \frac{1}{2\kappa^2}\int d^4x\sqrt{-q}\left(R-(\nabla\Phi)^2-\frac{K_-(\eta,\omega)(\nabla\eta)^2+K_+(\eta,\omega)(\nabla\omega)^2}{e^{\sqrt{\frac{2}{3}}\Phi}}\right.$$
$$\left.-\frac{V\left(\beta(\eta+\omega)\right)+U\left(e^{\sqrt{\frac{2}{3}}\Phi}+\frac{(\eta-\omega)^2}{6}\right)}{e^{2\sqrt{\frac{2}{3}}\Phi}}\right), \tag{D3}$$

where the kinetic coefficients $K_\mp(\eta,\omega)$ are defined as

$$K_\mp(\eta,\omega) \equiv 2 \mp \frac{\eta-\omega}{3}\left.\frac{d\beta}{d\Psi}\right|_{\Psi=\eta+\omega}. \tag{D4}$$

D.3 Expressions for the G function

In this section we derive the functions $G(\chi_2)$ introduced in Section 6.2. Following the procedure described in Subsection 6.3.1, the explicit forms of the non-local function $G(\chi_2)$ corresponding to a power-law kinetic coupling in the EF are given by:

$$G(\chi_2) = G_0 + \frac{1}{nk}\left[\Psi_0^{-n} - \left(\Psi_0^{n+2} + \frac{n+2}{k}\left(\chi_2-\chi_{2,0}\right)\right)^{-\frac{n}{n+2}}\right], \qquad n\neq 2, \tag{D5}$$

$$G(\chi_2) = G_0 + \frac{\Psi_0^2}{2k}\left(e^{\frac{2(\chi_2-\chi_{2,0})}{k}}-1\right), \qquad n=2. \tag{D6}$$

In contrast, for an exponential kinetic coupling, the resulting expression reads

$$G(\chi_2) = G_0 + \frac{\chi_2-\chi_{2,0}}{ke^{n\Psi_0}\left(ke^{n\Psi_0}+n(\chi_2-\chi_{2,0})\right)}. \tag{D7}$$

Bibliography

[1] M. De Angelis and C. van de Bruck. "Adiabatic and isocurvature perturbations in extended theories with kinetic couplings". *JCAP* **10**, 023 (2023), arXiv: 2304.12364 [hep-th].

[2] W. Giarè et al. "Tracking the multifield dynamics with cosmological data: a Monte Carlo approach". *JCAP* **12**, 014 (2023), arXiv: 2306.12414 [astro-ph.CO].

[3] C. Cecchini et al. "Testing scale-invariant inflation against cosmological data". *JCAP* **07**, 058 (2024), arXiv: 2403.04316 [astro-ph.CO].

[4] M. Rinaldi et al. "Scale-invariant inflation". *J. Phys. Conf. Ser.* **2531**, 012012 (2023), arXiv: 2303.16107 [gr-qc].

[5] F. Bombacigno et al. "Inflation in non-local hybrid metric-Palatini gravity". *JCAP* **05**, 025 (2025), arXiv: 2412.15064 [hep-th].

[6] M. De Angelis et al. "Gravitational waves in a cyclic Universe: resilience through cycles and vacuum state". *JCAP* **06**, 036 (2024), arXiv: 2403.00533 [hep-th].

[7] A. H. Guth. "Inflationary universe: A possible solution to the horizon and flatness problems". *Phys. Rev. D* **23**, 347–356 (1981).

[8] S. Weinberg. *Cosmology* (Oxford University Press, 2008).

[9] N. Aghanim et al. "Planck 2018 results. VI. Cosmological parameters". *Astron. Astrophys.* **641**, A6 (2020), arXiv: 1807.06209 [astro-ph.CO]. [Erratum: Astron. Astrophys. 652, C4 (2021)].

[10] A. G. Riess et al. "Observational evidence from supernovae for an accelerating universe and a cosmological constant". *Astron. J.* **116**, 1009–1038 (1998), arXiv: astro-ph/9805201.

[11] A. R. Liddle and D. H. Lyth. *Cosmological inflation and large scale structure* (Cambridge University Press, 2000).

[12] J. Martin, C. Ringeval, and V. Vennin. "Encyclopædia Inflationaris: Opiparous Edition". *Phys. Dark Univ.* **5-6**, 75–235 (2014), arXiv: 1303.3787 [astro-ph.CO].

[13] S. M. Carroll. "In What Sense Is the Early Universe Fine-Tuned?" (2014), arXiv: 1406.3057 [astro-ph.CO].

[14] C. P. Burgess. "Quantum gravity in everyday life: General relativity as an effective field theory". *Living Rev. Rel.* **7**, 5–56 (2004), arXiv: gr-qc/0311082.

[15] K. S. Stelle. "Renormalization of Higher Derivative Quantum Gravity". *Phys. Rev. D* **16**, 953–969 (1977).

[16] R. P. Woodard. "How Far Are We from the Quantum Theory of Gravity?" *Rept. Prog. Phys.* **72**, 126002 (2009), arXiv: 0907.4238 [gr-qc].

[17] L. Susskind. "Dynamics of spontaneous symmetry breaking in the Weinberg-Salam theory". *Phys. Rev. D* **20**, 2619–2625 (1979).

[18] M. E. Peskin and D. V. Schroeder. *An Introduction to quantum field theory* (Addison-Wesley, Reading, USA, 1995).

[19] S. Deser and R. P. Woodard. "Nonlocal Cosmology". *Phys. Rev. Lett.* **99**, 111301 (2007).

[20] A. D. Linde. "A New Inflationary Universe Scenario: A Possible Solution of the Horizon, Flatness, Homogeneity, Isotropy and Primordial Monopole Problems". *Phys. Lett. B* **108**, 389–393 (1982).

[21] V. F. Mukhanov and G. V. Chibisov. "Quantum fluctuations and a nonsingular universe". *JETPL* **33**, 532 (1981).

[22] A. A. Starobinskiĭ. "Spectrum of relict gravitational radiation and the early state of the universe". *JETPL* **30**, 682 (1979).

[23] P. G. Ferreira et al. "Inflation in a scale invariant universe". *Phys. Rev. D* **97**, 123516 (2018), arXiv: 1802.06069 [astro-ph.CO].

[24] P. G. Ferreira, C. T. Hill, and G. G. Ross. "Scale-Independent Inflation and Hierarchy Generation". *Phys. Lett. B* **763**, 174–178 (2016), arXiv: 1603.05983 [hep-th].

[25] M. Shaposhnikov and D. Zenhausern. "Scale invariance, unimodular gravity and dark energy". *Phys. Lett. B* **671**, 187–192 (2009), arXiv: 0809.3395 [hep-th].

[26] S. Kachru et al. "Towards inflation in string theory". *JCAP* **10**, 013 (2003), arXiv: hep-th/0308055.

[27] C. Gordon et al. "Adiabatic and entropy perturbations from inflation". *Phys. Rev. D* **63**, 023506 (2000), arXiv: astro-ph/0009131.

[28] D. Langlois et al. "Primordial Fluctuations and Non-Gaussianities in Multifield Dirac-Born-Infeld Inflation". *Phys. Rev. Lett.* **101**, 061301 (2008).

[29] C. T. Byrnes, K.-Y. Choi, and L. M. H. Hall. "Conditions for large non-Gaussianity in two-field slow-roll inflation". *JCAP* **10**, 008 (2008), arXiv: 0807.1101 [astro-ph].

[30] J. Khoury. "A Briefing on the ekpyrotic / cyclic universe", *6th RESCEU International Symposium on Frontier in Astroparticle Physics and Cosmology*, pp. Ed. by K. Sato and S. Nagataki (Universal Academy Press, 2004), arXiv: astro-ph/0401579.

[31] R. Brandenberger and P. Peter. "Bouncing Cosmologies: Progress and Problems". *Found. Phys.* **47**, 797–850 (2017), arXiv: 1603.05834 [hep-th].

[32] D. Battefeld and P. Peter. "A Critical Review of Classical Bouncing Cosmologies". *Phys. Rept.* **571**, 1–66 (2015), arXiv: 1406.2790 [astro-ph.CO].

[33] J. Khoury, P. J. Steinhardt, and N. Turok. "Designing cyclic universe models". *Phys. Rev. Lett.* **92**, 031302 (2004), arXiv: hep-th/0307132.

[34] J. Khoury et al. "The Ekpyrotic universe: Colliding branes and the origin of the hot big bang". *Phys. Rev. D* **64**, 123522 (2001), arXiv: hep-th/0103239.

[35] P. J. Steinhardt, N. Turok, and N. Turok. "A Cyclic model of the universe". *Science* **296**, 1436–1439 (2002), arXiv: hep-th/0111030.

[36] P. J. Steinhardt and N. Turok. "Cosmic evolution in a cyclic universe". *Phys. Rev. D* **65**, 126003 (2002), arXiv: hep-th/0111098.

[37] J.-L. Lehners. "Ekpyrotic and Cyclic Cosmology". *Phys. Rept.* **465**, 223–263 (2008), arXiv: 0806.1245 [astro-ph].

[38] L. A. Boyle, P. J. Steinhardt, and N. Turok. "The Cosmic gravitational wave background in a cyclic universe". *Phys. Rev. D* **69**, 127302 (2004), arXiv: hep-th/0307170.

[39] A. A. Starobinsky. "A New Type of Isotropic Cosmological Models Without Singularity". *Phys. Lett. B* **91**, 99–102 (1980).

[40] R. Kallosh and A. Linde. "Planck, LHC, and α-attractors". *Phys. Rev. D* **91**, 083528 (2015), arXiv: 1502.07733 [astro-ph.CO].

[41] S. Weinberg. *The Quantum theory of fields. Vol. 1: Foundations* (Cambridge University Press, 2005).

[42] S. Capozziello and M. D. Laurentis. "Extended Theories of Gravity". *Phys. Rept.* **509**, 167–321 (2011).

[43] S. Nojiri and S. D. Odintsov. "Unified cosmic history in modified gravity: From F(R) theory to Lorentz non-invariant models". *Phys. Rept.* **505**, 59–144 (2011).

[44] C. M. Will. "The confrontation between general relativity and experiment". *Living Reviews in Relativity* **17**, 4 (2014).

[45] C. M. Will. "Gravity: Newtonian, Post-Newtonian, and General Relativistic", *Gravity: Where Do We Stand?*, pp. 9–72. Ed. by R. Peron et al. (Springer International Publishing, 2016).

[46] J. F. Donoghue. "General Relativity as an Effective Field Theory: The Leading Quantum Corrections". *Phys. Rev. D* **50**, 3874–3888 (1994).

[47] L. Modesto. "Super-renormalizable Quantum Gravity". *Phys. Rev. D* **86**, 044005 (2012).

[48] T. Biswas et al. "Towards singularity and ghost free theories of gravity". *Phys. Rev. Lett.* **108**, 031101 (2012), arXiv: 1110.5249 [gr-qc].

[49] F. Briscese et al. "Inflation in (super-)renormalizable gravity". *Phys. Rev. D* **87**, 083507 (2013).

[50] M. Maggiore and M. Mancarella. "Nonlocal gravity and dark energy". *Phys. Rev. D* **90**, 023005 (2014), arXiv: 1402.0448 [hep-th].

[51] A. De Felice and S. Tsujikawa. "f(R) theories". *Living Rev. Rel.* **13**, 3 (2010), arXiv: 1002.4928 [gr-qc].

[52] T. Clifton et al. "Modified Gravity and Cosmology". *Phys. Rept.* **513**, 1–189 (2012), arXiv: 1106.2476 [astro-ph.CO].

[53] C. P. L. Berry and J. R. Gair. "Linearized f(R) Gravity: Gravitational Radiation and Solar System Tests". *Phys. Rev. D* **83**, 104022 (2011), arXiv: 1104.0819 [gr-qc]. [Erratum: Phys.Rev.D 85, 089906 (2012)].

[54] F. Bombacigno, F. Moretti, and G. Montani. "Scalar modes in extended hybrid metric-Palatini gravity: Weak field phenomenology". *Phys. Rev. D* **100**, 124036 (2019).

[55] S. M. Carroll. "The Cosmological constant". *Living Rev. Rel.* **4**, 1 (2001), arXiv: astro-ph/0004075.

[56] J. C. Hwang. "Cosmological perturbations in generalized gravity theories: Formulation". *Class. Quant. Grav.* **7**, 1613–1631 (1990).

[57] D. C. Rodrigues et al. "Auxiliary fields representation for modified gravity models". *Phys. Rev. D* **83**, 084028 (2011), arXiv: 1101.5028 [gr-qc].

[58] S. Nojiri, S. D. Odintsov, and V. K. Oikonomou. "Modified Gravity Theories on a Nutshell: Inflation, Bounce and Late-time Evolution". *Phys. Rept.* **692**, 1–104 (2017), arXiv: 1705.11098 [gr-qc].

[59] T. P. Sotiriou and V. Faraoni. "f(R) Theories Of Gravity". *Rev. Mod. Phys.* **82**, 451–497 (2010), arXiv: 0805.1726 [gr-qc].

[60] G. J. Olmo. "Limit to general relativity in f(R) theories of gravity". *Phys. Rev. D* **75**, 023511 (2007), arXiv: gr-qc/0612047.

[61] C. Brans and R. H. Dicke. "Mach's Principle and a Relativistic Theory of Gravitation". *Phys. Rev.* **124**, 925–935 (1961).

[62] I. Quiros. "Selected topics in scalar–tensor theories and beyond". *Int. J. Mod. Phys. D* **28**, 1930012 (2019), arXiv: 1901.08690 [gr-qc].

[63] J. Khoury and A. Weltman. "Chameleon fields: Awaiting surprises for tests of gravity in space". *Phys. Rev. Lett.* **93**, 171104 (2004), arXiv: astro-ph/0309300.

[64] A. Palatini. "Deduzione invariantiva delle equazioni gravitazionali dal principio di Hamilton". *Rend. Circ. Mat. Palermo* **43**, 203–212 (1919).

[65] G. Magnano and L. M. Sokolowski. "On physical equivalence between nonlinear gravity theories and a general relativistic selfgravitating scalar field". *Phys. Rev. D* **50**, 5039–5059 (1994), arXiv: gr-qc/9312008.

[66] M. Ferraris, M. Francaviglia, and I. Volovich. "The Universality of vacuum Einstein equations with cosmological constant". *Class. Quant. Grav.* **11**, 1505–1517 (1994), arXiv: gr-qc/9303007.

[67] A. Delhom and D. Rubiera-Garcia. "Palatini Theories of Gravity and Cosmology", *Modified Gravity and Cosmology: An Update by the CANTATA Network*, pp. 163–175. Ed. by E. N. Saridakis et al. (Springer International Publishing, Cham, 2021).

[68] G. J. Olmo. "Cosmology in Palatini theories of gravity". *AIP Conf. Proc.* **1458**, 222–237 (2012), arXiv: 1207.4815 [gr-qc].

[69] N. J. Poplawski. "The Cosmic snap parameter in f(R) gravity". *Class. Quant. Grav.* **24**, 3013–3020 (2007), arXiv: gr-qc/0610133.

[70] S. Capozziello et al. "First Order Extended Gravity and the Dark Side of the Universe: The General Theory". *AIP Conf. Proc.* **1241**, 844–853 (2010), arXiv: 0911.2159 [gr-qc].

[71] S. Capozziello, F. Darabi, and D. Vernieri. "Correspondence between Jordan-Einstein frames and Palatini-metric formalisms". *Mod. Phys. Lett. A* **25**, 3279–3289 (2010), arXiv: 1009.2580 [gr-qc].

[72] F. Shojai and A. Shojai. "Geodesic Congruences in the Palatini f(R) Theory". *Phys. Rev. D* **78**, 104011 (2008), arXiv: 0811.2832 [gr-qc].

[73] S. Capozziello, F. Darabi, and D. Vernieri. "Equivalence between Palatini and metric formalisms of f(R)-gravity by divergence free current". *Mod. Phys. Lett. A* **26**, 65–72 (2011), arXiv: 1006.0454 [gr-qc].

[74] G. Allemandi et al. "Conformal aspects of Palatini approach in extended theories of gravity". *Gen. Rel. Grav.* **38**, 33–60 (2006), arXiv: hep-th/0409198.

[75] M. Roshan and F. Shojai. "Palatini f(R) gravity and Noether symmetry". *Phys. Lett. B* **668**, 238–240 (2008), arXiv: 0809.1272 [gr-qc].

[76] A. Izadi and A. Shojai. "Speed of light in the extended gravity theories". *Class. Quant. Grav.* **26**, 195006 (2009), arXiv: 0909.0341 [gr-qc].

[77] T. P. Sotiriou. "f(R) gravity and scalar-tensor theory". *Class. Quant. Grav.* **23**, 5117–5128 (2006), arXiv: gr-qc/0604028.

[78] E Barausse, T. P. Sotiriou, and J. C. Miller. "Curvature singularities, tidal forces and the viability of Palatini f(R) gravity". *Class. Quant. Grav.* **25**, 105008 (2008).

[79] A. Mana, L. Fatibene, and M. Ferraris. "A further study on Palatini f(R)-theories for polytropic stars". *JCAP* **2015**, 040 (2015).

[80] S. Capozziello et al. "Hybrid metric-Palatini gravity". *Universe* **1**, 199–238 (2015), arXiv: 1508.04641 [gr-qc].

[81] N. Tamanini and C. G. Boehmer. "Generalized hybrid metric-Palatini gravity". *Phys. Rev. D* **87**, 084031 (2013), arXiv: 1302.2355 [gr-qc].

[82] J. a. L. Rosa, J. P. S. Lemos, and F. S. N. Lobo. "Wormholes in generalized hybrid metric-Palatini gravity obeying the matter null energy condition everywhere". *Phys. Rev. D* **98**, 064054 (2018).

[83] J. a. L. Rosa et al. "Cosmological solutions in generalized hybrid metric-Palatini gravity". *Phys. Rev. D* **95**, 124035 (2017), arXiv: 1703.03335 [gr-qc].

[84] J. a. L. Rosa, S. Carloni, and J. P. S. Lemos. "Cosmological phase space of generalized hybrid metric-Palatini theories of gravity". *Phys. Rev. D* **101**, 104056 (2020).

[85] S. Capozziello et al. "Hybrid modified gravity unifying local tests, galactic dynamics and late-time cosmic acceleration". *Int. J. Mod. Phys. D* **22**, 1342006 (2013), arXiv: 1305.3756 [gr-qc].

[86] S. Capozziello et al. "Cosmology of hybrid metric-Palatini f(X)-gravity". *JCAP* **04**, 011 (2013), arXiv: 1209.2895 [gr-qc].

[87] S. Capozziello et al. "The virial theorem and the dark matter problem in hybrid metric-Palatini gravity". *JCAP* **07**, 024 (2013), arXiv: 1212.5817 [physics.gen-ph].

[88] T. S. Koivisto and N. Tamanini. "Ghosts in pure and hybrid formalisms of gravity theories: A unified analysis". *Phys. Rev. D* **87**, 104030 (2013), arXiv: 1304.3607 [gr-qc].

[89] S. Carloni, T. Koivisto, and F. S. N. Lobo. "Dynamical system analysis of hybrid metric-Palatini cosmologies". *Phys. Rev. D* **92**, 064035 (2015), arXiv: 1507.04306 [gr-qc].

[90] S. Capozziello et al. "Galactic rotation curves in hybrid metric-Palatini gravity". *Astropart. Phys.* **50-52**, 65–75 (2013), arXiv: 1307.0752 [gr-qc].

[91] C. G. Böhmer, F. S. N. Lobo, and N. Tamanini. "Einstein static Universe in hybrid metric-Palatini gravity". *Phys. Rev. D* **88**, 104019 (2013), arXiv: 1305.0025 [gr-qc].

[92] N. A. Lima and V. S. Barreto. "Constraints on Hybrid Metric-palatini Gravity from Background Evolution". *Astrophys. J.* **818**, 186 (2016), arXiv: 1501.05786 [astro-ph.CO].

[93] S. Capozziello et al. "The Cauchy problem in hybrid metric-Palatini f(X)-gravity". *Int. J. Geom. Meth. Mod. Phys.* **11**, 1450042 (2014), arXiv: 1312.1320 [gr-qc].

[94] L. Modesto. "Super-renormalizable quantum gravity". *Phys. Rev. D* **86**, 044005 (2012).

[95] A. O. Barvinsky. "Aspects of Nonlocality in Quantum Field Theory, Quantum Gravity and Cosmology". *Mod. Phys. Lett. A* **30**, 1540003 (2015), arXiv: 1408.6112 [hep-th].

[96] A. De Felice and M. Sasaki. "Ghosts in classes of non-local gravity". *Phys. Lett. B* **743**, 189–197 (2015), arXiv: 1412.1575 [gr-qc].

[97] M. Rinaldi and L. Vanzo. "Inflation and reheating in theories with spontaneous scale invariance symmetry breaking". *Phys. Rev. D* **94**, 024009 (2016), arXiv: 1512.07186 [gr-qc].

[98] R. Carballo-Rubio, L. J. Garay, and G. García-Moreno. "Unimodular gravity vs general relativity: a status report". *Class. Quant. Grav.* **39**, 243001 (2022).

[99] W. Buchmüller and N. Dragon. "Einstein gravity from restricted coordinate invariance". *Phys. Lett. B* **207**, 292–294 (1988).

[100] W. Buchmüller and N. Dragon. "Gauge fixing and the cosmological constant". *Phys. Lett. B* **223**, 313–317 (1989).

[101] M. Henneaux and C. Teitelboim. "The cosmological constant and general covariance". *Phys. Lett. B* **222**, 195–199 (1989).

[102] A. Eichhorn. "An asymptotically safe guide to quantum gravity and matter". *Front. Astron. Space Sci.* **5**, 47 (2019), arXiv: 1810.07615 [hep-th].

[103] G. Gubitosi, C. Ripken, and F. Saueressig. "Scales and hierachies in asymptotically safe quantum gravity: a review". *Found. Phys.* **49**, 972–990 (2019), arXiv: 1901.01731 [gr-qc].

[104] S. M. Carroll. *Spacetime and Geometry: An Introduction to General Relativity* (Cambridge University Press, 2019).

[105] S. W. Hawking and G. F. R. Ellis. *The Large Scale Structure of Space-Time*, Cambridge Monographs on Mathematical Physics (Cambridge University Press, 2023).

[106] D. Baumann. "Inflation", *Theoretical Advanced Study Institute in Elementary Particle Physics: Physics of the Large and the Small*, pp. 523–686. Ed. by C. Csaki and S. Dodelson (World Scientific, 2011), arXiv: 0907.5424 [hep-th].

[107] R. L. Arnowitt, S. Deser, and C. W. Misner. "The Dynamics of general relativity". *Gen. Rel. Grav.* **40**, 1997–2027 (2008), arXiv: gr-qc/0405109.

[108] V. Mukhanov. *Physical Foundations of Cosmology* (Cambridge University Press, Oxford, 2005).

[109] S. Perlmutter et al. "Measurements of Ω and Λ from 42 High Redshift Supernovae". *Astrophys. J.* **517**, 565–586 (1999), arXiv: astro-ph/9812133.

[110] D. N. Spergel et al. "First year Wilkinson Microwave Anisotropy Probe (WMAP) observations: Determination of cosmological parameters". *Astrophys. J. Suppl.* **148**, 175–194 (2003), arXiv: astro-ph/0302209.

[111] L. Heisenberg. "A systematic approach to generalisations of General Relativity and their cosmological implications". *Phys. Rept.* **796**, 1–113 (2019).

[112] S. Weinberg. "The cosmological constant problem". *Rev. Mod. Phys.* **61**, 1–23 (1989).

[113] K. Freese. "Status of Dark Matter in the Universe". *Int. J. Mod. Phys.* **1**, 325–355 (2017), arXiv: 1701.01840 [astro-ph.CO].

[114] D. Brout et al. "The Pantheon+ Analysis: Cosmological Constraints". *Astrophys. J.* **938**, 110 (2022), arXiv: 2202.04077 [astro-ph.CO].

[115] S. Vagnozzi. "Seven Hints That Early-Time New Physics Alone Is Not Sufficient to Solve the Hubble Tension". *Universe* **9**, 393 (2023), arXiv: 2308.16628 [astro-ph.CO].

[116] S. Vagnozzi. "New physics in light of the H_0 tension: An alternative view". *Phys. Rev. D* **102**, 023518 (2020).

[117] T. Schiavone, G. Montani, and F. Bombacigno. "f(R) gravity in the Jordan frame as a paradigm for the Hubble tension". *Mon. Not. Roy. Astron. Soc.* **522**, L72–L77 (2023), arXiv: 2211.16737 [gr-qc].

[118] G. Montani et al. "Metric f(R) gravity with dynamical dark energy as a scenario for the Hubble tension". *Mon. Not. Roy. Astron. Soc.* **527**, L156–L161 (2023), arXiv: 2306.11101 [gr-qc].

[119] L. Verde, T. Treu, and A. G. Riess. "Tensions between the Early and the Late Universe". *Nature Astron.* **3**, 891 (2019), arXiv: 1907.10625 [astro-ph.CO].

[120] E. Di Valentino et al. "Snowmass2021 - Letter of interest cosmology intertwined II: The hubble constant tension". *Astropart. Phys.* **131**, 102605 (2021), arXiv: 2008.11284 [astro-ph.CO].

[121] E. Di Valentino et al. "In the realm of the Hubble tension—a review of solutions". *Class. Quant. Grav.* **38**, 153001 (2021), arXiv: 2103.01183 [astro-ph.CO].

[122] L. Perivolaropoulos and F. Skara. "Challenges for ΛCDM: An update". *New Astron. Rev.* **95**, 101659 (2022), arXiv: 2105.05208 [astro-ph.CO].

[123] N. Schöneberg et al. "The H0 Olympics: A fair ranking of proposed models". *Phys. Rept.* **984**, 1–55 (2022), arXiv: 2107.10291 [astro-ph.CO].

[124] P. Shah, P. Lemos, and O. Lahav. "A buyer's guide to the Hubble constant". *Astron. Astrophys. Rev.* **29**, 9 (2021), arXiv: 2109.01161 [astro-ph.CO].

[125] E. Abdalla et al. "Cosmology intertwined: A review of the particle physics, astrophysics, and cosmology associated with the cosmological tensions and anomalies". *JHEAp* **34**, 49–211 (2022), arXiv: 2203.06142 [astro-ph.CO].

[126] E. Di Valentino. "Challenges of the Standard Cosmological Model". *Universe* **8**, (2022).

[127] M. Kamionkowski and A. G. Riess. "The Hubble Tension and Early Dark Energy". *Ann. Rev. Nucl. Part. Sci.* **73**, 153–180 (2023), arXiv: 2211.04492 [astro-ph.CO].

[128] W. Giarè. "CMB Anomalies and the Hubble Tension" (2023), arXiv: 2305.16919 [astro-ph.CO].

[129] J.-P. Hu and F.-Y. Wang. "Hubble Tension: The Evidence of New Physics". *Universe* **9**, 94 (2023), arXiv: 2302.05709 [astro-ph.CO].

[130] L. Verde, N. Schöneberg, and H. Gil-Marín. "A Tale of Many H0". *Ann. Rev. Astron. Astrophys.* **62**, 287–331 (2024), arXiv: 2311.13305 [astro-ph.CO].

[131] T. M. C. Abbott et al. "Dark Energy Survey Year 3 results: Cosmological constraints from galaxy clustering and weak lensing". *Phys. Rev. D* **105**, 023520 (2022), arXiv: 2105.13549 [astro-ph.CO].

[132] E. Di Valentino et al. "Cosmology Intertwined III: $f\sigma_8$ and S_8". *Astropart. Phys.* **131**, 102604 (2021), arXiv: 2008.11285 [astro-ph.CO].

[133] T. M. C. Abbott et al. "DES Y3 + KiDS-1000: Consistent cosmology combining cosmic shear surveys". *Open J. Astrophys.* **6**, 2305.17173 (2023), arXiv: 2305.17173 [astro-ph.CO].

[134] T. Tröster et al. "Cosmology from large-scale structure: Constraining ΛCDM with BOSS". *Astron. Astrophys.* **633**, L10 (2020), arXiv: 1909.11006 [astro-ph.CO].

[135] C. Heymans et al. "KiDS-1000 Cosmology: Multi-probe weak gravitational lensing and spectroscopic galaxy clustering constraints". *Astron. Astrophys.* **646**, A140 (2021), arXiv: 2007.15632 [astro-ph.CO].

[136] R. Dalal et al. "Hyper Suprime-Cam Year 3 results: Cosmology from cosmic shear power spectra". *Phys. Rev. D* **108**, 123519 (2023), arXiv: 2304.00701 [astro-ph.CO].

[137] L. Faga et al. "Dark energy survey year 3 results: cosmology from galaxy clustering and galaxy–galaxy lensing in harmonic space". *Mon. Not. Roy. Astron. Soc.* **536**, 1586–1609 (2024), arXiv: 2406.12675 [astro-ph.CO].

[138] J. Yokoyama. "Relic Magnetic Monopoles in the Inflationary Universe". *Phys. Lett. B* **231**, 49–52 (1989).

[139] C. Zhang et al. "On the cosmological abundance of magnetic monopoles". *JHEP* **08**, 220 (2024), arXiv: 2404.04926 [hep-ph].

[140] M. V. Medvedev and A. Loeb. "Plasma Constraints on the Cosmological Abundance of Magnetic Monopoles and the Origin of Cosmic Magnetic Fields". *JCAP* **06**, 058 (2017), arXiv: 1704.05094 [astro-ph.CO].

[141] Planck Collaboration et al. "Planck 2018 results - IV. Diffuse component separation". *A&A* **641**, A4 (2020).

[142] A. Rajantie. "Introduction to Magnetic Monopoles". *Contemp. Phys.* **53**, 195–211 (2012), arXiv: 1204.3077 [hep-th].

[143] H. Georgi and S. L. Glashow. "Unity of All Elementary Particle Forces". *Phys. Rev. Lett.* **32**, 438–441 (1974).

[144] J. C. Pati and A. Salam. "Erratum: Lepton number as the fourth "color"". *Phys. Rev. D* **11**, 703–703 (1975).

[145] G. 't Hooft. "Magnetic Monopoles in Unified Gauge Theories". *Nucl. Phys. B* **79**, 276–284 (1974).

[146] A. H. Guth and S. H. H. Tye. "Phase Transitions and Magnetic Monopole Production in the Very Early Universe". *Phys. Rev. Lett.* **44**, 631 (1980). [Erratum: Phys.Rev.Lett. 44, 963 (1980)].

[147] M. Einhorn, D. Stein, and D. Toussaint. "Are grand unified theories compatible with standard cosmology?" *Phys. Rev. D* **21**, 3295–3298 (1980).

[148] A. D. Linde. "Inflationary Cosmology". *Lect. Notes Phys.* **738**, 1–54 (2008), arXiv: 0705.0164 [hep-th].

[149] D. H. Lyth and A. R. Liddle. *The Primordial Density Perturbation: Cosmology, Inflation and the Origin of Structure* (Cambridge University Press, 2009).

[150] D. Baumann and L. McAllister. *Inflation and String Theory*, Cambridge Monographs on Mathematical Physics (Cambridge University Press, 2015).

[151] W. H. Kinney. "TASI Lectures on Inflation" (2009), arXiv: 0902.1529 [astro-ph.CO].

[152] A. Riotto. "Inflation and the theory of cosmological perturbations". *ICTP Lect. Notes Ser.* **14**, 317–413 (2003), arXiv: hep-ph/0210162.

[153] L. Senatore. "Lectures on inflation.", *Theoretical Advanced Study Institute in Elementary Particle Physics: New Frontiers in Fields and Strings*, pp. 447–543. Ed. by J. Polchinski, P. Vieira, and O. DeWolfe (World Scientific, 2017), arXiv: 1609.00716 [hep-th].

[154] A. R. Liddle. "An Introduction to cosmological inflation", *ICTP Summer School in High-Energy Physics and Cosmology*, pp. 260–295. Ed. by A. Masiero, G. Senjanovic, and A. Smirnov (World Scientific, 1999), arXiv: astro-ph/9901124.

[155] D. Langlois. "Lectures on inflation and cosmological perturbations". *Lect. Notes Phys.* **800**, 1–57 (2010), arXiv: 1001.5259 [astro-ph.CO].

[156] A. R. Liddle, P. Parsons, and J. D. Barrow. "Formalizing the slow-roll approximation in inflation". *Phys. Rev. D* **50**, 7222–7232 (1994).

[157] L. Kofman, A. D. Linde, and A. A. Starobinsky. "Towards the theory of reheating after inflation". *Phys. Rev. D* **56**, 3258–3295 (1997), arXiv: hep-ph/9704452.

[158] B. A. Bassett, S. Tsujikawa, and D. Wands. "Inflation dynamics and reheating". *Rev. Mod. Phys.* **78**, 537–589 (2006), arXiv: astro-ph/0507632.

[159] Y. Shtanov, J. H. Traschen, and R. H. Brandenberger. "Universe reheating after inflation". *Phys. Rev. D* **51**, 5438–5455 (1995), arXiv: hep-ph/9407247.

[160] R. Allahverdi et al. "Reheating in Inflationary Cosmology: Theory and Applications". *Ann. Rev. Nucl. Part. Sci.* **60**, 27–51 (2010), arXiv: 1001.2600 [hep-th].

[161] D. J. H. Chung, E. W. Kolb, and A. Riotto. "Production of massive particles during reheating". *Phys. Rev. D* **60**, 063504 (1999), arXiv: hep-ph/9809453.

[162] M. A. Amin et al. "Nonperturbative Dynamics Of Reheating After Inflation: A Review". *Int. J. Mod. Phys. D* **24**, 1530003 (2014), arXiv: 1410.3808 [hep-ph].

[163] J. Martin and C. Ringeval. "First CMB Constraints on the Inflationary Reheating Temperature". *Phys. Rev. D* **82**, 023511 (2010), arXiv: 1004.5525 [astro-ph.CO].

[164] R. Allahverdi et al. "MSSM flat direction inflation: Slow roll, stability, fine tunning and reheating". *JCAP* **06**, 019 (2007), arXiv: hep-ph/0610134.

[165] J. M. Bardeen, P. J. Steinhardt, and M. S. Turner. "Spontaneous creation of almost scale-free density perturbations in an inflationary universe". *Phys. Rev. D* **28**, 679–693 (1983).

[166] A. H. Guth and S. Y. Pi. "Fluctuations in the New Inflationary Universe". *Phys. Rev. Lett.* **49**, 1110–1113 (1982).

[167] S. W. Hawking. "The Development of Irregularities in a Single Bubble Inflationary Universe". *Phys. Lett. B* **115**, 295 (1982).

[168] D. Baumann, H. Lee, and G. L. Pimentel. "High-Scale Inflation and the Tensor Tilt". *JHEP* **01**, 101 (2016), arXiv: 1507.07250 [hep-th].

[169] S. Hawking and I. Moss. "Fluctuations in the inflationary universe". *Nuclear Physics B* **224**, 180–192 (1983).

[170] H. Kodama and M. Sasaki. "Cosmological Perturbation Theory". *Prog. Theor. Phys. Suppl.* **78**, 1–166 (1984).

[171] M. Crocce and R. Scoccimarro. "Renormalized cosmological perturbation theory". *Phys. Rev. D* **73**, 063519 (2006), arXiv: astro-ph/0509418.

[172] R. Durrer. "Cosmological perturbation theory". *Lect. Notes Phys.* **653**, 31–70 (2004), arXiv: astro-ph/0402129.

[173] D. H. Lyth and A. Riotto. "Particle physics models of inflation and the cosmological density perturbation". *Phys. Rept.* **314**, 1–146 (1999), arXiv: hep-ph/9807278.

[174] V. Mukhanov, H. Feldman, and R. Brandenberger. "Theory of cosmological perturbations". *Phys. Rept.* **215**, 203–333 (1992).

[175] P. Dona and A. Marciano. "Non Bunch Davies group coherent states, and their quantum signatures in CMB observables" (2016), arXiv: 1612.00760 [gr-qc].

[176] A. Ashoorioon et al. "Non-Bunch–Davis initial state reconciles chaotic models with BICEP and Planck". *Phys. Lett. B* **737**, 98–102 (2014), arXiv: 1403.6099 [hep-th].

[177] D. Anninos et al. "Late-time Structure of the Bunch-Davies De Sitter Wavefunction". *JCAP* **11**, 048 (2015), arXiv: 1406.5490 [hep-th].

[178] M. Wrochna. "Conformal extension of the Bunch-Davies state across the de Sitter boundary". *J. Math. Phys.* **60**, 022301 (2019).

[179] J. M. Bardeen. "Gauge-invariant cosmological perturbations". *Phys. Rev. D* **22**, 1882–1905 (1980).

[180] R. H. Brandenberger. "Lectures on the theory of cosmological perturbations". *Lect. Notes Phys.* **646**, 127–167 (2004), arXiv: hep-th/0306071.

[181] A. Notari and A. Riotto. "Isocurvature perturbations in the ekpyrotic universe". *Nucl. Phys. B* **644**, 371–382 (2002), arXiv: hep-th/0205019.

[182] H. Ooguri et al. "Distance and de Sitter Conjectures on the Swampland". *Phys. Lett. B* **788**, 180–184 (2019), arXiv: 1810.05506 [hep-th].

[183] A. Achúcarro and G. A. Palma. "The string swampland constraints require multi-field inflation". *JCAP* **2019**, 041 (2019).

[184] K. N. Abazajian et al. "CMB-S4 Science Book, First Edition" (2016), arXiv: 1610.02743 [astro-ph.CO].

[185] T. Matsumura et al. "Mission design of LiteBIRD". *J. Low Temp. Phys.* **176**, 733 (2014), arXiv: 1311.2847 [astro-ph.IM].

[186] P. Ade et al. "The Simons Observatory: Science goals and forecasts". *JCAP* **02**, 056 (2019), arXiv: 1808.07445 [astro-ph.CO].

[187] S. Hanany et al. "PICO: Probe of Inflation and Cosmic Origins" (2019), arXiv: 1902.10541 [astro-ph.IM].

[188] A. Aghamousa et al. "The DESI Experiment Part I: Science,Targeting, and Survey Design" (2016), arXiv: 1611.00036 [astro-ph.IM].

[189] LSST Science Collaboration et al. "LSST Science Book, Version 2.0". *arXiv e-prints* (2009), arXiv: 0912.0201 [astro-ph.IM].

[190] S. Camera, M. G. Santos, and R. Maartens. "Probing primordial non-Gaussianity with SKA galaxy redshift surveys: a fully relativistic analysis". *Mon. Not. Roy. Astron. Soc.* **448**, 1035–1043 (2015), arXiv: 1409.8286 [astro-ph.CO]. [Erratum: Mon.Not.Roy.Astron.Soc. 467, 1505–1506 (2017)].

[191] P. D. Meerburg et al. "Primordial Non-Gaussianity". *Bull. Am. Astron. Soc.* **51**, 107 (2019), arXiv: 1903.04409 [astro-ph.CO].

[192] D. Baumann and L. McAllister. *Inflation and String Theory*, Cambridge Monographs on Mathematical Physics (Cambridge University Press, 2015).

[193] F. Di Marco, F. Finelli, and R. Brandenberger. "Adiabatic and isocurvature perturbations for multifield generalized Einstein models". *Phys. Rev. D* **67**, 063512 (2003), arXiv: astro-ph/0211276.

[194] S. Renaux-Petel and K. Turzyński. "On reaching the adiabatic limit in multi-field inflation". *JCAP* **2015**, 010 (2015).

[195] A. Achucarro et al. "Features of heavy physics in the CMB power spectrum". *JCAP* **01**, 030 (2011), arXiv: 1010.3693 [hep-ph].

[196] Z. Lalak et al. "Curvature and isocurvature perturbations in two-field inflation". *JCAP* **07**, 014 (2007), arXiv: 0704.0212 [hep-th].

[197] S. Garcia-Saenz, S. Renaux-Petel, and J. Ronayne. "Primordial fluctuations and non-Gaussianities in sidetracked inflation". *JCAP* **07**, 057 (2018), arXiv: 1804.11279 [astro-ph.CO].

[198] M. Sasaki and E. D. Stewart. "A General Analytic Formula for the Spectral Index of the Density Perturbations Produced during Inflation". *Prog. Theor. Phys.* **95**, 71–78 (1996).

[199] S. Groot Nibbelink and B. J. W. van Tent. "Scalar perturbations during multiple field slow-roll inflation". *Class. Quant. Grav.* **19**, 613–640 (2002), arXiv: hep-ph/0107272.

[200] D. Langlois and S. Renaux-Petel. "Perturbations in generalized multi-field inflation". *JCAP* **2008**, 017 (2008).

[201] J.-O. Gong. "Multi-field inflation and cosmological perturbations". *Int. J. Mod. Phys. D* **26**, 1740003 (2017).

[202] N. S. Sugiyama, E. Komatsu, and T. Futamase. "δN formalism". *Phys. Rev. D* **87**, 023530 (2013), arXiv: 1208.1073 [gr-qc].

[203] M. Sasaki and E. D. Stewart. "A General analytic formula for the spectral index of the density perturbations produced during inflation". *Prog. Theor. Phys.* **95**, 71–78 (1996), arXiv: astro-ph/9507001.

[204] D. Wands and J. Garcia-Bellido. "Density perturbations from two field inflation". *Helv. Phys. Acta* **69**, 211–214 (1996), arXiv: astro-ph/9608042.

[205] F. Finelli and R. Brandenberger. "On the generation of a scale invariant spectrum of adiabatic fluctuations in cosmological models with a contracting phase". *Phys. Rev. D* **65**, 103522 (2002), arXiv: hep-th/0112249.

[206] S. Renaux-Petel and K. Turzyński. "Geometrical Destabilization of Inflation". *Phys. Rev. Lett.* **117**, 141301 (2016), arXiv: 1510.01281 [astro-ph.CO].

[207] S. Garcia-Saenz and S. Renaux-Petel. "Flattened non-Gaussianities from the effective field theory of inflation with imaginary speed of sound". *JCAP* **11**, 005 (2018), arXiv: 1805.12563 [hep-th].

[208] O. Grocholski et al. "On backreaction effects in geometrical destabilisation of inflation". *JCAP* **05**, 008 (2019), arXiv: 1901.10468 [astro-ph.CO].

[209] A. Starobinsky. "A new type of isotropic cosmological models without singularity". *Phys. Lett. B* **91**, 99–102 (1980).

[210] T. d. P. Netto et al. "From stable to unstable anomaly-induced inflation". *Eur. Phys. J. C* **76**, 544 (2016), arXiv: 1509.08882 [hep-th].

[211] P. Jizba, H. Kleinert, and F. Scardigli. "Inflationary cosmology from quantum Conformal Gravity". *Eur. Phys. J. C* **75**, 245 (2015), arXiv: 1410.8062 [hep-th].

[212] P. Davies et al. "Energy-momentum tensor of a massless scalar quantum field in a Robertson-Walker universe". *Ann. Phys.* **109**, 108–142 (1977).

[213] T. S. Bunch and P. C. W. Davies. "Covariant Point Splitting Regularization for a Scalar Quantum Field in a Robertson-Walker Universe with Spatial Curvature". *Proc. Roy. Soc. Lond. A* **357**, 381–394 (1977).

[214] R. Penrose. "The Basic Ideas of Conformal Cyclic Cosmology". *AIP Conf. Proc.* **1446**, 233–243 (2012).

[215] V. G. Gurzadyan and R. Penrose. "On CCC-predicted concentric low-variance circles in the CMB sky". *Eur. Phys. J. Plus* **128**, 22 (2013), arXiv: 1302.5162 [astro-ph.CO].

[216] D. L. Jow and D. Scott. "Re-evaluating evidence for Hawking points in the CMB". *JCAP* **03**, 021 (2020), arXiv: 1909.09672 [astro-ph.CO].

[217] M. Novello and S. E. P. Bergliaffa. "Bouncing Cosmologies". *Phys. Rept.* **463**, 127–213 (2008), arXiv: 0802.1634 [astro-ph].

[218] R. H. Brandenberger. "Alternatives to the inflationary paradigm of structure formation". *Int. J. Mod. Phys. Conf. Ser.* **01**, 67–79 (2011), arXiv: 0902.4731 [hep-th].

[219] R. H. Brandenberger. "String Gas Cosmology", pp. Ed. by J. Erdmenger (Wiley-VCH, 2008), arXiv: 0808.0746 [hep-th].

[220] D. Wands. "Multiple field inflation". *Lect. Notes Phys.* **738**, 275–304 (2008), arXiv: astro-ph/0702187.

[221] S. Cremonini, Z. Lalak, and K. Turzynski. "Strongly Coupled Perturbations in Two-Field Inflationary Models". *JCAP* **03**, 016 (2011), arXiv: 1010.3021 [hep-th].

[222] L. McAllister and E. Silverstein. "String Cosmology: A Review". *Gen. Rel. Grav.* **40**, 565–605 (2008), arXiv: 0710.2951 [hep-th].

[223] X. Gao, D. Langlois, and S. Mizuno. "Influence of heavy modes on perturbations in multiple field inflation". *JCAP* **10**, 040 (2012), arXiv: 1205.5275 [hep-th].

[224] C. M. Peterson and M. Tegmark. "Testing two-field inflation". *Phys. Rev. D* **83**, 023522 (2011).

[225] D. I. Kaiser and E. I. Sfakianakis. "Multifield Inflation after Planck: The Case for Nonminimal Couplings". *Phys. Rev. Lett.* **112**, 011302 (2014), arXiv: 1304.0363 [astro-ph.CO].

[226] S. R. Geller et al. "Primordial black holes from multifield inflation with nonminimal couplings". *Phys. Rev. D* **106**, 063535 (2022), arXiv: 2205.04471 [hep-th].

[227] A. Achúcarro et al. "Shift-symmetric orbital inflation: Single field or multifield?" *Phys. Rev. D* **102**, 021302 (2020), arXiv: 1901.03657 [astro-ph.CO].

[228] E. Silverstein and A. Westphal. "Monodromy in the CMB: Gravity Waves and String Inflation". *Phys. Rev. D* **78**, 106003 (2008), arXiv: 0803.3085 [hep-th].

[229] S. Cespedes, V. Atal, and G. A. Palma. "On the importance of heavy fields during inflation". *JCAP* **05**, 008 (2012), arXiv: 1201.4848 [hep-th].

[230] T. Bjorkmo and M. C. D. Marsh. "Hyperinflation generalised: from its attractor mechanism to its tension with the 'swampland conditions'". *JHEP* **04**, 172 (2019), arXiv: 1901.08603 [hep-th].

[231] A. Achúcarro, V. Atal, and Y. Welling. "On the viability of $m^2\phi^2$ and natural inflation". *JCAP* **07**, 008 (2015), arXiv: 1503.07486 [astro-ph.CO].

[232] P. Christodoulidis, D. Roest, and E. I. Sfakianakis. "Angular inflation in multi-field α-attractors". *JCAP* **11**, 002 (2019), arXiv: 1803.09841 [hep-th].

[233] A. Linde et al. "Hypernatural inflation". *JCAP* **07**, 035 (2018), arXiv: 1803.09911 [hep-th].

[234] A. R. Brown. "Hyperbolic Inflation". *Phys. Rev. Lett.* **121**, 251601 (2018), arXiv: 1705.03023 [hep-th].

[235] F. Di Marco and F. Finelli. "Slow-roll inflation for generalized two-field Lagrangians". *Phys. Rev. D* **71**, 123502 (2005).

[236] D. Wands et al. "An Observational test of two-field inflation". *Phys. Rev. D* **66**, 043520 (2002), arXiv: astro-ph/0205253.

[237] L. Pinol. "Multifield inflation beyond Nfield=2: non-Gaussianities and single-field effective theory". *JCAP* **2021**, 002 (2021).

[238] S. Weinberg. "Must cosmological perturbations remain nonadiabatic after multifield inflation?" *Phys. Rev. D* **70**, 083522 (2004).

[239] S. Tsujikawa and H. Yajima. "New constraints on multifield inflation with nonminimal coupling". *Phys. Rev. D* **62**, 123512 (2000).

[240] D. I. Kaiser and A. T. Todhunter. "Primordial perturbations from multifield inflation with nonminimal couplings". *Phys. Rev. D* **81**, 124037 (2010).

[241] R. Easther et al. "Simple predictions from multifield inflationary models". *Phys. Rev. Lett.* **112**, 161302 (2014), arXiv: 1312.4035 [astro-ph.CO].

[242] A. Achúcarro et al. "Correlating features in the primordial spectra". *Phys. Rev. D* **87**, 121301 (2013).

[243] C. van de Bruck and M. Robinson. "Power Spectra beyond the Slow Roll Approximation in Theories with Non-Canonical Kinetic Terms". *JCAP* **08**, 024 (2014), arXiv: 1404.7806 [astro-ph.CO].

[244] M. Dias, J. Frazer, and D. Seery. "Computing observables in curved multifield models of inflation—A guide (with code) to the transport method". *JCAP* **2015**, 030 (2015).

[245] M. Dias et al. "Numerical evaluation of the bispectrum in multiple field inflation—the transport approach with code". *JCAP* **12**, 033 (2016), arXiv: 1609.00379 [astro-ph.CO].

[246] M. Braglia et al. "Generating primordial features at large scales in two field models of inflation". *JCAP* **2020**, 025 (2020).

[247] M. Braglia, X. Chen, and D. K. Hazra. "Comparing multi-field primordial feature models with the Planck data". *JCAP* **06**, 005 (2021), arXiv: 2103.03025 [astro-ph.CO].

[248] G. Cabass et al. "Constraints on multifield inflation from the BOSS galaxy survey". *Phys. Rev. D* **106**, 043506 (2022), arXiv: 2204.01781 [astro-ph.CO].

[249] S. R. Geller et al. "Primordial black holes from multifield inflation with nonminimal couplings". *Phys. Rev. D* **106**, 063535 (2022).

[250] X.-B. Li, X.-G. Zheng, and J.-Y. Zhu. "Spectra and entropy of multifield warm inflation". *Phys. Rev. D* **99**, 043528 (2019).

[251] L. McAllister, S. Renaux-Petel, and G. Xu. "A statistical approach to multifield inflation: many-field perturbations beyond slow roll". *JCAP* **2012**, 046 (2012).

[252] C. M. Peterson and M. Tegmark. "Testing multifield inflation: A geometric approach". *Phys. Rev. D* **87**, 103507 (2013).

[253] G. Leung et al. "Reheating, multifield inflation and the fate of the primordial observables". *JCAP* **2012**, 008 (2012).

[254] D. Dutcher et al. "Measurements of the E-mode polarization and temperature-E-mode correlation of the CMB from SPT-3G 2018 data". *Phys. Rev. D* **104**, 022003 (2021).

[255] L. C. Price et al. "MULTIMODECODE: an efficient numerical solver for multifield inflation". *JCAP* **2015**, 005 (2015).

[256] J. Silk and M. S. Turner. "Double inflation". *Phys. Rev. D* **35**, 419–428 (1987).

[257] D. Polarski and A. Starobinsky. "Spectra of perturbations produced by double inflation with an intermediate matter-dominated stage". *Nucl. Phys. B* **385**, 623–650 (1992).

[258] D. Langlois. "Correlated adiabatic and isocurvature perturbations from double inflation". *Phys. Rev. D* **59**, 123512 (1999).

[259] R. Kallosh, A. Linde, and D. Roest. "Large field inflation and double α-attractors". *JHEP* **08**, 052 (2014), arXiv: 1405.3646 [hep-th].

[260] D. Blas, J. Lesgourgues, and T. Tram. "The Cosmic Linear Anisotropy Solving System (CLASS). Part II: Approximation schemes". *JCAP* **2011**, 034 (2011).

[261] A. Lewis, A. Challinor, and A. Lasenby. "Efficient computation of CMB anisotropies in closed FRW models". *Astrophys. J.* **538**, 473–476 (2000), arXiv: astro-ph/9911177.

[262] C. Howlett et al. "CMB power spectrum parameter degeneracies in the era of precision cosmology". *JCAP* **2012**, 027 (2012).

[263] Y. Akrami et al. "Planck 2018 results. X. Constraints on inflation". *Astron. Astrophys.* **641**, A10 (2020), arXiv: 1807.06211 [astro-ph.CO].

[264] P. A. R. Ade et al. "Improved Constraints on Primordial Gravitational Waves using Planck, WMAP, and BICEP/Keck Observations through the 2018 Observing Season". *Phys. Rev. Lett.* **127**, 151301 (2021), arXiv: 2110.00483 [astro-ph.CO].

[265] N. Aghanim et al. "Planck 2018 results. V. CMB power spectra and likelihoods". *Astron. Astrophys.* **641**, A5 (2020), arXiv: 1907.12875 [astro-ph.CO].

[266] N. Aghanim et al. "Planck 2018 results. I. Overview and the cosmological legacy of Planck". *Astron. Astrophys.* **641**, A1 (2020), arXiv: 1807.06205 [astro-ph.CO].

[267] N. Aghanim et al. "Planck 2018 results. VIII. Gravitational lensing". *Astron. Astrophys.* **641**, A8 (2020), arXiv: 1807.06210 [astro-ph.CO].

[268] C. P. Burgess, J. M. Cline, and R. Holman. "Effective field theories and inflation". *JCAP* **10**, 004 (2003), arXiv: hep-th/0306079.

[269] C. Wetterich. "Cosmology and the Fate of Dilatation Symmetry". *Nucl. Phys. B* **302**, 668–696 (1988), arXiv: 1711.03844 [hep-th].

[270] M. Shaposhnikov and D. Zenhausern. "Quantum scale invariance, cosmological constant and hierarchy problem". *Phys. Lett. B* **671**, 162–166 (2009), arXiv: 0809.3406 [hep-th].

[271] C. Wetterich. "Fundamental scale invariance". *Nucl. Phys. B* **964**, 115326 (2021), arXiv: 2007.08805 [hep-th].

[272] C. Wetterich. "Quantum scale symmetry" (2019), arXiv: 1901.04741 [hep-th].

[273] S. Mooij, M. Shaposhnikov, and T. Voumard. "Hidden and explicit quantum scale invariance". *Phys. Rev. D* **99**, 085013 (2019), arXiv: 1812.07946 [hep-th].

[274] A. Ghoshal, D. Mukherjee, and M. Rinaldi. "Inflation and primordial gravitational waves in scale-invariant quadratic gravity with Higgs". *JHEP* **05**, 023 (2023), arXiv: 2205.06475 [gr-qc].

[275] S. Vicentini, L. Vanzo, and M. Rinaldi. "Scale-invariant inflation with one-loop quantum corrections". *Phys. Rev. D* **99**, 103516 (2019), arXiv: 1902.04434 [gr-qc].

[276] G. Tambalo and M. Rinaldi. "Inflation and reheating in scale-invariant scalar-tensor gravity". *Gen. Rel. Grav.* **49**, 52 (2017), arXiv: 1610.06478 [gr-qc].

[277] J. Garcia-Bellido et al. "Higgs-Dilaton Cosmology: From the Early to the Late Universe". *Phys. Rev. D* **84**, 123504 (2011), arXiv: 1107.2163 [hep-ph].

[278] K. S. Stelle. "Renormalization of higher-derivative quantum gravity". *Phys. Rev. D* **16**, 953–969 (1977).

[279] A. Salvio. "Quadratic Gravity". *Front. in Phys.* **6**, 77 (2018), arXiv: 1804.09944 [hep-th].

[280] A. De Felice et al. "Starobinsky inflation with a quadratic Weyl tensor". *Phys. Rev. D* **108**, 123524 (2023), arXiv: 2309.01835 [gr-qc].

[281] R. N. Greenwood, D. I. Kaiser, and E. I. Sfakianakis. "Multifield Dynamics of Higgs Inflation". *Phys. Rev. D* **87**, 064021 (2013), arXiv: 1210.8190 [hep-ph].

[282] S. Casas, M. Pauly, and J. Rubio. "Higgs-dilaton cosmology: An inflation–dark-energy connection and forecasts for future galaxy surveys". *Phys. Rev. D* **97**, 043520 (2018), arXiv: 1712.04956 [astro-ph.CO].

[283] G. D'Amico et al. "Limits on primordial non-Gaussianities from BOSS galaxy-clustering data". *Phys. Rev. D* **111**, 063514 (2025), arXiv: 2201.11518 [astro-ph.CO].

[284] S. Casas et al. "Scale-invariant alternatives to general relativity. III. The inflation-dark energy connection". *Phys. Rev. D* **99**, 063512 (2019), arXiv: 1811.05984 [astro-ph.CO].

[285] C. van de Bruck and R. Daniel. "Inflation and scale-invariant R^2 gravity". *Phys. Rev. D* **103**, 123506 (2021), arXiv: 2102.11719 [gr-qc].

[286] M. Cicoli et al. "On the choice of entropy variables in multifield inflation". *Class. Quant. Grav.* **40**, 025008 (2023), arXiv: 2107.03391 [astro-ph.CO].

[287] T. Mori, K. Kohri, and J. White. "Multi-field effects in a simple extension of R^2 inflation". *JCAP* **10**, 044 (2017), arXiv: 1705.05638 [astro-ph.CO].

[288] J.-O. Gong and T. Tanaka. "A covariant approach to general field space metric in multi-field inflation". *JCAP* **03**, 015 (2011), arXiv: 1101.4809 [astro-ph.CO]. [Erratum: JCAP 02, E01 (2012)].

[289] D. H. Lyth and D. Wands. "Generating the curvature perturbation without an inflaton". *Phys. Lett. B* **524**, 5–14 (2002), arXiv: hep-ph/0110002.

[290] N. Bartolo et al. "Non-Gaussianity from inflation: Theory and observations". *Phys. Rept.* **402**, 103–266 (2004), arXiv: astro-ph/0406398.

[291] D. Seery and J. E. Lidsey. "Primordial non-Gaussianities from multiple-field inflation". *JCAP* **09**, 011 (2005), arXiv: astro-ph/0506056.

[292] C. T. Byrnes. "Lecture notes on non-Gaussianity". *Astrophys. Space Sci. Proc.* **45**, 135–165 (2016), arXiv: 1411.7002 [astro-ph.CO].

[293] A. A. Abolhasani and M. Sasaki. "Single-field consistency relation and δN-formalism". *JCAP* **08**, 025 (2018), arXiv: 1805.11298 [astro-ph.CO].

[294] Y. Akrami et al. "Planck 2018 results. IX. Constraints on primordial non-Gaussianity". *Astron. Astrophys.* **641**, A9 (2020), arXiv: 1905.05697 [astro-ph.CO].

[295] G. Cabass et al. "Constraints on Single-Field Inflation from the BOSS Galaxy Survey". *Phys. Rev. Lett.* **129**, 021301 (2022), arXiv: 2201.07238 [astro-ph.CO].

[296] A. Barreira. "Can we actually constrain f_{NL} using the scale-dependent bias effect? An illustration of the impact of galaxy bias uncertainties using the BOSS DR12 galaxy power spectrum". *JCAP* **11**, 013 (2022), arXiv: 2205.05673 [astro-ph.CO].

[297] M. S. Cagliari et al. "Optimal constraints on Primordial non-Gaussianity with the eBOSS DR16 quasars in Fourier space". *JCAP* **08**, 036 (2024), arXiv: 2309.15814 [astro-ph.CO].

[298] J. M. Maldacena. "Non-Gaussian features of primordial fluctuations in single field inflationary models". *JHEP* **05**, 013 (2003).

[299] P. Creminelli and M. Zaldarriaga. "Single field consistency relation for the 3-point function". *JCAP* **10**, 006 (2004).

[300] D. Wands. "Local non-Gaussianity from inflation". *Class. Quant. Grav.* **27**, 124002 (2010).

[301] P. Creminelli. "On non-Gaussianities in single-field inflation". *JCAP* **10**, 003 (2003).

[302] X. Chen, R. Easther, and E. A. Lim. "Large non-Gaussianities in single field inflation". *JCAP* **06**, 023 (2007).

[303] L. Senatore, K. M. Smith, and M. Zaldarriaga. "Non-Gaussianities in single field inflation and their optimal limits from the WMAP 5-year data". *JCAP* **01**, 028 (2010).

[304] F. L. Bezrukov and D. S. Gorbunov. "Distinguishing between R^2-inflation and Higgs-inflation". *Phys. Lett. B* **713**, 365–368 (2012), arXiv: 1111.4397 [hep-ph].

[305] W. K. Hastings. "Monte Carlo sampling methods using Markov chains and their applications". *Biometrika* **57**, 97–109 (1970).

[306] A. Gelman and D. B. Rubin. "Inference from Iterative Simulation Using Multiple Sequences". *Statist. Sci.* **7**, 457–472 (1992).

[307] S. K. Choi et al. "The Atacama Cosmology Telescope: a measurement of the Cosmic Microwave Background power spectra at 98 and 150 GHz". *JCAP* **12**, 045 (2020), arXiv: 2007.07289 [astro-ph.CO].

[308] S. Aiola et al. "The Atacama Cosmology Telescope: DR4 Maps and Cosmological Parameters". *JCAP* **12**, 047 (2020), arXiv: 2007.07288 [astro-ph.CO].

[309] W. Handley and P. Lemos. "Quantifying the global parameter tensions between ACT, SPT and Planck". *Phys. Rev. D* **103**, 063529 (2021), arXiv: 2007.08496 [astro-ph.CO].

[310] W. Giarè et al. "Is the Harrison-Zel'dovich spectrum coming back? ACT preference for ns ∼ 1 and its discordance with Planck". *Mon. Not. Roy. Astron. Soc.* **521**, 2911–2918 (2023), arXiv: 2210.09018 [astro-ph.CO].

[311] R. Calderón et al. "On the consistency of ΛCDM with CMB measurements in light of the latest Planck, ACT and SPT data". *JCAP* **08**, 059 (2023), arXiv: 2302.14300 [astro-ph.CO].

[312] V. Poulin et al. "Early Dark Energy Can Resolve The Hubble Tension". *Phys. Rev. Lett.* **122**, 221301 (2019), arXiv: 1811.04083 [astro-ph.CO].

[313] G. Ye and Y.-S. Piao. "Is the Hubble tension a hint of AdS phase around recombination?" *Phys. Rev. D* **101**, 083507 (2020), arXiv: 2001.02451 [astro-ph.CO].

[314] G. Ye, B. Hu, and Y.-S. Piao. "Implication of the Hubble tension for the primordial Universe in light of recent cosmological data". *Phys. Rev. D* **104**, 063510 (2021), arXiv: 2103.09729 [astro-ph.CO].

[315] J.-Q. Jiang and Y.-S. Piao. "Testing AdS early dark energy with Planck, SPTpol, and LSS data". *Phys. Rev. D* **104**, 103524 (2021), arXiv: 2107.07128 [astro-ph.CO].

[316] D. K. Hazra, A. Antony, and A. Shafieloo. "One spectrum to cure them all: signature from early Universe solves major anomalies and tensions in cosmology". *JCAP* **08**, 063 (2022), arXiv: 2201.12000 [astro-ph.CO].

[317] J.-Q. Jiang and Y.-S. Piao. "Toward early dark energy and ns=1 with Planck, ACT, and SPT observations". *Phys. Rev. D* **105**, 103514 (2022), arXiv: 2202.13379 [astro-ph.CO].

[318] J.-Q. Jiang, G. Ye, and Y.-S. Piao. "Return of Harrison–Zeldovich spectrum in light of recent cosmological tensions". *Mon. Not. Roy. Astron. Soc.* **527**, L54–L59 (2023), arXiv: 2210.06125 [astro-ph.CO].

[319] V. Poulin, T. L. Smith, and T. Karwal. "The Ups and Downs of Early Dark Energy solutions to the Hubble tension: A review of models, hints and constraints circa 2023". *Phys. Dark Univ.* **42**, 101348 (2023), arXiv: 2302.09032 [astro-ph.CO].

[320] J.-Q. Jiang, G. Ye, and Y.-S. Piao. "Impact of the Hubble tension on the r-n_s contour" (2023), arXiv: 2303.12345 [astro-ph.CO].

[321] Z.-Y. Peng and Y.-S. Piao. "Testing the ns-H0 scaling relation with Planck-independent CMB data". *Phys. Rev. D* **109**, 023519 (2024), arXiv: 2308.01012 [astro-ph.CO].

[322] M.-X. Lin et al. "Acoustic Dark Energy: Potential Conversion of the Hubble Tension". *Phys. Rev. D* **100**, 063542 (2019), arXiv: 1905.12618 [astro-ph.CO].

[323] S. Vagnozzi. "Consistency tests of ΛCDM from the early integrated Sachs-Wolfe effect: Implications for early-time new physics and the Hubble tension". *Phys. Rev. D* **104**, 063524 (2021), arXiv: 2105.10425 [astro-ph.CO].

[324] E. Di Valentino et al. "Bayesian evidence against the Harrison-Zel'dovich spectrum in tensions with cosmological data sets". *Phys. Rev. D* **98**, 063508 (2018), arXiv: 1808.09201 [astro-ph.CO].

[325] W. Giarè. "Inflation, the Hubble Tension and Early Dark Energy: an alternative overview" (2024), arXiv: 2404.12779 [astro-ph.CO].

[326] F. L. Bezrukov and M. Shaposhnikov. "The Standard Model Higgs boson as the inflaton". *Phys. Lett. B* **659**, 703–706 (2008), arXiv: 0710.3755 [hep-th].

[327] F. Bezrukov et al. "Higgs inflation: consistency and generalisations". *JHEP* **01**, 016 (2011), arXiv: 1008.5157 [hep-ph].

[328] J. Rubio. "Higgs inflation". *Front. Astron. Space Sci.* **5**, 50 (2019), arXiv: 1807.02376 [hep-ph].

[329] J. L. F. Barbon and J. R. Espinosa. "On the Naturalness of Higgs Inflation". *Phys. Rev. D* **79**, 081302 (2009), arXiv: 0903.0355 [hep-ph].

[330] C. P. Burgess, H. M. Lee, and M. Trott. "Comment on Higgs Inflation and Naturalness". *JHEP* **07**, 007 (2010), arXiv: 1002.2730 [hep-ph].

[331] X. Calmet and R. Casadio. "Self-healing of unitarity in Higgs inflation". *Phys. Lett. B* **734**, 17–20 (2014), arXiv: 1310.7410 [hep-ph].

[332] A. Salvio and A. Mazumdar. "Classical and Quantum Initial Conditions for Higgs Inflation". *Phys. Lett. B* **750**, 194–200 (2015), arXiv: 1506.07520 [hep-ph].

[333] W. Giarè et al. "Inflationary potential as seen from different angles: model compatibility from multiple CMB missions". *JCAP* **09**, 019 (2023), arXiv: 2305.15378 [astro-ph.CO].

[334] W. Giarè et al. "Testing α-attractor quintessential inflation against CMB and low-redshift data". *Phys. Dark Univ.* **46**, 101713 (2024), arXiv: 2402.01560 [astro-ph.CO].

[335] M. H. Abitbol et al. "The Simons Observatory: Astro2020 Decadal Project Whitepaper". *Bull. Am. Astron. Soc.* **51**, 147 (2019), arXiv: 1907.08284 [astro-ph.IM].

[336] K. Abazajian et al. "CMB-S4: Forecasting Constraints on Primordial Gravitational Waves". *Astrophys. J.* **926**, 54 (2022), arXiv: 2008.12619 [astro-ph.CO].

[337] E. Allys et al. "Probing Cosmic Inflation with the LiteBIRD Cosmic Microwave Background Polarization Survey". *PTEP* **2023**, 042F01 (2023), arXiv: 2202.02773 [astro-ph.IM].

[338] R. Kallosh and A. Linde. "Universality Class in Conformal Inflation". *JCAP* **07**, 002 (2013), arXiv: 1306.5220 [hep-th].

[339] R. Kallosh, A. Linde, and D. Roest. "Superconformal Inflationary α-Attractors". *JHEP* **11**, 198 (2013), arXiv: 1311.0472 [hep-th].

[340] M. Galante et al. "Unity of Cosmological Inflation Attractors". *Phys. Rev. Lett.* **114**, 141302 (2015), arXiv: 1412.3797 [hep-th].

[341] R. Kallosh and A. Linde. "Polynomial α-attractors". *JCAP* **04**, 017 (2022), arXiv: 2202.06492 [astro-ph.CO].

[342] D. Roest and M. Scalisi. "Cosmological attractors from α-scale supergravity". *Phys. Rev. D* **92**, 043525 (2015), arXiv: 1503.07909 [hep-th].

[343] A. Linde. "Single-field α-attractors". *JCAP* **05**, 003 (2015), arXiv: 1504.00663 [hep-th].

[344] E. V. Linder. "Dark Energy from α-Attractors". *Phys. Rev. D* **91**, 123012 (2015), arXiv: 1505.00815 [astro-ph.CO].

[345] M. Scalisi. "Cosmological α-attractors and de Sitter landscape". *JHEP* **12**, 134 (2015), arXiv: 1506.01368 [hep-th].

[346] S. D. Odintsov and V. K. Oikonomou. "Inflationary α-attractors from $F(R)$ gravity". *Phys. Rev. D* **94**, 124026 (2016), arXiv: 1612.01126 [gr-qc].

[347] M. Braglia et al. "Unified framework for early dark energy from α-attractors". *Phys. Rev. D* **102**, 083513 (2020), arXiv: 2005.14053 [astro-ph.CO].

[348] J. G. Rodrigues, S. Santos da Costa, and J. S. Alcaniz. "Observational constraints on α -attractor inflationary models with a Higgs-like potential". *Phys. Lett. B* **815**, 136156 (2021), arXiv: 2007.10763 [astro-ph.CO].

[349] R. Shojaee, K. Nozari, and F. Darabi. "α-Attractors and reheating in a nonminimal inflationary model". *Int. J. Mod. Phys. D* **29**, 2050077 (2020), arXiv: 2101.03981 [astro-ph.CO].

[350] S. Bhattacharya et al. "α-attractor inflation: Models and predictions". *Phys. Rev. D* **107**, 103530 (2023), arXiv: 2212.13363 [astro-ph.CO].

[351] L. Brissenden, K. Dimopoulos, and S. Sánchez López. "Non-oscillating early dark energy and quintessence from α-attractors". *Astropart. Phys.* **157**, 102925 (2024), arXiv: 2301.03572 [astro-ph.CO].

[352] T. Harko et al. "Metric-Palatini gravity unifying local constraints and late-time cosmic acceleration". *Phys. Rev. D* **85**, 084016 (2012), arXiv: 1110.1049 [gr-qc].

[353] R. P. Woodard. "Ostrogradsky's theorem on Hamiltonian instability". *Scholarpedia* **10**, 32243 (2015), arXiv: 1506.02210 [hep-th].

[354] C. M. Bender and P. D. Mannheim. "Exactly solvable PT-symmetric Hamiltonian having no Hermitian counterpart". *Phys. Rev. D* **78**, 025022 (2008), arXiv: 0804.4190 [hep-th].

[355] K. Hinterbichler. "Theoretical Aspects of Massive Gravity". *Rev. Mod. Phys.* **84**, 671–710 (2012), arXiv: 1105.3735 [hep-th].

[356] D. Iosifidis, A. C. Petkou, and C. G. Tsagas. "Torsion/non-metricity duality in f(R) gravity". *Gen. Rel. Grav.* **51**, 66 (2019), arXiv: 1810.06602 [gr-qc].

[357] A. Delhom. "Minimal coupling in presence of non-metricity and torsion". *Eur. Phys. J. C* **80**, 728 (2020), arXiv: 2002.02404 [gr-qc].

[358] G. J. Olmo. "Palatini Approach to Modified Gravity: f(R) Theories and Beyond". *Int. J. Mod. Phys. D* **20**, 413–462 (2011), arXiv: 1101.3864 [gr-qc].

[359] V. I. Afonso, G. J. Olmo, and D. Rubiera-Garcia. "Mapping Ricci-Based Theories of Gravity into General Relativity". *Phys. Rev. D* **97**, 021503 (2018).

[360] A. Albrecht and P. J. Steinhardt. "Cosmology for Grand Unified Theories with Radiatively Induced Symmetry Breaking". *Phys. Rev. Lett.* **48**, 1220–1223 (1982).

[361] A. Vilenkin. "The Birth of Inflationary Universes". *Phys. Rev. D* **27**, 2848 (1983).

[362] J. M. Bardeen, P. J. Steinhardt, and M. S. Turner. "Spontaneous Creation of Almost Scale - Free Density Perturbations in an Inflationary Universe". *Phys. Rev. D* **28**, 679 (1983).

[363] E. R. Harrison. "Fluctuations at the threshold of classical cosmology". *Phys. Rev. D* **1**, 2726–2730 (1970).

[364] Y. B. Zeldovich. "A Hypothesis, unifying the structure and the entropy of the universe". *Mon. Not. Roy. Astron. Soc.* **160**, 1P–3P (1972).

[365] P. J. E. Peebles and J. T. Yu. "Primeval adiabatic perturbation in an expanding universe". *Astrophys. J.* **162**, 815–836 (1970).

[366] C. L. Bennett et al. "NINE-YEAR WILKINSON MICROWAVE ANISOTROPY PROBE (WMAP) OBSERVATIONS: FINAL MAPS AND RESULTS". *ApJS* **208**, 20 (2013).

[367] G. Hinshaw et al. "NINE-YEAR WILKINSON MICROWAVE ANISOTROPY PROBE (WMAP) OBSERVATIONS: COSMOLOGICAL PARAMETER RESULTS". *ApJS* **208**, 19 (2013).

[368] B. A. Benson et al. "SPT-3G: A Next-Generation Cosmic Microwave Background Polarization Experiment on the South Pole Telescope". *Proc. SPIE Int. Soc. Opt. Eng.* **9153**, 91531P (2014), arXiv: 1407.2973 [astro-ph.IM].

[369] D. Dutcher et al. "Measurements of the E-mode polarization and temperature-E-mode correlation of the CMB from SPT-3G 2018 data". *Phys. Rev. D* **104**, 022003 (2021), arXiv: 2101.01684 [astro-ph.CO].

[370] P. J. Steinhardt and N. Turok. "The Cyclic universe: An Informal introduction". *Nucl. Phys. B Proc. Suppl.* **124**, 38–49 (2003), arXiv: astro-ph/0204479.

[371] N. Turok and P. J. Seinhardt. "Beyond inflation: A Cyclic universe scenario". *Phys. Scripta T* **117**, 76–85 (2005), arXiv: hep-th/0403020.

[372] A. Ashtekar, M. Bojowald, and J. Lewandowski. "Mathematical structure of loop quantum cosmology". *Adv. Theor. Math. Phys.* **7**, 233–268 (2003), arXiv: gr-qc/0304074.

[373] M. Bojowald, R. Maartens, and P. Singh. "Loop quantum gravity and the cyclic universe". *Phys. Rev. D* **70**, 083517 (2004), arXiv: hep-th/0407115.

[374] H.-H. Xiong et al. "Cyclic universe with quintom matter in loop quantum cosmology". *Mod. Phys. Lett. A* **24**, 1237–1246 (2009), arXiv: 0711.4469 [hep-th].

[375] P. H. Frampton. "Cyclic Universe and Infinite Past". *Mod. Phys. Lett. A* **22**, 2587–2592 (2007), arXiv: 0705.2730 [astro-ph].

[376] J. V. Narlikar, G. Burbidge, and R. G. Vishwakarma. "Cosmology and Cosmogony in a Cyclic Universe". *J. Astrophys. Astron.* **28**, 67–99 (2007), arXiv: 0801.2965 [astro-ph].

[377] L. Baum and P. H. Frampton. "Entropy of contracting universe in cyclic cosmology". *Mod. Phys. Lett. A* **23**, 33–36 (2008), arXiv: hep-th/0703162.

[378] T. Biswas. "The Hagedorn Soup and an Emergent Cyclic Universe" (2008), arXiv: 0801.1315 [hep-th].

[379] T. Cailleteau, P. Singh, and K. Vandersloot. "Non-singular Ekpyrotic/Cyclic model in Loop Quantum Cosmology". *Phys. Rev. D* **80**, 124013 (2009), arXiv: 0907.5591 [gr-qc].

[380] R. H. Brandenberger. "Processing of Cosmological Perturbations in a Cyclic Cosmology". *Phys. Rev. D* **80**, 023535 (2009), arXiv: 0905.1514 [hep-th].

[381] A. R. El-Nabulsi. "Accelerated Dilatonic-Brans-Dicke cyclic and non-singular universe from string theory". *Res. Astron. Astrophys.* **11**, 1249–1256 (2011).

[382] Y.-F. Cai, C. Gao, and E. N. Saridakis. "Bounce and cyclic cosmology in extended nonlinear massive gravity". *JCAP* **10**, 048 (2012), arXiv: 1207.3786 [astro-ph.CO].

[383] Y.-F. Cai and E. N. Saridakis. "Cyclic cosmology from Lagrange-multiplier modified gravity". *Class. Quant. Grav.* **28**, 035010 (2011), arXiv: 1007.3204 [astro-ph.CO].

[384] S. Nojiri, S. D. Odintsov, and D. Saez-Gomez. "Cyclic, ekpyrotic and little rip universe in modified gravity". *AIP Conf. Proc.* **1458**, 207–221 (2012), arXiv: 1108.0767 [hep-th].

[385] H.-Y. Chang and R. J. Scherrer. "Coincidence Problem in Cyclic Phantom Models of the Universe". *Phys. Rev. D* **86**, 027303 (2012), arXiv: 1204.6329 [astro-ph.CO].

[386] R. I. Ivanov and E. M. Prodanov. "Cyclic Universe with an Inflationary Phase from a Cosmological Model with Real Gas Quintessence". *Phys. Rev. D* **86**, 083536 (2012), arXiv: 1210.0186 [gr-qc].

[387] K. Saaidi, H. Sheikhahmadi, and A. H. Mohammadi. "Interacting New Agegraphic Dark Energy in a Cyclic Universe". *Astrophys. Space Sci.* **338**, 355–361 (2012), arXiv: 1201.0275 [gr-qc].

[388] I. Bars, P. J. Steinhardt, and N. Turok. "Cyclic Cosmology, Conformal Symmetry and the Metastability of the Higgs". *Phys. Lett. B* **726**, 50–55 (2013), arXiv: 1307.8106 [gr-qc].

[389] Y. Tavakoli and J. C. Fabris. "Creation of particles in a cyclic universe driven by loop quantum cosmology". *Int. J. Mod. Phys. D* **24**, 1550062 (2015), arXiv: 1412.0775 [gr-qc].

[390] D. Oriti, L. Sindoni, and E. Wilson-Ewing. "Emergent Friedmann dynamics with a quantum bounce from quantum gravity condensates". *Class. Quant. Grav.* **33**, 224001 (2016), arXiv: 1602.05881 [gr-qc].

[391] M. de Cesare, A. G. A. Pithis, and M. Sakellariadou. "Cosmological implications of interacting Group Field Theory models: cyclic Universe and accelerated expansion". *Phys. Rev. D* **94**, 064051 (2016), arXiv: 1606.00352 [gr-qc].

[392] P. Pavlovic and M. Sossich. "Cyclic cosmology in modified gravity". *Phys. Rev. D* **95**, 103519 (2017), arXiv: 1701.03657 [gr-qc].

[393] E. N. Saridakis, S. Banerjee, and R. Myrzakulov. "Bounce and cyclic cosmology in new gravitational scalar-tensor theories". *Phys. Rev. D* **98**, 063513 (2018), arXiv: 1807.00346 [gr-qc].

[394] P. Das et al. "Cosmological time crystal: Cyclic universe with a small cosmological constant in a toy model approach". *Phys. Rev. D* **98**, 024004 (2018), arXiv: 1801.07970 [hep-th].

[395] A. Ijjas. "Cyclic completion of the anamorphic universe". *Class. Quant. Grav.* **35**, 075010 (2018), arXiv: 1610.02752 [astro-ph.CO].

[396] N. Ahmed and S. Z. Alamri. "A cyclic universe with varying cosmological constant in $f(R,T)$ gravity". *Can. J. Phys.* **97**, 1075–1082 (2019), arXiv: 1902.03104 [gr-qc].

[397] S.-L. Li et al. "Emergent universe scenario, bouncing universes, and cyclic universes in degenerate massive gravity". *Phys. Rev. D* **99**, 104057 (2019), arXiv: 1903.03940 [gr-qc].

[398] R. J. Scherrer. "The Coincidence Problem and the Swampland Conjectures in the Ijjas-Steinhardt Cyclic Model of the Universe". *Phys. Lett. B* **798**, 134981 (2019), arXiv: 1907.11293 [gr-qc].

[399] A. Ijjas and P. J. Steinhardt. "Entropy, black holes, and the new cyclic universe". *Phys. Lett. B* **824**, 136823 (2022), arXiv: 2108.07101 [gr-qc].

[400] N. Gorkavyi. "Gravitational wave background discovered by NANOGrav as evidence of a cyclic universe". *New Astron.* **91**, 101698 (2022), arXiv: 2110.10218 [astro-ph.CO].

[401] M. Martín-Benito, R. B. Neves, and J. Olmedo. "States of Low Energy in bouncing inflationary scenarios in Loop Quantum Cosmology". *Phys. Rev. D* **103**, 123524 (2021), arXiv: 2104.03035 [gr-qc].

[402] A. Calcinari and S. Gielen. "Towards anisotropic cosmology in group field theory". *Class. Quant. Grav.* **40**, 085004 (2023), arXiv: 2210.03149 [gr-qc].

[403] J. Khoury et al. "Density perturbations in the ekpyrotic scenario". *Phys. Rev. D* **66**, 046005 (2002), arXiv: hep-th/0109050.

[404] J.-L. Lehners et al. "Generating ekpyrotic curvature perturbations before the big bang". *Phys. Rev. D* **76**, 103501 (2007), arXiv: hep-th/0702153.

[405] E. I. Buchbinder, J. Khoury, and B. A. Ovrut. "On the initial conditions in new ekpyrotic cosmology". *JHEP* **11**, 076 (2007), arXiv: 0706.3903 [hep-th].

[406] J.-L. Lehners and P. J. Steinhardt. "Planck 2013 results support the cyclic universe". *Phys. Rev. D* **87**, 123533 (2013), arXiv: 1304.3122 [astro-ph.CO].

[407] C.-G. Park and B. Ratra. "Using the tilted flat-ΛCDM and the untilted non-flat ΛCDM inflation models to measure cosmological parameters from a compilation of observational data". *Astrophys. J.* **882**, 158 (2019), arXiv: 1801.00213 [astro-ph.CO].

[408] W. Handley. "Curvature tension: evidence for a closed universe". *Phys. Rev. D* **103**, L041301 (2021), arXiv: 1908.09139 [astro-ph.CO].

[409] E. Di Valentino, A. Melchiorri, and J. Silk. "Planck evidence for a closed Universe and a possible crisis for cosmology". *Nature Astron.* **4**, 196–203 (2019), arXiv: 1911.02087 [astro-ph.CO].

[410] G. Efstathiou and S. Gratton. "The evidence for a spatially flat Universe". *Mon. Not. Roy. Astron. Soc.* **496**, L91–L95 (2020), arXiv: 2002.06892 [astro-ph.CO].

[411] E. Di Valentino, A. Melchiorri, and J. Silk. "Investigating Cosmic Discordance". *Astrophys. J. Lett.* **908**, L9 (2021), arXiv: 2003.04935 [astro-ph.CO].

[412] D. Benisty and D. Staicova. "Testing late-time cosmic acceleration with uncorrelated baryon acoustic oscillation dataset". *Astron. Astrophys.* **647**, A38 (2021), arXiv: 2009.10701 [astro-ph.CO].

[413] S. Vagnozzi et al. "The galaxy power spectrum take on spatial curvature and cosmic concordance". *Phys. Dark Univ.* **33**, 100851 (2021), arXiv: 2010.02230 [astro-ph.CO].

[414] S. Vagnozzi, A. Loeb, and M. Moresco. "Eppur è piatto? The Cosmic Chronometers Take on Spatial Curvature and Cosmic Concordance". *Astrophys. J.* **908**, 84 (2021), arXiv: 2011.11645 [astro-ph.CO].

[415] E. Di Valentino et al. "Interacting Dark Energy in a closed universe". *Mon. Not. Roy. Astron. Soc.* **502**, L23–L28 (2021), arXiv: 2011.00283 [astro-ph.CO].

[416] W. Yang et al. "2021-H0 odyssey: closed, phantom and interacting dark energy cosmologies". *JCAP* **10**, 008 (2021), arXiv: 2101.03129 [astro-ph.CO].

[417] S. Cao, J. Ryan, and B. Ratra. "Using Pantheon and DES supernova, baryon acoustic oscillation, and Hubble parameter data to constrain the Hubble constant, dark energy dynamics, and spatial curvature". *Mon. Not. Roy. Astron. Soc.* **504**, 300–310 (2021), arXiv: 2101.08817 [astro-ph.CO].

[418] S. Dhawan, J. Alsing, and S. Vagnozzi. "Non-parametric spatial curvature inference using late-Universe cosmological probes". *Mon. Not. Roy. Astron. Soc.* **506**, L1–L5 (2021), arXiv: 2104.02485 [astro-ph.CO].

[419] B. R. Dinda. "Cosmic expansion parametrization: Implication for curvature and H0 tension". *Phys. Rev. D* **105**, 063524 (2022), arXiv: 2106.02963 [astro-ph.CO].

[420] J. E. Gonzalez et al. "Testing the consistency between cosmological data: the impact of spatial curvature and the dark energy EoS". *JCAP* **11**, 060 (2021), arXiv: 2104.13455 [astro-ph.CO].

[421] O. Akarsu et al. "Testing spatial curvature and anisotropic expansion on top of the ΛCDM model". *Phys. Dark Univ.* **39**, 101162 (2023), arXiv: 2112.07807 [astro-ph.CO].

[422] S. Cao and B. Ratra. "Using lower redshift, non-CMB, data to constrain the Hubble constant and other cosmological parameters". *Mon. Not. Roy. Astron. Soc.* **513**, 5686–5700 (2022), arXiv: 2203.10825 [astro-ph.CO].

[423] A. Glanville, C. Howlett, and T. M. Davis. "Full-shape galaxy power spectra and the curvature tension". *Mon. Not. Roy. Astron. Soc.* **517**, 3087–3100 (2022), arXiv: 2205.05892 [astro-ph.CO].

[424] J. Bel et al. "Constraining spatial curvature with large-scale structure". *JCAP* **09**, 076 (2022), arXiv: 2206.03059 [astro-ph.CO].

[425] W. Yang et al. "Revealing the effects of curvature on the cosmological models". *Phys. Rev. D* **107**, 063509 (2023), arXiv: 2210.09865 [astro-ph.CO].

[426] J. Stevens, H. Khoraminezhad, and S. Saito. "Constraining the spatial curvature with cosmic expansion history in a cosmological model with a non-standard sound horizon". *JCAP* **07**, 046 (2023), arXiv: 2212.09804 [astro-ph.CO].

[427] A. Favale, A. Gómez-Valent, and M. Migliaccio. "Cosmic chronometers to calibrate the ladders and measure the curvature of the Universe. A model-independent study". *Mon. Not. Roy. Astron. Soc.* **523**, 3406–3422 (2023), arXiv: 2301.09591 [astro-ph.CO].

[428] J. Khoury, P. J. Steinhardt, and N. Turok. "Inflation versus cyclic predictions for spectral tilt". *Phys. Rev. Lett.* **91**, 161301 (2003), arXiv: astro-ph/0302012.

[429] S. Gratton et al. "Conditions for generating scale-invariant density perturbations". *Phys. Rev. D* **69**, 103505 (2004), arXiv: astro-ph/0301395.

[430] C. Caprini and D. G. Figueroa. "Cosmological Backgrounds of Gravitational Waves". *Class. Quant. Grav.* **35**, 163001 (2018), arXiv: 1801.04268 [astro-ph.CO].

[431] T. Kobayashi, M. Yamaguchi, and J. Yokoyama. "G-inflation: Inflation driven by the Galileon field". *Phys. Rev. Lett.* **105**, 231302 (2010), arXiv: 1008.0603 [hep-th].

[432] M. Kawasaki, N. Kitajima, and S. Yokoyama. "Gravitational waves from a curvaton model with blue spectrum". *JCAP* **08**, 042 (2013), arXiv: 1305.4464 [astro-ph.CO].

[433] K. Nozari and S. Shafizadeh. "Realization of blue spectrum in generalized Galileon super-inflation models". *Int. J. Mod. Phys. D* **26**, 1750016 (2016), arXiv: 1712.09530 [gr-qc].

[434] W. Giarè and F. Renzi. "Propagating speed of primordial gravitational waves". *Phys. Rev. D* **102**, 083530 (2020), arXiv: 2007.04256 [astro-ph.CO].

[435] L. C. Price et al. "Gravitational wave consistency relations for multifield inflation". *Phys. Rev. Lett.* **114**, 031301 (2015), arXiv: 1409.2498 [astro-ph.CO].

[436] S. Mukohyama et al. "Blue Tensor Spectrum from Particle Production during Inflation". *JCAP* **08**, 036 (2014), arXiv: 1405.0346 [astro-ph.CO].

[437] R. Namba et al. "Scale-dependent gravitational waves from a rolling axion". *JCAP* **01**, 041 (2016), arXiv: 1509.07521 [astro-ph.CO].

[438] M. Peloso, L. Sorbo, and C. Unal. "Rolling axions during inflation: perturbativity and signatures". *JCAP* **09**, 001 (2016), arXiv: 1606.00459 [astro-ph.CO].

[439] O. Özsoy. "Synthetic Gravitational Waves from a Rolling Axion Monodromy". *JCAP* **04**, 040 (2021), arXiv: 2005.10280 [astro-ph.CO].

[440] E. Dimastrogiovanni, M. Fasiello, and T. Fujita. "Primordial Gravitational Waves from Axion-Gauge Fields Dynamics". *JCAP* **01**, 019 (2017), arXiv: 1608.04216 [astro-ph.CO].

[441] L. Iacconi et al. "Interferometer Constraints on the Inflationary Field Content". *JCAP* **03**, 031 (2020), arXiv: 1910.12921 [astro-ph.CO].

[442] S. Endlich, A. Nicolis, and J. Wang. "Solid Inflation". *JCAP* **10**, 011 (2013), arXiv: 1210.0569 [hep-th].

[443] D. Cannone, G. Tasinato, and D. Wands. "Generalised tensor fluctuations and inflation". *JCAP* **01**, 029 (2015), arXiv: 1409.6568 [astro-ph.CO].

[444] L. Graef and R. Brandenberger. "Breaking of Spatial Diffeomorphism Invariance, Inflation and the Spectrum of Cosmological Perturbations". *JCAP* **10**, 009 (2015), arXiv: 1506.00896 [astro-ph.CO].

[445] A. Ricciardone and G. Tasinato. "Primordial gravitational waves in supersolid inflation". *Phys. Rev. D* **96**, 023508 (2017), arXiv: 1611.04516 [astro-ph.CO].

[446] G. Capurri et al. "Let Effective Field Theory of Inflation flow: stochastic generation of models with red/blue tensor tilt". *JCAP* **11**, 037 (2020), arXiv: 2006.10781 [astro-ph.CO].

[447] W. Giarè et al. "Towards a reliable calculation of relic radiation from primordial gravitational waves". *Mon. Not. Roy. Astron. Soc.* **520**, 2 (2023), arXiv: 2210.14159 [astro-ph.CO].

[448] Y. Cai. "Generating enhanced parity-violating gravitational waves during inflation with violation of the null energy condition". *Phys. Rev. D* **107**, 063512 (2023), arXiv: 2212.10893 [gr-qc].

[449] G. Ye, M. Zhu, and Y. Cai. "Null energy condition violation during inflation and pulsar timing array observations". *JHEP* **02**, 008 (2024), arXiv: 2312.10685 [gr-qc].

[450] A. Ashoorioon et al. "Reconciliation of High Energy Scale Models of Inflation with Planck". *JCAP* **02**, 025 (2014), arXiv: 1306.4914 [hep-th].

[451] S. Choudhury. "Single field inflation in the light of Pulsar Timing Array Data: quintessential interpretation of blue tilted tensor spectrum through Non-Bunch Davies initial condition". *Eur. Phys. J. C* **84**, 278 (2024), arXiv: 2307.03249 [astro-ph.CO].

[452] Y.-F. Cai et al. "Sound speed resonance of the stochastic gravitational wave background". *Phys. Rev. Lett.* **126**, 071303 (2021), arXiv: 2009.09833 [gr-qc].

[453] A. Gruzinov. "Elastic inflation". *Phys. Rev. D* **70**, 063518 (2004), arXiv: astro-ph/0404548.

[454] R. H. Brandenberger et al. "Tensor Modes from a Primordial Hagedorn Phase of String Cosmology". *Phys. Rev. Lett.* **98**, 231302 (2007), arXiv: hep-th/0604126.

[455] R. H. Brandenberger, A. Nayeri, and S. P. Patil. "Closed String Thermodynamics and a Blue Tensor Spectrum". *Phys. Rev. D* **90**, 067301 (2014), arXiv: 1403.4927 [astro-ph.CO].

[456] M. Baumgart, J. J. Heckman, and L. Thomas. "CFTs blueshift tensor fluctuations universally". *JCAP* **07**, 034 (2022), arXiv: 2109.08166 [hep-ph].

[457] A. Stewart and R. Brandenberger. "Observational Constraints on Theories with a Blue Spectrum of Tensor Modes". *JCAP* **08**, 012 (2008), arXiv: 0711.4602 [astro-ph].

[458] Y.-F. Cai et al. "On the possibility of blue tensor spectrum within single field inflation". *Nucl. Phys. B* **900**, 517–532 (2015), arXiv: 1412.7241 [hep-th].

[459] Y. Wang and W. Xue. "Inflation and Alternatives with Blue Tensor Spectra". *JCAP* **10**, 075 (2014), arXiv: 1403.5817 [astro-ph.CO].

[460] S. Kuroyanagi, T. Takahashi, and S. Yokoyama. "Blue-tilted Tensor Spectrum and Thermal History of the Universe". *JCAP* **02**, 003 (2015), arXiv: 1407.4785 [astro-ph.CO].

[461] S. Kuroyanagi, T. Takahashi, and S. Yokoyama. "Blue-tilted inflationary tensor spectrum and reheating in the light of NANOGrav results". *JCAP* **01**, 071 (2021), arXiv: 2011.03323 [astro-ph.CO].

[462] W. Giarè and A. Melchiorri. "Probing the inflationary background of gravitational waves from large to small scales". *Phys. Lett. B* **815**, 136137 (2021), arXiv: 2003.04783 [astro-ph.CO].

[463] S. Vagnozzi. "Implications of the NANOGrav results for inflation". *Mon. Not. Roy. Astron. Soc.* **502**, L11–L15 (2021), arXiv: 2009.13432 [astro-ph.CO].

[464] S. Vagnozzi. "Inflationary interpretation of the stochastic gravitational wave background signal detected by pulsar timing array experiments". *JHEAp* **39**, 81–98 (2023), arXiv: 2306.16912 [astro-ph.CO].

[465] V. K. Oikonomou, P. Tsyba, and O. Razina. "Red or Blue Tensor Spectrum from GW170817-compatible Einstein-Gauss-Bonnet Theory: A Detailed Analysis" (2024), arXiv: 2402.02049 [gr-qc].

[466] N. K. Stein and W. H. Kinney. "Simple single-field inflation models with arbitrarily small tensor/scalar ratio". *JCAP* **03**, 027 (2023), arXiv: 2210.05757 [astro-ph.CO].

[467] J. K. Erickson et al. "Cosmic perturbations through the cyclic ages". *Phys. Rev. D* **75**, 123507 (2007), arXiv: hep-th/0607164.

[468] A. J. Tolley, N. Turok, and P. J. Steinhardt. "Cosmological perturbations in a big-crunch–big-bang space-time". *Phys. Rev. D* **69**, 106005 (2004).

[469] D. H. Lyth. "The Primordial curvature perturbation in the ekpyrotic universe". *Phys. Lett. B* **524**, 1–4 (2002), arXiv: hep-ph/0106153.

[470] A. Aravind, D. Lorshbough, and S. Paban. "Non-Gaussianity from Excited Initial Inflationary States". *JHEP* **07**, 076 (2013), arXiv: 1303.1440 [hep-th].

[471] R. Holman and A. J. Tolley. "Enhanced Non-Gaussianity from Excited Initial States". *JCAP* **05**, 001 (2008), arXiv: 0710.1302 [hep-th].

[472] J. Torrado and A. Lewis. "Cobaya: Code for Bayesian Analysis of hierarchical physical models". *JCAP* **05**, 057 (2021), arXiv: 2005.05290 [astro-ph.IM].

[473] R. M. Neal. "Taking Bigger Metropolis Steps by Dragging Fast Variables" (2005), arXiv: math/0502099 [math.ST].